# MEASUREMENT OF STEREOSELECTIVE BUPROPION DISPOSITION IN RAT BRAIN TO SUPPORT TRANSLATIONAL PBPK/PD MODEL DEVELOPMENT AND APPLICATION

by

**Chandrali S. Bhattacharya**

**A Dissertation**

*Submitted to the Faculty of Purdue University*

*In Partial Fulfillment of the Requirements for the degree of*

**Doctor of Philosophy**


Department of Pharmacy Practice

West Lafayette, Indiana

August 2020

# THE PURDUE UNIVERSITY GRADUATE SCHOOL
# STATEMENT OF COMMITTEE APPROVAL

**Dr. Brian R. Overholser, Chair**

Department of Pharmacy Practice

**Dr. Robert E. Stratford, Co-chair**

Division of Clinical Pharmacology, Indiana University School of Medicine

**Dr. Kevin M. Sowinski**

Department of Pharmacy Practice

**Dr. David R. Foster**

Department of Pharmacy Practice

**Dr. Zeruesenay Desta**

Division of Clinical Pharmacology, Indiana University School of Medicine

**Approved by:**

Dr. Alan J. Zillich

*Dedicated to my sister Paulami Bhattacharya-Patil, my parents Meera and Sampad Bhattacharya and my late grandfather Ramesh Tailor.*

# ACKNOWLEDGMENTS

I am grateful to my many mentors and colleagues during my graduate tenure at Duquesne University, Purdue University and Indiana University, who have provided me with expertise, training, advice, and support.

Foremost, I express my sincerest gratitude to my primary mentor, Dr. Robert E. Stratford for accepting me as his first graduate student and investing in my professional and personal development. I would also like to thank him and his family for their constant support in this journey from Pittsburgh to Indianapolis.

I would like to thank the Indiana Clinical and Translational Sciences Institute (CTSI) for the pre doctoral grant (Grant Number UL1TR002529, A. Shekhar, PI), from the National Institutes of Health, National Center for Advancing Translational Sciences, Clinical and Translational Sciences Award to support my research. I would also like to acknowledge grant from the Charles Henry Leach II fund to support my in vitro microsomal incubation work. I would like to thank the Cancer Center at Indiana University School of Medicine funded by the IU Simon Comprehensive Cancer Center Support Grant (P30CA082709). I also want to thank Anthony L. Sinn & Melissa A. Trowbridge from the In Vivo Therapeutics Core of the IU Simon Comprehensive Cancer Center for technical assistance with in vivo studies. I would like to thank Andi Masters and Christine Bach (Indiana University) for their patience and support with method development, analysis of bupropion and accommodating me in their lab.

I would like to thank Dr. Sara Quinney (Indiana University) who was my unofficial co-mentor and provided invaluable advice on my project and career. I would like to thank Dr. Ahmed Elmokadem (Metrum Research Group) for his constant encouragement, mentorship and invaluable support with mrgsolve/R for PBPK model development. I would also like to thank Dr. Devendra Pade (Certara) for his support with Simcyp®.

I also owe a great deal of thanks to members of my committee. I am honored to have Dr. Zeruesenay Desta on my committee whose pioneering efforts to characterize bupropion`s stereoselective pathways have greatly improved understanding of bupropion`s disposition in scientific community and has paved way for my research. Over the last couple of years, I have

begun to appreciate his unique way of challenging and at the same time supporting my work. I would like to thank Dr. Brian Overholser who has always happily stepped in to bridge the transition from Duquesne to Purdue University and his input on my project and overall graduate school progress. Drs. Dave Foster and Kevin Sowinski have been excellent professional role models and I deeply appreciate their valuable support and feedback through committee meetings.

I am also thankful to the other members of Purdue's Department of Pharmacy Practice who have provided me with daily support and assistance. Many members within the Division of Clinical Pharmacology at the Indiana University School of Medicine have also made essential contributions to my graduate training. Through formal didactic sessions, departmental seminars, the Division has contributed enormously to my graduate training. I would like to thank my former internship mentors at Vertex Pharmaceuticals and AbbVie Inc, for the learning opportunities and contribution towards my professional development. I also owe a great deal of gratitude to my graduate colleagues at Duquesne University, Indiana University, Purdue's Department of Pharmacy Practice for their support throughout my time in the program, including scientific, social, and emotional support. I would like to thank my roommate Sarah Holt and her family and other Brottier Hall roommates Jessica Rebello, Leah Woodard for their support and instantly making me feel at home in this foreign land. At last, I would like to thank my sister who encouraged me to move to USA to follow my dreams and has been a constant pillar of strength through all the ups and downs in life and of course, I would like to thank my parents who have instilled in me and my sister the value of hard work, good work ethics, honesty and perseverance.

# TABLE OF CONTENTS

# LIST OF TABLES

# LIST OF FIGURES

# ABSTRACT

**Background:** Bupropion, an atypical antidepressant and smoking cessation aid, is associated with wide inter-subject variability in its efficacy and safety. Variability in response to bupropion therapy is thought to be driven by variability in metabolism. Bupropion undergoes complex phase 1 and 2 stereoselective metabolism. Though bupropion`s pharmacology is not fully understood, much of it is thought to be due to its metabolites, specially, S, S-hydroxybupropion. In vitro studies (functional assays measuring $IC_{50}$ at dopamine transporter-DAT, norepinephrine transporter-NET, various subtypes of nicotinic receptors-nAChR) and mouse models (forced swim test to assess antidepressant effect, antinociceptive models to assess antagonism of nicotine effects) indicate S, S-hydroxybupropion to contribute more towards efficacy as an antidepressant and smoking cessation aid than racemic bupropion and R, R-hydroxybupropion, respectively. Both pharmacokinetics (PK) and pharmacodynamics (PD) of bupropion and its metabolites are complex and reported to be stereoselective. As bupropion is known to act on multiple central nervous system (CNS) targets (DAT, NET nAChR), understanding CNS disposition (target site) is critical to explain variability in bupropion`s therapeutic and toxic effects.

**Objective:** The objective of our study was to characterize the exposure of bupropion enantiomers and corresponding phase 1 metabolite diastereomers in plasma and brain in a surrogate non-clinical species, and to subsequently develop animal-to-human-translational population-PK and Physiologically Based PK (PBPK) models to predict human brain concentrations of bupropion and its active metabolite S, S-hydroxybupropion. Application of these PK modeling approaches to map the time course of unbound brain concentration can then be compared to in vitro potency measures at DAT, NET and nAChRs to predict target engagement over time (PD). Establishing relationships between plasma PK, target site PK along with PD would elucidate possible cause(s) of inter-patient variability to bupropion therapy.

**Methods:** The first step towards development of a CNS model was to identify a nonclinical species with phase 1 metabolism closest to humans. To accomplish this, hepatic microsomal incubations of four species-rat, mouse, non-human primates (NHPs) and humans were conducted separately for the R- and S-bupropion enantiomers, and the formation of enantiomer-specific

metabolites was determined using LC-MS/MS. Intrinsic formation clearance ($CL_{int}$) of metabolites across the four species (rats, mice, NHPs, humans) was determined from the formation rate versus substrate concentration relationship.

Racemic bupropion (10 mg/kg) and preformed S, S-hydroxybupropion (2 mg/kg) were administered subcutaneously to adult male Sprague Dawley rats (n = 24/compound). Brain and plasma were collected from rats (n = 3) at eight time points for 6 hours and analyzed using a chiral LC-MS/MS method. Rat plasma protein and brain homogenate binding studies were conducted for all analytes to correct for unbound fraction using equilibrium dialysis method.

A plasma-brain compartmental pharmacokinetic approach was used to describe the blood–brain-barrier transport of both bupropion and S, S-hydroxybupropion. Also, a 2-compartment permeability-limited brain model consisting of brain blood, brain mass compartments was developed and incorporated into a whole body physiologically-based pharmacokinetic (PBPK) parent-metabolite model for bupropion and S, S-hydroxybupropion. Both population PK and PBPK modeling approaches were subsequently translated to humans to predict human plasma and brain site exposure and its relationship to DAT and NET $IC_{50}$ potencies.

**Results:** The total clearance of S-bupropion was higher than that of R-bupropion in monkey and human liver microsomes. The contribution of hydroxybupropion to the total racemic bupropion clearance was 38%, 62%, 17%, and 96% in human, monkey, rat, and mouse, respectively. In the same species order, threohydrobupropion contributed 53%, 23%, 17%, and 3%, and erythrohydrobupropion contributed 9%, 14%, 66%, and 1.3%, respectively, to racemic bupropion clearance. Hepatic microsomal incubation studies indicated non-human primates to be the appropriate species to model CNS disposition. However, the cost and limited pharmacokinetic and pharmacodynamic data in NHPs were insurmountable barriers to conducting in vivo studies in NHPs. After considering multiple factors, such as the formation of reductive metabolites (higher in rats than mice), which are also thought to contribute to bupropion`s therapeutic efficacy, availability of microdialysis data measuring bupropion and dopamine, norepinephrine levels in brain extracellular fluid (ECF) and other in vitro potency evaluations in rats, rat was chosen as the surrogate species to model bupropion`s disposition.

In rats, unbound plasma and brain exposures and plasma clearances of both R and S-bupropion were similar. The exposure to parent was higher (50 to 100-fold) than to metabolites. The exposure of oxidative metabolites (R, R- and S, S-hydroxybupropion) was 2 to 3-fold higher in brain and plasma than reductive metabolites (R, R- and S, S-threohydrobupropion, S, R- and R, S-erythrohydrobupropion). Hepatic clearances of R- and S-bupropion scaled from in vitro rat hepatic microsomal incubation studies were 3-fold and 25-fold lower than their respective in vivo unbound apparent clearances. This could possibly be due to substantial contribution of metabolic pathways not characterized in this in vivo study and/or possible extrahepatic disposition in the rat. The unbound brain to unbound plasma $AUC_{0\text{-}6h}$ ratio ($K_{p,uu}$) of R- and S-bupropion were 0.43 and 0.38 respectively. $K_{p,uu}$ of oxidative metabolites (R, R- and S, S-hydroxybupropion) and reductive metabolites (R, R- and S, S-threohydrobupropion) were close to 1. $K_{p,uu}$ of S, R-erythrohydrobupropion was 0.43 and that of pre-formed S, S-hydroxybupropion was 5.

With respect to population PK modeling of both bupropion and S, S-hydroxybupropion, a plasma-brain compartmental model structure with time dependent change in brain influx clearance was required to adequately characterize the BBB transport of parent and this active metabolite. Using a physiologically-based pharmacokinetic model (PBPK) approach too, incorporation of active efflux and carrier mediated uptake terms in addition to passive permeability was necessary to adequately characterize brain disposition of bupropion and S, S-hydroxybupropion. Both modeling approaches (population-PK and PBPK) when translated to humans indicated that the predicted human brain exposures fall below the reported DAT and NET $IC_{50}$ measures of bupropion and S, S-hydroxybupropion.

**Conclusion:** Specific to our work in the rat, the discrepancy between in vitro scaled hepatic clearance and in vivo plasma clearance of R and S-bupropion suggests alternative non-CYP mediated clearance pathways and/or extra hepatic disposition of bupropion. Both translational PK models indicate active process such as efflux transporter or carrier mediated uptake could be involved in bupropion`s disposition in the brain. Variability in expression of these speculated active/carrier mediated transporters could possibly cause variability in response. Also, other CNS targets could contribute to bupropion`s therapeutic efficacy, elucidation of which would require further investigation.

# CHAPTER 1. INTRODUCTION

## 1.1 Clinical indication, controversy and off-label use.

Bupropion was initially developed as a new structural-type antidepressant to improve on the safety and tolerability of existing antidepressants (Carroll et al., 2014; Fava et al., 2005). Bupropion`s pharmacological properties are different from those of tricyclic antidepressants, which were earlier considered to be the first choice of treatment for clinical depression (Carroll et al., 2014). Unlike tricyclic antidepressants (TCAs), bupropion does not possess anticholinergic activity (Carroll et al., 2014; Fabre J., Louis, & McLendon, 1978; Ferris, Cooper, & Maxwell, 1983; Soroko, Mehta, Maxwell, Ferris, & Schroeder, 1977). Hence, it does not possess antimuscarinic side effects of TCAs such as dry mouth, constipation, and urinary retention (Stahl et al., 2004). Also, bupropion is reported to act on norepinephrine (NE) and dopamine (DA) neurotransmitter systems with no appreciable serotogenic activity (Fava et al., 2005; Stahl et al., 2004). As a result of this, bupropion is thought to cause less sexual dysfunction than selective serotonin reuptake inhibitors (SSRIs) and not result in weight gain, which is typically seen with SSRIs (Fava et al., 2005; Stahl et al., 2004).

Bupropion is currently available in three distinct but bioequivalent formulations-immediate release (IR), sustained-release (SR), and extended release (XL)(Fava et al., 2005). When it was first approved in 1989 by US FDA, it was available as IR tablet, which required thrice-daily dosing (Stahl et al., 2004). Although clinically effective, due to reported association of adverse events such as seizures (seizure rate 0.4%) associated with peak plasma concentrations (Dunner et al., 1998), and also the inconvenience due to dosing regimen faced by the patients, SR formulation was later developed (Fava et al., 2005). The time to maximum plasma concentration was prolonged in twice daily SR formulation, and the peak plasma concentrations of bupropion were somewhat lower (15%), and, along with convenience of a twice-daily dosing schedule, the SR formulation improved tolerability/safety profile (seizure rate is 0.1%) (Connarn et al., 2017). However, in a study which compared SR-bupropion formulation to SSRIs, reported greater non-compliance with bupropion due to dose frequency and difficulty remembering to take the

medication led to development of XL formulation which provides a 24-hour plasma concentration of bupropion following a single therapeutic dose (Fava et al., 2005).

There were reports of adverse events in patients being treated for major depressive disorder when switching from Wellbutrin XL (brand name) to Budeprion XL (generic), which on further investigation revealed that generic Budeprion XL 300 mg was bio-inequivalent to Wellbutrin XL formulation (Woodcock , Khan , & Yu 2012). This was surprising and fairly controversial as bupropion is a BCS class 1 drug (Connarn et al., 2017). Despite a higher risk of seizures associated with higher dose of bupropion, approval of Budeprion XL 300 mg was based on the results of a bioequivalence study of Budeprion XL 150 mg and Wellbutrin XL 150 mg, which were extrapolated to the 300-mg product (Woodcock et al., 2012). The comparative area-under-the-curve and $C_{max}$ values for the generic 150-mg products fell within FDA bioequivalent criteria (entire 90% confidence interval associated with the generic to reference ratio of geometric means should fall within the bioequivalence limits of 80 to 125%) (Kharasch et al., 2019). However, a disparity in $t_{max}$ in both 150 mg and 300 mg XL generic versus brand product was observed, which could be due to difference in formulation technology (Woodcock et al., 2012). Also, FDA guidance does not include $t_{max}$ as a criterion for bioequivalence (Kharasch et al., 2019). Later a study by Kharasch et al (Kharasch et al., 2019), which evaluated the bioequivalence and therapeutic equivalence of three generic products versus brand bupropion in adults with major depression, reported that the three bupropion XL 300 mg generic products were both bioequivalent and not therapeutically different from brand drug and each other.

Despite its controversies, due to its dual action on norepinephrine and dopamine systems, bupropion has been evaluated for use in a number of on- and off-label indications. It was approved as a smoking cessation aid (Zyban®) using the sustained release formulation (*U.S. Food and Drug Administration Center for Drug Evaluation (1997). Zyban NDA 20-711 Approval*). Later, bupropion was also approved as a weight loss aid in combination with naltrexone-marketed as Contrave® (fixed dose combination of naltrexone SR and bupropion SR) (Apovian, 2015; *U.S. Food and Drug Administration, Center for Drug Evaluation and Research (2014). Contrave NDA 20006Orig1s000 Approval Letter.*). A number of studies have evaluated bupropion for the treatment of attention-deficit/hyperactivity disorder (ADHD), though its use has not been approved

by the FDA (Reimherr, Hedges, Strong, Marchant, & Williams, 2005; Timothy E. Wilens et al., 2001). Bupropion has showed promising results on reducing methamphetamine dependence (Newton et al., 2006) and also in a study which evaluated combined contingency management with bupropion for the treatment of cocaine addiction (Poling et al., 2006).

## 1.2 Metabolism

Bupropion is extensively metabolized (Schroeder, May 1983; Welch, Lai, & Schroeder, 1987). The absolute bioavailability in humans is currently unknown, as the pharmacokinetics of intravenous (IV) administration have not been reported in humans. Studies in beagle dogs following IV and oral adminstration of 100 mg bupropion indicate absolute oral bioavailability to be < 10 % (Butz et al., 1981). Following a single oral dose of $^{14}$C-bupropion in humans and rats, less than 1% of the dose was recovered as unchanged bupropion in urine, and 10% recovered in the feces was predominantly made up of metabolites (Schroeder, May 1983).

Despite its proven efficacy, bupropion therapy is associated with wide intersuject variability (Benowitz, Zhu, Tyndale, Dempsey, & Jacob, 2013; Connarn et al., 2017; Connarn et al., 2016; Golden, De Vane, et al., 1988; Hesse et al., 2004; Laizure, DeVane, Stewart, Dommisse, & Lai, 1985; Woodcock et al., 2012; A. Z. X. Zhu et al., 2012; Andy Z. X. Zhu et al., 2014). Variability regarding bupropion metabolism is considered chiefly responsible for variability in its response (Benowitz et al., 2013; Gufford, Lu, Metzger, Jones, & Desta, 2016; Hesse et al., 2004; Kharasch, Mitchell, & Coles, 2008; Masters et al., 2016; A. Z. X. Zhu et al., 2012; Andy Z. X. Zhu et al., 2014). To address the issue of intersubject variability, there have been extensive efforts to elucidate its metabolic pathways, with special emphasis on characterizing stereoselective metabolism through in vitro and in vivo studies (Coles & Kharasch, 2008; Gufford et al., 2016; Kharasch et al., 2008; Masters et al., 2016; Sager, Price, & Isoherranen, 2016). A schematic of bupropion`s metabolic pathway is shown in **Figure 1.1**. It is now known that despite being administered in humans as a racemate, systemic exposures of R-bupropion is five to six fold greater than S-form (Dash, Rais, & Srinivas, 2018; Masters et al., 2016). Both the R and S enantiomers of bupropion undergo phase 1 oxidative metabolism, which involves hydroxylation of bupropion catalysed by cytochrome P450 2B6 (major enzyme) to form an hydroxy intermediate;subsequent

cyclization results in the creation of a second chiral center with the potential for the generation of two diastereomers(Carroll et al., 2014). Only the trans-diastereomers, S, S- and R, R-hydroxybupropion have been found in plasma in humans and when synthesized de novo, indicating that they are the thermodynamically more stable isomers (Carroll et al., 2014; Fang et al., 2000). Steric hindrance is thought to reduce cyclization to the cis-diastereomers, R, S- and S, R-hydroxybupropion (Carroll et al., 2014; Fang et al., 2000). Following administration of racemate bupropion, the exposure of hydroxybupropion is about thirty fold higher than bupropion (Kharasch et al., 2019; Masters et al., 2016). R, R-hydroxybupropion exposure is forty to sixty fold higher than S, S-hydroxybupropion (Dash et al., 2018; Fang et al., 2000; Masters et al., 2016). The amino ketone group of bupropion undergoes reductive metabolism to produce R, S- and S, R-erythrohydrobupropion and R, R- and S, S-threohydrobupropion. This reaction is reported to be catalysed by carbonyl reductases and 11β-hydroxysteroid dehydrogenase 1(Connarn, Zhang, Babiskin, & Sun, 2015; Skarydova et al., 2014). Plasma exposure of threohydrobupropion is five-fold higher than bupropion (Masters et al., 2016). Exposure of R, R-threohydrobupropion is about four-fold higher than S, S-threohydrobupropion. The exposure of erythrohydrobupropion is similar to bupropion. The exposure of S, R-erythrohydrobupropion is higher is six fold higher than than R, S-hydrobupropion (Dash et al., 2018; Masters et al., 2016). These phase 1 metabolites (dervived through oxidative or reductive metabolism) further undergo phase 2 metabolism, which is mediated by several glucuronosyltransferase isoforms, to form their respective glucuronide conjugates, which are polar and exreted in urine (Gufford et al., 2016). Overall, based on plasma exposure, R-bupropion and its metabolites were found to dominate over S-bupropion and its metabolites. In vivo, bupropion has an elimination half-life of approximately 12 hours and reaches steady state within a week (Masters et al., 2016). Hydroxybupropion has a half-life of about 20 hours, while threo- and erythrohydrobupropion have longer half-lives (33 and 37 hours, respecitvely) than the parent drug (Masters et al., 2016). The half life of the phase 1 metabolites is greater than parent, suggesting elimination rate limited kinetics. In contrast to this interpretation, S, S-hydroxybupropion was reported to have formation rate limited kinetics with a half life of 14.6 hours (Masters et al., 2016).

Although hydroxybupropion, threohydrobupropion and erythrohydrobupropion are the main circulating metabolites, the amount of these metabolites and their conjugates excreted in urine only account for 23% of the oral dose (Welch et al., 1987). Twenty-two percent of the dose has been reported to be excreted in urine as m-chlorohippuric acid, a glycine conjugate of m-chlorobenzoic acid and nearly 36% of the dose is recovered in urine as unidentified polar metabolites (Welch et al., 1987).

A debate exists over bupropion`s use as a CYP2B6 probe (Coles & Kharasch, 2008; Faucette et al., 2000; Sager et al., 2016). The formation of hydroxybupropion from bupropion is thought to be a selective marker of CYP2B6 activity (Faucette et al., 2000). A study using recombinant enzymes by Sager et al suggest CYP2B6 contributes similarly to the R, R-hydroxybupropion and S, S-hydroxybupropion formation (90% of hydroxybupropion formation is by CYP2B6) (Sager et al., 2016). Hepatic microsomal and S9 incubation studies suggest the hepatic formation clearance of R, R-hydroxybupropion is 2-fold higher S, S-hydroxybupropion and doesn't explain the sixty fold difference in plasma exposures (Bhattacharya, Kirby, Van Stipdonk, & Stratford, 2019; Sager et al., 2016). Three-fold higher formation clearance of R, R-hydroxybupropion glucuronide than S, S-hydroxybupropion glucuronide from human liver microsomal study agrees reasonably well with three-fold higher recovery of R, R-hydroxybupropion glucuronide than S, S-hydroxbupropion glucuronide in urine following administration of 100 mg IR bupropion to healthy human volunteers (Gufford et al., 2016; Masters et al., 2016). The renal clearance of S, S-hydroxybupropion is only ten fold higher than R, R-hydroxybupropion and still does not explain the difference in plasma exposure of these diasteromers. This implies that the overall total clearance of S, S-hydroxybupropion is higher than R, R-hydroxybupropion. However, the pathways involved in hydroxybupropion elimination have not been fully characterized. Altogether, it suggests that in cases where hydroxybupropion metabolism may potentially be altered, use of a metabolite to parent AUC ratio may not a dependable marker of CYP2B6 activity.

However, hydroxybupropion formation plays a minor role in overall bupropion clearance as seen by fraction contribution using in vitro recombinant studies (Sager et al., 2016) and reduced hydroxybupropion formation without alteration in bupropion concentrations in carriers of lower-

activity CYP2B6 alleles CYP2B6*6 and *18 (Benowitz et al., 2013). Genetic variation in CYP2B6, the enzyme that mediates bupropion hydroxylation, was identified as a significant source of variation in hydroxybupropion levels.

Further, species difference in bupropion`s metabolism supports the hypothesis that variability in metabolism drives the variability in resposne, especially as metabolites are thought to contribute to bupropion`s therpaeutic atctivity. In rats, bupropion is reported to be metabolized by side chain oxidation predominantly to acidic metabolites such as m-chlorohippuric acid and m-benzoic acid which is confirmed by their major recovery in urine (Schroeder, May 1983; Welch et al., 1987). These acidic metabolites are reported to be pharmacologically inactive ("National Center for Biotechnology Information. PubChem Database. m-Chlorohippuric acid, CID=448, https://pubchem.ncbi.nlm.nih.gov/compound/m-Chlorohippuric-acid (accessed on May 20, 2020),"). In contrast, mice, dogs, and humans form a major side hydroxylated product, which appears in higher concentration in plasma of mice, dogs and humans and to minor extent in rats (Welch et al., 1987).

Animal safety studies suggest that chronic dosing of bupropion induces its own metabolism (Welch et al., 1987). High single daily oral dose (≥ 150 mg/kg for 14 days) of bupropion to rats, dogs and mice indicated that bupropion increased the extent of its own metabolism through possibly liver enzyme induction (Welch et al., 1987). In rats, plasma bupropion AUC was 17 fold lower and the plasma half life reduced two-fold after 14 days of daily high dose of bupropion compared to first day. In rats, the plasma hydroxybupropion exposure reduced three-fold, and its plasma half-life did not change, which suggested that metabolism via side chain cleavage was the induced pathway. In both mice and dogs, plasma exposure of bupropion decreased ten-fold and the plasma half life also reduced six-fold in mice and three-fold in dogs. In mice, the plasma hydroxybupropion exposure and half-lives remained unchanged. In beagle dogs, exposure of hydroxybupropion increased four-fold, and half life of hydroxybupropion slighlty decreased (Welch et al., 1987). However, the current bupropion label indicates that at recommended doses in humans, bupropion does not induce its own metabolism (GlaxoSmithKline).

## 1.3 Pharmacology

Pharmacology of bupropion is not fully understood. Much of bupropion's pharmacological activity is attributed to its metabolites, specially S, S-hydroxybupropion (Damaj et al., 2004). Bupropion and its metabolites increase extracellular dopamine and norepinephrine concentations (hypofunctioning of noradrenergic and/or dopaminergic pathways thought to be implicated in depression) in synapses by inhibiting reuptake by NET and DAT transporters (Nomikos GG1, 1992 ; Stahl et al., 2004). This is thought to contribute toward its antidepressant activity and also in part its smoking cessation activity as it aids in alleviating withdrawal symptoms stemming smoking abstinence (Carroll et al., 2014; Stahl et al., 2004). This mechanism of action is supported by in vitro dopamine and norepinephrine inhibition in mouse brain synaptosomes and in vivo microdialysis studies where bupropion caused a dose-dependent decrease in dopamine and norephinephrine neuronal firing as well as increased synaptic and brain concentrations of dopamine and norepinephrine (Ascher et al., 1995; Cooper et al., 1994; Li, Perry, & Wong, 2002; Nomikos GG1, 1992 ). Results from a study by Musso et al comparing in vitro (dopamine or norepinephrine reuptake inhibition in mice brain synaptosomes) and in vivo potency (tetrabenazine induced sedation model in mice) of bupropion enantiomers are presented below in **Table 1.1** (Musso et al., 1993).

**Table 1.1.** Summary of in vitro and in vivo potency measures of bupropion enantiomers from study by Musso et al (Musso et al., 1993).

| Compound | Antitetrabenazine activity ($ED_{50}$ mg/kg, IP ± SE) | NET $IC_{50}$ (µM) | DAT $IC_{50}$ (µM) |
|---|---|---|---|
| Racemic bupropion | 18± 3 | 6.7 ± 1.9 | 2.1 ± 0.8 |
| (+)-1 bupropion | 23 ± 4 | 4.0 ± 1.1 | 2.3 ± 0.9 |
| (-)-1 bupropion | 17± 4 | 10.5 ± 3.2 | 4.2 ± 1.9 |

ED: Effective dose; IP: intraperitoneal.

Studies suggest that (+)- and (-)-isomers had (S)- and (R)-configurations, respectively (Carroll et al., 2014; Fang et al., 2000). Musso et al indicated that the rapid racemization of the

enantiomers confounded the absolute measures of potency and this limited drawing conclusions from studies towards understanding the pharmacological effects of the individual isomers (Musso et al., 1993).

As previously discussed, the hypothesis that variability in bupropion metabolism leads to variability in response is further substantiated by significant species differences in bupropion`s antidepressant effect (Butz, Welch, & Findlay, 1982; Carroll et al., 2014; Suckow, Smith, Perumal, & Cooper, 1986). Animal studies suggest that bupropion has greater efficacy in mice versus rats in rodent models of depression (indicated by anti-tetrabenazine activity) (Suckow et al., 1986). Higher formation of S, S-hydroxybupropion in mice than rats, as indicated by in vitro hepatic microsomal incubations, could possible explain this discrepancy in efficacy between species (**Chapter 2**) (Bhattacharya et al., 2019). In vitro studies indicate S, S-hydroxybupropion to be a much more potent inhibitor of both dopamine and norepinephrine uptake than R, R-hydroxybupropion (Carroll et al., 2014; Damaj et al., 2004; Lukas et al., 2010). Also, the S, S-hydroxybupropion $IC_{50}$ value for the norepinephrine transporter was about four-fold lower than that of bupropion and the $IC_{50}$ value for the dopamine transporter was comparable to that of bupropion. Interestingly it was noted that at high doses, mice were more susceptible to convulsive effects of bupropion than rats, which could possibly be attributed to higher hydroxybupropion exposure as well (Welch et al., 1987).

Efforts to understand bupropion`s mechanism of action still continue. Over the years, different studies have been conducted to determine dopamine transporter occupancy after dosing patients with bupropion to gain information about the contribution of inhibition of the DAT to the pharmacological mechanism of action of bupropion. PET studies by Meyers et al, Learned Coughlin et al indicate that DAT occupancy after bupropion treatment in patients during 24 hours is about 20% (Árgyelán et al., 2005; Learned-Coughlin et al., 2003; J. H. Meyer et al., 2002). A 20.8% DAT occupancy during bupropion treatment was also observed in a SPECT study, but this study did not find a significant difference between baseline DAT occupancies in depressed patients relative to that in healthy volunteers (Árgyelán et al., 2005). Further, study by Egerton et al used $^{11}C$ raclopride PET (binding to DAT) to determine whether bupropion administration increases extracellular dopamine levels in the rat and human striatum (Egerton et al., 2010). In rats,

bupropion administration decreased striatal $^{11}$C raclopride-specific binding, consistent with increases in extracellular DA concentrations resulting from inhibition of DA reuptake. However, when this approach was translated to humans, bupropion administration did not decrease striatal $^{11}$C raclopride binding potential, indicating that extracellular DA levels were not increased to levels detectable using this approach (Egerton et al., 2010).

DAT blockade of 22% occurred in imaging studies following administration of preformed metabolite S, S-hydroxybupropion (radafaxine) (Nora D. Volkow et al., 2005). Similar to bupropion, the relatively low potency of DAT blockade by S, S-hydroxybupropion combined with its slow onset suggested that it lacked reinforcing effects. PET imaging studies show that DAT-blocking drugs are not reinforcing if they block less than 50% of DAT within a relatively short period and clear the brain rapidly (N. D. Volkow et al., 1997; Nora D. Volkow et al., 1998). Altogether, these results suggest that in humans, bupropion's or S, S-hydroxybupropion`s therapeutic efficacy is unlikely to be solely due to increase in striatal dopaminergic transmission.

The mechanism of bupropion’s smoking cessation activity is not clear. Part of the smoking cessation effects of bupropion are attributed to antagonism at nicotinic acetylcholine receptors (nAChRs). Bupropion and hydroxybupropion are reported to be noncompetitive antagonists at several of these receptors (Damaj et al., 2004; Damaj et al., 2010; Lukas et al., 2010; Slemmer, Martin, & Damaj, 2000). nAChR antagonist activity of bupropion, R, R- and S, S-hydroxybupropion determined using human neuroblastoma cells are shown below in **Table 1.2**.

**Table 1.2.** In vitro potency measures of bupropion, R, R- and S, S-hydroxybupropion on DAT, NET and nicotinic acetylcholine receptors (Damaj et al., 2004)

| Compound | DAT (μM) | NET (μM) | nAChR$\alpha_4\beta_2$ (μM) | nAChR$\alpha_3\beta_4$ (μM) | nAChR$\alpha_4\beta_4$ (μM) |
|---|---|---|---|---|---|
| Bupropion | 0.55 ± 65 | 1.9 ±12 | 12 ±1.1 | 1.8 ±1.1 | 14±1.1 |
| S, S-hydroxybupropion | 0.790 ± 11 | 0.5 ± 35 | 3.3±1.1 | 10 ± 1.5 | 30 ±1.1 |
| R, R-hydroxybupropion | >10 | >10 | 31 ±1.1 | 6.5 ± 1.2 | 41±1.1 |

DAT: dopamine transporter; NET: norepinephrine transporter; nAChR: nicotinic acetylcholine receptors.

In mouse models, S, S-hydroxybupropion has been reported to be a more potent nicotine antagonist than R, R-hydroxybupropion and bupropion (Carroll et al., 2014; Damaj et al., 2004; Damaj et al., 2010; Slemmer et al., 2000). Bupropion and S, S-hydroxybupropion, but not R, R-hydroxybupropion, significantly decreased the development of nicotine reward as measured in the conditioned place preference and withdrawal paradigm in mice (Damaj et al., 2010). Bupropion and both of its metabolites reversed affective and somatic withdrawal signs in nicotine-dependent mice, but the S, S-hydroxymetabolite had higher potency than bupropion and R, R-hydroxybuproion (Damaj et al., 2010). Bupropion and S, S-, but not R, R- hydroxybupropion, produced partial substitution for nicotine in drug discrimination test. No smoking cessation clinical studies using S, S-hydroxybupropion have been conducted to our knowledge (Carroll et al., 2014; Nora D. Volkow et al., 2005).

Although R, R-hydroxybupropion has lower potency at reported targets (DAT, NET and several of the nAChRs subtypes) relative to S, S-hydroxybupropion and bupropion (Carroll et al., 2014; Damaj et al., 2004; Damaj et al., 2010; Slemmer et al., 2000), since its overall plasma exposure is much higher than bupropion ($C_{max}$-three to four fold, AUC-thirty fold) and S, S-hydroxybupropion ($C_{max}$ thirty fold, AUC-forty to sixty fold) following 100 mg single dose of IR bupropion to healthy human volunteers (Masters et al., 2016; Masters, McCoy, Jones, & Desta), it is possible that its concentrations in brain might reach sufficient levels to produce clinically meaningful blockade of these targets (Benowitz et al., 2013; Dash et al., 2018; Masters et al., 2016; A. Z. X. Zhu et al., 2012). In humans, plasma hydroxybupropion levels following bupropion

treatment have been reported to be predictive of smoking cessation outcomes (Benowitz et al., 2013; A. Z. X. Zhu et al., 2012). Yet no studies have assessed the relationship between the concentrations of the individual R, R and S, S-hydroxybupropion diastereomers and rates of smoking cessation.

Another example of bupropion`s action on multiple targets which is not fully understood regards its approval in combination with naltrexone, an opiate receptor antagonist, for obesity management. This combination product is known as Contrave® (Nainggolan, September 10, 2014). Though mechanism by which the combination of naltrexone SR/bupropion SR induces weight loss is not fully understood (Apovian et al., 2013; Ornellas & Chavez, 2011), it is suggested that bupropion stimulates the pro-opiomelanocortin (POMC) neurons (in hypothalamus), that release α–melanocyte-stimulating hormone (MSH) and β-endorphin. α–MSH mediates the anorectic effect of POMC, whereas β-endorphin is responsible for autoinhibitory feedback, which inactivates the anorectic effect. Naltrexone is thought to block opioid receptor-mediated POMC auto-inhibition, thus augmenting POMC firing in a synergistic manner. It is also thought that bupropion`s action on mesolimbic reward pathways (dopaminergic systems) that modulate reward values and goal-oriented behaviors may lead to further weight reduction (Ornellas & Chavez, 2011).

### 1.4 Central nervous system (CNS) disposition

The blood-brain-barrier selectively restricts the blood-to-brain paracellular diffusion of compounds due to its well-developed tight junctions, thus potentially creating a situation where plasma exposure may not be a good indicator of brain exposure (Luissint, Artus, Glacial, Ganeshamoorthy, & Couraud, 2012). Early studies were conducted to understand CNS disposition of racemic bupropion and formed metabolites in multiple species-rat, mouse, guinea pig (Suckow et al., 1986). In these studies, brain to plasma ratios of bupropion following a 40 mg intraperitoneal (IP) dose of bupropion in these species were similar, ranging from 7.5 to 9 (Suckow et al., 1986; Welch et al., 1987). The hydroxybupropion brain to plasma ratios were 6.3, 9.5, 3.5 in rats, mouse and guinea pig, respectively. Threohydrobupropion brain to plasma ratios were 18.1, 21.6 and 5 in rats, mouse, guinea pigs, respectively (Suckow et al., 1986). However, all ratios from this and prior

studies in nonclinical species represent total brain and plasma ratios, not corrected for fraction unbound in both matrices. Correction for unbound concentration is necessary as it represents the concentration that is available to interact with the targets (DAT, NET) to elicit pharmacological response (Liu & Chen, 2015).

Cerebral microdialysis, a gold standard technique that gives direct measures of unbound extracellular fluid concentration, has not been conducted for bupropion and metabolites in multiple species, largely because of its cost, it is technically demanding and is low throughput. Microdialysis studies that have been reported for bupropion have mostly employed rats, possibly because of ease of handling. The unbound brain to unbound plasma ratio of bupropion and formed hydroxybupropion from a study by Yenicelli using microdialysis following administration of 10 mg/kg IP bupropion were 0.47 and 0.32 for bupropion and hydroxybupropion, respectively (Yeniceli, Şener, Korkmaz, Doğrukol-Ak, & Tuncel, 2011).

An early study by Golden et al measured plasma and cerebrospinal fluid (CSF) concentrations of bupropion and three metabolites in depressed patients at steady state (Golden, De Vane, et al., 1988). The mean CSF to plasma ratio of bupropion, hydroxybupropion, threohydrobupropion and erythrohydrobupropion were 0.43, 0.04, 0.5 and 0.36 respectively. Importantly, the metabolite to parent ratio (hydroxybupropion/bupropion) in CSF did not mirror that in plasma (Golden, De Vane, et al., 1988). This study nor any of the earlier studies did not characterize stereoselective disposition of bupropion in brain. These clinical observations along with the aforementioned pre-clinical findings provide only limited insight regarding CNS disposition of bupropion and its pharmacologically active metabolites. Further, they do not satisfactorily address the use of plasma as a reliable surrogate for brain exposure. Hence elucidation of stereoselective disposition of bupropion and its pharmacologically active metabolites in the brain is necessary to better understand the effects of this complex drug. Suggestion of two additional factors further complicate CNS disposition of bupropion and its metabolites. A recent study conducted in rats measured bupropion and S, S- hydroxybupropion clearance across the blood-brain-barrier. Evidence of carrier mediated transport, which may be stereoselective (Cremers, Flik, Folgering, Rollema, & Stratford, 2016), was presented. Secondly, CYP2B6, a key enzyme involved in bupropion`s oxidative metabolism, is also expressed in brain

(Stingl, Brockmoller, & Viviani, 2013). Contribution of CNS localized CYP2B6 to bupropion and CYP2B6 formed metabolite concentrations in brain has not been investigated. Thus, the possibilities of stereoselective carrier mediated transport across the blood-brain-barrier, and stereoselective metabolism in brain may lead to CNS exposures that are not simply determined by physicochemical properties of bupropion and its metabolites. These pharmacokinetic factors, in addition to stereoselective pharmacology, may contribute towards the observed interpatient variability in bupropion's effect.

## 1.5 Hypothesis and specific aims

The overall hypothesis of this thesis is that relative exposures of bupropion enantiomers to each other and to their corresponding phase 1 diastereomeric pharmacologically active metabolites are different between plasma and brain; these differences prevent reliance solely on systemic exposure measures to understand interpatient differences in response to racemic bupropion administration. Despite bupropion's several clinical and research applications, the stereoselective disposition of bupropion at its target site, that is brain, has not been characterized. This could possibly be due to ethical and safety reasons which limit direct assessment of stereoselective disposition in human brain extracellular fluid. An approach to understand bupropion stereoselective disposition in the brain as a potential source of its inter-subject response variability is to first conduct plasma and brain pharmacokinetic studies in surrogate non-clinical species. Subsequently, application of animal-to-human translational modeling approaches could be used to identify and evaluate hypothesized factors (system and drug specific) influencing dose-concentration (systemic and brain PK)-response (PD) relationships contributing to inter-subject variability in response to bupropion therapy.

We addressed the overall hypothesis through the following specific hypotheses (below) and associated specific aims:

**Hypothesis 1.** Marmoset monkeys demonstrate stereoselective bupropion metabolism comparable to human. These non-human primates (NHPs) metabolize bupropion to produce hydroxybupropion and respective conjugates to similar degree as humans and would be appropriate surrogate species to understand bupropion`s CNS disposition.

**Specific aim 1.** Compare the intrinsic hepatic clearance of bupropion enantiomers and their metabolites in liver microsomes from several non-clinical species to that observed in human liver microsomes to identify species for CNS disposition model development.

**Hypothesis 2.** Plasma is not a good surrogate for brain exposure. The plasma exposure of bupropion enantiomers and metabolite diastereomers of the surrogate non clincal species are different than brain.

**Specific aim 2.** Measure exposures of bupropion enantiomers and their corresponding phase 1 metabolite isomers in plasma and brain following administration of racemic and a key pharmacologically active metabolite, S, S-hydroxybupropion, to surrogate non-clinical species. Use stereospecific quantitative analyses to measure bupropion-related substances in rat brain following administration of racemic bupropion.

**Hypothesis 3.** Stability of bupropion enantiomers is different in plasma, brain and buffer. Instability and inversion of bupropion enantiomers alters estimates of the in vitro unbound fraction estimates for plasma and brain.

**Specific aim 3.** Characterize chiral inversion/stability of bupropion enantiomers in rat plasma, brain and buffer (0.1 M phosphate buffer pH 7.4) to estimate the kinetics of chiral inversion and degradation through a population modeling approach, and application to estimate unbound fractions in plasma and brain matrices.

**Hypothesis 4.** Development of rat-to-human translational population-pharmacokinetic model that describes the central nervous system disposition of bupropion and its metabolite (S, S-hydroxybupropion) will advance our understanding of intersubject variability in human bupropion response.

**Specific aim 4.** Develop a translational population-pharmacokinetic model characterizing plasma-brain transfer (blood-brain-barrier transport) to predict bupropion and pharmacologically active metabolite S, S-hydroxybupropion exposures in human brain (target site), and their relationship to pharmacologic potency measures at the dopamine transporter (DAT) and the norepinephrine transporter (NET).

**Hypothesis 5.** Development of rat-to-human translational physiologically-based pharmacokinetic model that describes the central nervous system disposition of bupropion and its

metabolite (S, S-hydroxybupropion) will advance our understanding of intersubject variability in human bupropion response.

**Specific aim 5.** Develop a translational physiologically-based pharmacokinetic model to predict bupropion and pharmacologically active metabolite S, S-hydroxybupropion exposures in human brain (target site), and their relationship to pharmacologic potency measures at the dopamine transporter (DAT) and the norepinephrine transporter (NET).

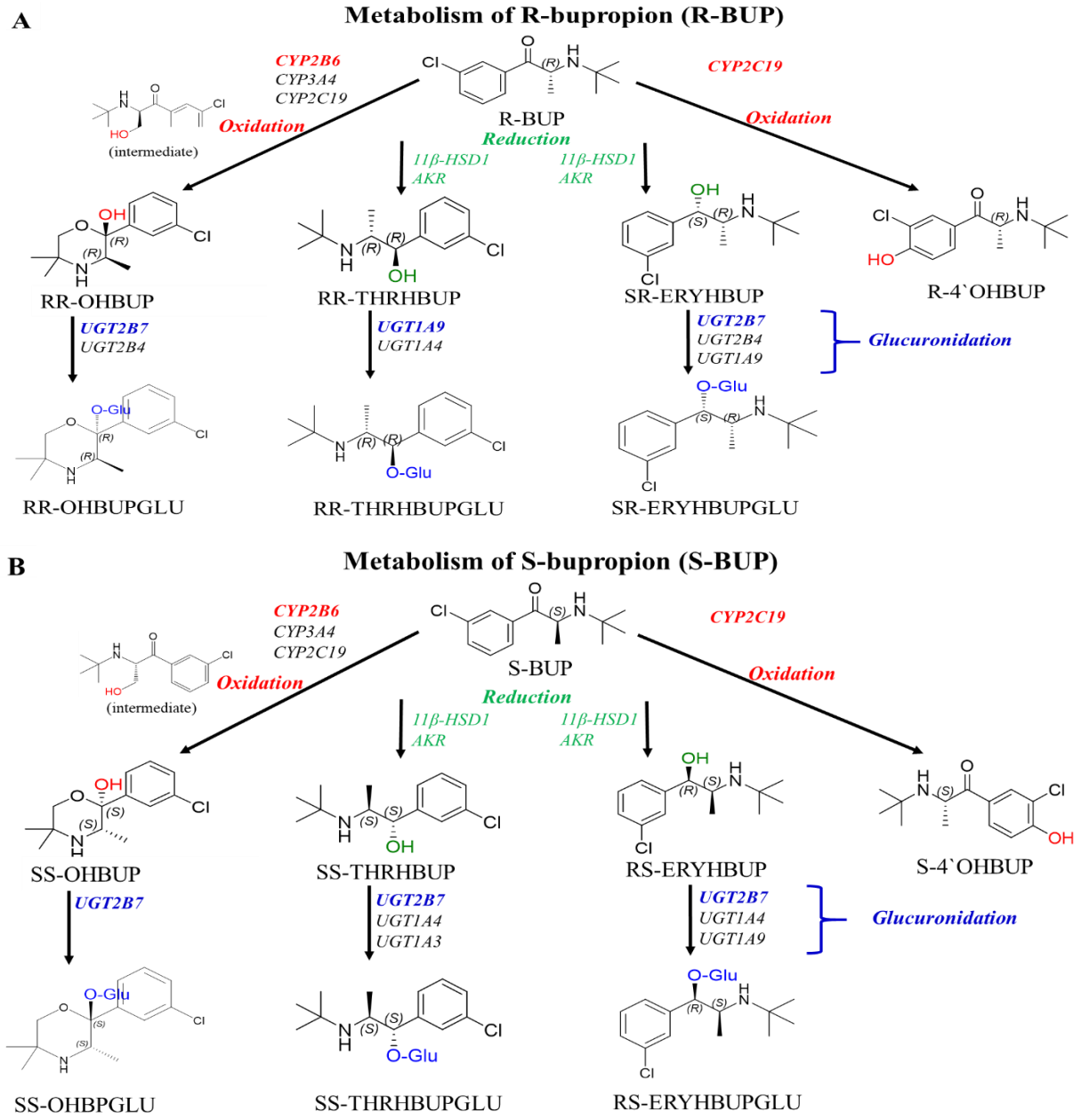


**Figure 1.1.** Bupropion is administered as a racemic mixture and undergoes stereoselective metabolism. Metabolic pathways of R-bupropion (**A, Top**) and S-bupropion (**B, Bottom**) adapted from Sager et al (Sager et al., 2016) and Gufford et al (Gufford et al., 2016). In addition to the shown pathways, bupropion is also metabolized to m-chlorohippuric acid, m-chlorobenzoic acid and some unidentified polar metabolites (Welch et al., 1987). Major enzymes contributing to particular pathway are highlighted in red or green or blue. BUP: bupropion; OHBUP: hydroxybupropion; THRHBUP: Threohydrobupropion; ERYHBUP: erythrohydrobupropion; GLU: glucuronide; 11β-HSD1: 11β-Hydroxysteroid dehydrogenase 1, AKR, Aldo-keto reductase. Figures drawn using ChemDraw Professional 15.1

# CHAPTER 2. COMPARISON OF STEREOSELECTIVE METABOLISM OF BUPROPION IN HUMAN, MONKEY, RAT AND MOUSE LIVER MICROSOMES

*A version of this chapter has been published in part, in European Journal of Drug Metabolism and Pharmacokinetics.*

*Reprinted by permission from Springer Nature, European Journal of Drug Metabolism and Pharmacokinetics. Bhattacharya, C., Kirby, D., Van Stipdonk, M., & Stratford, R. E. "Comparison of In Vitro Stereoselective Metabolism of Bupropion in Human, Monkey, Rat, and Mouse Liver Microsomes", 44(2), 261-274. doi:10.1007/s13318-018-0516-4, copyright, (2019)*

*The final publication is available at https://link.springer.com/article/10.1007/s13318-018-0516-4.*

**Hypothesis 1.** Marmoset monkeys demonstrate stereoselective bupropion metabolism comparable to human. These non-human primates (NHPs) metabolize bupropion to produce hydroxybupropion and respective conjugates to similar degree as humans and would be appropriate surrogate species to understand bupropion`s CNS disposition.

**Specific aim 1.** Compare the intrinsic hepatic clearance of bupropion enantiomers and their metabolites in liver microsomes from several non-clinical species to that observed in human liver microsomes to identify species for CNS disposition model development.

## 2.1 Introduction

Bupropion has been marketed as Wellbutrin® and Zyban® for the management of depression and as a smoking cessation aid, respectively, since the early 1990s (Fava et al., 2005). Its recent approval by the U.S. FDA in combination with naltrexone, Contrave®, for obesity, and a recent positive outcome in clinical trials for attention-deficit/hyperactivity disorder (ADHD), further exemplify the multifaceted therapeutic potential of this drug (Berigan, 2002; Hamedi et al., 2014; Ornellas & Chavez, 2011; Reimherr et al., 2005; Wilens et al.). However, despite being a biopharmaceutical classification system (BCS) class I drug, failure of generic bupropion to meet U.S. FDA bioequivalence standards has drawn attention to the problem of interpatient variability in its clinical response (Benowitz et al., 2013; Connarn et al., 2017; Connarn et al., 2016; Golden,

De Vane, et al., 1988; Hesse et al., 2004; Laizure et al., 1985; Woodcock et al., 2012; A. Z. X. Zhu et al., 2012; Andy Z. X. Zhu et al., 2014). This is of concern due to its high propensity to induce seizures and other side effects (Beyens, Guy, Mounier, Laporte, & Ollagnier, 2008; Davidson, 1990; Grandas & López-Manzanares, 2007; Hesse et al., 2004; Johnston JA, 1991 ; Laizure et al., 1985; Woodcock et al., 2012). With over 40 million patients worldwide prescribed bupropion (Fava et al., 2005), understanding causes of inter-subject variability is critical. Variability regarding bupropion metabolism is considered chiefly responsible for variability in its response (Benowitz et al., 2013; Gufford et al., 2016; Hesse et al., 2004; Kharasch et al., 2008; Masters et al., 2016; A. Z. X. Zhu et al., 2012; Andy Z. X. Zhu et al., 2014).

The disposition and pharmacology of bupropion are complex, since both bupropion and its metabolites have diverse pharmacokinetic (PK) and pharmacodynamic (PD) profiles (Carroll et al., 2014; Coles & Kharasch, 2008; Damaj et al., 2004; Damaj et al., 2010; Gufford et al., 2016; Kharasch et al., 2008; Masters et al., 2016; Sager et al., 2016; Silverstone, Williams, McMahon, Fleming, & Fogarty, 2008; Skarydova et al., 2014; Suckow et al., 1986). Though bupropion is clinically administered as a racemate, plasma exposure of R-bupropion and its metabolites are reported to be higher than exposure to the S enantiomer and its metabolites (Gufford et al., 2016; Kharasch et al., 2008; Masters et al., 2016). Both enantiomers are reported to undergo stereoselective phase 1 and 2 metabolism mediated by multiple enzymes (Coles & Kharasch, 2008; Gufford et al., 2016; Sager et al., 2016). In-vitro and in-vivo studies indicate stereoselective phase 1 and 2 metabolic pathways contribute to observed differences in plasma profiles of bupropion enantiomers and their metabolites (Coles & Kharasch, 2008; Gufford et al., 2016; Kharasch et al., 2008; Masters et al., 2016). Furthermore, several of the isoforms of these metabolizing enzymes and pharmacological targets are polymorphic (Spraggs CF, 2005; Swan et al., 2004), making this also a potential factor contributing to inter-subject variability.

Despite lower plasma exposure of S, S-hydroxybupropion than R, R-hydroxybupropion and bupropion enantiomers, in vitro (Damaj et al., 2004; Damaj et al., 2010) and rodent behavioural studies (Bondarev, Bondareva, Young, & Glennon, 2003; Damaj et al., 2004; Damaj et al., 2010; Grabus, Carroll, & Damaj, 2012) indicate this metabolite plays an important role in the efficacy of the marketed product, both as an antidepressant and smoking cessation aid. Yet,

attempts to bring S,S-hydroxybupropion or its structural analogs to the clinic have met with limited success (Deveaugh-Geiss et al., 2002; Nora D. Volkow et al., 2005), implying that other metabolites may also contribute to bupropion`s overall therapeutic activity. This argument is strengthened by findings from studies that attribute pharmacological activity at several targets (dopamine and norepinephrine transporter inhibition, and agonist and/or antagonist effects at multiple central nicotinic receptors) to reductive metabolites (Ascher et al., 1995; Bondarev et al., 2003; Martin, Massol, Colin, Lacomblez, & Puech, 1990; Schroeder, May 1983).

Previous studies of other centrally acting drugs have suggested that, despite lower brain cytochrome P450 (CYPs) expression than liver, local metabolism by CYPs may also influence exposure in brain, and that this might contribute to inter-individual variability in response (Agarwal et al., 2008; Ferguson & Tyndale, 2011; Khokhar & Tyndale, 2011; Miksys & Tyndale, 2004; V. Ravindranath, Kommaddi, & Pai, 2006; Sharon & Tyndale, 2009; Toselli, Dodd, & Gillam, 2016). The possibility of stereoselective brain disposition as a potential source of inter-subject variability in bupropion response is supported by rodent studies demonstrating nicotine-mediated induction of brain CYP2B (Khokhar, Miksys, & Tyndale, 2010). Interestingly, metabolite-to-bupropion exposure ratios in plasma were different relative to those observed in rat brain (Suckow et al., 1986) and human cerebrospinal fluid (CSF) (Golden, De Vane, et al., 1988), suggesting that plasma may not be an adequate indicator of brain exposure. One approach to understanding bupropion stereoselective disposition in the brain as a potential source of its inter-subject response variability would be to conduct plasma and brain PK studies in surrogate non-clinical species. In-vitro and in-vivo studies conducted in mice, rats and monkeys have not comprehensively evaluated relative systemic exposure and, hence, potential pharmacologic contributions of individual R- or S-bupropion enantiomers and their metabolites (Cremers et al., 2016; Damaj et al., 2004; Hansard, Jackson, Smith, Rose, & Jenner, 2011; A. Meyer et al., 2013; Silverstone et al., 2008; Suckow et al., 1986; Welch et al., 1987).

Thus, the aim of the present work was to compare the stereoselective phase 1 metabolism of bupropion in liver microsomes in three animal species with that in humans. Ideally, this would enable selection of the animal species most resembling bupropion stereoselective systemic metabolism in humans, and subsequently to be used for in-vivo experiments to measure bupropion

enantiomer and corresponding metabolite diastereomer exposure in brain interstitial fluid using microdialysis. This comprehensive exposure profile in brain interstitial fluid that bathes the multiple targets postulated to contribute to bupropion efficacy would ultimately support translational physiologic-based PK modeling and simulation to predict their contribution to target engagement in human brain, much like what has been done with atomoxetine and duloxetine (William Kielbasa, Kalvass, & Stratford, 2009; W. Kielbasa & Stratford, 2012). It is hoped these efforts will help predict the full gamut of bupropion and metabolite disposition in CNS, and so further our understanding of factors contributing to variability in bupropion's effectiveness in depression, weight loss and as adjunctive therapy in smoking cessation programs.

## 2.2 Materials and methods

### 2.2.1 Materials

R-bupropion (Lot # 7- DHL-47-), S-bupropion (Lot # 7- DHL-52-1), R, R-hydroxybupropion (Lot # 20-MVI-123-4), S, S-hydroxybupropion (Lot # 21-MVI-35-1), racemic (rac)-threohydrobupropion (Lot# 1-SHG-39-2), rac-erythrohydrobupropion (Lot# 4-TKA-11-3) and acetaminophen (Lot # 2-GBL-176-1) were purchased from Toronto Research Chemicals (Toronto, Ontario). Nicotinamide adenine dinucleotide phosphate (NADPH) (Lot # 16898425) was purchased from Sigma Aldrich Chemical Co. (St. Louis, MO). Magnesium chloride heptahydrate (Lot # 144052), dibasic potassium phosphate anhydrous (Lot # 153822), monobasic potassium phosphate (Lot # 157503), HPLC grade methanol (Lot # 152929), and HPLC grade acetonitrile (Lot # 152667) were purchased from Fisher Scientific (Fair Lawn, NJ). Pooled human liver microsomes (Lot # 38291), rat (adult male Sprague Dawley) liver microsomes (Lot # 5118007) and mouse (female CD-1) liver microsomes (Lot # 4338001) were purchased from Corning (Woburn, MA). Monkey (adult male marmoset) liver microsomes (Lot # 73474) were purchased from BD Gentest.

### 2.2.2 Liquid chromatography-tandem mass spectrometry (LC-MS/MS) method development and validation

***Standard curve and quality control samples***

Individual standard stock solutions (1 mg/mL) each of R-bupropion, S-bupropion, S, S-hydroxybupropion, R, R-hydroxybupropion, rac-threohydrobupropion, and rac-erythrohydrobupropion were prepared in 2 mL polypropylene tubes by dissolving the compounds in methanol. All solutions were stored at -20 °C. On the day of an analysis, standards were prepared from the standard stock solutions. Standard curves for R-bupropion, R, R-hydroxybupropion, rac-threohydrobupropion, and rac-erythrohydrobupropion had the following concentrations: 0.025, 0.05, 0.20, 1.0, 5.0, 20, 100, and 500 ng/mL. S-bupropion, S,S-hydroxybupropion, rac-threohydrobupropion, and rac-erythrohydrobupropion had the following concentrations: 0.050, 0.25, 0.50, 1.0, 2.5, 5.0, and 10 ng/mL. The smaller concentration range for S-bupropion and its metabolites was in response to observations from R-bupropion incubations in which metabolite concentrations did not exceed 10 ng/mL. Quality control (QC) samples were run in triplicate along with standards to generate statistical data for assay accuracy and precision. QC samples had the following concentrations for R-bupropion, R, R-hydroxybupropion, rac-threohydrobupropion, and rac -erythrohydrobupropion: 1 ng/mL (low QC), 100 ng/mL (medium QC), and 500 ng/mL (high QC). For S-bupropion and S, S-hydroxybupropion, QC samples had the following concentrations: 0.10 ng/mL (low QC), 1.0 ng/mL (medium QC), and 10 ng/mL (high QC). Samples were run in a matrix consisting of a 1:4 phosphate buffer (pH 7.4): acetonitrile mixture with the addition of 0.1% formic acid, containing 100 nM acetaminophen (APAP) as the internal standard. In addition, standards and QC samples also contained 0.5 mg/mL of hepatic microsomes from the relevant species to be consistent with the incubated sample preparations.

***HPLC conditions***

Chromatography was performed using a Phenomenex KINTEX Luna® (150 x 4.6 mm) 3.0-micron C18 column. Achiral chromatography conditions were used; this was possible because separate incubations were conducted with the individual bupropion enantiomers. Injection volume

was held constant at 3 μL, and the mobile phase was delivered as a gradient with a constant flow rate of 0.5 mL/min. A binary mobile phase was employed, which consisted of A) aqueous solution of 20 mM ammonium acetate plus 0.1% ammonium hydroxide (pH 5.7) and B) methanol. The mobile phase was delivered as a gradient that began at 55% A and decreased to 45% of mobile phase A over 8 minutes. From 8-12 minutes, mobile phase A was decreased to 35%. From 12 to 14 minutes, mobile phase A was decreased from 35% to 25%. Next, mobile phase A was decreased from 25% to 10% over 2 minutes and was held for 2 minutes. From 18 minutes to 18.1 minutes mobile phase A was increased from 10% to 55% and held for 4.4 minutes to re-equilibrate the column for the next run.

***Triple-quadrupole mass spectrometer (QqQ/MS) conditions***

An Agilent 6460 with Agilent Jet Stream (AJS) Thermal Focusing Technology was used for the identification of analytes following LC separation. A multiple reaction monitoring (MRM) scanning method was used, because of its sensitivity. The optimal parameters for the AJS-ESI source were the following: gas temperature (320 °C); nebulizer pressure (45 psi); sheath gas temperature (400 °C); sheath gas flow (11 L/min); capillary voltage (4000 V); and nozzle voltage (500 V). Bupropion and its metabolites were detected by positive ion electrospray ionization (ESI) using the mass transitions. Mass transitions are identical for S-bupropion and its derived metabolites versus the respective stereoisomers of R-bupropion parent and its derived metabolites.

***Assay performance***

Calibration curves were analyzed by least squares regression analysis using Agilent MassHunter Workstation Quantitative Software™. The model used for each calibration curve was linear with a weighting of 1/y for optimization for each analyte. Accuracy and precision for each analyte were determined based on the QC concentrations. Intra-assay precision and accuracy were calculated from three samples per QC concentration. Samples from each species were run on a single day, thus obviating the need for evaluation of inter-assay accuracy and precision.

### 2.2.3 Microsomal incubations

Microsomal incubation mixtures consisted of 100 mM potassium phosphate buffer pH 7.4, 5 mM magnesium chloride ($MgCl_2$), 0.5 mg/mL hepatic microsomes of a given species (human, monkey, rat, mouse), and bupropion (R or S enantiomer). To determine initial rate, time-dependent experiments of R- and S-bupropion (at 3.2 µM) was conducted in liver microsomes of each species (human, marmoset monkey, rat, mouse). Formation rate of the metabolite across the four species was determined at six different substrate (R- or S-bupropion) concentrations ranging from 0.4 to 10 µM. This range is identical to that used by Sager et al using human liver S9 fractions, and which encompasses clinically relevant bupropion concentrations (Masters et al., 2016; Sager et al., 2016). It also encompasses the range of racemic bupropion and S, S-hydroxybupropion concentrations observed in rats following a 10 mg/kg dose of racemic bupropion or 2 mg/kg S, S-hydroxybupropion, which were maximal at 1 µM and 3 µM, respectively (Cremers et al., 2016). Because similar systemic concentrations would be targeted for any of the three non-clinical species potentially used to evaluate in vivo plasma and brain pharmacokinetics of bupropion enantiomers and corresponding metabolites, the same concentration range used in the human incubations was also used for the non-clinical species. Reactions were initiated by adding NADPH (1 mM) following a 5-minute preincubation at 37˚C in a water-bath. Total incubation volume after addition of NADPH was 100 µL. All concentrations stated above represent the final concentration in the 100 µL incubation volume. The reaction was stopped with 400 µL of ice-cold acetonitrile containing 0.1% (v/v) formic acid and acetaminophen (final internal standard concentration in 500 µL was 0.1 µM). After stopping the reaction, all samples were centrifuged for 15 minutes at 3000g, 4˚C and the supernatant was transferred to microcentrifuge tubes and stored at -80˚C until analysis. Incubations were performed in triplicate and controls (no NADPH) were run in parallel. Microsomal protein binding was assumed to be negligible in all four species. In support of this assumption, Sager, et al demonstrated negligible binding of both bupropion enantiomers in human S9 fraction at 5 mg/mL protein (Sager et al., 2016). Data was analyzed using JMP®, Version 13.2.0. SAS Institute Inc., Cary, NC and tested for statistical differences by one-way ANOVA with post-hoc Tukey`s test.

Since S- or R- 4`hydroxybupropion are reported as minor metabolites in humans (contributing < 10% to overall bupropion clearance) (Sager et al., 2016), and with no reported pharmacological activity or commercially available standards, these metabolites were not evaluated. As shown in **Figure 2.1**, a specific threohydrobupropion (S, S vs. R, R) or erythrohydrobupropion (R, S vs S, R) metabolite is formed when incubations are conducted with a specific enantiomer. This obviated the need to correct standard concentrations of the racemic mixture of these two metabolite types (threo and erythro) for the individual diastereomers when calculating unknown concentrations of these metabolites from the incubations.

Formation rate of a metabolite was plotted against substrate concentration and fit via linear or nonlinear regression models in JMP®, Version 13.2.0. SAS Institute Inc., Cary, NC and GraphPad Prism version 6.00 for Windows (GraphPad Software, CA, USA). Final model selection was guided by precision of parameter estimates, objective function and examination of goodness-of-fit plots. When metabolite formation kinetics followed linear kinetics, intrinsic clearance ($CL_{int}$) was calculated from the slope of formation rate (v) versus substrate concentration (S) plots. When non-linear kinetics were observed, $CL_{int}$ was calculated as the ratio of $V_{max}$ and $K_m$ based on the Michaelis–Menten equation (1) that reduces to concentration-independent kinetics when [S] << $K_m$.

$$V = \frac{V_{max} \cdot [S]}{K_m + [S]} \quad \text{.....Equation 2.1}$$

Intrinsic clearance ($CL_{int}$) was scaled to intrinsic hepatic clearance ($CL_{int,H}$) using the equation below (2) for the four species. Values for the two ratios that are specific to each species are summarized in the respective table legends.

$$CL_{int,H} = CL_{int} \cdot \frac{\text{mg microsomes}}{\text{gram (g) of liver}} \cdot \frac{\text{liver weight (g)}}{\text{body weight (kg)}} \quad \text{.....Equation 2.2}$$

## 2.3 Results

### 2.3.1 LC-MS/MS method development and validation

Chromatographic separation of bupropion (R or S), hydroxybupropion (S, S or R, R), rac-erythrohydrobupropion and rac-threohydrobupropion was successfully achieved using a Phenomenex KINTEX Luna® (150 x 4.6 mm) 3.0-micron C18 column. As achiral conditions were used, the developed method was employed for both R- and S-bupropion and their corresponding metabolites and was successfully reproducible for the four animal species. Bupropion enantiomer inversion was avoided by using a short incubation time of seven minutes (Sager et al., 2016). Calibration curves generated were linear for all analytes where the common $r^2$ values were $\geq 0.99$. Assay accuracy and precision were $\leq 20\%$ for all QC samples.

### 2.3.2 Microsomal incubation kinetics

**Figure 2.1** depicts the initial rate kinetics of R and S-bupropion in human, marmoset money, rat and mouse liver microsomes at 3.2 µM. 7 minutes was chosen as the incubation time. At this time and microsomal protein concentration, there was no observable substrate depletion; furthermore, formation of metabolites was linear with respect to time.

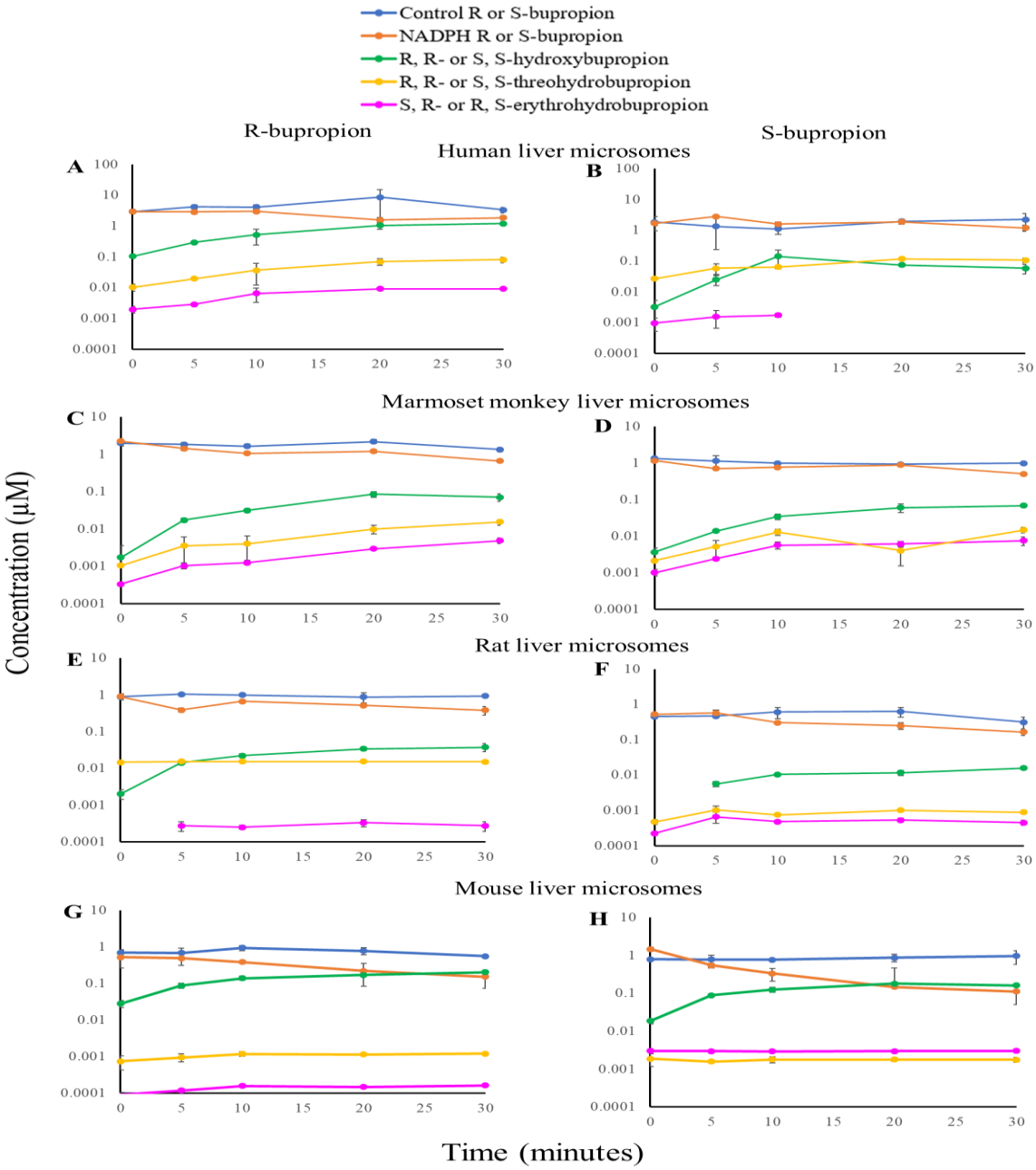


**Figure 2.1.** Initial rate determination of R (**Left**) and S-bupropion (**Right**) in human (**A** and **B**), marmoset monkey (**C** and **D**), rat (**E** and **F**) and mouse (**G** and **H**) liver microsomes. These studies were conducted at 3.2 µM bupropion (R or S) concentration. Data are represented as the mean ± S.D (n=3). Blue line indicates R or S-bupropion control with no NADPH, orange line indicates R or S bupropion with NADPH, green indicates R, R- or S, S-hydroxybupropion, yellow line indicates R, R- or S, S-threohydrobupropion, pink line indicates S, R- or R, S-erythrohydrobupropion.

**Tables 2.1 – 2.4** summarize the kinetics of R- and S-bupropion phase 1 metabolism in human, marmoset, rat and mouse liver microsomes, respectively. Formation clearance ($CL_{int}$) of each metabolite was estimated from the relationship between formation rate relative to the range of substrate concentrations evaluated (0.4-10 μM). These relationships are summarized in **Figures. 2.2 – 2.5** for each species, respectively. In marmoset, a linear relationship was observed for all six metabolites; whereas, in the mouse, saturable kinetics were observed for all six metabolites. Human and rat formation kinetics were mixed linear and non-linear. **Table 2.5** summarizes $V_{max}$ and $K_m$ estimates in cases where non-linear kinetics were observed. In such cases, $CL_{int}$ represents the ratio $V_{max}/K_m$, which would apply to conditions in which substrate concentration << $K_m$ according to Equation 2.1.

***Characterization of bupropion metabolism in human liver microsomes (HLMs)***

With respect to the two bupropion isomers, total $CL_{int}$ of S-bupropion was 5.6-fold higher than R-bupropion (**Table 2.1**). The various fractions of this total contributed by the measured metabolites are also summarized in **Table 2.1**. R, R-hydroxybupropion was found to be the major metabolite of R-bupropion, while S, S-threohydrobupropion was the major metabolite of S-bupropion. All three metabolites derived from S-bupropion had higher $CL_{int}$ of formation compared to their corresponding diastereoisomers derived from R-bupropion. **Figure 2.6** summarizes the fractional clearance ($f_{m,\ racemic}$) that each metabolite contributes to the clearance of racemic bupropion. In human liver microsomes, S, S-threohydrobupropion was found to be the major metabolite, contributing 37% to total racemic bupropion clearance.

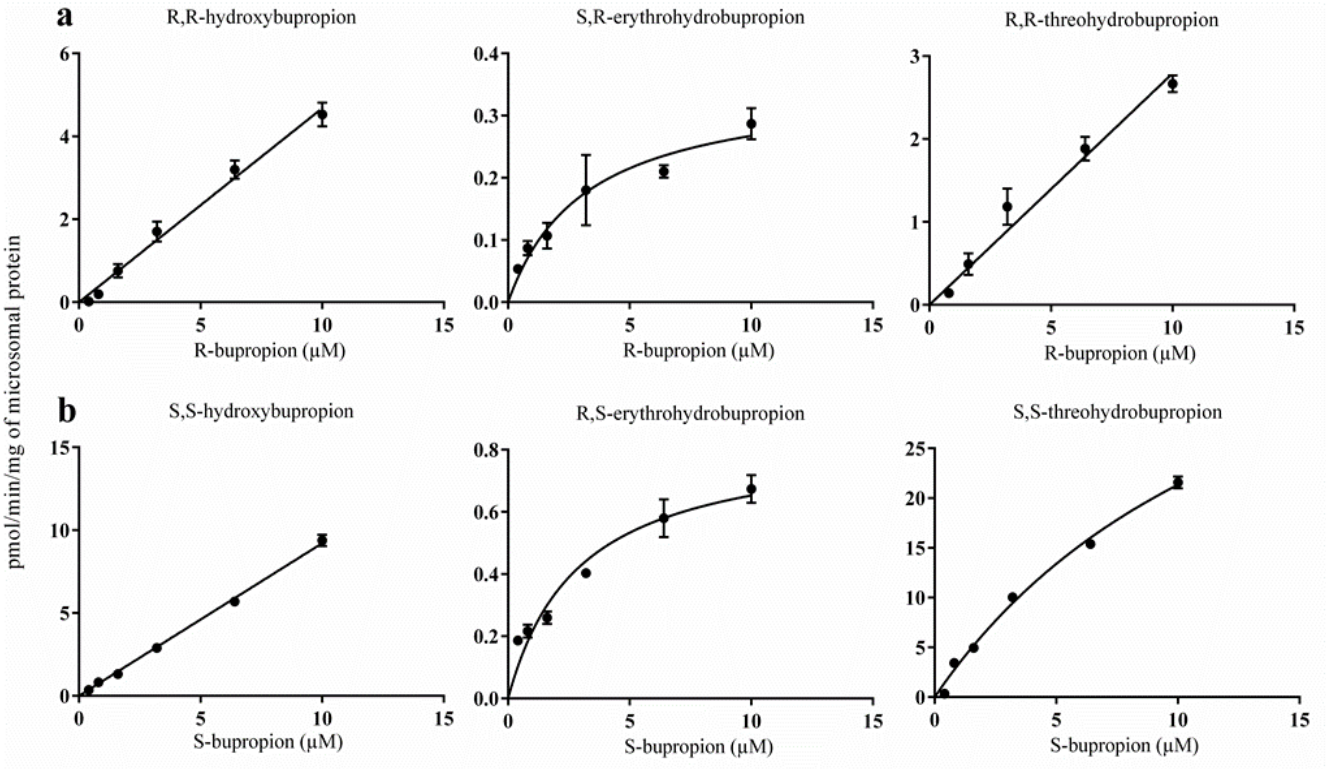


**Figure 2.2.** Metabolite formation kinetics of R- and S-bupropion in human liver microsomes. (a) Concentration dependent formation of R, R-hydroxybupropion, S, R-erythrohydrobupropion, R, R-threohydrobupropion from R-bupropion. (b) Concentration dependent formation of S, S-hydroxybupropion, R, S-erythrohydrobupropion, S, S-threohydrobupropion from S-bupropion. Data are represented as the mean ± S.D (n=3)

**Table 2.1.** Kinetics of R- and S-bupropion metabolism in human liver microsomes

| Substrate and metabolites | $CL_{int}$ | $CL_{int, H}$[a] | $f_{m, enantiomer}$[b] |
|---|---|---|---|
| | µl/min/mg of microsomal protein | L/h | |
| R-bupropion | | | |
| R, R-hydroxybupropion | 0.48 | 2.12 | 0.56 |
| R, R-threohydrobupropion | 0.27 | 1.19 | 0.31 |
| S, R-erythrohydrobupropion | 0.11 | 0.49 | 0.13 |
| Total R-bupropion $CL_{int}$ | 0.86 | 3.80 | |
| S-bupropion | | | |
| S, S-hydroxybupropion | 0.93 | 4.14 | 0.19 |
| S, S-threohydrobupropion | 3.59 | 16.01 | 0.75 |
| R, S-erythrohydrobupropion | 0.29 | 1.29 | 0.06 |
| Total S-bupropion $CL_{int}$ | 4.81 | 21.4 | |

[a] Microsomal intrinsic clearance ($CL_{int}$) values were scaled to hepatic intrinsic clearance ($CL_{int, H}$) using the scaling factor of 40 mg microsomal protein/g liver. Assuming a body weight of 81 kg and 22 g liver/kg body weight results in 1782 g liver weight. These values are from SIMCYP® simulator, version 17, Certara®.

[b] Fractional contribution of a metabolite to the total bupropion enantiomer $CL_{int, H}$ ($f_{m, enantiomer}$).

***Characterization of bupropion metabolism in marmoset monkey liver microsomes (MMLMs)***

In MMLMs, total $CL_{int}$ of S-bupropion was 1.3-fold relative to R-bupropion (**Table 2.2**). As with HLMs, R, R-hydroxybupropion was found to be the major metabolite of R-bupropion; however, unlike HLMs, in which S, S-threohydrobupropion was the major metabolite derived from S-bupropion, S, S-hydroxybupropion was the major metabolite in MMLMs. Formation clearance ($CL_{int}$) of S, S-hydroxybupropion and R, R-hydroxybupropion were similar in MMLMs. $CL_{int}$ of the two-remaining metabolite diastereoisomer pairs was faster from S-bupropion; namely, S, S-threohydrobupropion was nearly 2-fold higher than R, R-threohydrobupropion; R, S-erythrohydrobupropion was 3-fold higher than S, R-erythrohydrobupropion. For both enantiomers, the rank order for formation of the three metabolites was the same in this species. Considering the overall contribution of each of the measured metabolites to total racemic bupropion clearance (**Figure 2.6**), R, R-hydroxybupropion was the major metabolite, contributing 36% to overall bupropion clearance (0.71/2). Comparing to HLMs, the rank order of R-bupropion-derived metabolite formation kinetics ($f_{m, enantiomer}$) was the same in MMLMs. However, the rank order of

S-bupropion-derived metabolite formation kinetics was different between the two species, with $f_{m,\ enantiomer}$ of S, S-hydroxybupropion being 3-fold higher, S, S-threohydrobupropion 3-fold lower and R, S-erythrohydrobupropion 3.5-fold higher in MMLMs relative to HLMs.

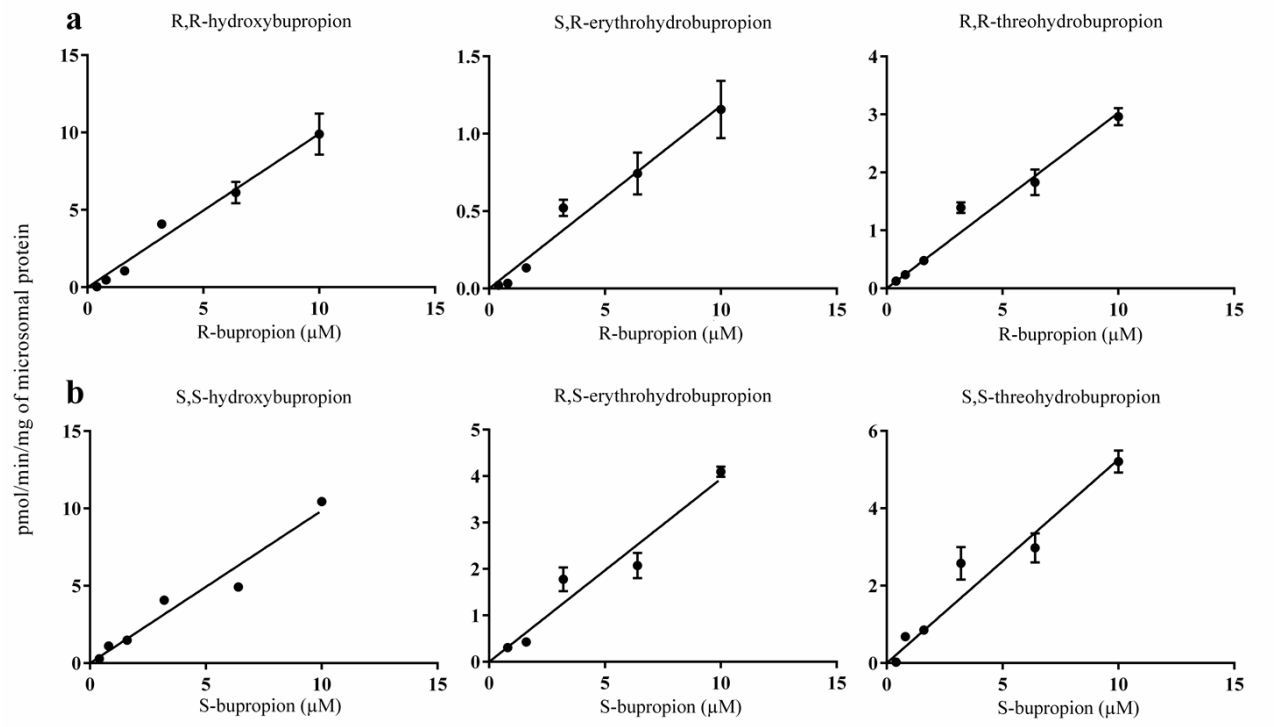


**Figure 2.3.** Metabolite formation kinetics of R- and S-bupropion in monkey liver microsomes. (a) Concentration dependent formation of R, R-hydroxybupropion, S, R-erythrohydrobupropion, R, R-threohydrobupropion from R-bupropion. (b) Concentration dependent formation of S, S-hydroxybupropion, R, S-erythrohydrobupropion, S, S-threohydrobupropion from S-bupropion. Data are represented as the mean ± S.D (n=3)

**Table 2.2.** Kinetics of R- and S-bupropion metabolism in monkey liver microsomes

| Substrate and metabolites | $CL_{int}$ | $CL_{int, H}$[a] | $f_{m, enantiomer}$[b] |
|---|---|---|---|
| | µl/min/mg of microsomal protein | L/h | |
| R-bupropion | | | |
| R, R-hydroxybupropion | 1.02 | 0.16 | 0.71 |
| R, R-threohydrobupropion | 0.29 | 0.04 | 0.20 |
| S, R-erythrohydrobupropion | 0.12 | 0.02 | 0.08 |
| Total R-bupropion $CL_{int}$ | 1.43 | 0.22 | |
| S-bupropion | | | |
| S, S-hydroxybupropion | 0.97 | 0.15 | 0.52 |
| S, S-threohydrobupropion | 0.50 | 0.08 | 0.27 |
| R, S-erythrohydrobupropion | 0.39 | 0.06 | 0.21 |
| Total S-bupropion $CL_{int}$ | 1.86 | 0.29 | |

[a] Microsomal intrinsic clearance values were scaled to $CL_{int, H}$ using the scaling factor of 31 mg microsomal protein/g liver. Assuming a body weight of 4 kg and 19.67 g liver/kg body weight results in 78.7 g liver weight. These values are from SIMCYP® simulator, version 17, Certara®.
[b] Fractional contribution of a metabolite to the total bupropion enantiomer $CL_{int, H}$ ($f_{m,\ enantiomer}$).

***Characterization of bupropion metabolism in rat liver microsomes (RLMs)***

In striking contrast to HLMs and MMLMs, total $CL_{int}$ of S-bupropion in RLMs was 7-fold lower than R-bupropion (**Table 2.3**), and the erythrohydrobupropion isomers were the dominant metabolites formed for both R- and S-bupropion. While formation of R, R-hydroxybupropion, R, R-threohydrobupropion and S, S-hydroxybupropion followed linear kinetics, formation of S, R-erythrohydrobupropion, R, S-erythrohydrobupropion and S, S-threohydrobupropion followed Michaelis-Menten kinetics (**Figure 2.4**). Considering, the relative contribution of all the measured metabolites to racemic bupropion clearance, S, R-erythrohydrobupropion was the chief metabolite, contributing 44% to overall bupropion clearance (**Figure 2.6**). In comparison to HLMs, $f_{m, enantiomer}$ of R, R-hydroxybupropion in RLMs was 5-fold lower; R, R-threohydrobupropion was 31-fold lower and that of S, R -erythrohydrobupropion was 7-fold higher in RLMs. The $f_{m, enantiomer}$ of S, S-hydroxybupropion in RLMs was nearly the same as HLMs; S, S-threohydrobupropion was 2-fold lower and R, S-erythrohydrobupropion was 7-fold higher in RLMs.

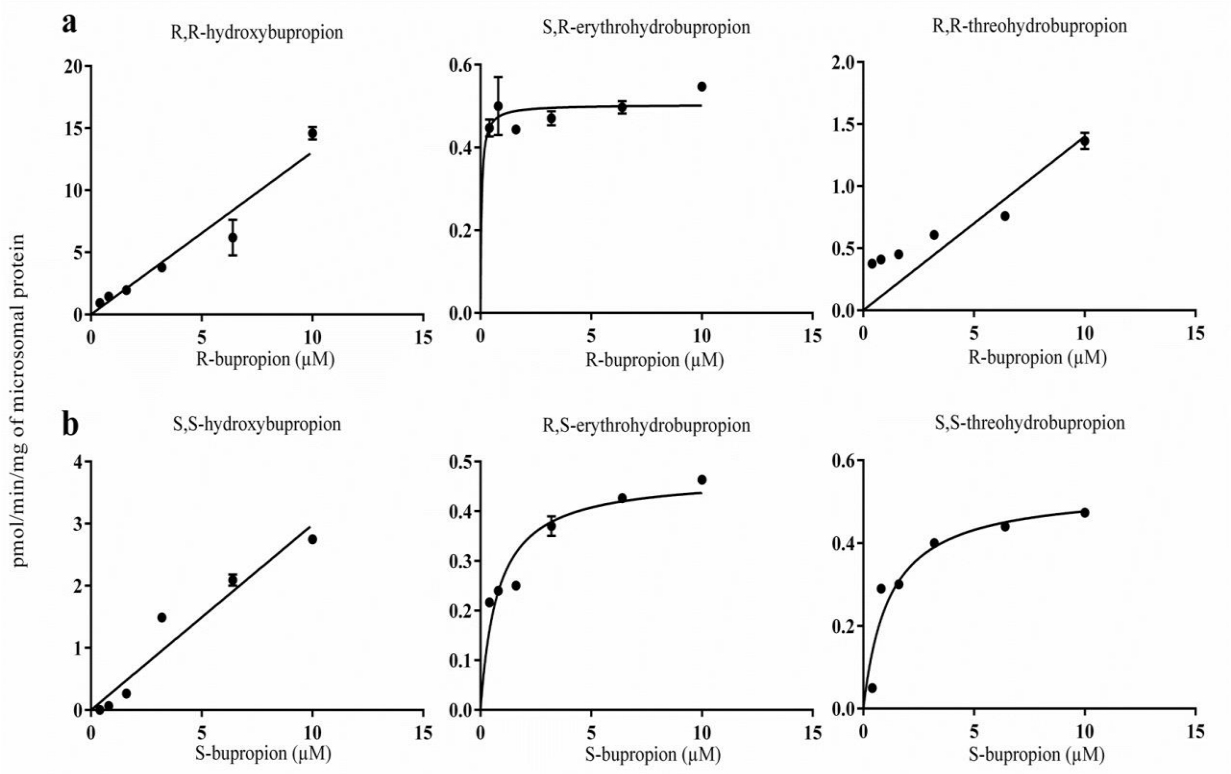


**Figure 2.4.** Metabolite formation kinetics of R- and S-bupropion in rat liver microsomes. (a) Concentration dependent formation of R, R-hydroxybupropion, S, R-erythrohydrobupropion, R, R-threohydrobupropion from R-bupropion. (b) Concentration dependent formation of S,S-hydroxybupropion, R, S-erythrohydrobupropion, S, S-threohydrobupropion from S-bupropion. Data are represented as the mean ± S.D (n=3).

**Table 2.3.** Kinetics of R- and S-bupropion metabolism in rat liver microsomes

| Substrate and metabolites | $CL_{int}$ | $CL_{int, H}$[a] | $f_{m, enantiomer}$[b] |
|---|---|---|---|
| | µl/min/mg of microsomal protein | L/h | |
| R-bupropion | | | |
| R, R-hydroxybupropion | 1.33 | 0.034 | 0.12 |
| R, R-threohydrobupropion | 0.10 | 0.003 | 0.01 |
| S, R-erythrohydrobupropion | 10.00 | 0.256 | 0.88 |
| Total R-bupropion $CL_{int}$ | 11.43 | 0.29 | |
| S-bupropion | | | |
| S, S-hydroxybupropion | 0.30 | 0.008 | 0.22 |
| S, S-threohydrobupropion | 0.46 | 0.012 | 0.34 |
| R, S-erythrohydrobupropion | 0.60 | 0.015 | 0.44 |
| Total S-bupropion $CL_{int}$ | 1.36 | 0.04 | |

[a] Microsomal intrinsic clearance values were scaled to $CL_{int, H}$ using the scaling factor of 46 mg microsomal protein/g liver. Assuming a body weight of 0.25 kg and 35.6 g liver/kg body weight results in 8.9 g liver weight. These values are from SIMCYP® simulator, version 17, Certara®.
[b] Fractional contribution of a metabolite to the total bupropion enantiomer $CL_{int, H}$ ($f_{m,\ enantiomer}$).

***Characterization of bupropion metabolism in mouse liver microsomes (MLMs)***

In MLMs, total $CL_{int}$ of S-bupropion was nearly 2-fold lower than R-bupropion (**Table 2.4**). Like rats, and in contrast to humans, total R-bupropion $CL_{int}$ was faster than S-bupropion. R, R-hydoxybupropion was responsible for 95% of total R-bupropion clearance; likewise, S, S-hydroxybupropion was the main metabolite from S-bupropion phase 1 metabolism ($f_{m, enantiomer}$ = 95%). Of all the measured metabolites, both S, S- and R, R-hydroxybupropion were found to contribute 48% each towards racemic bupropion clearance (**Figure 2.6**). Comparing the fraction that each metabolite contributes to $CL_{int, H}$ for an enantiomer ($f_{m, enantiomer}$), it was observed that R, R-hydroxybupropion formation was 2-fold higher, R, R-threohydrobupropion was 8-fold lower and that of S, R-erythrohydrobupropion was 13-fold lower than HLMs. The $f_{m, enantiomer}$ of S, S-hydroxybupropion in MLMs was 5-fold higher; S, S-threohydrobupropion was 38-fold lower and R, S-erythrohydrobupropion was 2-fold lower than HLMs.

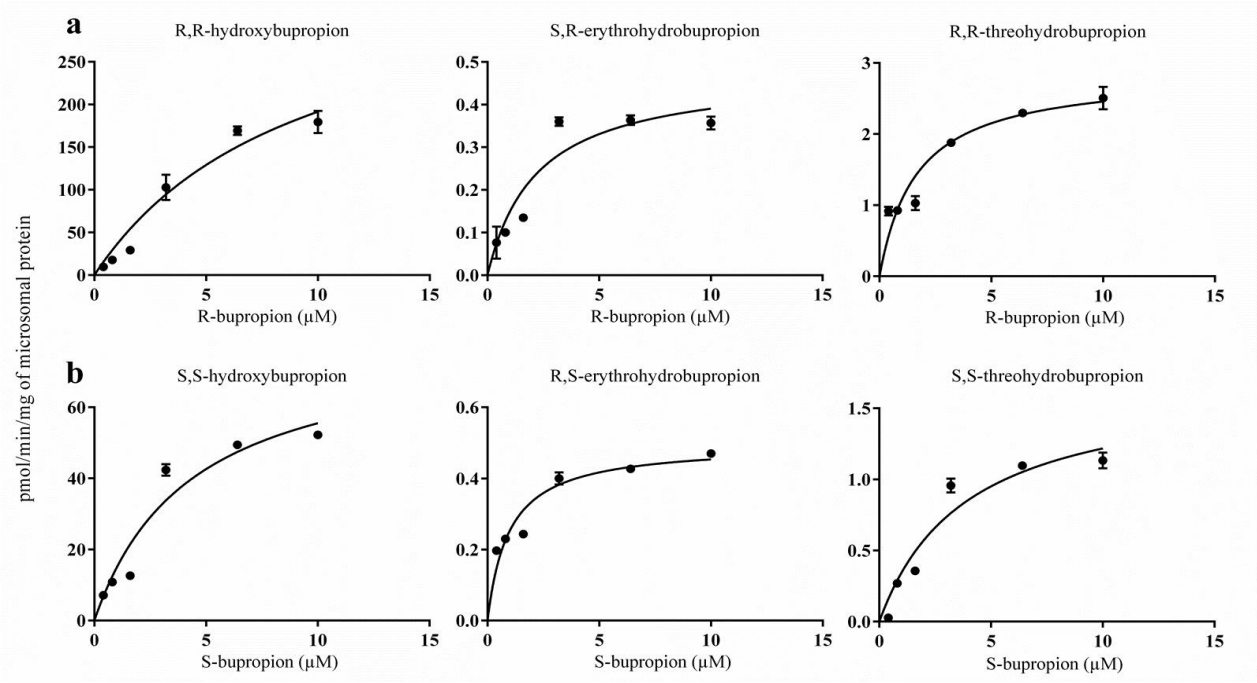


**Figure 2.5.** Metabolite formation kinetics of R- and S-bupropion in mouse liver microsomes. (a) Concentration dependent formation of R, R-hydroxybupropion, S, R-erythrohydrobupropion, R, R-threohydrobupropion from R-bupropion. (b) Concentration dependent formation of S, S-hydroxybupropion, R, S-erythrohydrobupropion, S, S-threohydrobupropion from S-bupropion. Data are represented as the mean ± S.D (n=3).

**Table 2.4**. Kinetics of R- and S-bupropion metabolism in mouse liver microsomes

| Substrate and metabolites | $CL_{int}$ | $CL_{int, H}$[a] | $f_{m, enantiomer}$[b] |
|---|---|---|---|
| | µl/min/mg of microsomal protein | L/h | |
| R-bupropion | | | |
| R, R-hydroxybupropion | 39.63 | 0.15 | 0.95 |
| R, R-threohydrobupropion | 1.73 | 0.007 | 0.04 |
| S, R-erythrohydrobupropion | 0.22 | 0.001 | 0.01 |
| Total R-bupropion $CL_{int}$ | 41.58 | 0.158 | |
| S-bupropion | | | |
| S, S-hydroxybupropion | 18.30 | 0.071 | 0.95 |
| S, S-threohydrobupropion | 0.43 | 0.002 | 0.02 |
| R, S-erythrohydrobupropion | 0.52 | 0.002 | 0.03 |
| Total S-bupropion $CL_{int}$ | 19.25 | 0.074 | |

[a] Microsomal intrinsic clearance values were scaled to $CL_{int, H}$ using the scaling factor of 48 mg microsomal protein/g liver. Assuming a body weight of 0.025 kg and 51.2 g liver/kg body weight results in 1.2 g liver weight. These values are from SIMCYP® simulator, version 17, Certara®.
[b] Fractional contribution of a metabolite to the total bupropion enantiomer $CL_{int, H}$ ($f_{m, enantiomer}$).

**Table 2.5.** Michaelis-Menten parameters for metabolites displaying saturable formation kinetics in liver microsomes

| Species | Substrate | Metabolite | $V_{max}$ | $K_m$ | $CL_{int}$ ($V_{max}/K_m$) |
|---|---|---|---|---|---|
| | | | pmol/min/mg microsomal protein | µM | µl/min/mg of microsomal protein |
| Human | R-BUP | SR-ERYHBUP | 0.35 ± 0.03 | 3.19 ± 0.76 | 0.11 |
| | S-BUP | SS-THRHBUP | 52.56 ± 5.88 | 14.63 ± 2.32 | 3.59 |
| | | RS-ERYHBUP | 0.84 ± 0.06 | 2.89 ± 0.56 | 0.29 |
| Rat | R-BUP | SR-ERYHBUP | 0.50 ± 0.01 | 0.05 ± 0.028 | 10 |
| | S-BUP | SS-THRHBUP | 0.53 ± 0.03 | 1.16 ± 0.24 | 0.46 |
| | | RS-ERYHBUP | 0.47 ± 0.02 | 0.78 ± 0.14 | 0.60 |
| Mouse | R-BUP | RR-OHBUP | 370.44 ± 71.12 | 9.34 ± 3.10 | 39.66 |
| | | RR-THRHBUP | 2.86 ± 0.17 | 1.65 ± 0.32 | 1.73 |
| | | SR-ERYHBUP | 0.47 ± 0.04 | 2.20 ± 0.62 | 0.21 |
| | S-BUP | SS-OHBUP | 79.65 ± 9.44 | 4.35 ± 1.15 | 18.31 |
| | | SS-THRBUP | 1.69 ± 0.18 | 3.9 ± 1.0 | 0.43 |
| | | RS-ERYHBUP | 0.49 ± 0.02 | 0.96 ± 0.16 | 0.51 |

RR-OHBUP: R, R-hydroxybupropion, RR-THRBUP: R, R-threohydrobupropion, SR-ERYHBUP: S, R-Erythrohydrobupropion. SS-OHBUP: S, S-hydroxybupropion, SS-THRBUP: S, S-threohydrobupropion, RS-ERYHBUP: R, S-erythrohydrobupropion

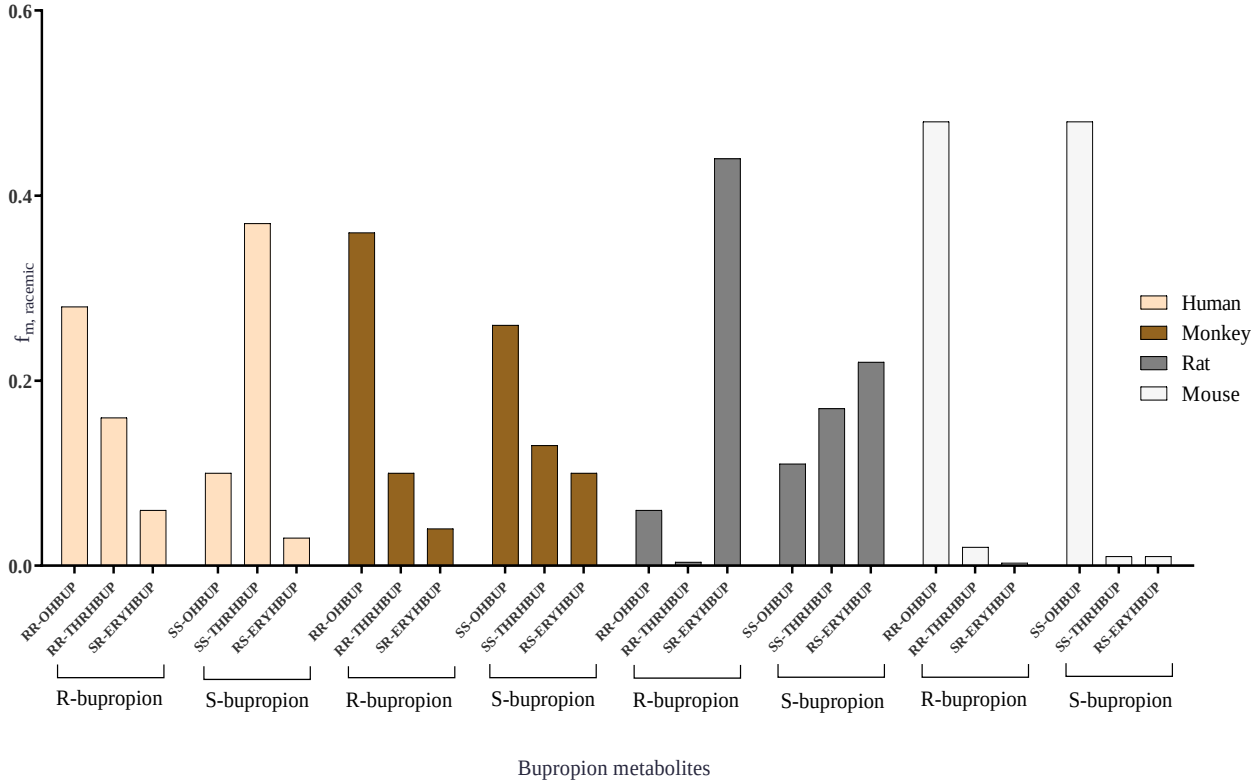


**Figure 2.6.** Interspecies comparison of the fraction of racemic bupropion metabolized to a specific metabolite ($f_{m,\ racemic}$). RR-OHBUP: R, R-hydroxybupropion, RR-THRBUP: R, R-threohydrobupropion, SR-ERYHBUP: S, R-Erythrohydrobupropion. SS-OHBUP: S, S-hydroxybupropion, SS-THRBUP: S, S-threohydrobupropion, RS-ERYHBUP: R, S-erythrohydrobupropion

As summarized in **Figure 2.6**, comparing across the four species, the total hydroxybupropion proportion contributing to racemic bupropion clearance was highest in the mouse (96%), followed by monkey (62%), human (38%) and least in rat (17%). Threohydrobupropion was the most prevalent metabolite in human microsomes (53%), followed by monkey (23%), rat (17%) and least in mouse (3%). The highest fraction of total erythrohydrobupropion was observed in the rat (66%), followed by monkey (14%), human (9%) and least in mouse liver microsomes (1.3%).

## 2.4 Discussion

Despite proven efficacy, bupropion therapy is associated with wide inter-subject variability in clinical response (Dunner DL, 1998; Johnston JA, 1991 ; Laizure et al., 1985; Masters et al., 2016). Complex pharmacokinetics and pharmacology of this drug, which includes formation of several active metabolites displaying variations in their own clearance to secondary metabolites, are the attributed causes (Bondarev et al., 2003; Damaj et al., 2004; Gufford et al., 2016; Kharasch et al., 2008; Masters et al., 2016; A. Meyer et al., 2013; Sager et al., 2016; Skarydova et al., 2014; Stahl et al., 2004). In order to advance understanding of this variability and its sources, application of non-clinical animal experiments designed to enable chiral resolution of bupropion enantiomers and phase 1 metabolite diastereomers in plasma and brain might be useful. Preference in species selection would be based on similarity of metabolite formation kinetics relative to humans. The objective of the study reported herein was to compare phase 1 metabolite formation kinetics in rodents and NHPs to those in human in order to justify species selection for stereospecific CNS disposition studies.

The 5.6-fold higher S-bupropion relative to R-bupropion total $CL_{int}$ in HLMs is close to the 5-fold difference observed in human liver S9 fractions (Sager et al., 2016). This preferential loss of S-bupropion observed in two in vitro studies agrees with clinical results (Masters et al., 2016) identifying S-bupropion as the higher clearance enantiomer. The presently reported relative $CL_{int}$ for R, R- and S, S-hydroxybupropion in HLMs (0.48 versus 0.93 µl/min/mg of microsomal protein, respectively) is in excellent agreement with the difference reported in human liver S9 fraction (0.47 versus 0.81 µl/min/mg of S9 protein, respectively) (Sager et al., 2016). This agreement confirms that hydroxybupropion formation is primarily by microsomal enzymes (Coles & Kharasch, 2008; Connarn et al., 2015; Sager et al., 2016; Skarydova et al., 2014). For both diastereomers, CYP2B6 was shown to be responsible for 90% of their formation, with minor contributions from CYP2C19 and CYP3A4 (Sager et al., 2016). The linear formation rate observed for these two metabolites over the concentration range evaluated is also consistent with the estimated CYP2B6 $K_m$ values being > 100 µM for R- and S-bupropion (Sager et al., 2016). Disparity in $CL_{int}$ of R, R- and S, S-threohydrobupropion formation between HLMs (0.27 and 3.59 µL/min/mg protein, respectively) and the S9 fraction (0.69 and 5.61 µL/min/mg protein,

respectively) (Sager et al., 2016) is attributed to cytoplasmic aldo-keto reductase contribution in the S9 fraction (Connarn et al., 2015; Skarydova et al., 2014). The $CL_{int}$ of S, R and R, S-erythrohydrobupropion (0.11 and 0.29 µl/min/mg of microsomal protein, respectively) observed in our study is in close agreement with reported values (0.11 and 0.25 µl/min/mg of S9 protein, respectively) in liver S9 (Sager et al., 2016). As with hydroxybupropion, this similarity supports that microsomal 11β-HSD1 is primarily responsible for the production of erythrohydrobupropion diastereomers at clinically relevant bupropion concentrations (Masters et al., 2016). It is also consistent with reports of minor contribution by cytosolic aldo-keto reductase in the formation of total erythrohydrobupropion (Connarn et al., 2015; Skarydova et al., 2014). Overall, the finding that racemic bupropion clearance in HLMs is mainly by carbonyl reduction (62% combined for threo- and erythrohydrobupropion isomers, as summarized in **Figure 2.6**) is consistent with published in-vitro and in-vivo results (Benowitz et al., 2013; Connarn et al., 2015; Gufford et al., 2016; Masters et al., 2016; A. Meyer et al., 2013; Sager et al., 2016; Skarydova et al., 2014).

Studies conducted in rats and mice are unclear regarding the contribution of phase 1 metabolites to observed pharmacologic effects (Bruijnzeel & Markou, 2003; Carroll et al., 2014; Damaj et al., 2004; Damaj et al., 2010; Martin et al., 1990; A. Meyer et al., 2013; Schroeder, May 1983; Silverstone et al., 2008; Suckow et al., 1986; Welch et al., 1987). In part, this is due to different metabolic profiles between rats and mice. Our finding of higher hydroxybupropion formation in MLMs relative to RLMs is consistent with higher systemic exposure of this metabolite in-vivo in mice (Carroll et al., 2014; Suckow et al., 1986; Welch et al., 1987). S,S-hydroxybupropion is an active metabolite, possessing potency comparable to bupropion at dopamine active transporter (DAT) and norepinephrine transporter (NET) and nicotinic receptors (Bondarev et al., 2003; Damaj et al., 2004; Damaj et al., 2010). Combined, these PK and pharmacologic data are the basis for speculation for the superior translational efficacy of mice to humans (Damaj et al., 2004; Damaj et al., 2010; Martin et al., 1990; Silverstone et al., 2008; Suckow et al., 1986; Welch et al., 1987). However, our findings summarized in **Figure 2.6** that threohydrobupropion diastereomers account for < 5% of racemic bupropion clearance in the MLMs versus 54% in HLMs, and that threohydrobupropion possesses exposure-related

pharmacologic or toxic activity (Bondarev et al., 2003; Martin et al., 1990; Silverstone et al., 2008), limits the translational value of the mouse from the standpoint of safety.

Based simply on the close genetic homology of NHPs to humans (Dalgaard, 2015), it is reasonable to expect they would be a superior translational model to understand bupropion CNS disposition and ensuing central effects in humans. However, in vitro metabolite kinetics, and in vivo metabolite disposition in NHPs is limited (Banks, Smith, & Blough, 2016; Hansard et al., 2011; Schindler, Gilman, Panlilio, McCann, & Goldberg, 2011; Wang et al., 2011), and reports of stereoselective analysis are absent. We found that the total percentage of hydroxybupropion, threohydrobupropion, erythrohydrobupropion in marmoset monkey liver microsomes (62%, 23%,14%, respectively) is in good agreement with a previously published report (62%, 28%, 10%) in baboon hepatic microsomes (Wang et al., 2011). Of note, the Wang et al study identified the CYP2B subfamily was responsible for hydroxybupropion formation, which is the case in humans, and supports similarity of bupropion metabolism between NHPs and humans. However, the Wang et al study did not delineate the proportions of the diastereomer metabolites, which would be important to determine both systemically and centrally in order to more fully comprehend the complex CNS pharmacology of bupropion. Despite marked differences between bupropion metabolism in rodents and humans, in-vivo studies in rodents have identified an important contribution of phase 1 metabolites to bupropion effects (Bondarev et al., 2003; Damaj et al., 2010; Silverstone et al., 2008; Suckow et al., 1986; Welch et al., 1987). Rodent studies also provide evidence that relative metabolite-to-bupropion exposure in brain is different than plasma (Suckow et al., 1986). Potential causes of the latter could be due to different permeability properties of metabolites relative to bupropion (Cremers et al., 2016) and/or metabolism of bupropion in brain (Miksys, Lerman, Shields, Mash, & Tyndale, 2003). Overall, given the relative similarity of stereoselective bupropion phase 1 metabolism between MMLMs and HLMs we observed, in vivo systemic and brain disposition studies conducted in NHPs would be preferred over rodent studies to support development of translational physiologic-based PK models to improve our understanding of bupropion CNS pharmacology, including its potential to elicit seizures, in the context of its complex metabolic disposition.

A limitation of our analysis is that we did not measure blood-to-plasma concentration ratios of the two enantiomers in the four species, nor did we measure unbound plasma fractions ($f_u$) of these enantiomers across species. These determinations would have enabled a determination of hepatic blood clearances of the two enantiomers in each species, which would have provided a more comprehensive comparison. However, Sager et al (Sager et al., 2016) who did estimate plasma binding and blood-plasma concentration ratios for the two enantiomers, indicated that differences in hepatic extraction alone were sufficient to explain bupropion stereoselective disposition. We invoke this argument on behalf of the other species (Avdeef, 2012). As well, racemic bupropion $f_u$ in rats ranges from 0.31 to 0.49 (Avdeef, 2012) which is close to humans (Avdeef, 2012; Sager et al., 2016) and therefore, considered similar.

Our findings demonstrate that phase 1 metabolism in NHPs best approximates that observed in humans, thereby supporting, based on similarity of stereoselective metabolite formation patterns alone, preferential use of this species to extend our understanding of stereoselective bupropion CNS disposition. For example, awareness of carrier-mediated transport at the BBB and/or metabolism within brain would generate new possibilities for causation of the unpredictable CNS adverse effects observed with this drug.

# CHAPTER 3. MEASUREMENT OF STEREOSELECTIVE BUPROPION DISPOSITION IN RAT BRAIN AND PLASMA

**Hypothesis 2.** Plasma is not a good surrogate for brain exposure. The plasma exposure of bupropion enantiomers and metabolite diastereomers of the surrogate non-clinical species are different than brain.

**Specific aim 2.** Measure exposures of bupropion enantiomers and their corresponding phase 1 metabolite isomers in plasma and brain following administration of racemic and a key pharmacologically active metabolite, S, S-hydroxybupropion, to surrogate non-clinical species. Use stereospecific quantitative analyses to measure bupropion-related substances in rat brain following administration of racemic bupropion.

## 3.1 Introduction

Bupropion, a known antidepressant and smoking cessation aid, demonstrates wide inter-subject variability in its effectiveness (Benowitz et al., 2013; Connarn et al., 2017; Connarn et al., 2016; Golden, De Vane, et al., 1988; Hesse et al., 2004; Laizure et al., 1985; Woodcock et al., 2012; A. Z. X. Zhu et al., 2012; Andy Z. X. Zhu et al., 2014). This is of concern due to its high propensity to induce seizures and other side effects (Beyens et al., 2008; Davidson, 1990; Grandas & López-Manzanares, 2007; Hesse et al., 2004; Johnston JA, 1991 ; Laizure et al., 1985; Woodcock et al., 2012). Variability regarding bupropion metabolism is considered chiefly responsible for variability in its response (Benowitz et al., 2013; Gufford et al., 2016; Hesse et al., 2004; Kharasch et al., 2008; Masters et al., 2016; A. Z. X. Zhu et al., 2012; Andy Z. X. Zhu et al., 2014). To address this issue, there have been extensive efforts to elucidate stereoselective metabolic pathways (Coles & Kharasch, 2008; Gufford et al., 2016; Kharasch et al., 2008; Masters et al., 2016; Sager et al., 2016). It is now known that despite being administered to humans as a racemate, systemic exposures of R-bupropion and its metabolites are greater than the corresponding S form. In vitro and in vivo studies indicate stereoselective phase 1 and 2 metabolism to contribute towards the observed differences in plasma profiles of metabolites (Gufford et al., 2016; Masters et al., 2016; Sager et al., 2016). Several of the isoforms of these

metabolizing enzymes are polymorphic in nature, making them a potential factor contributing to inter-subject variability (Benowitz et al., 2013; Bhasker et al., 2000).

Despite S, S-hydroxybupropion`s low plasma exposure in humans, in vitro studies and studies in mouse models indicate it to contribute more towards efficacy as an antidepressant and smoking cessation aid than racemic bupropion and R, R-hydroxybupropion, respectively (Damaj et al., 2004).

The basis that variability in bupropion metabolism leads to variability in response is further substantiated by significant species differences in bupropion`s effects in models of depression (Butz et al., 1982; Carroll et al., 2014; Suckow et al., 1986). Animal studies suggest that bupropion has greater efficacy in mice versus rats in these models (indicated by anti-tetrabenazine activity) (Suckow et al., 1986). This difference corresponds to higher systemic exposure to hydroxybupropion in mice than rats (Carroll et al., 2014; Suckow et al., 1986). However, stereoselective disposition of bupropion and its metabolites, particularly S, S-hydroxybupropion, in any of the preclinical species has not been determined.

The blood-brain-barrier selectively restricts the blood-to-brain paracellular diffusion of compounds due to its well-developed tight junctions, thus potentially creating a situation where plasma exposure may not be a good indicator of brain exposure (Luissint et al., 2012). This argument is substantiated by early clinical studies where the metabolite to parent ratio (hydroxybupropion/bupropion) in cerebrospinal fluid (CSF) did not mirror that in plasma (Golden, De Vane, et al., 1988). Elucidation of stereoselective disposition of bupropion and its pharmacologically active metabolites in the brain is necessary to better understand the effects of this complex drug. Evidence of carrier mediated transport, which may be stereoselective (Cremers et al., 2016), was presented by a recent study conducted in rats that measured bupropion and S, S-hydroxybupropion clearance across the blood-brain-barrier. Secondly, CYP2B6, a key enzyme involved in bupropion`s oxidative metabolism, is also expressed in brain (Stingl et al., 2013). Contribution of CNS localized CYP2B6 to bupropion`s metabolism in brain has not been investigated. Thus, stereoselective carrier mediated transport across the blood-brain-barrier, and stereoselective metabolism in brain may lead to CNS exposures that are not simply determined by physicochemical properties of bupropion and its metabolites. These PK factors, in addition to

stereoselective pharmacology, may contribute towards the observed interpatient variability in bupropion's effect. However, ethical and safety considerations limit direct assessment of stereoselective disposition in human CSF.

Previously, our lab published the first comprehensive characterization of phase 1 stereoselective metabolism of bupropion in rodents (rats and mice) and non-human primate (NHP) liver microsomes (Bhattacharya et al., 2019) to establish suitability and limitations for subsequent use of non-clinical species to model bupropion CNS disposition in humans.

Our results suggest the relative proportions of stereospecific phase 1 metabolite production in NHPs best approximates those observed in humans. However, the cost and limited PK and PD data in NHPs impedes us from conducting in vivo studies in NHPs. Although the mouse might seem as the second-best species to support physiology basked pharmacokinetic-pharmacodynamic (PBPK/PD) model development, one must exert caution, as mice don`t produce substantial reductive metabolites that can be quantified. This is an important shortcoming, as reductive metabolites are thought to contribute to some of bupropion`s therapeutic efficacy (Ascher et al., 1995; Bondarev et al., 2003; Martin et al., 1990; Schroeder, May 1983). Also, there is substantial PK and PD information from prior studies in rats that would support development of PK and PK/PD models (Cremers et al., 2016; Damaj et al., 2010; William Kielbasa et al., 2009; Yeniceli et al., 2011). However, none of these studies have characterized stereoselective disposition in plasma and brain. Based on the above stated reasons, rats would be our surrogate animal of choice to characterize plasma and brain exposures of bupropion enantiomers and corresponding phase 1 diastereomer metabolites and subsequent development of translational PBPK/PD model.

## 3.2 Material and methods

### 3.2.1 Drugs and chemicals

Racemic bupropion hydrochloride (catalog # B689625; lot # 9-MWC-72-1), R-bupropion (R-Bupropion D-Tartaric Acid Salt, catalog # B689615), S-bupropion (S-Bupropion L-Tartaric Acid Salt, catalog # B689620), R, R-hydroxybupropion (catalog # H830665), S, S-hydroxybupropion (catalog # H830670; lot # 3-WBZ-85-4), racemic threo-dihydro bupropion

(catalog # D448675) racemic erythron-dihydro bupropion (catalog # D448650) were purchased from Toronto Research Chemicals (Toronto, Ontario). Acetaminophen (catalog # A5000; lot # 122K0021), ammonium bicarbonate (catalog # 09830; lot # BCBL6295V), hydrochloric acid, ACS reagent 37% (catalog # 320331; lot # SHBG1273V) were purchased from Sigma Aldrich Chemical Co (St. Louis, MO). Sprague Dawley rat brains (catalog # IRTBR0000; lot # 2699601-15) were purchased from Innovative Research (Novi, MI). Sprague Dawley rat plasma (K3EDTA, pooled, catalog # RAT00PLK3PNN; lot # RAT386832) was purchased from BioIVT (Westbury, NY). Methanol (lot # A465-4), ethyl acetate (lot # E195SK-4), sodium phosphate monobasic (catalog # S381-3; lot # 007029) were purchased from Fisher Scientific (Fairlawn, NJ).

### 3.2.2 Evaluation of plasma and brain binding of bupropion enantiomers and metabolite diastereomers

Unbound plasma and brain fractions of bupropion enantiomers (R and S-bupropion) and metabolite diastereomers (R, R and S, S-hydroxybupropion, threohydrobupropion, erythrohydrobupropion) were determined in a 96-well equilibrium dialysis apparatus (HTD96b, HTDialysis, Gales Ferry CT). Dialysis membrane (molecular weight cut off 12,000-16,000; catalog # S25645, Fisher Scientific) was activated by first soaking in deionized water for 30 minutes at room temperature, then in 25% v/v methanol water for 30 minutes and finally in 0.1 M pH 7.4 sodium phosphate buffer for about 60 minutes until being assembled into dialysis apparatus (Kalvass, Maurer, & Pollack, 2007).

Rat brain tissue was diluted 3-fold with 0.1 M sodium phosphate buffer, pH 7.4 (room temperature, 25 ℃) and homogenized with a sonic probe (TissueRuptor Homogenizer, Qiagen) at room temperature (25 ℃). Unbound fractions were similar from preliminary experiments conducted for R and S-bupropion at 1 µM and 10 µM concentration in rat plasma. This range covers the therapeutic-supratherapeutic range in humans. Due to superior analytical quantification at 10 µM, determination of unbound fractions of bupropion related entities in plasma and brain were conducted at this concentration (10 µM). 10 µM plasma or brain stocks of bupropion related entities were prepared from their respective 0.1 mg/mL methanolic stocks and final volume to 1000 µL was made with rat plasma or brain homogenate and vortexed (Vortex Maxi Mix 1 Model

M16715) for 10-15 seconds. 20 µL was immediately aliquoted into tubes and stored at -80 ºC as zero-time ($T_0$) samples.

The activated dialysis membrane was assembled into the dialysis apparatus as per the manufacturer`s instructions.100 µL of pH 7.4 phosphate buffer was first loaded to one side of dialysis membrane and 100 µL rat plasma or brain homogenate was loaded to other side of dialysis membrane. There were n = 3 wells/per compound/matrix in this experiment.

The apparatus was sealed using an adhesive sealing film (lot # 1102, HTDialysis, Gales Ferry, CT) and then placed in shaking water bath (Dubnoff metabolic shaking incubator, Precision Scientific) at 37 ºC for 5 hours. The remainder of rat plasma or brain was placed on shaking water bath for 5 hours sample ($T_5$). At the end of 5-hr incubation, 20 µL of the contents (rat plasma, brain homogenate and buffer) from the 96 well equilibrium dialysis apparatus, $T_0$ and $T_5$ samples were transferred to 96 well plate and stored immediately at -80 ºC. Fraction unbound determination for bupropion enantiomers (R and S) and hydroxybupropion diastereomers (R, R- and S, S-) in both matrices (plasma and brain) were repeated in triplicate twice.

### 3.2.3 Pharmacokinetic study in Sprague Dawley rats

#### *Animal preparation*

Adult male Sprague-Dawley rats (290–330 g) were used for the experiments. The experiments were approved by Institutional Animal Care and Use Committee (IACUC, Indiana University School of Medicine). After arrival, animals were housed in individually ventilated microisolator shoebox cages (10.25″ W x 18.75″ D x 8″ H) in a temperature-controlled (22 ± 2 ºC) and humidity controlled (30% to 70% relative humidity) environment on a 12:12 hour light: dark cycle (lights on, 7 AM) at Laboratory Animal Resource Center (LARC), IU School of Medicine. Standard diet (Teklad Global 2018SX) and domestic-quality mains water (filtered by reverse osmosis) were available ad libitum. Direct contact bedding was used (Sani-Chip, Envigo). The rats were monitored daily. General appearance, body weight and loss of body condition were used to assess animal health.

***Drug administration and sample collection***

On the day of experiment, 2 mg/mL dosing solution of racemic bupropion hydrochloride and S, S-hydroxybupropion in 0.9% NaCl were prepared. 0.01 N HCl was used to aid solubilization of S, S-hydroxybupropion. Racemic bupropion (10 mg/kg) and S, S-hydroxybupropion (2 mg/kg) were administered subcutaneously to adult male Sprague Dawley rats (n = 24/compound). Blood and brain were collected from rats (n = 3) at eight time points (0-hour, 0.25-hour, 0.5-hour, 1-hour, 2-hour, 3-hour, 4-hour, 6-hour). 0.2 mL blood was collected via 27G butterfly needle inserted into tail vein into disodium EDTA tubes (Greiner Bio-One Vacuette #454222) and centrifuged (Sorvall Legend RT) at 3000 rpm for 10 minutes to generate plasma. Brain were harvested post euthanasia via $CO_2$. The samples were stored at -80 ºC until bioanalysis by LC-MS/MS.

***Sample analysis***

*Standard curve and quality control samples*

Standard stock solutions (1 mg/mL each) of racemic bupropion, R, R-hydroxybupropion, S, S-hydroxybupropion, racemic erythro-dihydrobupropion, racemic threo-dihydrobupropion, and acetaminophen (internal standard), were prepared separately in polypropylene tubes by adding methanol. Assumption was racemic mixtures are 50:50 racemate. Therefore, the adjusted concentration of the stock solutions was 0.5 mg/mL each for R-bupropion, S-bupropion, S, R-erythrohydrobupropion, R, S-erythrohydrobupropion, R, R-erythrohydrobupropion, and S, S-threohydrobupropion. Separate stock solutions of the analytes were created for quality control (QC) samples. All solutions were stored at −20˚C. Working standard solutions were prepped from the standard stock solutions daily by performing 1:10 serial dilutions in methanol into 12 × 75 polypropylene tubes. An aliquot from the working solutions was added to human plasma (total volume of 200 µL) and 20 µL was transferred to clean 12 × 75 polypropylene tubes. The standard curves for R, R-hydroxybupropion and S, S-hydroxybupropion had the following concentrations: 0.3, 1, 3, 10, 30, 100, 300, 1000, and 3000 ng/mL. The standard curves for R-bupropion, S-bupropion, S, R-erythrohydrobupropion, R, S-erythrohydrobupropion, R, R-

erythrohydrobupropion, and S, S-threohydrobupropion had the following concentrations: 0.15, 0.5, 1.5, 5, 15, 50, 150, 500, and 1500 ng/mL. Quality control (QC) samples were prepared in duplicate. The QC samples had the following concentrations for R, R-hydroxybupropion and S, S-hydroxybupropion: 1 ng/mL (low QC), 30 ng/mL (medium QC), and 2000 ng/mL (high QC). The QC samples had the following concentrations for R-bupropion, S-bupropion, S, R-erythrohydrobupropion, R, S-erythrohydrobupropion, R, R-erythrohydrobupropion, and S, S-threohydrobupropion: 0.5 ng/mL (low QC), 15 ng/mL (medium QC), and 1000 ng/mL (high QC).

*Sample preparation*

Frozen rat plasma or brain homogenate samples (stored in a −80 ˚C freezer) were thawed to ambient temperature and 20 µL were transferred to 12 × 75 polypropylene tubes. Then, 20 µL of 0.1 ng/ µL of acetaminophen (internal standard) and 1 mL of ethyl acetate were added to the tube, and the sample was vortex mixed for 20 seconds. After centrifugation at 4000 rpm at ambient temperature for three minutes, the organic phase was transferred to a clean 12 × 75 polypropylene tube and evaporated to dryness. The samples were reconstituted with 50 µL of methanol then vortex mixed for 20 seconds. A 10 µL aliquot of each sample was injected into the HPLC.

*Conditions for HPLC–MS/MS*

Chromatographic separation was achieved using an Agilent1290 series HPLC coupled with a PAL HTC-XT Leap autosampler using reverse phase chromatography, at 40°C, with a Phenomenex Lux 3 µm AMP 150X4.6 mm column. Mobile phase (methanol: 5mM ammonium bicarbonate, pH= 10.0; 80:20; v/v) was delivered isocratically at a constant flow rate of 400µL/min. The column effluent was monitored using a Sciex 5500 QTRAP triple-quadrupole mass spectrometer (Foster City, CA) equipped with an electrospray ionization probe in positive mode. The mass spectrometer was controlled by Analyst software (version 1.6.2) in conjunction with Windows 7®. A flow injection analysis was performed on each analyte to maximize sensitivity. The responses of the analytes were optimized at a source temperature of 650°C, under unit resolution for quadrupole 1 and 3. In addition, the analytes were given a dwell time of 200 ms and a settling time of 10 ms. The ion spray voltage was 5500 V and the interface heater was on. Optimal

gas pressures (psi) for all of the analytes were as follows: collision gas medium, curtain gas 10, ion source gas (1) 25, ion source gas (2) 25. Multiple reaction monitoring was used to measure Q1/Q3transitions for: R-bupropion and S-bupropion at 240.1/184.0; R, R-hydroxybupropion and S, S-hydroxybupropion at 255.9/139.0; S, R-erythrohydrobupropion, R, S-erythrohydrobupropion, R, R-threohydrobupropion, and S, S-threohydrobupropion at 241.9/116.0; and acetaminophen at 152.0/109.9. Mass spectrometry settings for the voltages are listed in **Table 3.1**.

### 3.2.4 Data analysis

Fraction unbound in plasma and brain was calculated using the below equations. Percent recovery was calculated from the sum of the concentration in the buffer side (free) plus the plasma or brain side (bound) relative to the $T_5$ sample (Zamek-Gliszczynski et al., 2011). Percent stability was calculated from the concentration in the spiked matrix incubated ($T_5$) at 37 °C relative to the $T_0$ sample.

$$f_{u,plasma} = \frac{\text{concentration in buffer}}{\text{concentration in plasma}} \quad \text{Equation 3.1}$$

$$f_{u,brain} = \frac{1/D}{[1/f_{u,measured}]-1]+1/D} \quad \text{Equation 3.2}$$

Unbound brain volume of distribution ($V_{u,\ brain}$) was calculated using the below equation (Fridén, Gupta, Antonsson, Bredberg, & Hammarlund-Udenaes, 2007). D in the equation is dilution and $f_{u,measured}$ was calculated from the ratio of the concentration in buffer relative to the brain homogenate.

$$V_{u,brain} = 1 + D\left(\frac{1}{f_{u,measured}} - 1\right) \quad \text{Equation 3.3}$$

Intracellular to extracellular unbound brain drug concentration ratio ($K_{p,uu,cell}$) was calculated using the below equation. $V_{ISF}$, $V_{cyto}$, $V_{lyso}$ are volumes of brain interstitial fluid (0.2 mL, pH 7.3), cytosol (0.8 mL, pH 7) and lysosomes (0.01 mL, pH 5) (Fridén et al., 2011; Fridén et al., 2007). pKa (base) of bupropion, hydroxybupropion, threohydrobupropion and erythrohydrobupropion were 8.6, 7.6, 7.4, 9.6 respectively (Fridén et al., 2011; Xue, Zhang, & Cai, 2018).

$$K_{p,uu,cell} = V_{ISF} + K_{p,uu,cyto} \cdot (V_{cyto} + V_{lyso} * K_{p,uu,lyso}) \quad \text{.....Equation 3.4}$$

$$K_{p,uu,lyso,base} = \frac{10^{pKa-pH_{lyso}}+1}{10^{pKa-pH_{cyto}}+1} \quad \text{.....Equation 3.5}$$

$$K_{p,uu,cyto,base} = \frac{10^{pKa-pH_{cyto}}+1}{10^{pKa-pH_{ISF}}+1} \quad \text{.....Equation 3.6}$$

Unbound brain to unbound plasma ratio ($K_{p,uu}$) was calculated using below equation, where AUC is area under curve, $CL_{in}$ is brain influx clearance, $CL_{out}$ is brain efflux clearance, $CL_{passive}$ is passive permeability clearance, $CL_{active\ uptake}$ is clearance due to active uptake, $CL_{active\ efflux}$ is clearance due to active efflux, $CL_{metabolism}$ is clearance due to within brain metabolism and $CL_{bulk\ flow}$ is clearance due to bulk flow (Hammarlund-Udenaes, Fridén, Syvänen, & Gupta, 2008; Andreas Reichel, 2015).

$$K_{p,uu} = \frac{AUC_{0-6hr,brain}}{AUC_{0-6hr,plasma}} \quad \text{.....Equation 3.7}$$

$$K_{p,uu} = \frac{CL_{in}}{CL_{out}} \quad \text{.....Equation 3.8}$$

$$K_{p,uu} = \frac{CL_{passive} + CL_{active\ uptake} - CL_{active\ efflux}}{Cl_{passive} + CL_{active\ efflux} - CL_{active\ uptake} + CL_{metabolism} + CL_{bulk\ flow}} \quad \text{.....Equation 3.9}$$

All statistical analysis was conducted using JMP®, version 13.2.0 (SAS Institute Inc., Cary, NC, USA). Comparison of fraction unbound values between enantiomeric or diastereomeric pairs and between enantiomers and diastereomers for a given matrix (plasma or brain) was done using ANOVA followed by Tukey's Honest Significant Difference test with a priori alpha set to 0.05. Comparison between $f_{u,plasma}$ and $f_{u,brain}$ values for enantiomers or diastereomers using paired two tailed test with alpha of 0.05.

All pharmacokinetic analysis was conducted using Phoenix Winonlin 8.2 (Pharsight Corporation, Certara, L.P., Princeton, NJ). Non-compartmental analysis (NCA) was conducted on mean total and unbound plasma and brain concentration (unbound concentration obtained by multiplying fraction unbound with total concentrations for each matrix/compound). The terminal elimination-rate constant (k) was estimated by linear regression of the terminal portion of the log-transformed concentration-time profile using at least three data points. The area under the curve from time zero to the last time point (6 hours) was determined using the trapezoidal rule with linear-up/log-down interpolation. Statistical data comparisons of exposures between enantiomeric or diastereomeric pairs for a given matrix (plasma or brain), or comparison between plasma and brain exposure values for a given enantiomer or diastereomer, or metabolite to parent ratios were evaluated using a paired two-tailed t test or Wilcoxon signed-rank test after testing for normality of residuals using Shapiro Wilks test. A p value of 0.05 was considered statistically significant.

### 3.3 Results

Chromatographic separation of bupropion enantiomers and metabolite diastereomers was successfully achieved with the Phenomenex Lux 3 µm AMP (150 × 4.6 mm) chiral column.

**Table 3.1.** MS/MS settings (ABSciex 5500) for R-bupropion, S-bupropion, R, R-hydroxybupropion, S, S-hydroxybupropion, erythrohydrobupropion (S, R and R, S-), threohydrobupropion (R, R- and S, S-), and acetaminophen

| Compound | Q1 (m/z) | Q3 (m/z) | Mode | Time (msec) | DP (V) | EP (V) | CE (V) | Exit Potential (V) |
|---|---|---|---|---|---|---|---|---|
| R-BUP | 240.18 | 184.20 | + | 200 | 50 | 8 | 25 | 16 |
| S-BUP | 240.18 | 184.20 | + | 200 | 50 | 8 | 25 | 16 |
| RR-OHBUP | 256.16 | 139.10 | + | 200 | 50 | 4 | 35 | 8 |
| SS-OHBUP | 256.16 | 139.10 | + | 200 | 50 | 4 | 35 | 8 |
| THRHBUP | 242.03 | 116.10 | + | 200 | 60 | 8 | 45 | 6 |
| ERYHBUP | 242.03 | 116.10 | + | 200 | 60 | 8 | 45 | 6 |
| APAP | 152.32 | 110.10 | + | 200 | 40 | 14 | 25 | 6 |

BUP: Bupropion; OHBUP: Hydroxybupropion; THRHBUP: Threohydrobupropion; ERYHBUP: Erythrohydrobupropion; APA: Acetaminophen. +: Positive; DP: Declustering Potential; EP: Entrance Potential; CE: Collision Energy.

**Figures 3.1 to 3.4**, show chromatograms of bupropion related entities in rat plasma and brain. LC-MS/MS (ABSciex 5500) settings are summarized in **Table 3.1**. The calibration curves generated were linear for all analytes, and $r^2$ values were generally $\geq 0.99$. Assay accuracy and precision were $\geq 80\%$ for all QC samples.

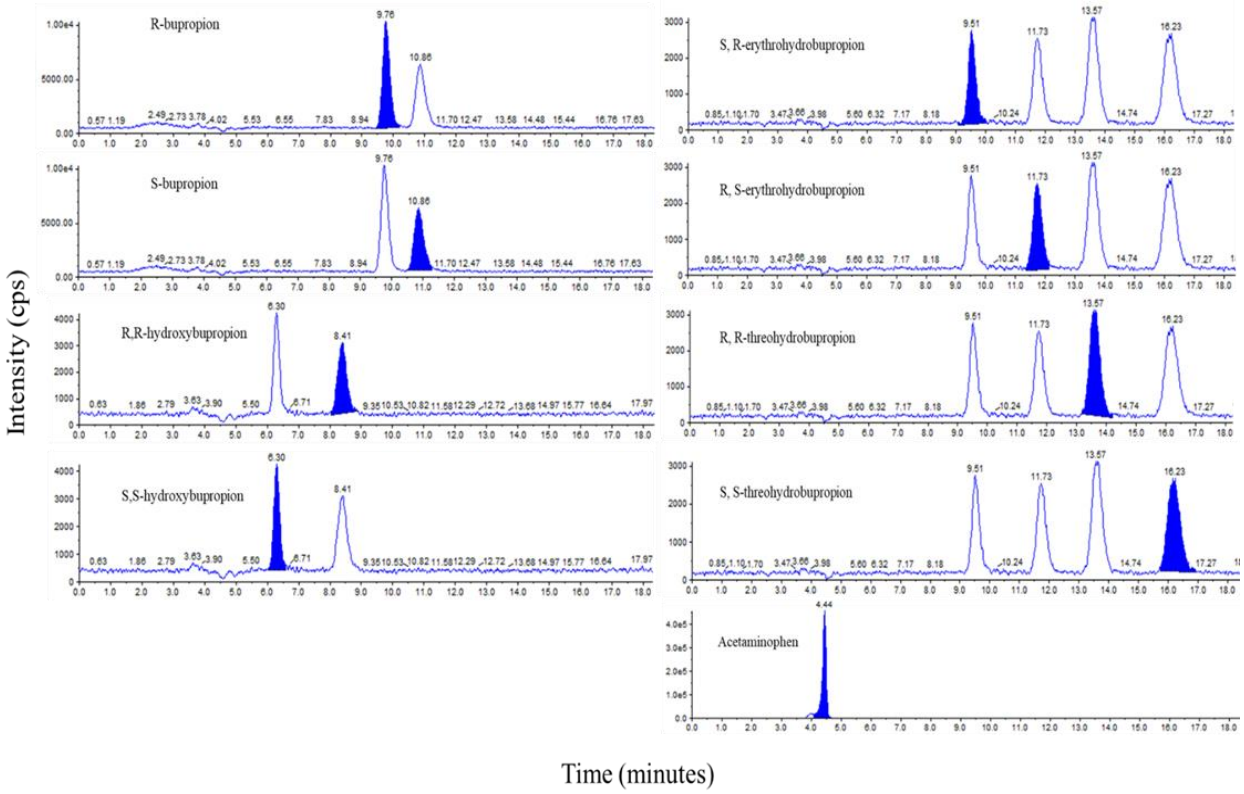


**Figure 3.1.** Chromatograms of bupropion and metabolites at the lowest limit of quantification in rat plasma. 3 ng/mL for bupropion (R and S), hydroxybupropion (R, R and S, S) and 1.5 ng/mL for erythrohydrobupropion (S, R and R, S) and threohydrobupropion (R, R and S, S). The filled peak is the analyte of interest.

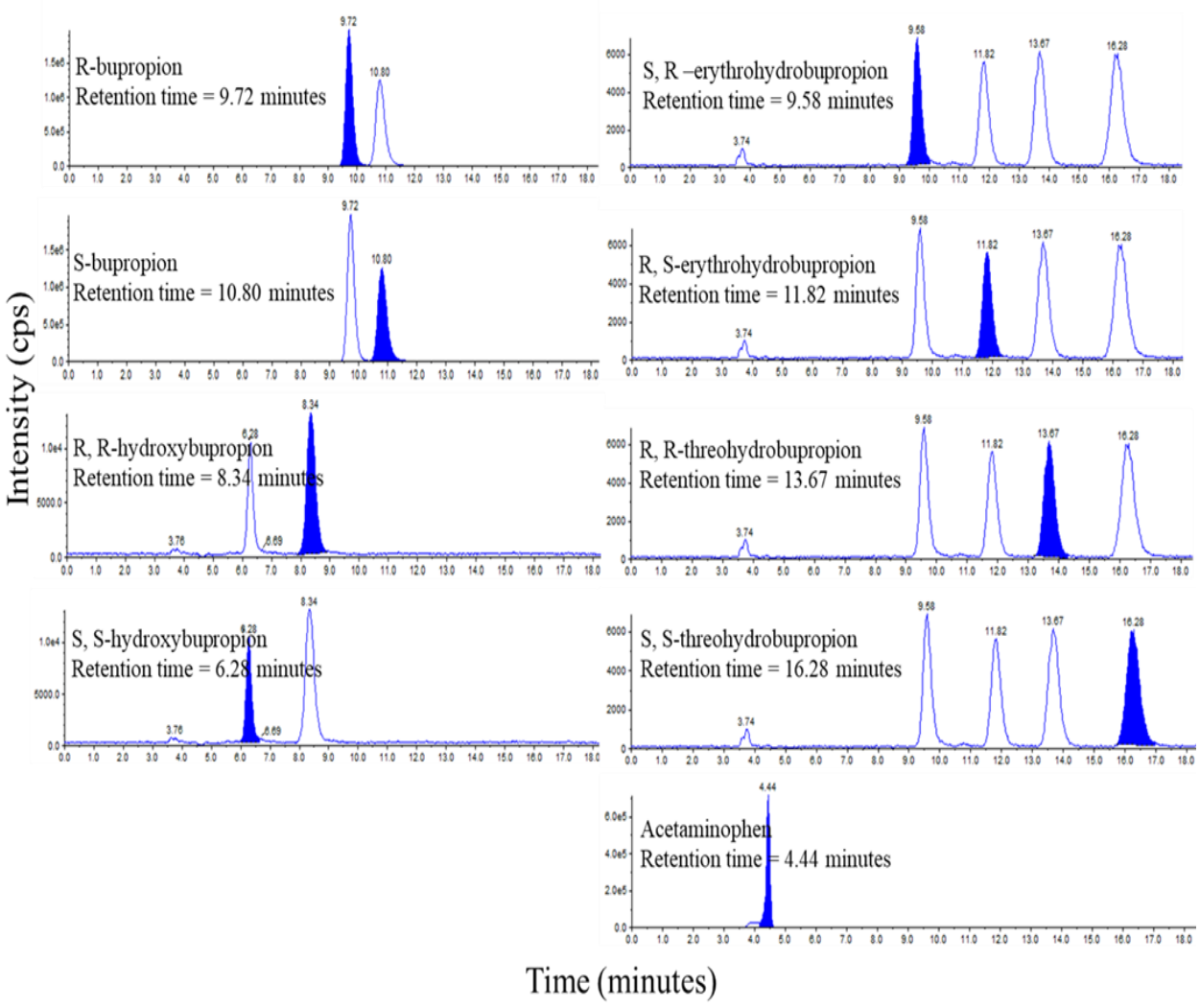


**Figure 3.2.** Chromatogram of bupropion and metabolites in rat plasma after single 10 mg/kg dose of racemic bupropion. The filled peak is the analyte of interest.

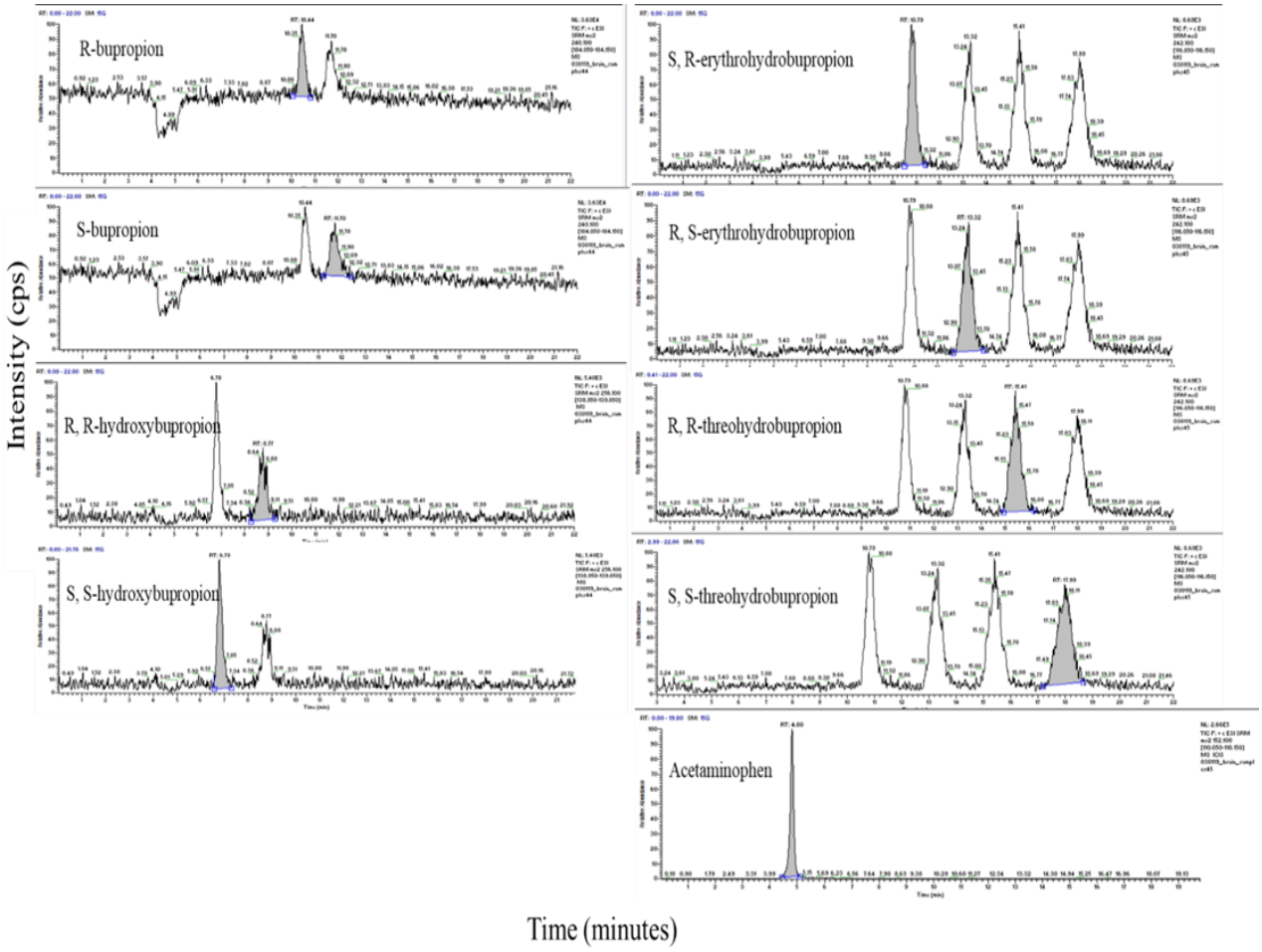


**Figure 3.3.** Chromatograms of bupropion and metabolites at the lowest limit of quantification in rat brain. 0.15 ng/sample for bupropion (R and S), hydroxybupropion (R, R and S, S) and 0.23 ng/sample for erythrohydrobupropion (S, R and R, S) and threohydrobupropion (R, R and S, S). The filled peak is the analyte of interest. The filled peak is the analyte of interest.

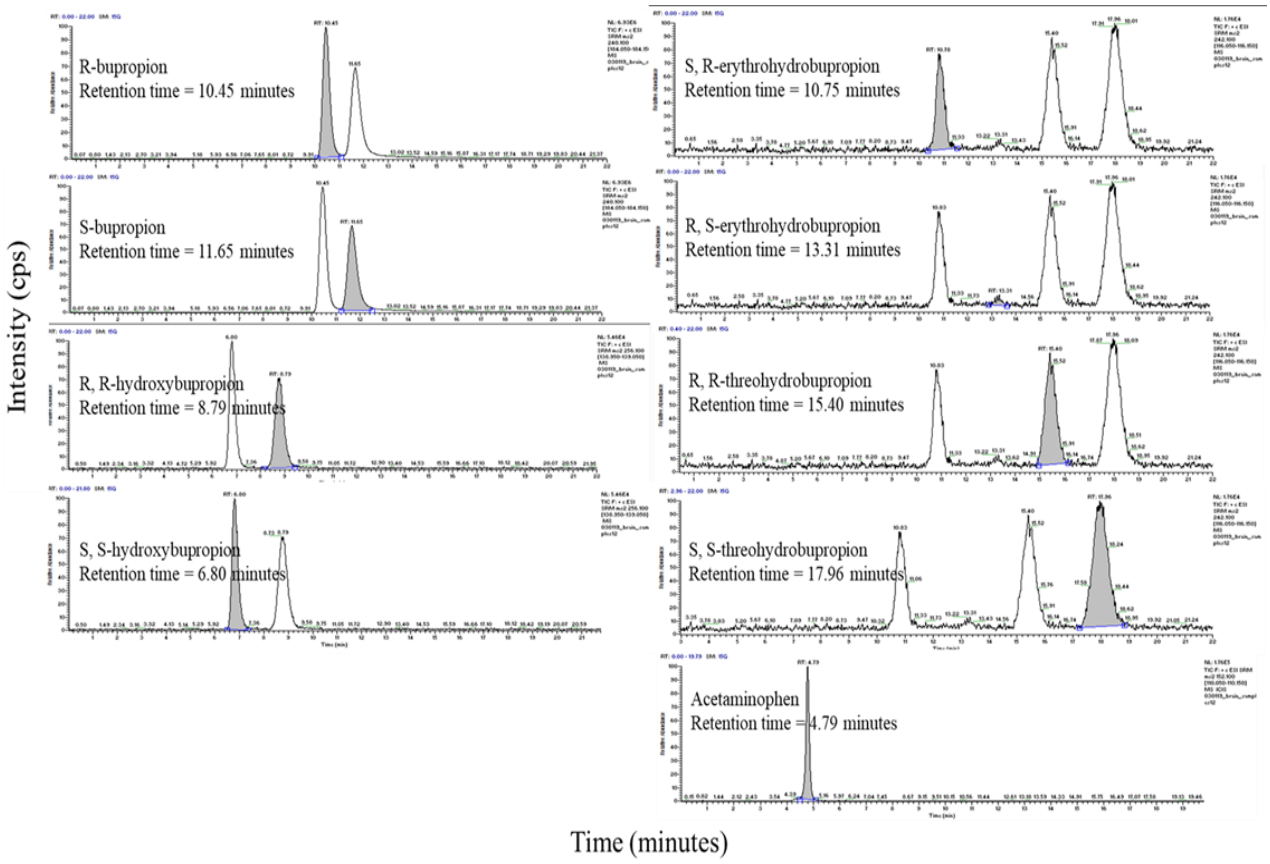


**Figure 3.4.** Chromatogram of bupropion and metabolites in rat brain after single 10 mg/kg dose of racemic bupropion. The filled peak is the analyte of interest.

### 3.3.1 Plasma and brain binding assessment

Results from rat plasma and brain binding assays are displayed in **Table 3.2**. The $f_{u,plasma}$ values for bupropion enantiomers or reductive diastereomers were not different ($p>0.05$). However, $f_{u,plasma}$ R, R-hydroxybupropion was found to be ~2 fold lower than S, S-hydroxybupropion ($p<0.001$). For a given enantiomer or diastereomer, $f_{u,plasma}$ was 3-7 fold higher than $f_{u,brain}$ ($p<0.0001$). A low $f_{u,brain}$ and high $V_{u,brain}$ (> 0.8 ) of all the entities, indicates high affinity for brain tissue/non-specific binding. The physicochemical parameter $K_{p,uu,cell}$ value > 2 for all entities suggests intracellular accumulation (Fridén et al., 2007; Hammarlund-Udenaes et al., 2008). Both bupropion enantiomers were unstable in plasma and brain, see **Table 3.2**. However, bupropion

enantiomers were 3 to 5-fold more stable in brain than plasma. Greater than 200 % recovery of bupropion enantiomers was observed at the end of the five-hour plasma binding incubation.

**Table 3.2.** Parameters derived from rat plasma and brain homogenate binding.

| Compound | $f_{u,plasma}$ | Plasma recovery % | Plasma stability % | $f_{u,brain}$ | Brain recovery % | Brain stability % | $V_{u,brain}$ | $K_{p,uu,cell}$ |
|---|---|---|---|---|---|---|---|---|
| R-BUP* | 0.51 ± 0.06 | 591 | 9.12 | 0.14 ± 0.04 | 133 | 26 | 7.61 | 2.68 |
| S-BUP* | 0.59± 0.08 | 457 | 9.44 | 0.12 ± 0.01 | 87 | 45.1 | 5.25 | 2.68 |
| RR-OHBUP* | 0.40 ± 0.07 | 105 | 116.5 | 0.20 ± 0.04 | 98.5 | 102 | 6.12 | 2.27 |
| SS-OHBUP* | 0.70 ± 0.16 | 139 | 96.4 | 0.16 ± 0.06 | 102 | 197 | 8.36 | 2.27 |
| RR-THRHBUP | 0.63± 0.02 | 117 | 84.2 | 0.19± 0.02 | 96.6 | 117 | 5.35 | 2.05 |
| SS-THRHBUP | 0.73 ± 0.03 | 121 | 79.7 | 0.20 ± 0.03 | 98.4 | 114 | 4.97 | 2.05 |
| SR-ERYHBUP | 0.79 ± 0.02 | 119 | 103 | 0.15 ± 0.01 | 89.1 | 119 | 6.41 | 2.88 |
| RS-ERYBBUP | 0.78± 0.04 | 118 | 101 | 0.154± 0.01 | 88.8 | 118 | 6.53 | 2.88 |

* represents mean of 3 replicate studies, each conducted in triplicate ± SD
$f_u$ fraction unbound; $V_u$ unbound apparent brain volume of distribution; $K_{p,uu,cell}$ intracellular to extracellular unbound drug concentration ratio. BUP: Bupropion; OHBUP: Hydroxybupropion; THRHBUP: Threohydrobupropion; ERYHBUP: Erythrohydrobupropion.

### 3.3.2 Model-independent pharmacokinetic analyses

Results from non-compartmental analysis of total and unbound concentrations of bupropion enantiomers and their phase 1 metabolites in rat plasma and brain are shown in **Tables 3.3** and **3.4**.

**Table 3.3.** Total pharmacokinetic parameters in rat plasma and brain derived from non-compartmental analysis.

| Analyte | k | $t_{1/2}$ | $t_{max}$ | $C_{max}$ | $AUC_{0\text{-}6hr}$ | $AUC_{0\text{-}\infty}$ | %AUC $extrapolated_{observed}$ | CL/F | Vz/F |
|---|---|---|---|---|---|---|---|---|---|
| units | ($hr^{-1}$) | h | h | nM | nM*h | nM*h | % | L/h | L |
| **Rat plasma pharmacokinetic parameters (total)** | | | | | | | | | |
| R-BUP | 0.4 | 1.8 | 1 | 1235 | 4676 | 5328 | 12.2 | 1.1 | 1.7 |
| S-BUP | 0.4 | 1.6 | 1 | 1050 | 3800 | 4245 | 10.5 | 1.4 | 2.0 |
| *Total BUP* | | | | *2286* | *8476* | *9573* | | *2.6* | |
| BUP R-/S- Ratio | | | | 1.17 | 1.23 | 1.25 | | | |
| RR-OHBUP | 0.3 | 2.4 | 2 | 25.7 | 72.0 | 125 | 42.1 | | |
| SS-OHBUP | 0.3 | 2.5 | 2 | 9.6 | 37.5 | 49 | 23.4 | | |
| *Total OHBUP Formed* | | | | *35.4* | *110* | *174* | | | |
| OHBUP RR-/SS- Ratio | | | | 2.67 | 1.94 | 2.55 | | | |
| *Preformed SS-OHBUP* | *0.6* | *1.1* | *1* | *119* | *389* | *404* | *3.8* | *5.8* | *9.8* |
| RR-THRHBUP | 0.1 | 4.8 | 3 | 7.8 | 24.9 | 70.5 | 64.7 | | |
| SS-THRHBUP | 0.1 | 3.9 | 3 | 8.2 | 25 | 63.7 | 60.7 | | |
| *Total THRHBUP* | | | | *16.0* | *49.9* | *134* | | | |
| THRHBUP RR-/SS- Ratio | | | | 0.95 | 1 | 1.10 | | | |
| SR-ERYHBUP | 0.03 | 21.9 | 1 | 7.5 | 20.7 | 245 | 91.6 | | |
| R,S-ERYHBUP | 0.2 | 4.3 | 0.2 | 7.4 | 6.2 | 47.6 | 87.0 | | |
| *Total ERYHBUP* | | | | *15* | *26.9* | *293* | | | |
| ERYHBUP SR-/RS- Ratio | | | | 1.01 | 3.33 | 5.14 | | | |
| **Rat brain pharmacokinetic parameters (total)** | | | | | | | | | |
| R-BUP | 0.5 | 1.3 | 0.5 | 3780 | 6993 | 7354 | 4.9 | | |
| S-BUP | 0.5 | 1.3 | 0.5 | 4013 | 7119 | 7434 | 4.2 | | |
| *Total BUP* | | | | *7793* | *14112* | *14787* | | | |
| BUP R-/S- Ratio | | | | 0.94 | 0.98 | 0.98 | | | |
| RR-OHBUP | 0.3 | 2 | 1 | 59.1 | 216 | 252 | 14.6 | | |
| SS-OHBUP | 0.3 | 1.9 | 0.5 | 55.6 | 177 | 203 | 12.7 | | |
| *Total OHBUP* | | | | *115* | *392* | *455* | | | |
| OHBUP RR-/SS- Ratio | | | | 1.06 | 1.22 | 1.24 | | | |
| *Preformed SS-OHBUP* | *0.9* | *0.7* | *0.5* | *4187* | *9917* | *9976* | *0.5* | | |
| RR-THRHBUP | 0.3 | 2.6 | 2 | 21.2 | 79.1 | 102 | 22.6 | | |
| SS-THRHBUP | 0.3 | 2.4 | 2 | 26.6 | 105 | 135 | 22 | | |
| *Total THRHBUP* | | | | *47.8* | *185* | *237* | | | |
| THRHBUP RR-/SS- Ratio | | | | 0.79 | 0.75 | 0.75 | | | |
| SR-ERYHBUP | 0.3 | 2.7 | 2 | 14.4 | 56.4 | 74.6 | 24.4 | | |

BUP: Bupropion; OHBUP: Hydroxybupropion; THRHBUP: Threohydrobupropion; ERYHBUP: Erythrohydrobupropion; k: elimination rate constant; $t_{1/2}$-Half-life = 0.693/k; $t_{max}$, time to reach maximum concentration; $C_{max}$: maximum concentration; AUC: Area under curve; CL/F: apparent oral clearance calculated from Dose/AUC; Vz/F: apparent volume of distribution.

**Table 3.4.** Unbound pharmacokinetic parameters in rat plasma and brain derived from non-compartmental analysis.

| Analyte | k | $t_{1/2}$ | $t_{max}$ | $C_{max}$ | $AUC_{0-6hr}$ | $AUC_{0-\infty}$ | % AUC $extrapolated_{observed}$ | CL/F | Vz/F |
|---|---|---|---|---|---|---|---|---|---|
| units | ($hr^{-1}$) | h | h | nM | nM*h | nM*h | % | L/h | L |
| **Rat plasma pharmacokinetic parameters (unbound)** | | | | | | | | | |
| R-BUP | 0.4 | 1.8 | 1 | 642 | 2432 | 2771 | 12.2 | 2.3 | 32.5 |
| S-BUP | 0.4 | 1.6 | 1 | 620 | 2242 | 2505 | 10.5 | 2.5 | 30.7 |
| Total BUP | | | | *1262* | *4674* | *5275* | | *4.8* | |
| BUP R-/S- Ratio | | | | *1.04* | *1.08* | *1.11* | | | |
| RR-OHBUP | 0.3 | 2.6 | 2 | 10.3 | 38.3 | 51.6 | 25.8 | | |
| SS-OHBUP | 0.3 | 2.5 | 2 | 6.8 | 26.3 | 34.3 | 23.4 | | |
| Total OHBUP Formed | | | | *17* | *64.6* | *85.9* | | | |
| OHBUP RR-/SS- Ratio | | | | 1.53 | 1.46 | 1.50 | | | |
| Preformed SS-OHBUP | *0.6* | *1.2* | *1* | *83.4* | *272* | *283* | *3.7* | *8.2* | *14.1* |
| RR-THRHBUP | 0.1 | 4.8 | 3 | 4.9 | 15.7 | 44.5 | 64.7 | | |
| SS-THRHBUP | 0.2 | 3.9 | 3 | 6.1 | 17.3 | 45.4 | 62 | | |
| Total THRHBUP | | | | *11* | *33* | *89.9* | | | |
| THRHBUP RR-/SS- Ratio | | | | 0.81 | 0.91 | 0.98 | | | |
| SR-ERYHBUP | 0.03 | 21.9 | 1 | 5.9 | 16.3 | 193 | 91.5 | | |
| RS-ERYHBUP | 0.16 | 4.3 | 0.25 | 5.8 | 4.8 | 37.4 | 87.1 | | |
| Total ERYHBUP | | | | *11.8* | *21.2* | *230* | | | |
| ERYHBUP SR-/RS- Ratio | | | | 1.02 | 3.38 | 5.16 | | | |
| **Rat brain pharmacokinetic parameters (unbound)** | | | | | | | | | |
| R-BUP | 0.5 | 1.3 | 1 | 567 | 1049 | 1103 | 4.9 | | |
| S-BUP | 0.5 | 1.3 | 1 | 482 | 854 | 892 | 4.2 | | |
| Total BUP | | | | *1049* | *1903* | *1995* | | | |
| BUP R-/S- Ratio | | | 1 | 1.17 | 1.22 | 1.23 | | | |
| RR-OHBUP | 0.3 | 2 | 1 | 11.8 | 43.1 | 50.5 | 14.5 | | |
| SS-OHBUP | 0.3 | 1.9 | 1 | 8.9 | 28.3 | 32.4 | 12.7 | | |
| Total OHBUP | | | | *20.7* | *71.4* | *82.9* | | | |
| OHBUP RR-/SS- Ratio | | | | 1.33 | 1.52 | 1.56 | | | |
| Preformed SS-OHBUP | *0.9* | *0.8* | *1* | *586* | *1388* | *1397* | *0.5* | | |
| RR-THRHBUP | 0.3 | 2.6 | 2 | 4 | 15 | 19.4 | 22.7 | | |
| SS-THRHBUP | 0.3 | 2.4 | 2 | 5.6 | 22.2 | 28.4 | 22.0 | | |
| Total THRHBUP | | | | *9.6* | *37.2* | *47.8* | | | |
| THRHBUP RR-/SS- Ratio | | | | 0.71 | 0.67 | 0.68 | | | |
| SR-ERYHBUP | 0.3 | 2.7 | 2 | 2.3 | 9 | 11.9 | 24.4 | | |

BUP: Bupropion; OHBUP: Hydroxybupropion; THRHBUP: Threohydrobupropion; ERYHBUP: Erythrohydrobupropion; k: elimination rate constant; $t_{1/2}$-Half-life = 0.693/k; $t_{max}$: time to reach maxi maximum concentration; $C_{max}$: maximum concentration; AUC: Area under curve; CL/F: apparent oral clearance calculated from Dose/AUC; Vz/F: apparent volume of distribution.

***Concentration time courses of bupropion enantiomers and metabolite diastereomers in plasma and brain***

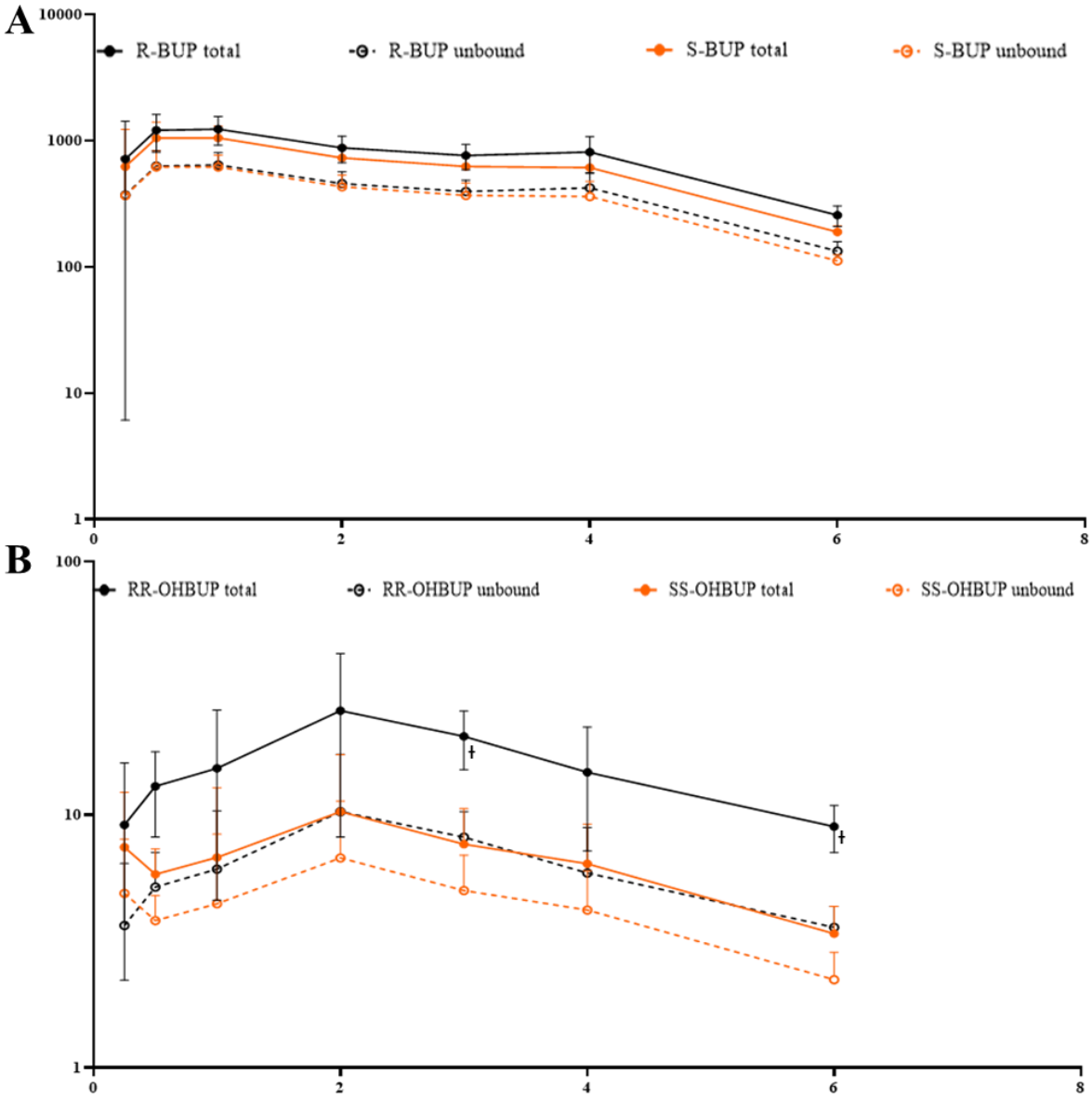


**Figure 3.5.** Mean unbound and total plasma concentration time profiles of **A)** R vs S bupropion **B)** R, R- vs S, S-hydroxybupropion **C)** R, R-threohydrobupropion vs S, S-threohydrobupropion **D)** S, R-erythrohydrobupropion vs R, S-erythrohydrobupropion, following 10 mg/kg, subcutaneous administration of racemic bupropion to adult male Sprague Dawley rats. Symbols and error bars denote observed means and standard deviation (n = 3 at each time point), respectively. BUP: bupropion; OHBUP: hydroxybupropion; THRHBUP: threohydrobupropion; ERYHBUP: erythrohydrobupropion. ǂ indicates timepoints at which the concentrations between two enantiomers or diastereomers were statistically different ($p<0.05$).

Figure 3.5 continued

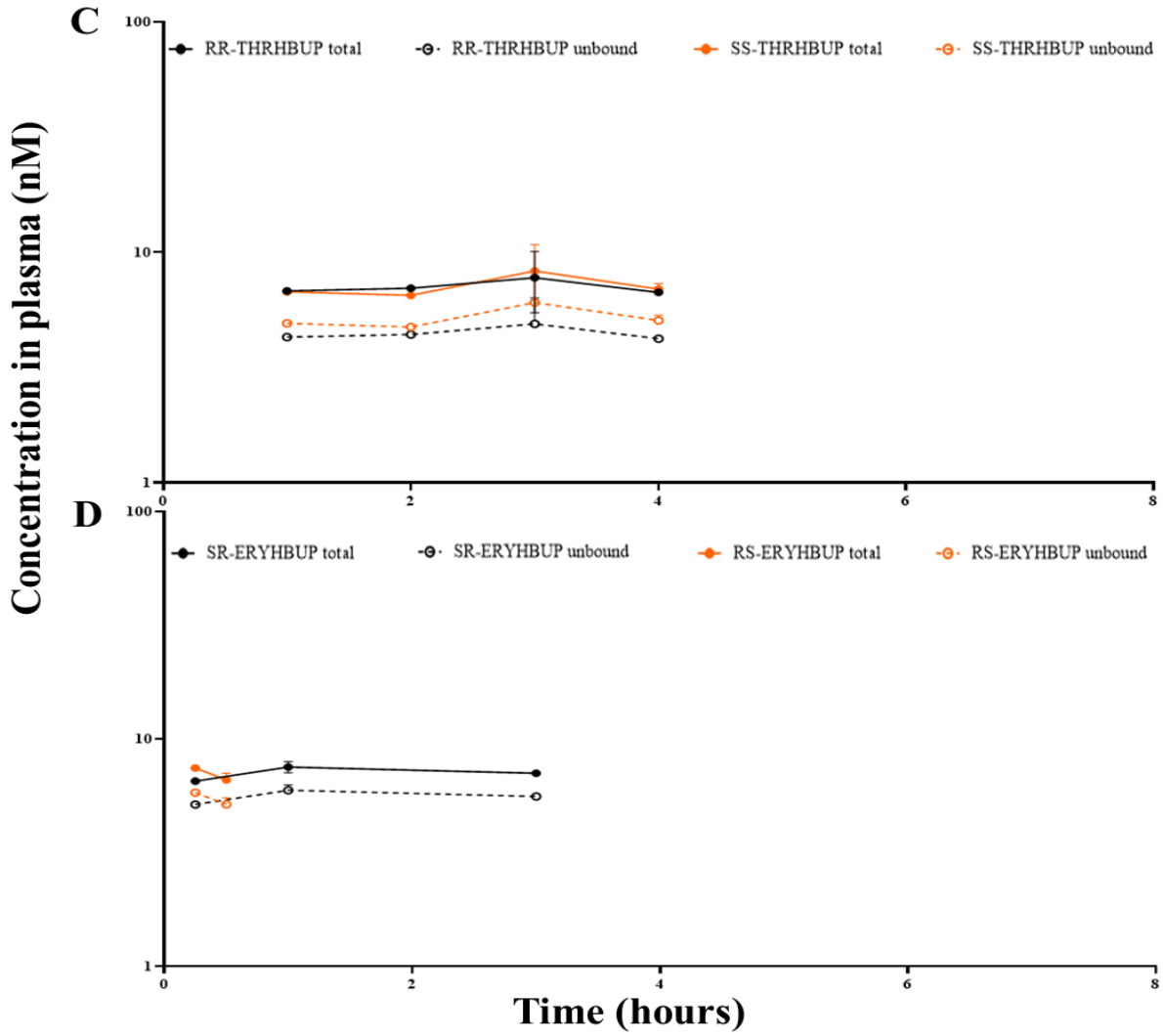

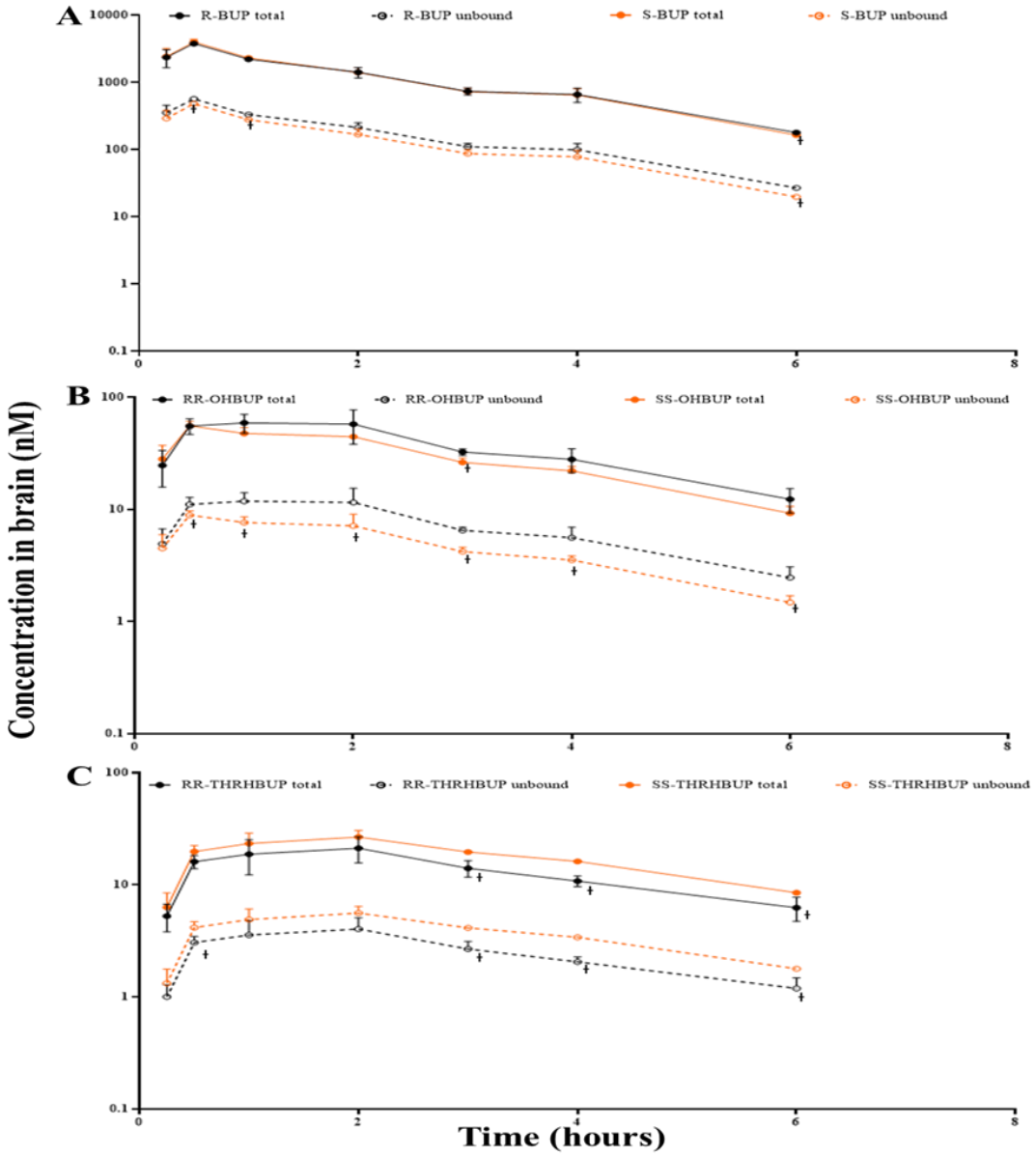


**Figure 3.6.** Mean unbound and total brain concentration time profiles of **A)** R vs S bupropion **B)** R, R- vs S, S-hydroxybupropion **C)** R, R-threohydrobupropion vs S, S-threohydrobupropion **D)** S, R-erythrohydrobupropion vs R, S-erythrohydrobupropion, following 10 mg/kg, subcutaneous administration of racemic bupropion to adult male Sprague Dawley rats. Symbols and error bars denote observed means and standard deviation (n = 3 at each time point), respectively. BUP: bupropion; OHBUP: hydroxybupropion; THRHBUP: threohydrobupropion; ERYHBUP: erythrohydrobupropion. ɨ indicates timepoints at which the concentrations between two enantiomers or diastereomers were statistically different ($p < 0.05$).

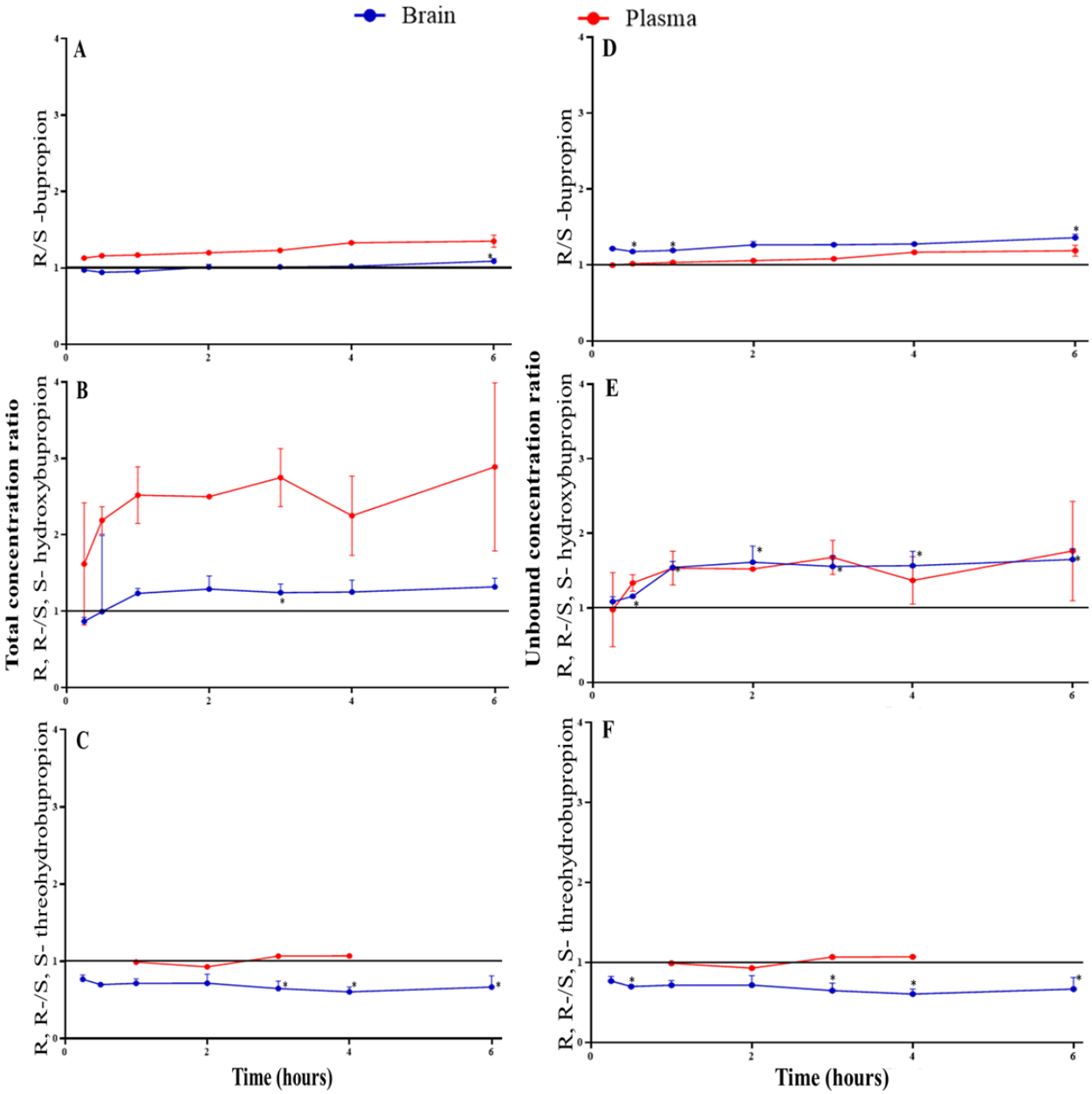


**Figure 3.7.** Mean ratios of R/S-bupropion; R, R/S, S- hydroxybupropion and R, R/ S, S-threohydrobupropion in plasma (red) and brain (blue) over time following 10 mg/kg, subcutaneous administration of racemic bupropion to adult male Sprague Dawley rats. **Left panel** (**A** to **C**) represents ratios of total concentration in plasma and brain. **Right panel** (**D** to **F**) represents ratios of unbound concentration in plasma and brain. Symbols and error bars denote observed means and standard deviation (n=3 at each time point), respectively. * indicates timepoints at which the concentrations between two enantiomers or diastereomers (plasma or brain) were statistically different.

Graphically, **Figures 3.5 A, 3.6 A, 3.7A, 3.7 D** and statistically, the total and unbound exposures of R-bupropion (**Table 3.3** and **3.4**) were similar to the corresponding S-bupropion concentrations in plasma and brain. Total exposure of R, R-hydroxybupropion was higher in plasma ($p = 0.004$), not brain, than S, S-hydroxybupropion (**Figure 3.5 B, 3.6 B, 3.7 B**). On correcting for fraction unbound in both matrices, diastereomeric ratios were found to be similar during the course of the study in plasma (**Figure 3.7 B**). Unbound exposure ($AUC_{0\text{-}6hr}$) of R, R-hydroxybupropion was greater ($p = 0.006$) than S, S-hydroxybupropion in brain, suggesting stereoselective disposition in brain (**Figure 3.7 B**). Total and unbound $AUC_{0\text{-}6hr}$ of S, S-threohydrobupropion (**Figure 3.5 C, 3.6 C, 3.7 C, 3.7 F**) was observed to be higher than R, R-threohydrobupropion in plasma and brain. However, no statistically significant difference between exposures of these diastereomers was observed in the two matrices. Plasma $AUC_{0\text{-}6hr}$ of S, R-erythrohydrobupropion was 4-fold higher than R, S-erythrohydrobupropion. There were not enough data to determine if the difference between erythrohydrobupropion diastereomers was statistically significant in plasma. Concentrations of R, S-erythrohydrobupropion in brain were below the quantification limit (1.5 ng/mL).

***Stereospecific parent versus metabolite concentrations in plasma and brain***

Exposures (total and unbound AUC) of metabolites in both matrices were 50-100 lower than the parent, as shown in **Figures 3.8** and **3.9**. In our present study, comparing unbound plasma exposures ($AUC_{0\text{-}6hr}$) of formed S, S-hydroxybupropion to bupropion and correcting for differences in clearance between bupropion and that of preformed S, S-hydroxybupropion, the fraction of bupropion metabolized to S, S-hydroxybupropion was 1.5 %. Based on total and unbound exposures ($AUC_{0\text{-}6h}$) in the two matrices (**Table 3.3** and **3.4**), exposure to oxidative metabolites was higher than reductive metabolite exposure, with R, R-hydroxybupropion being the major metabolite in both the matrices. Overall, exposure of R-bupropion metabolites was higher than its S-counterpart in both matrices.

Parallel post-absorption and post-distribution plasma kinetics, as shown in **Figure 3.8**, and similar elimination rates (**Table 3.3** and **3.4**) between parent and formed hydroxybupropion diastereomers, suggest elimination of the metabolites is formation-rate limited. This conclusion is supported by

consistent shorter half-life estimates following pre-formed S, S-hydroxybupropion administration (**Tables 3.3** and **3.4**), and with prior studies (Cremers et al., 2016). Slower elimination rates from plasma of reductive metabolites compared to parent suggest possible elimination related kinetics of reductive metabolites (**Tables 3.3** and **3.4**). However, this needs further confirmation by separate administration of reductive metabolites.

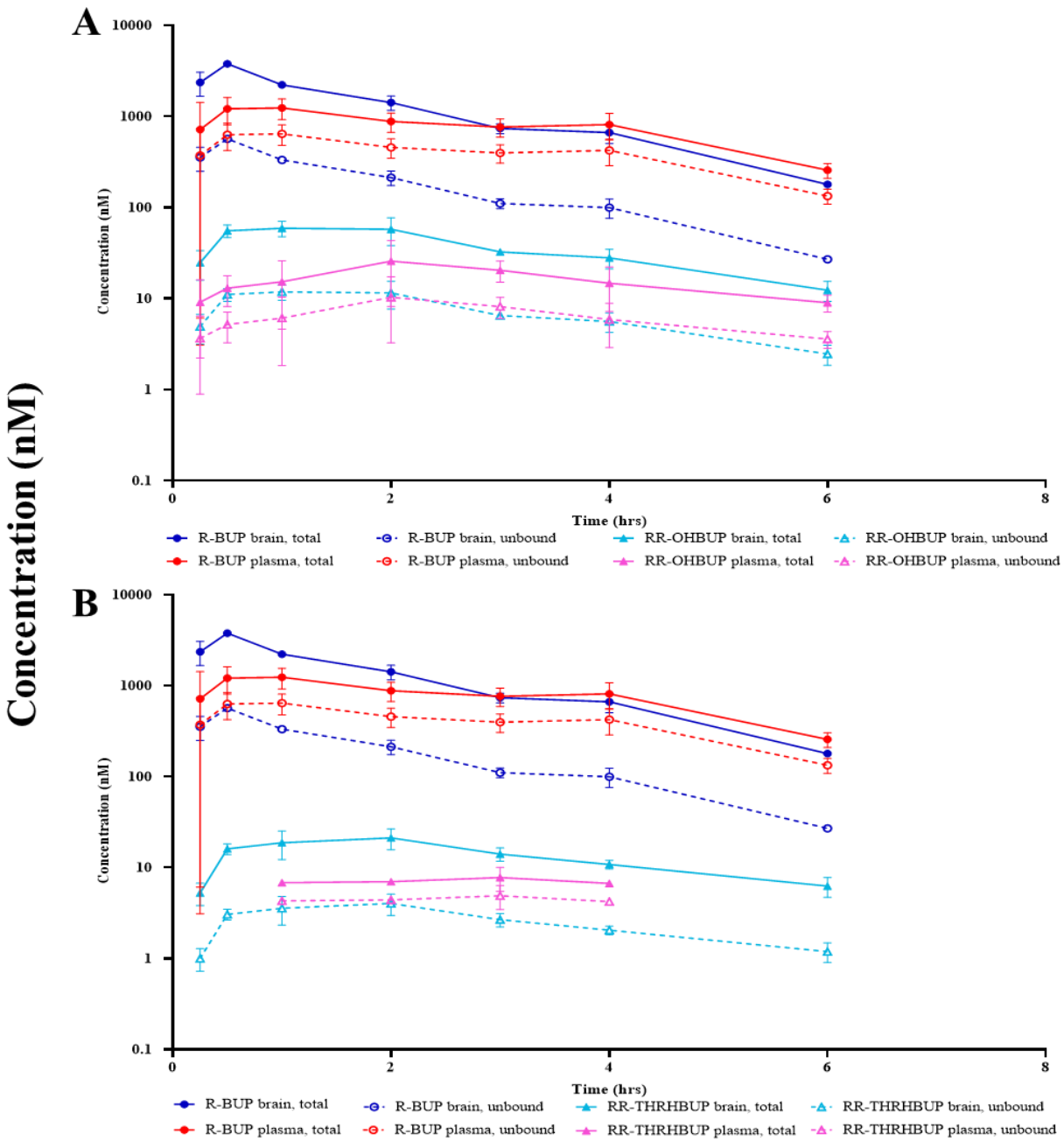


**Figure 3.8.** Mean unbound (dashed lines) and total (solid line) parent-metabolite concentration-time profiles in plasma and brain following 10 mg/kg, subcutaneous administration of racemic bupropion to adult male Sprague Dawley rats. Symbols and error bars denote observed means and standard deviation (n = 3 at each time point) respectively. Panel **A to C** depicts profiles of R-bupropion and its metabolites. Panel **D** to **E** depicts profiles of S-bupropion and metabolites. BUP: bupropion; OHBUP: hydroxybupropion; THRHBUP: Threohydrobupropion; ERYHBUP: ErythrohydrobupropionFigure 3.8 continued

Figure 3.8 continued

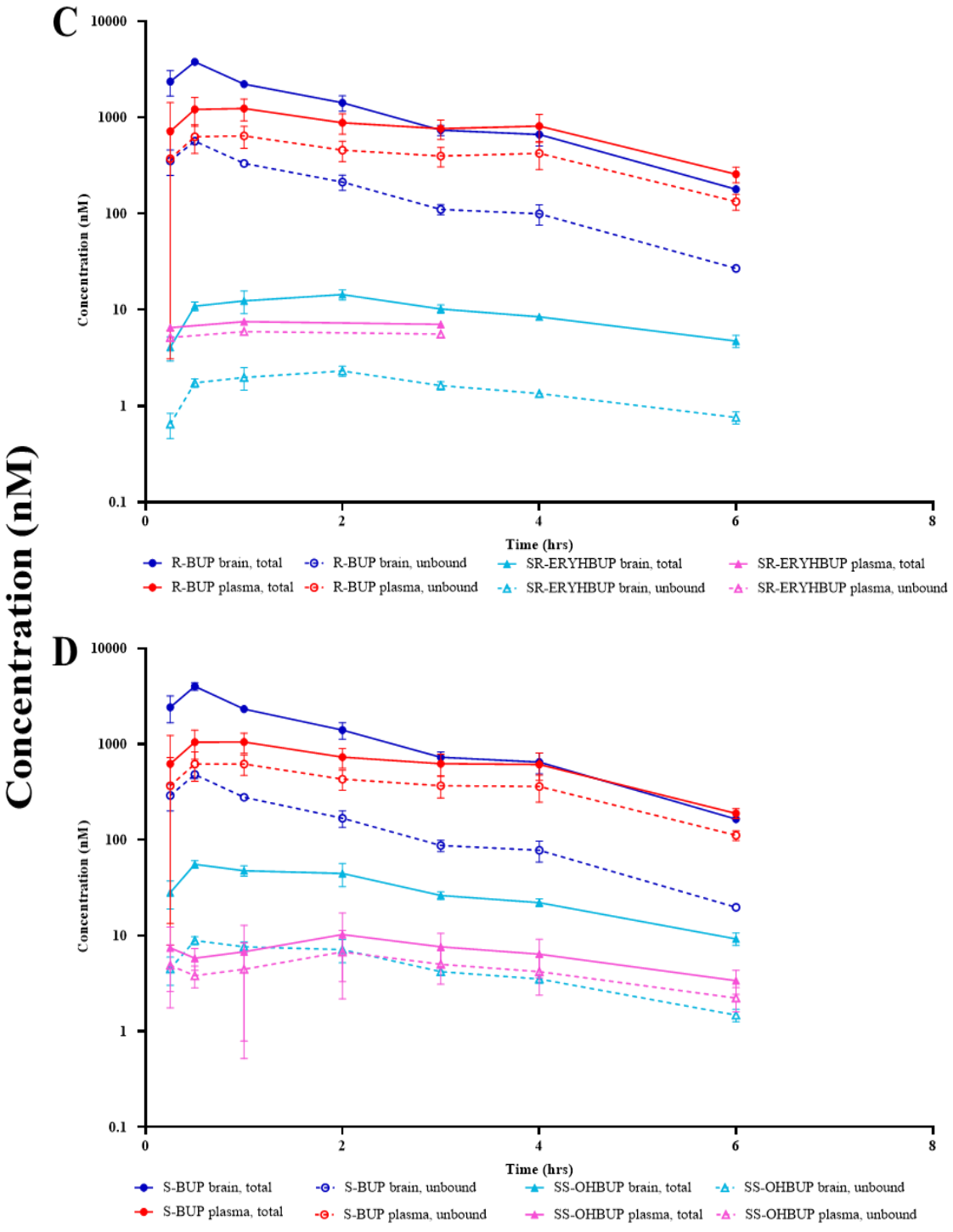

Figure 3.8 continued

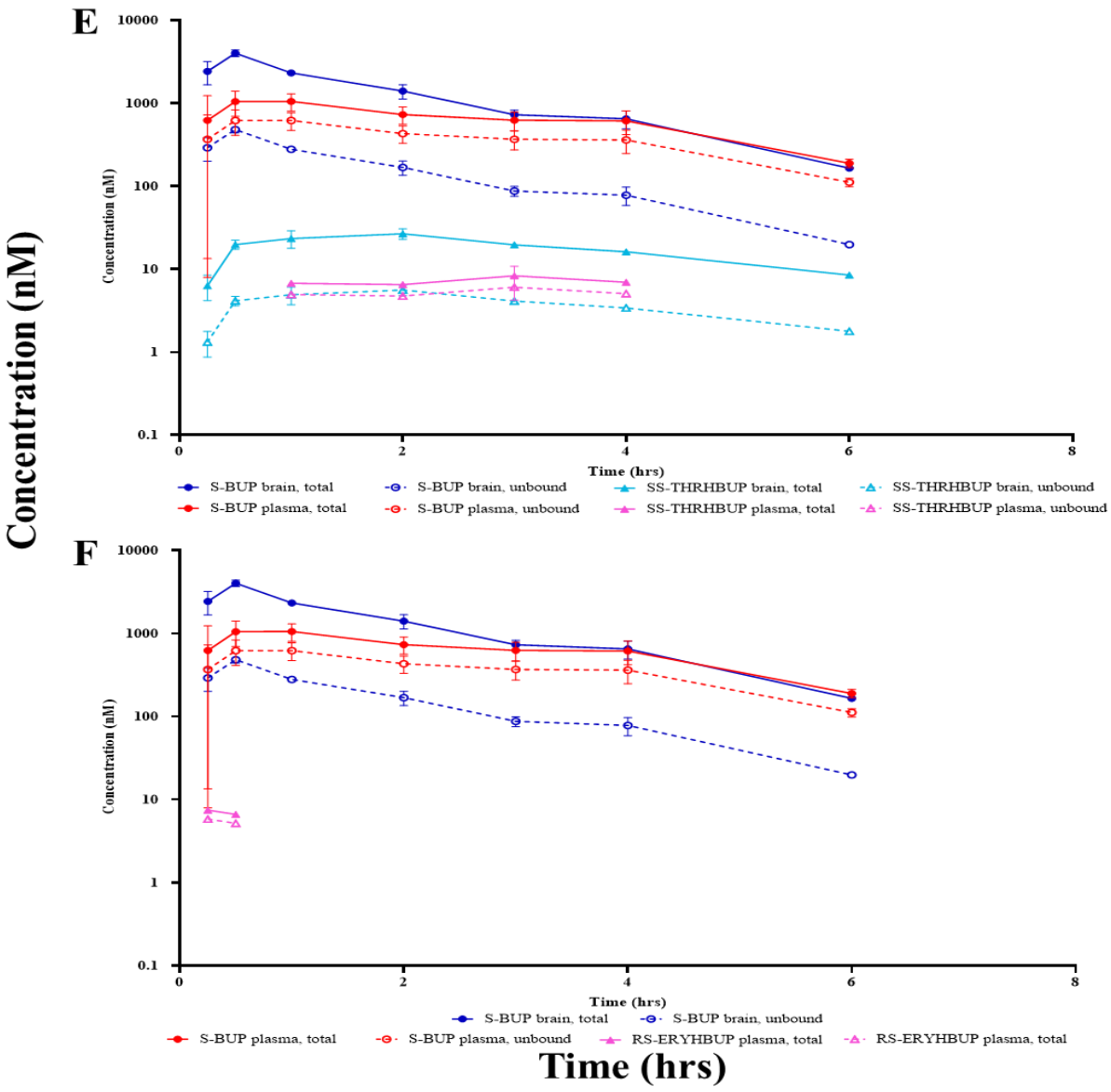


.

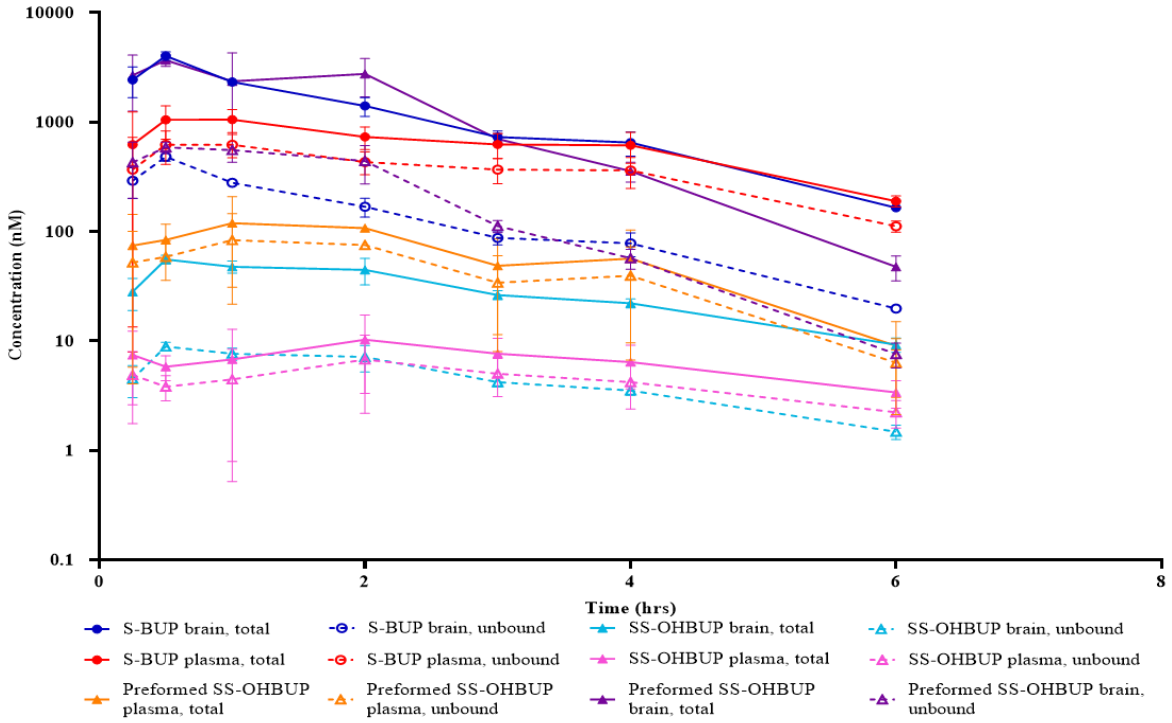


**Figure 3.9.** Mean unbound (dashed lines) and total (solid lines) S-bupropion, formed S,S-hydroxybupropion and preformed S,S-hydroxybupropion concentration-time profiles in plasma and brain following 10 mg/kg, subcutaneous administration of racemic bupropion and 2 mg/kg of preformed S, S-hydroxybupropion (separate groups) to adult male Sprague Dawley rats. Symbols and error bars denote observed means and standard deviation (n=3 at each time point) respectively. BUP: bupropion; OHBUP: hydroxybupropion

A time dependent change in total brain to total plasma concentration ratios of bupropion and its metabolites ($K_p$ **Figure 3.10 A**, **3.10 B**), and corresponding unbound brain to unbound plasma concentration ratios ($K_{p,uu}$ **Figure 3.10 C**, **3.10 D**) over time was noted. As shown in **Figures 10 C** and **D**, from 1 to 6 hours, unbound exposures of bupropion enantiomers were lower ($p<0.05$) in brain than plasma. Unbound brain concentrations of pre-formed S, S-hydroxybupropion were consistently higher in brain than in plasma. The result was a 5-fold higher unbound brain to plasma exposure from 0 to 6 hours (**Table 3.5**).

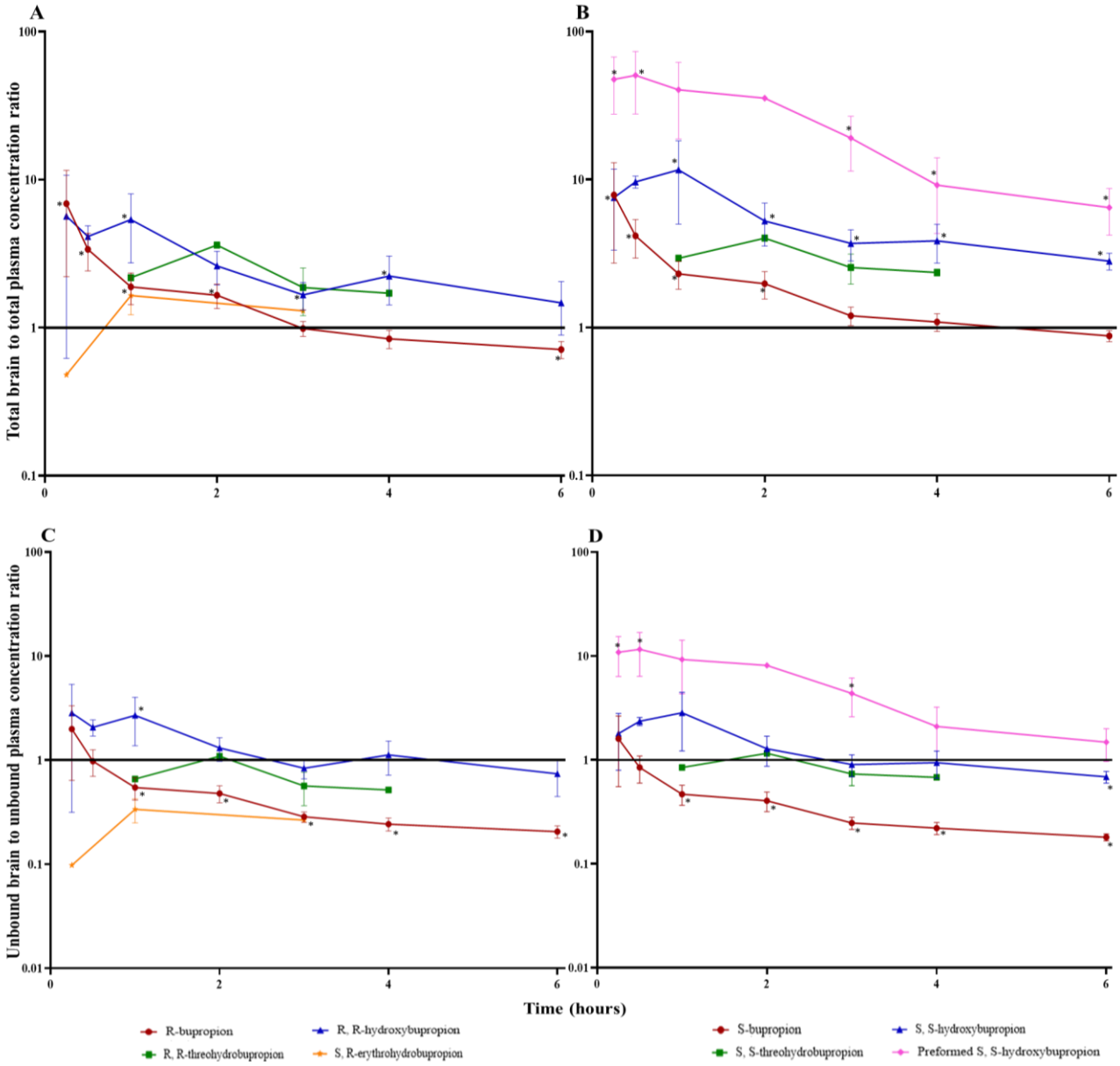


**Figure 3.10.** Mean unbound brain to unbound plasma concentration ratio time profiles of bupropion and metabolites following 10 mg/kg subcutaneous administration of racemic bupropion or 2 mg/kg preformed S, S-hydroxybupropion to adult male Sprague Dawley rats. Top panel represents total brain to total plasma concentration ratio versus time profile of **A)** R-bupropion and metabolites and **B)** S-bupropion and metabolites and preformed S, S-hydroxybupropion. Bottom panel represents unbound brain to unbound plasma concentration ratio versus time profiles of **C)** R-bupropion and metabolites and **D)** S-bupropion and metabolites and preformed S, S-hydroxybupropion. Symbols and error bars denote observed means and standard deviation (n=3 at each time point). * indicates timepoints at which the concentrations between plasma and brain were statistically different.

**Table 3.5.** Unbound brain to unbound plasma ($K_{p,uu}$) and total brain to total plasma ($K_p$) concentration ratios of bupropion and metabolites.

| Analyte | $K_{p,uu\ 0\text{-}6hr}$ | $K_{p,uu\ 4\text{-}6hr}$ | $K_{p,uu,t}$ | $K_{p,0\text{-}6hr}$ | $K_{p,4\text{-}6hr}$ | $K_{p,t}$ |
|---|---|---|---|---|---|---|
| R-BUP | 0.431 | 0.221 | 0.205 (6 hr) | 1.50 | 0.787 | 0.712 (6 hr) |
| S-BUP | 0.381 | 0.199 | 0.180 (6 hr) | 1.87 | 1.01 | 0.877 (6 hr) |
| RR-OHBUP | 1.13 | 0.822 | 0.737 (6 hr) | 2.99 | 1.70 | 1.47 (6 hr) |
| SS-OHBUP | 1.08 | 0.759 | 0.685 (6 hr) | 4.71 | 3.20 | 2.81 (6 hr) |
| RR-THRHBUP | 0.958 | - | 0.516 (4 hr) | 3.18 | - | 1.71 (4 hr) |
| SS-THRHBUP | 1.28 | - | 0.677 (4 hr) | 4.22 | - | 2.35 (4 hr) |
| SR-ERYHBUP | 0.426 | - | 0.265 (3 hr) | 2.73 | - | 1.30 (3 hr) |
| Preformed SS-OHBUP | 5.10 | 1.410 | 1.47 (6 hr) | 25.5 | 7.04 | 6.46 (6 hr) |

Subscripts 0-6 hr indicate Area Under Curve (AUC) calculated from 0 to 6 hour; 4-6 hr indicate partial AUCs calculated from 4 to 6-hour, t indicates concentration ratio at last timepoint (timepoint indicated in parenthesis). Plasma concentration of reductive metabolites were below limit of quantification at 6 hours. BUP: bupropion; OHBUP: hydroxybupropion; THRHBUP Threohydrobupropion; ERYHBUP: Erythrohydrobupropion.

From 3 to 6 hours, decline in formed metabolites in brain was similar to plasma (**Table 3.3**, **Figure 3.8**). Overall, unbound exposures ($AUC_{0\text{-}6hr}$) of formed metabolites were also similar in brain and plasma (**Table 3.5**). A transient overshoot (from 0.5 to 2 hours) followed by decline in $K_{p,uu}$ ratios was apparent for both formed R, R- and S, S-hydroxybupropion and threohydrobupropion. This transient overshoot, as shown in **Figures 3.10 B** and **3.10 D,** was more prominent with preformed S, S-hydroxybupropion. For these two metabolites, metabolite to parent ratios were consistently higher in brain than plasma (**Figure 3.11**, **Table 3.6**).

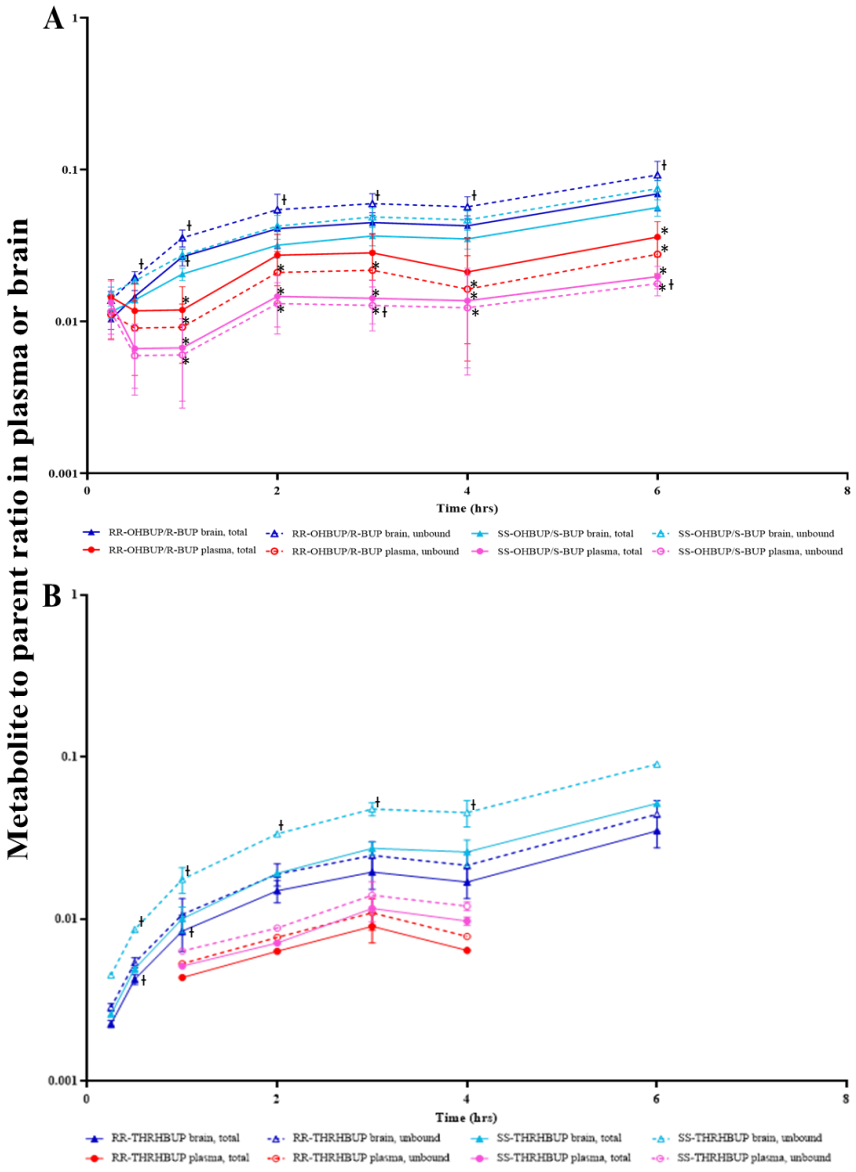


**Figure 3.11.** Mean unbound and total metabolite to parent ratio (R vs S) in plasma and brain following 10 mg/kg, subcutaneous administration of racemic bupropion to adult male Sprague Dawley rats. **A)** Represents unbound and total hydroxybupropion (R, R or S, S-) to parent bupropion (R or S) ratios in plasma and brain. **B)** Represents unbound and total threohydrobupropion (R, R or S, S-) to parent bupropion (R or S) ratios in plasma and brain. **C)** Represents unbound and total erythrohydrobupropion (S, R or R, S-) to parent bupropion (R or S) ratios in plasma and brain. Symbols and error bars denote observed means and standard deviation (n=3 at each time point) respectively. BUP: bupropion; OHBUP: hydroxybupropion; THRHBUP: threohydrobupropion; ERYHBUP: erythrohydrobupropion. The timepoints at which the ratios between two matrices were different are shown by Asterisk * in figure. Time points in which R, R/R-BUP versus S, S-/S-BUP were different are indicated by ɨ.

Figure 3.11 continued

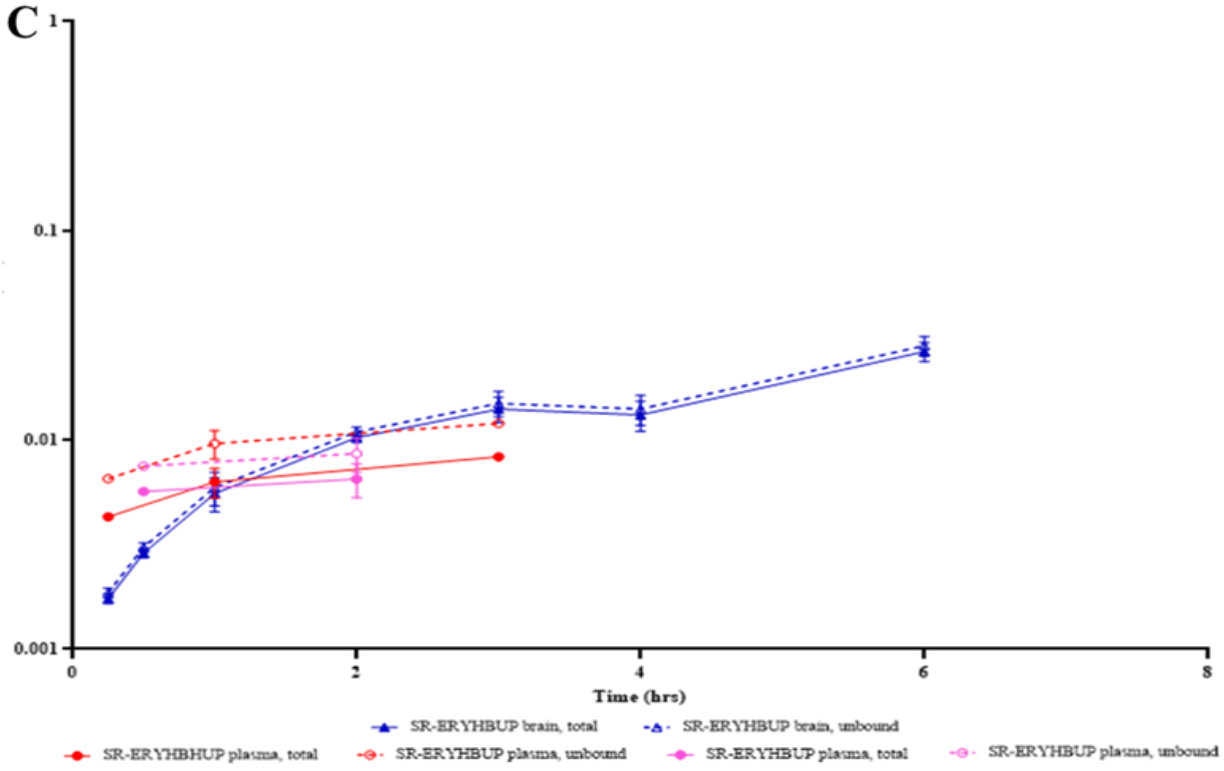

**Table 3.6.** Unbound and total metabolite to parent ratios in rat plasma and brain.

| Metabolite to parent exposure ratios $\frac{AUC_{0-6h,metabolite}}{AUC_{0-6h,parent}}$ | Unbound exposures | | | Total exposures | | |
|---|---|---|---|---|---|---|
| | Plasma (P) | Brain (B) | Fold difference (B/P) | Plasma (P) | Brain (B) | Fold difference (B/P) |
| RR-OHBUP/R-BUP | 0.016 | 0.041 | 2.61 | 0.015 | 0.031 | 2.00 |
| RR-THRHBUP/R-BUP | 0.006 | 0.014 | 2.22 | 0.005 | 0.011 | 2.12 |
| SR-ERYHBUP/R-BUP | 0.007 | 0.009 | 1.28 | 0.004 | 0.008 | 1.82 |
| SS-OHBUP/S-BUP | 0.011 | 0.036 | 3.36 | 0.010 | 0.025 | 2.51 |
| SS-THRHBUP/S-BUP | 0.018 | 0.026 | 1.43 | 0.007 | 0.015 | 2.25 |
| RS-ERYHBUP/S-BUP | 0.002 | | | 0.002 | | |

BUP: bupropion; OHBUP: hydroxybupropion; THRHBUP: threohydrobupropion; ERYHBUP: erythrohydrobupropion

## 3.4 Discussion

In this study we quantified bupropion related entities using a chiral assay to characterize differences in relative exposures of parent enantiomeric and metabolite diastereomeric pairs between plasma and brain. The overarching goal is to translate this understanding of relative exposures between plasma and brain to humans using translational modeling and simulation tools.

In vitro derived measures of binding in the two matrices enabled determination of unbound parent enantiomer and metabolite diastereomer concentrations in plasma and brain. A major assumption in this study is that the in vitro derived measures of fraction unbound (in both matrices) represent the in vivo unbound exposures. Correction for unbound fraction was critical because, as per the free drug hypothesis, it is the unbound brain concentration that is available for interacting with CNS drug targets (DAT and NET for bupropion) (Liu & Chen, 2015; Andreas Reichel, 2010). The $f_{u,plasma}$, $f_{u,brain}$ for bupropion enantiomers reported in our study are close to previously reported values for bupropion (Avdeef, 2012). Also, the unbound brain exposures of bupropion and unbound plasma and brain exposures for S, S hydroxybupropion from our present in vivo studies are close to values reported using microdialysis which gives direct measures of unbound concentration, suggesting that our in vitro unbound fractions adequately captured the in vivo unbound concentration (Cremers et al., 2016). Observed differences in $f_{u,plasma}$ versus $f_{u,brain}$ for a given enantiomer or diastereomer can be attributed to differences in composition of plasma versus

brain, with plasma having twice as much protein, while brain 20-fold more lipids (Andreas Reichel, 2010, 2014).

### 3.4.1 Stereoselective parent and metabolite kinetics in plasma

Absence of prominent in vivo stereoselective disposition in rat for bupropion enantiomers and metabolite diastereomers stands in contrast to that seen in humans (Masters et al., 2016). In humans, following a 100 mg oral dose of racemic bupropion, apparent oral clearance of S-bupropion was 6-fold higher than R-bupropion (Masters et al., 2016). In our present study, the apparent clearance values of both enantiomers were similar. Substantially reduced formation in rats of the specific metabolites we measured challenged our ability to detect possible differences. In addition, chiral inversion of the two bupropion enantiomers in vivo may occur sufficiently rapidly (**Chapter 3**) such that enantiomer concentrations reach a state of equilibrium within minutes.

Evidence from this study of formation-rate limited kinetics with oxidative metabolites (R, R- and S, S-hydroxybupropion) is in agreement with a previous study using microdialysis, and also with observations in humans (Cremers et al., 2016; Masters et al., 2016). The longer half-lives observed relevant to reductive metabolites compared to parent enantiomers in plasma are also consistent with longer elimination half-lives of reductive metabolites in humans (Masters et al., 2016).

### 3.4.2 Stereoselective brain relative to plasma kinetics

Observation of higher unbound bupropion exposure in plasma than brain is similar to observations from a microdialysis study reported by Yeniceli et al (Yeniceli et al., 2011). $K_{p,uu}$, a parameter reflecting unbound drug disposition in brain versus plasma, provides evidence regarding operation of carrier-mediated uptake or efflux across the BBB (Fridén et al., 2007; Hammarlund-Udenaes et al., 2008). The $K_{p,uu}$ value < 1 we observed with bupropion enantiomers in rats is close to a CSF-plasma ratio of 0.43 reported in humans by Golden et al (Golden, DeVane, et al., 1988). Both time dependent decline in $K_{p,uu}$ and $K_{p,uu}$ values < 1 for both bupropion enantiomers suggest net efflux and or metabolism at the blood-brain-barrier (BBB) (Fridén et al., 2007). Variations in

efflux transporter expression, such as P-gp expression at the BBB, may contribute to variability in response observed in individuals on bupropion therapy (O'Brien, Dinan, Griffin, & Cryan, 2012). The possibility of a transporter involved in bupropion disposition has also been suggested by a study wherein bupropion administration significantly increased digoxin renal clearance in rats, possibly due to alteration of OATP4C1 uptake of digoxin into renal proximal tubule epithelium, and/or alteration of subsequent P-gp efflux out of these cells (He, Yu, Prasad, Chen, & Unadkat, 2014). The 2 to 3-fold higher brain than plasma metabolite to parent unbound exposure ratios suggest preferential accumulation of metabolites in brain, possibly due to differences in carrier-mediated BBB transport of metabolites relative to parent, but also possibly due to additional metabolite formation within brain. Unlike liver, expression of metabolic enzymes, such as CYP450, in brain that could potentially contribute to local stereoselective bupropion metabolism, is lower and not well characterized. Unlike hepatic microsomes, use of brain microsomes is not popular due low expression and lower stability of cytochrome P450 during brain microsome preparation (Vijayalakshmi Ravindranath & Anandatheerthavarada, 1990). We used population modeling approach to test this hypothesis (within brain metabolism). Our model suggests brain formation clearance makes a negligible contribution to overall brain clearance (discussed in **Chapter 5**).

A $K_{p,uu}$ value ~1 for both oxidative and reductive metabolites suggests transport at the BBB is dominated by passive processes. A $K_{p,uu}$ value > 1 following preformed S, S-hydroxybupropion administration was also observed by Cremer et al (Cremers et al., 2016); however, the magnitude was 3-4 times lower than our study, possibly due to differences in techniques. Notwithstanding, both studies provide evidence of carrier-mediated uptake participation in the transport of preformed S, S-hydroxybupropion at the BBB. The discrepancy in $K_{p,uu}$ values of formed versus preformed S, S-hydroxybupropion could possibly be due to competition between bupropion and metabolites competing with formed S, S-hydroxybupropion at blood-brain-barrier. The relative exposure of S, S-hydroxybupropion or R, R-hydroxybupropion to bupropion is much lower, which would enhance the ability of bupropion to compete with stereoselective carrier mediated transport. A separate R, R-hydroxybupropion dosing group could shed more light into the observed difference. Due to reported significantly lower pharmacological potency than S, S-hydroxybupropion and bupropion, a separate R, R-hydroxybupropion was not included in this

study (Damaj et al., 2004). Lower bupropion doses may also help; however, this approach would be limited by low production of this metabolite in rat, compromising ability to measure it. The transient overshoot in $K_{p,uu}$ of S, S-hydroxybupropion, more prominent in preformed S, S-hydroxybupropion than formed hydroxybupropion enantiomers, imply involvement of pH-dependent proton-coupled antiporter at blood-brain-barrier as suggested in study by Cremers et al (Cremers et al., 2016). This antiporter is thought to be involved in transport of weakly basic CNS drugs such as oxycodone, apomorphine, clonidine (Cremers et al., 2016).

### 3.4.3 In vitro – in vivo correlation

The rank order of total concentrations of the racemic parent and metabolites (bupropion > hydroxybupropion > threohydrobupropion > erythrohydrobupropion) in both matrices are in agreement with those reported by Welch et al and Suckow et al (Suckow et al., 1986; Welch et al., 1987).

However, there was disagreement in the rank order based on metabolite to parent plasma $AUC_{0\text{-}6hr}$ ratios (unbound) from our in vivo study to that observed and reported in the rat hepatic liver microsomal incubation study we conducted (**Chapter 2**) (Bhattacharya et al., 2019). The rat hepatic microsomal studies suggested R-bupropion to be the higher clearance enantiomer than S-bupropion, whereas no differences in R vs S enantiomer clearance were observed in vivo. In our present rat study, higher oxidative than reductive metabolite formation was seen, whereas a higher proportion of reductive metabolites were observed in rat liver microsomes (Bhattacharya et al., 2019). Some agreement between in vitro and in vivo studies was seen. In both in vitro (hepatic microsomes) and in vivo (rat plasma) studies, 2-3 fold higher S, R-erythrohydrobupropion than R, S-erythrohydrobupropion was observed (Bhattacharya et al., 2019). Though not statistically significant, we see slightly higher (1.1-fold) S, S-threohydrobupropion plasma exposure than R, R-threohydrobupropion compared to a 34-fold higher formation clearance in rat hepatic microsomes.

Hepatic clearances of R- and S-bupropion scaled from in vitro rat hepatic microsomal incubation studies were 3-fold and 25-fold lower than their respective in vivo unbound apparent clearances. This could possibly be due to substantial contribution of metabolic pathways not

characterized in this in vivo study and/or possible extrahepatic disposition in the rat. We did not measure the major rat metabolites such as acidic metabolites formed through side chain cleavage (m-chlorobenzoic acid, m-chlorohippuric acid) and glucuronide conjugates of phase 1 metabolites (Suckow et al., 1986; Welch et al., 1987).

The similar in vivo clearance of the two enantiomers, but a six-fold lower hepatic clearance of S-bupropion than R-bupropion (based on our in vitro studies), suggests that rat liver forms S-bupropion metabolites less efficiently than R, and/or that S-bupropion undergoes extrahepatic disposition to a larger extent.

Kirby et al observed evidence of a bupropion-digoxin drug-drug interaction (DDI), in which staggered dosing of bupropion (150 mg, extended release tablet) and digoxin (0.5 mg) increased renal clearance of digoxin by 80% and decreased its plasma AUC by 40% (He et al., 2014; Kirby et al., 2011; Kirby et al., 2012). They also observed that in the presence of digoxin renal clearance of bupropion did not change, but the renal clearance of racemic hydroxybupropion, formation clearance of racemic hydroxybupropion and the racemic hydroxybupropion to bupropion urinary ratio and that of R, R-hydroxybupropion to R-bupropion urinary ratio were significantly increased. A significant effect of digoxin on S, S-hydroxybupropion/ S-bupropion urinary ratio was not observed (Kirby et al., 2011). Further studies to investigate the mechanism of this interaction through in vitro transport studies in Madin-Darby canine kidney II (MDCKII) cells suggested bupropion and its metabolites had no effect on human P-gp mediated transepithelial transport of [3H]-Digoxin, but bupropion and hydroxybupropion significantly stimulated H-OATP4C1 mediated transport of [3H]-Digoxin. A subsequent study in rats found bupropion significantly increased digoxin renal clearance by possibly inhibiting rat-Oatp4c1-mediated digoxin renal reabsorption.

However, the opposite localization of OATP4C1 in humans (localized at the basolateral membrane of proximal tubular cells) versus rats (Oatp4c1 is an apical uptake transporter in the rat kidney), suggest rat is not an appropriate animal model to elucidate the mechanisms underlying digoxin renal elimination (Shen et al., 2018).

Later, Shen et al studied the effect of multiple dosing of bupropion on the pharmacokinetics of digoxin in cynomolgus monkeys (Shen et al., 2018). They observed a significant decrease in

systemic exposure of digoxin mediated by an increase in its non-renal clearance with repeated dosing of bupropion compared to a single dose (Shen et al., 2018). This study did not evaluate the impact of bupropion-digoxin interaction on bupropion metabolite exposures. The mechanistic basis of this interaction is not fully understood, and the authors suggest possible dosage adjustment of digoxin and bupropion in heart failure patients with comorbid depression, as a possible clinical implication of this interaction.

Altogether, studies in humans and animals suggest possible extrahepatic disposition, and possible transporter involvement in bupropion`s disposition, both of which would benefit from further investigation.

### 3.4.4 Comparison to human plasma pharmacokinetics

Unlike humans, we did not observe prominent differences in clearances of R vs S-bupropion, or between exposures of diastereomeric metabolites (Gufford et al., 2016; Masters et al., 2016). Humans are reported to have higher exposure of phase 1 metabolite than parent; whereas, rats have higher parent than metabolite exposure (Masters et al., 2016). Like humans, oxidative phase 1 metabolites were more prominent than reductive metabolites in rats. We observed slightly higher exposure of R-bupropion and its metabolites than S-bupropion. Like humans, exposure to S, R-erythrohydrobupropion was higher than R, S-erythrohydrobupropion. Observation of higher S, S-threohydrobupropion than R, R-threohydrobupropion matches the 0-6-hour profile in humans (Masters et al., 2016). Overall, observed differences could be attributed to differences in metabolism between rats and humans (Suckow et al., 1986; Welch et al., 1987). Unlike humans, rats make very little of these basic metabolites; most of the administered bupropion is extensively metabolized to acidic metabolites (m-chlorobenzoic acid, m-chlorohippuric acid) through side chain cleavage (Suckow et al., 1986; Welch et al., 1987). These differences between rat and humans may challenge extrapolating our findings to humans.

Overall, high $V_{u,brain}$ (> 0.8) and $K_{p,uu,cell}$ from in vitro brain binding studies, and the time dependent change in $K_{p,uu}$ for bupropion and hydroxybupropion (formed diastereomers and preformed S, S-hydroxybupropion) observed in vivo, suggest involvement of a carrier-mediated uptake process at the BBB. Contribution of a pH-dependent proton-coupled antiporter at the BBB,

a transporter thought to be involved in transport of weakly basic drugs such as apomorphine, clonidine and diphenhydramine across this barrier (André, Debray, Scherrmann, & Cisternino, 2009; Okura et al., 2008; Okura, Higuchi, Kitamura, & Deguchi, 2014; Sadiq et al., 2011), may be involved. A similar observation and rationale was presented by a microdialysis study in Sprague Dawley rats by Cremers et al, which used the same dose and administration route of bupropion and pre-formed S, S-hydroxybupropion (Cremers et al., 2016). Additional studies, using in vitro human cell-derived BBB models, and possibly transfected with putative uptake transporters, may provide evidence supporting the functional presence of carrier-mediated blood-brain-barrier transport, and support its possible effect in vivo, providing impetus for additional in vivo studies. Incorporation of transporter-mediated disposition across the BBB into PBPK models would also be useful to project the role of carrier-mediated transport in brain disposition of bupropion and S, S-hydroxybupropion in humans. Comprehensive data regarding expression of transporters and metabolic enzymes in rat and human brain is lacking, which complicates extrapolating results to humans. However, developing such models facilitates identifying the gaps in our current knowledge and generating new hypotheses for future experiments.

In addition to substantially reduced formation in the rat of major metabolites produced in human, an additional limitation to our study approach was the use of whole brain homogenization, which results in disruption of entire brain cells. Hence, clear distinction between intracellular versus extracellular drug distribution in brain could not be made. However, similar (within 2-fold) unbound bupropion exposures, estimated from whole brain and in vitro brain binding, from our present study ($AUC_{0-\infty}$,1996 nM·hr) with Cremers (prefrontal cortex, 1644 nM·hr) and Yenicelli (Nucleus accumbens, 1146 nM·hr), and preformed S, S-hydroxybupropion (1263 nM·hr in our study vs 945 nM·hr in Cremers), obtained using microdialysis, which measures brain extracellular fluid, supports confidence using the present approach to measure extracellular fluid brain concentrations.

During our in vitro binding study, we observed > 200% recoveries of bupropion enantiomers and low stability (< 10%) in plasma at the end of 5-hour incubation. Both chiral inversion and low plasma stability are associated with bupropion, but mechanisms driving these processes are poorly understood (Laizure & DeVane, 1985; O'Byrne, Williams, Walsh, & Gilmer,

2010; Sager et al., 2016). This may reduce accuracy estimating unbound fraction in both matrices, and associate to reduced confidence applying these measured values to approximate unbound concentrations in vivo. To address these concerns, our next step was to measure chiral inversion and degradation of bupropion enantiomers in three matrices (plasma, brain and 0.1 M phosphate buffer, pH 7.4), and apply a modeling approach to ascertain bupropion fraction unbound in rat plasma and brain.

# CHAPTER 4. CHARACTERIZATION OF CHIRAL INVERSION AND STABILITY OF BUPROPION ENANTIOMERS IN RAT PLASMA, BRAIN AND BUFFER

**Hypothesis 3.** Stability of bupropion enantiomers is different in plasma, brain and buffer. Instability and inversion of bupropion enantiomers alters estimates of the in vitro unbound fraction estimates for plasma and brain.

**Specific aim 3.** Characterize chiral inversion/stability of bupropion enantiomers in rat plasma, brain and buffer (0.1 M phosphate buffer pH 7.4) to estimate the kinetics of chiral inversion and degradation through a population modeling approach, and application to estimate unbound fractions in plasma and brain matrices.

## 4.1 Introduction

Bupropion is a second-generation antidepressant also indicated for smoking cessation. Itis also being tested as a candidate treatment for psycho-stimulant drug abuse, and attention-deficit hyperactivity disorder (ADHD) (Laizure & DeVane, 1985). Despite its established efficacy in both approved indications, bupropion therapy is associated with wide intersubject variability, which is thought to be driven by variability in metabolism (Masters et al., 2016). Bupropion undergoes complex stereoselective metabolism that is still not fully understood and metabolites are reported to have stereoselective pharmacological activity (Bondarev et al., 2003; Damaj et al., 2004; Damaj et al., 2010). Bupropion is about twice as potent an inhibitor of dopamine reuptake compared to norepinephrine reuptake (Damaj et al., 2004; Damaj et al., 2010). Its active metabolite S, S-hydroxybupropion is twice as potent at inhibiting norepinephrine reuptake than bupropion, and almost as potent as bupropion in inhibiting dopamine reuptake (Damaj et al., 2004). There have been extensive efforts to understand stereoselective systemic disposition of bupropion in humans (Gufford et al., 2016; Masters et al., 2016).

Accurate and precise measurement of plasma and brain target site concentrations of bupropion, is important to generate valid pharmacokinetic data for research and clinical applications. The free base form of bupropion is reported to be unstable and hygroscopic, and there

have been efforts to improve stability of bupropion using inclusion complexes, different salt forms, and controlling moisture levels during its product manufacturing process. (O'Byrne et al., 2010). Degradation of bupropion is known to be pH and temperature dependent (Laizure & DeVane, 1985; O'Byrne et al., 2010). Below pH 5, protonation of the amine group is thought to inhibit its degradation, and at pH above 5 and approaching its pKa, bupropion becomes increasingly deprotonated and is reported to suffer from hydroxide ion catalyzed degradation (Laizure & DeVane, 1985; O'Byrne et al., 2010; Suma, Kosanam, & Sai Prakash, 2006). The choice of matrix also seems to influence bupropion stability. Bupropion half-life in phosphate buffer pH 7.4 is reported to be 7-9 days, while in human plasma it is reported to be 11 hours at 37 ºC and 54 hours at 22 ºC (Kiptoo et al., 2009; Laizure & DeVane, 1985; O'Byrne et al., 2010; Suma et al., 2006). Its stability in brain tissue in any species has not been reported.

Another phenomenon that can potentially complicate understanding both systemic and brain pharmacokinetics of bupropion is that of chiral inversion. Chiral-inversion between bupropion enantiomers is known to occur, however, the mechanism or what triggers chiral inversion is not fully understood (Musso et al., 1993; Sager et al., 2016). Further, the influence of matrix on inversion rates has also not been investigated. Following administration of racemic bupropion to humans, the plasma exposure of R-bupropion is reported to be 10-fold higher than S-bupropion (Masters et al., 2016). However, few studies have been conducted to evaluate pharmacodynamic difference between the two enantiomers. Musso et al determined that (+)-1 isomer had effective dose ($ED_{50}$) values of 23 mg/kg from the antitetrabenazine test, and half maximal inhibitory concentration ($IC_{50}$) of 4 µM for in vitro norepinephrine reuptake inhibiting activity (NET) and 2.3 µM for dopamine reuptake inhibiting activity (DAT) (Musso et al., 1993). The (-)-1 isomer had an $ED_{50}$ of 17 mg/kg and $IC_{50}$ of 10.5 µM at NET and 4.2 µM at DAT (Musso et al., 1993). Racemic bupropion in the tetrabenazine assay had an $ED_{50}$ of 18 mg/kg and $IC_{50}$ of 6.7 µM at NET and 2.1 µM at DAT (Musso et al., 1993). However, the rapid racemization of the enantiomers may confound the absolute measures of potency and this may have limited conclusions from studies towards understanding the pharmacological effects of the individual isomers. Studies suggest that (+)- and (-)-isomers had (S)- and (R)-configurations, respectively (Carroll et al., 2014; Fang et al., 2000).

Understanding chiral inversion is important because this may change the proportion of the enantiomers over time and impact prediction of steady state pharmacokinetics of the two isomers. Unlike bupropion, its metabolites are reported to be stable in human plasma; however, the inversion potential, particularly of hydroxybupropion, of which the S, S-hydroxybupropion form is pharmacologically active, has not been investigated (Dash et al., 2018).

In light of known low stability and chiral inversion associated with bupropion, coupled with our own experimentally observed low stability in plasma and brain (10-45%), and > 200 % recoveries observed at the end of in vitro plasma binding studies for both bupropion enantiomers, it was imperative to characterize degradation and inversion in three matrices (rat plasma, brain and 0.1 M phosphate buffer pH 7.4). It was important to ascertain the true unbound fraction, a parameter critical to estimate target site unbound concentration, that shall ultimately be used to translate understanding to human brain target site concentrations using modeling and simulation. Also, through this study, we hoped to gain a better understanding of discrepancies in plasma exposures between the present study and a previous microdialysis study of bupropion using the same dose, strength, rat strain (similar weight range and sex), and route of administration (Cremers et al., 2016). While unbound brain exposures of bupropion using microdialysis and through brain homogenate exposure corrected for fraction unbound in the present study were similar (within 2-fold), there was an almost 7-fold difference in unbound plasma exposure of bupropion between these two studies.

## 4.2 Material and methods

### 4.2.1 Drugs and chemicals

R-bupropion (R-Bupropion D-Tartaric Acid Salt, catalog # B689615), S-bupropion (S-Bupropion L-Tartaric Acid Salt, catalog # B689620) were purchased from Toronto Research Chemicals (Toronto, Ontario). Acetaminophen (catalog # A5000; lot # 122K0021), ammonium bicarbonate (catalog # 09830; lot # BCBL6295V) were purchased from Sigma Aldrich Chemical Co (St. Louis, MO). Sprague Dawley rat brains (catalog # IRTBR0000; lot # 2699601-15) were purchased from Innovative Research (Novi, MI). Sprague Dawley rat plasma (K3EDTA, pooled,

catalog # RAT00PLK3PNN; lot # RAT386832) was purchased from BioIVT (Westbury, NY). Methanol (lot # A465-4), ethyl acetate (lot # E195SK-4), sodium phosphate monobasic (catalog # S381-3; lot # 007029) were purchased from Fisher Scientific (Fairlawn, NJ).

### 4.2.2 Plasma and brain homogenate binding

Unbound plasma and brain fractions of bupropion enantiomers (R and S) were determined using a 96-well equilibrium dialysis apparatus (HTD96b, HTDialysis, Gales Ferry CT). Dialysis membranes (molecular weight cut off 12,000-16,000; catalog # S25645, Fisher Scientific) were conditioned successively in deionized water (30 minutes), 25% methanol (30 minutes) and 100 mM pH 7.4 sodium phosphate buffer (60 minutes). Rat brain tissue was diluted 3-fold with 0.1 M sodium phosphate buffer, pH 7.4 and homogenized with a sonic probe (TissueRuptor Homogenizer, Qiagen). 100 µL of pH 7.4 phosphate buffer was first loaded to one side of the dialysis membrane, and 100 µL rat plasma or brain homogenate was loaded to the other side. The 96-well equilibrium dialysis apparatus was incubated for 5 hours in a shaking water bath maintained at 37 ºC. After 5 hours, 20 µL of matrix sample (plasma or brain homogenate), and buffer from the other side of each well were aliquoted and analyzed by LC-MS/MS. Zero-time sample ($T_0$) and 5-hour sample ($T_5$) for each matrix (plasma and buffer, or brain homogenate and buffer) were also analyzed to determine stability and recovery.

### 4.2.3 Characterization of chiral inversion/stability of bupropion enantiomers in rat plasma, brain and 0.1 M phosphate buffer pH 7.4

For determination of inversion rates and irreversible loss of R and S-bupropion in plasma, brain and buffer, 100 µL of blank rat plasma, brain homogenates (prepared as described in the previous section), or 0.1 M phosphate pH 7.4 buffer spiked to 10 µM R or S-bupropion was incubated at 37 ºC in a shaking water bath (Dubnoff metabolic shaking incubator, Precision Scientific). Reactions were stopped at 0 hour, 0.25 hour, 0.5 hour, 1 hour, 2 hours, 4 hours, 6 hours, 8 hours, and 24 hours for each of the matrices by removing from the water bath and storing at -80 ºC immediately after sampling each time point until further processing for analysis by LC-MS/MS.

### 4.2.4 Sample analysis

Frozen rat plasma or brain homogenate samples (stored at −80 ˚C) were thawed to ambient temperature and 20 µL were transferred to 12 × 75 polypropylene tubes. Then, 20 µL of 0.1 ng/µL of acetaminophen (APAP- internal standard) and 1 mL of ethyl acetate were added to the tube, and the sample was vortex mixed for 20 seconds. After centrifugation at 4000 rpm at ambient temperature for three minutes, the organic phase was transferred to a clean 12 × 75 polypropylene tube and evaporated to dryness. Samples were reconstituted with 50 µL of methanol then vortex mixed for 20 seconds. A 10 µL aliquot of each sample was injected into the HPLC. Chromatographic separation was achieved using an Agilent1290 series HPLC coupled with a PAL HTC-XT Leap autosampler using reverse phase chromatography, at 40 °C, with a Phenomenex Lux 3 µm AMP 150 × 4.6 mm column. Mobile phase (methanol: 5mM ammonium bicarbonate, pH = 10.0; 80:20; v/v) was delivered isocratically at a constant flow rate of 400µL/min. The column effluent was monitored using a Sciex 5500 QTRAP triple-quadrupole mass spectrometer (Foster City, CA) equipped with an electrospray ionization probe in positive mode. The mass spectrometer was controlled by Analyst software (version1.6.2) in conjunction with Windows 7®. A flow injection analysis was performed on each analyte to maximize sensitivity. The responses of the analytes were optimized at a source temperature of 650 °C, under unit resolution for quadrupole 1 and 3. In addition, the analytes were given a dwell time of 200 ms and a settling time of 10 ms. The ion spray voltage was 5500 V and the interface heater was on. Optimal gas pressures for all of the analytes were as follows: collision gas medium, curtain gas 10, ion source gas (1) 25, ion source gas (2) 25. Multiple reaction monitoring was used to measure Q1/Q3 transitions for R-bupropion and S-bupropion at 240.1/184.0. Standard stock solutions (1 mg/mL) of R and S-bupropion and APAP were prepared separately in polypropylene tubes by adding methanol. Working standard solutions were prepped from the standard stock solutions daily by performing 1:10 serial dilutions in methanol into 12 × 75 polypropylene tubes. The standard curves for R-bupropion andS-bupropion ranged from 0.15 to 1500 ng/mL. Quality control (QC) samples were prepared in duplicate. The QC samples had the following concentrations: 0.5 ng/mL (low QC), 15 ng/mL (medium QC), and 1000 ng/mL (high QC).

### 4.2.5 Data analysis

Fraction unbound in plasma ($f_{u,plasma}$) and brain ($f_{u,brain}$) were calculated using the below equations (Kalvass et al., 2007). D in the equation refers to dilution of brain matrix (3-fold), and $f_{u,measured}$ was calculated from the ratio of concentration in buffer to diluted brain homogenate. Percent recovery was calculated based on the free (buffer side) plus bound (plasma or brain homogenate side) levels at 5 hours relative to the $T_5$ sample. Percent stability was calculated based on the spiked matrix incubated ($T_5$) at 37 °C relative to the $T_0$ sample.

$$f_{u,plasma} = \frac{\text{concentration in buffer}}{\text{concentration in plasma}} \quad \text{.....Equation 4.1}$$

$$f_{u,brain} = \frac{1/D}{[1/f_{u,\,measured}]-1]+1/D} \quad \text{.....Equation 4.2}$$

Since chiral inversion and degradation processes occurred simultaneously, k, reflecting the rate constant of the slowest step (degradation or inversion), was calculated from the slope of the monoexponential equation derived from terminal phase (last three or four) concentration-time points of each of the enantiomers in each matrix. Statistical analysis was done in JMP®, version 13.2.0 (SAS Institute Inc., Cary, NC, USA), and graphs were drawn using GraphPad Prism version 6.00 for Windows (GraphPad Software, La Jolla, CA, USA). Assuming normal distribution, statistical comparisons between enantiomeric pairs was conducted by ANOVA and post hoc Dunnett's was used to determine statistical differences in concentrations at specific timepoints for each enantiomer. A p value of 0.05 was considered significant.

### 4.2.6 Population-pharmacokinetic (Pop-PK) approach to estimate inversion and degradation rates of the bupropion enantiomers in three matrices and its application.

Population PK analysis was done by Phoenix NLME 8.1 (Pharsight Corporation, Certara, L.P., Princeton NJ). A population modeling approach was used for both R and S-bupropion in all matrices (rat plasma, brain, 0.1 M phosphate buffer pH 7.4) using first-order conditional estimation (FOCE). Chiral inversion and degradation rates were first estimated for each matrix for both

enantiomers. Models were parameterized as fixed volumes with clearance terms specific for chiral inversion and degradation. Different model structures, such as unique chiral inversion clearances for each enantiomer versus a single (equivalent) inversion clearance were evaluated. We also evaluated model structures based on only chiral inversion without degradation versus chiral inversion with degradation. Models based on two clearances (one clearance for each enantiomer, regardless of starting enantiomer) versus a single clearance (R-bupropion loss is due to S-bupropion loss, when S-bupropion was the starting enantiomer, and vice versa when R-bupropion was the starting enantiomer). There were 48 observations and 24 wells in the inversion/stability population model of R or S-bupropion in buffer and brain. There were 52 observations and 29 wells in the population model of R or S-bupropion in the plasma model, which included combining a preliminary chiral inversion experiment conducted over a 6-hour duration and a repeat experiment spanning 24 hours. Inter-well variability of inversion and loss parameters was estimated by assuming a log-normal distribution based on the exponential relationship, $P_i = P_{tv} \times \exp(\eta_i)$, where $P_i$ is the parameter estimate of clearance for the $i^{th}$ well, $P_{tv}$ is the population typical value and $\eta_i$ is the deviation from the population value of the $i^{th}$ well. Various residual error models were also evaluated. These were additive, proportional, and mixed additive - proportional. A proportional error model was eventually selected in the three matrices for both enantiomers, based on $Y = F \times (1 + EPS(1))$, where Y is the dependent-variable observations, F is the corresponding individual specific model predictions and EPS is the residual error.

Inversion and degradation clearances derived from chiral inversion/stability experiments conducted in individual matrices were used to estimate unbound fractions of the two enantiomers from the plasma and brain binding studies. Since these parameters (chiral inversion and degradation clearances) were derived from total concentrations in plasma/brain, they were incorporated in a model to predict unbound fractions from plasma/brain binding studies after factoring in $CL_{total} = CL_{unbound} \times f_u$ in the model, where $CL_{total}$ is the total clearance (chiral inversion or degradation), $CL_{unbound}$ is unbound clearance (chiral inversion or degradation) and $f_u$ is unbound fraction in rat plasma or brain. There were 54 observations and 9 wells each in the plasma and brain binding population models derived from bupropion enantiomer binding studies

Model evaluation was based on objective function and precision of estimates. In addition, visual inspection of goodness of fit plots (conditional weighted residual versus either population predicted or time after dose plots, as well as the observed versus individual predicted and population predicted concentration plots) were also used to support final model structure. A visual predictive check with 1000 replicates was also conducted.

## 4.3 Results

### 4.3.1 Plasma and brain binding assessment

Unbound fractions for both enantiomers were 3-fold higher in rat plasma than brain (**Table 4.1**). The stability of both enantiomers in brain and plasma were low (< 50 %). However, between the two matrices, enantiomers were approximately 3 to 4-fold more stable in brain than plasma.

**Table 4.1.** Unbound fractions ($f_u$) of R and S-bupropion in rat plasma and brain homogenate

| Compound | $f_{u,\ plasma}$ | % Plasma recovery | % Plasma stability | $f_{u,\ brain}$ | % Brain recovery | % Brain stability |
|---|---|---|---|---|---|---|
| R-bupropion | 0.518 ± 0.021 | 591 | 9.12 | 0.146 ± 0.015 | 133 | 26.0 |
| S-bupropion | 0.590 ± 0.030 | 457 | 9.44 | 0.122 ± 0.008 | 87 | 45.1 |

Fraction unbound measures represent the mean of 3 replicate studies, each study conducted in triplicate ± SEM.

### 4.3.2 Results from chiral inversion/stability experiments in three matrices (rat plasma, brain and 0.1 M phosphate buffer pH 7.4)

From **Figure 4.1**, it seems by about 4 hours, chiral inversion equilibrium (concentration of R = S) was attained in all three matrices. In plasma, from 0.5-hour timepoint onwards, statistically, there was no difference in R versus S-bupropion concentration (incubated versus formed enantiomer, for both R and S bupropion incubated separately). In brain, no statistical difference in concentration between enantiomers was observed from one to two hours onwards. In 0.1 M phosphate buffer pH 7.4, when R-bupropion was incubated, the concentrations of starting and formed enantiomer were similar from four-hour time point, whereas when S-bupropion was incubated the concentrations of R and S were not different from one hour onwards. From Dunnett`s test, we noted the plasma concentration of incubated R or S-bupropion was not different from

control (zero-hour timepoint) only until 15 minutes. In brain, the concentration of incubated R-bupropion was not different from control until eight hours and that of incubated S-bupropion was not different from control up to two hours. Concentration of R and S-bupropion (starting enantiomer) in buffer was not different from control over a period of twenty-four hours.

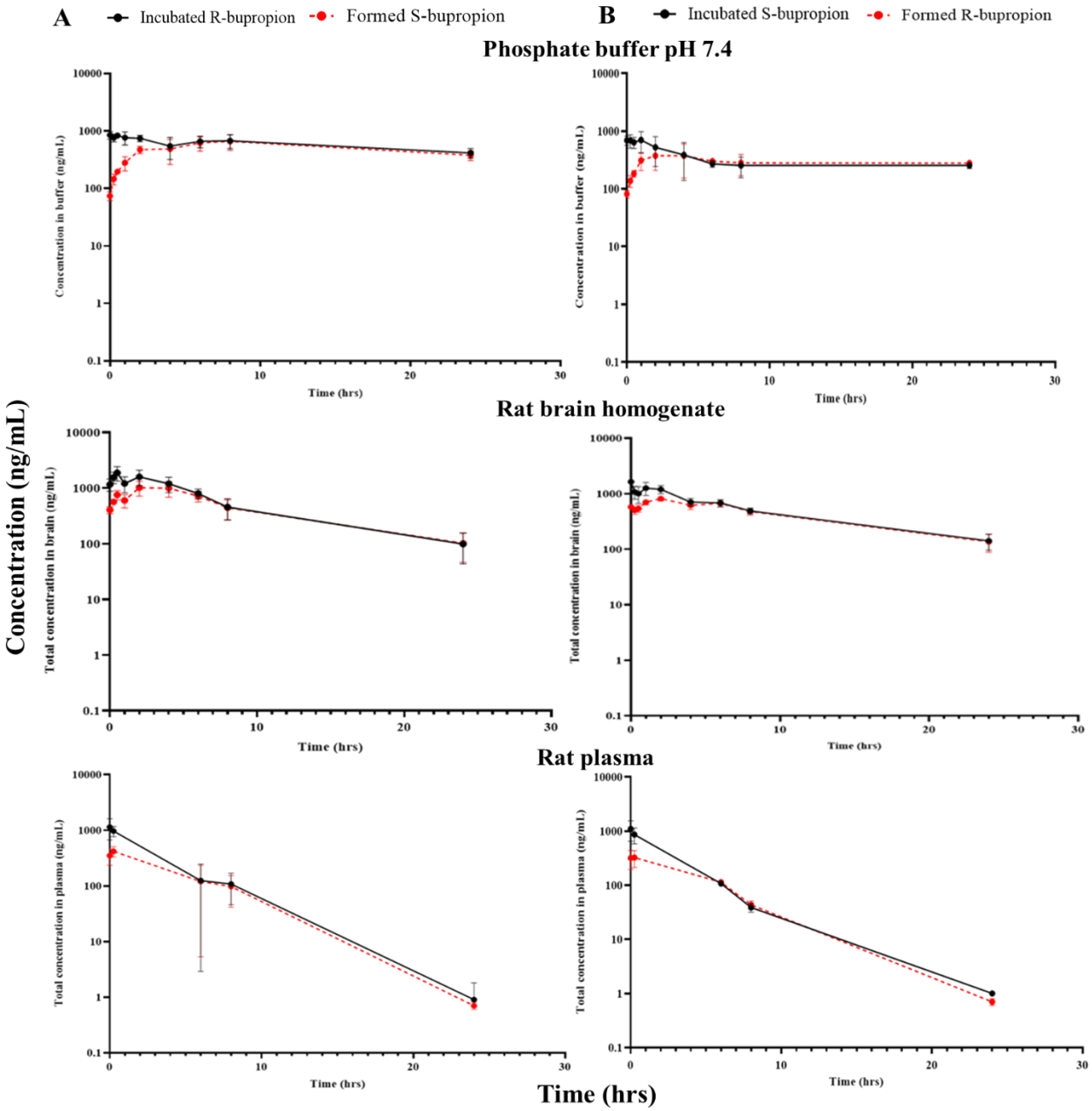


**Figure 4.1.** Twenty-four-hour chiral inversion/degradation profiles of bupropion enantiomers in the three matrices (in vitro) at 37 ˚C. **Panel A (Left)** represents chiral inversion/degradation profile of R-bupropion (10 µM) incubated in 0.1 M phosphate buffer pH 7.4, rat brain homogenate and rat plasma. **Panel B (Right)** represents chiral inversion/degradation profile of S-bupropion (10 µM) incubated in phosphate buffer pH 7.4, rat brain homogenate and rat plasma. Data are represented as the mean ± SD (n = 3) at each timepoint. Black lines with filled circles represent profiles of incubated enantiomer and red dashed lines with filled circles represent profiles of the formed enantiomer (due to chiral inversion) for a given matrix.

From **Table 4.2**, bupropion appears to be most stable in buffer and least stable in plasma. Between the two enantiomers, S-bupropion appears to be less stable than R-bupropion in plasma and buffer. However, in brain S-bupropion seems to be more stable than R-bupropion. **Figure 4.1**, suggest that two processes, namely, chiral inversion and degradation occur simultaneously, and this may limit our ability to get a true estimate of fraction unbound in plasma.

**Table 4.2.** First order rate constants (k) determined for chiral inversion/degradation of bupropion enantiomers in three matrices (rat plasma, rat brain and 0.1 M phosphate buffer pH 7.4)

| Enantiomer incubated | Analyte measured | Matrix | k ($hr^{-1}$) | Half-life (hours) |
|---|---|---|---|---|
| R-bupropion | R-bupropion | plasma | 0.282 | 2.45 |
| | | brain | 0.108 | 6.4 |
| | | buffer | 0.028 | 24.7 |
| | S-bupropion | plasma | 0.295 | 2.34 |
| | | brain | 0.102 | 6.7 |
| | | buffer | 0.03 | 23.1 |
| S-bupropion | R-bupropion | plasma | 0.276 | 2.51 |
| | | brain | 0.085 | 8.15 |
| | | buffer | 0.01 | 69.3 |
| | S-bupropion | plasma | 0.246 | 2.8 |
| | | brain | 0.084 | 8.25 |
| | | buffer | 0.034 | 20.3 |

k: first order rate constant, calculated from slope of monoexponential equation derived from terminal phase (last three-four) concentration-time points of each of the enantiomers in each matrix. Half-life = 0.693/ k

### 4.3.3 Population-PK model characterizing chiral inversion and degradation in three matrices

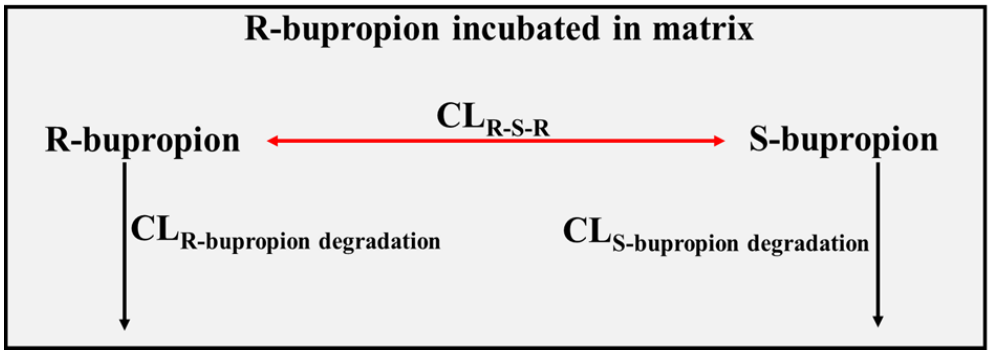


**Figure 4.2.** Schematic of chiral inversion and degradation occurring simultaneously in a matrix. Matrix, 0.1 M Phosphate buffer pH 7.4/rat plasma/rat brain homogenate; $CL_{R\text{-}S\text{-}R}$ chiral inversion clearance; $CL_R$ or $_{S\text{-}bupropion}$ degradation clearance.

Through our population-pharmacokinetic modeling approach, we were able to distinctly estimate chiral inversion and degradation clearances in the three matrices (**Tables 4.3-4.5**). The model structure is shown in **Figure 4.2**. Overall, from **Table 4.6** for both the enantiomers in all the three matrices, the models suggest that the rate of inversion between the enantiomers is faster than their degradation rates. The chiral inversion rate was faster in rat plasma than brain and buffer. For both the enantiomers, degradation was 5-fold more rapid in plasma than brain. S-bupropion appears to undergo inversion slightly (~1.5 fold) faster than R-bupropion in both plasma and brain but seems to be slightly more stable than R-bupropion in both matrices. For both bupropion enantiomers in plasma and brain, a model structure with two degradation terms (degradation of incubated and formed enantiomer) was determined to be a better model than one with single degradation term. However, in the case of bupropion enantiomers incubated in buffer, a model without any loss term (consisting only of chiral inversion) described the data best. This is consistent with reported stability (half-life of 7-9 days) of bupropion in buffer (O'Byrne et al., 2010). Also, two inversion terms ($CL_{R\text{-}S}$ and $CL_{S\text{-}R}$) instead of a single inversion ($CL_{R\text{-}S\text{-}R}$) did not improve the model fit. So, a single term was used to characterize the inversion between the enantiomers in all three matrices. Results of the present study indicate that at 37 ˚C, bupropion enantiomers are most stable in buffer followed by brain and least stable in rat plasma.

**Table 4.3.** Population pharmacokinetic parameter estimates of R and S-bupropion incubated in 0.1 M phosphate buffer pH 7.4.

| Parameter | Estimate (% CV) | Inter well variability (% CV) |
|---|---|---|
| R-bupropion incubated (buffer) | | |
| V (mL) | 0.232 (6.61) | 8.37 (2.4) |
| $CL_{R\text{-}S\text{-}R,\ buffer}$ (mL/hr) | 0.074 (7.1) | |
| Residual error (proportional) | | |
| R-bupropion | 0.095 (14.5) | |
| S-bupropion | 0.005 (108) | |
| S-bupropion incubated (buffer) | | |
| V (mL) | 0.349 (7.98) | 14.4 (4.19) |
| $CL_{S\text{-}R\text{-}S,\ buffer}$ (mL/hr) | 0.137 (13.1) | 20.4 (7.3) |
| Residual error (proportional) | | |
| R-bupropion | 0.003 (3.67) | |
| S-bupropion | 0.116 (11.3) | |

V: volume; $CL_{R\text{-}S\text{-}R}$ or $CL_{S\text{-}R\text{-}S}$: chiral inversion clearance.

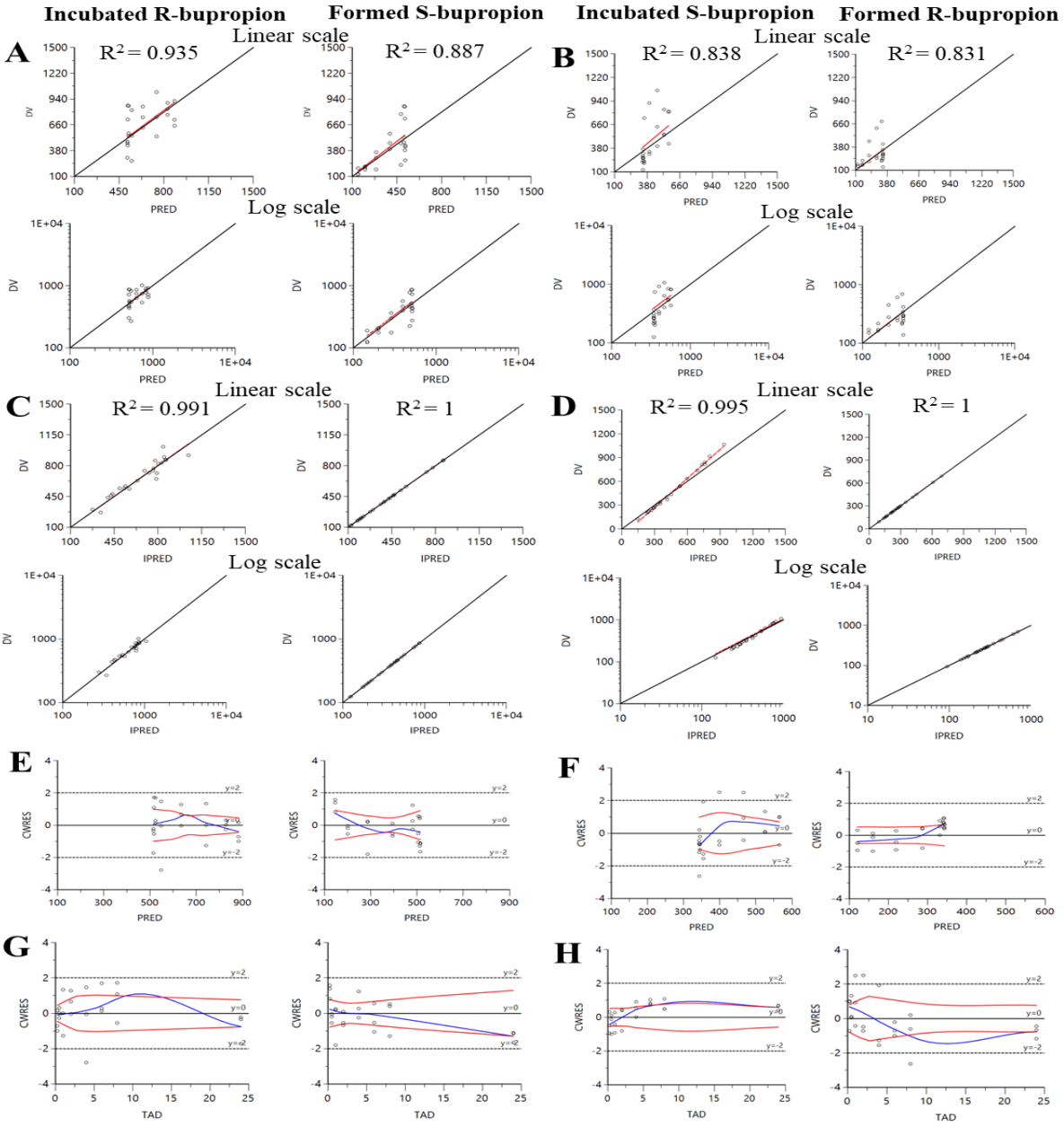


**Figure 4.3.** Model diagnostic plots for R and S-bupropion incubated in buffer. **A** and **B**: Population predicted concentrations versus observed concentrations for R and S-bupropion, respectively. The solid line is the line of unity. **C** and **D**: Individual predicted concentrations versus observed concentrations for R and S-bupropion, respectively. **E** and **F**: Conditional weighted residuals versus time for R and S- bupropion respectively. **G** and **H**: Conditional weighted residuals versus population predicted concentrations for R and S-bupropion, respectively. CWRES: Conditional weighted residuals; DV: observed concentration; IPRED: Individual predicted; PRED: Population predicted; TAD: Time After Dose. Units of concentration and time are nanomolar (nM) and hours respectively.

**Table 4.4**. Population pharmacokinetic parameter estimates of R and S-bupropion incubated in rat brain homogenate

| Parameter | Estimate (% CV) | Inter well variability (% CV) |
|---|---|---|
| R-bupropion incubated (brain) | | |
| V (mL) | 0.092 (12.1) | 11.14 (4.4) |
| $CL_{R\text{-bupropion degradation, brain}}$ (mL/hr) | 0.008 (21.2) | 28.61 (24) |
| $CL_{S\text{-bupropion degradation, brain}}$ (mL/hr) | 0.011 (13.7) | 4.65 (5.7) |
| $CL_{R\text{-S-R, brain}}$ (mL/hr) | 0.020 (23.3) | |
| Residual error (proportional) | | |
| R-bupropion | 0.131 (21.7) | |
| S-bupropion | 0.091 (60.6) | |
| S-bupropion incubated (brain) | | |
| V (mL) | 0.125 (6.7) | 3.44 (1.31) |
| $CL_{R\text{-bupropion degradation, brain}}$ (mL/hr) | 0.011 (10.1) | |
| $CL_{S\text{-bupropion degradation, brain}}$ (mL/hr) | 0.008 (15.1) | 24.2 (12.8) |
| $CL_{S\text{-R-S, brain}}$ (mL/hr) | 0.039 (20.6) | |
| Residual error (proportional) | | |
| R-bupropion | 0.008 (20.1) | |
| S-bupropion | 0.145 (15.4) | |

V: volume; $CL_{R\text{-S-R}}$ or $CL_{S\text{-R-S}}$: chiral inversion clearance; $CL_{R \text{ or } S\text{-bupropion degradation}}$: degradation clearance.

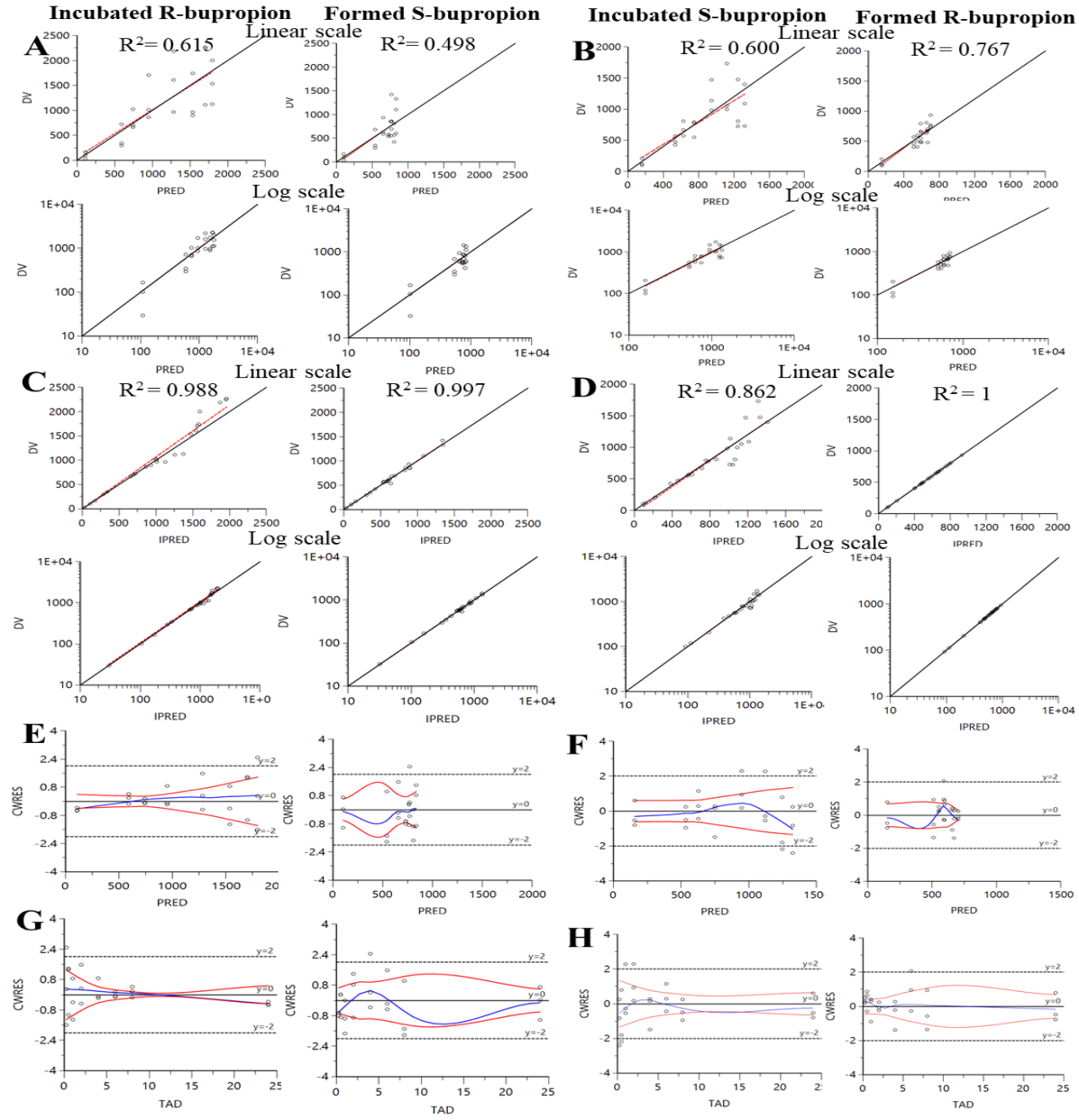


**Figure 4.4.** Model diagnostic plots for R and S-bupropion incubated in rat brain homogenate. **A** and **B**: Population predicted concentrations versus observed concentrations for R and S-bupropion, respectively. The solid line is the line of unity. **C** and **D**: Individual predicted concentrations versus observed concentrations for R and S bupropion, respectively. **E** and **F**: Conditional weighted residuals versus time for R and S- bupropion respectively. **G** and **H**: Conditional weighted residuals versus population predicted concentrations for R and S-bupropion, respectively. CWRES: Conditional weighted residuals; DV: observed concentration; IPRED: Individual predicted; PRED: Population predicted; TAD: Time After Dose. Units of concentration and time are nanomolar (nM) and hours respectively.

**Table 4.5.** Population pharmacokinetic parameter estimates of R and S-bupropion incubated in rat plasma.

| Parameter | Estimate (% CV) | Inter well variability (% CV) |
|---|---|---|
| R-bupropion incubated (plasma) | | |
| V (mL) | 0.107 (19.9) | |
| $CL_{R\text{-bupropion degradation, plasma}}$ (mL/hr) | 0.042 (24.1) | 83.1 (21.9) |
| $CL_{S\text{-bupropion degradation, plasma}}$ (mL/hr) | 0.022 (23.2) | |
| $CL_{R\text{-S-R, plasma}}$ (mL/hr) | 0.087 (25.8) | |
| Residual error (proportional) | | |
| R-bupropion | 0.593 (16.8) | |
| S-bupropion | 0.466 (14.9) | |
| S-bupropion incubated (plasma) | | |
| V (mL) | 0.078 (11.6) | |
| $CL_{R\text{-bupropion degradation, plasma}}$ (mL/hr) | 0.019 (21.2) | |
| $CL_{S\text{-bupropion degradation, plasma}}$ (mL/hr) | 0.023 (19.5) | |
| $CL_{S\text{-R-S, plasma}}$ (mL/hr) | 0.096 (14.7) | |
| Residual error (proportional) | | |
| R-bupropion | 0.388 (16.8) | |
| S-bupropion | 0.34 (17.5) | |

V: volume; $CL_{R\text{-S-R}}$ or $CL_{S\text{-R-S}}$: chiral inversion clearance; $CL_{R \text{ or } S\text{-bupropion degradation}}$ degradation clearance.

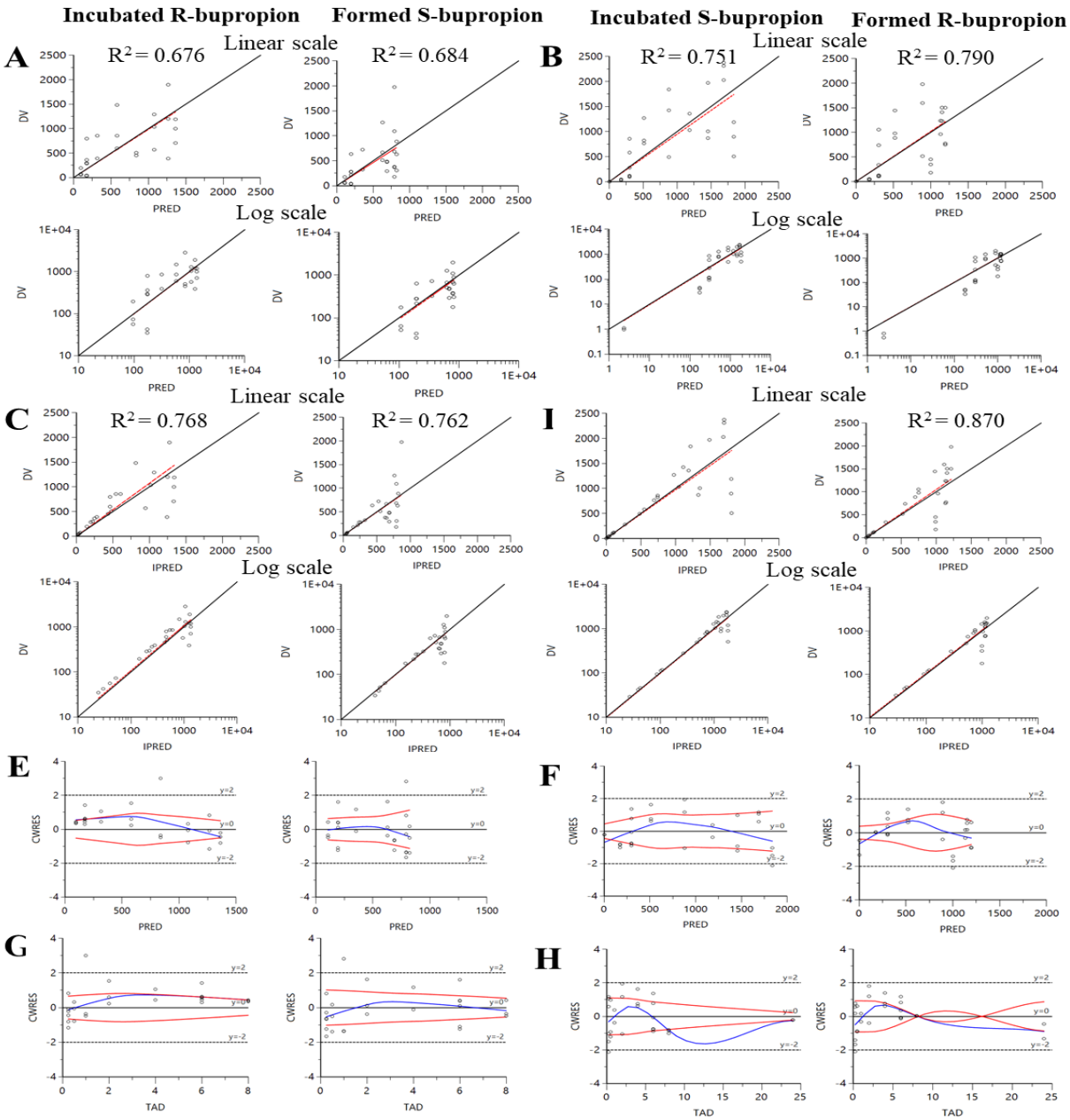


**Figure 4.5.** Model diagnostic plots for R and S-bupropion incubated in rat brain homogenate. **A** and **B**: Population predicted concentrations versus observed concentrations for R and S-bupropion, respectively. The solid line is the line of unity. **C** and **D**: Individual predicted concentrations versus observed concentrations for R and S-bupropion, respectively. **E** and **F**: Conditional weighted residuals versus time for R and S- bupropion respectively. **G** and **H**: Conditional weighted residuals versus population predicted concentrations for R and S-bupropion, respectively. CWRES: Conditional weighted residuals; DV: observed concentration; IPRED: Individual predicted; PRED: Population predicted; TAD: Time After Dose. Units of concentration and time are nanomolar (nM) and hours respectively.

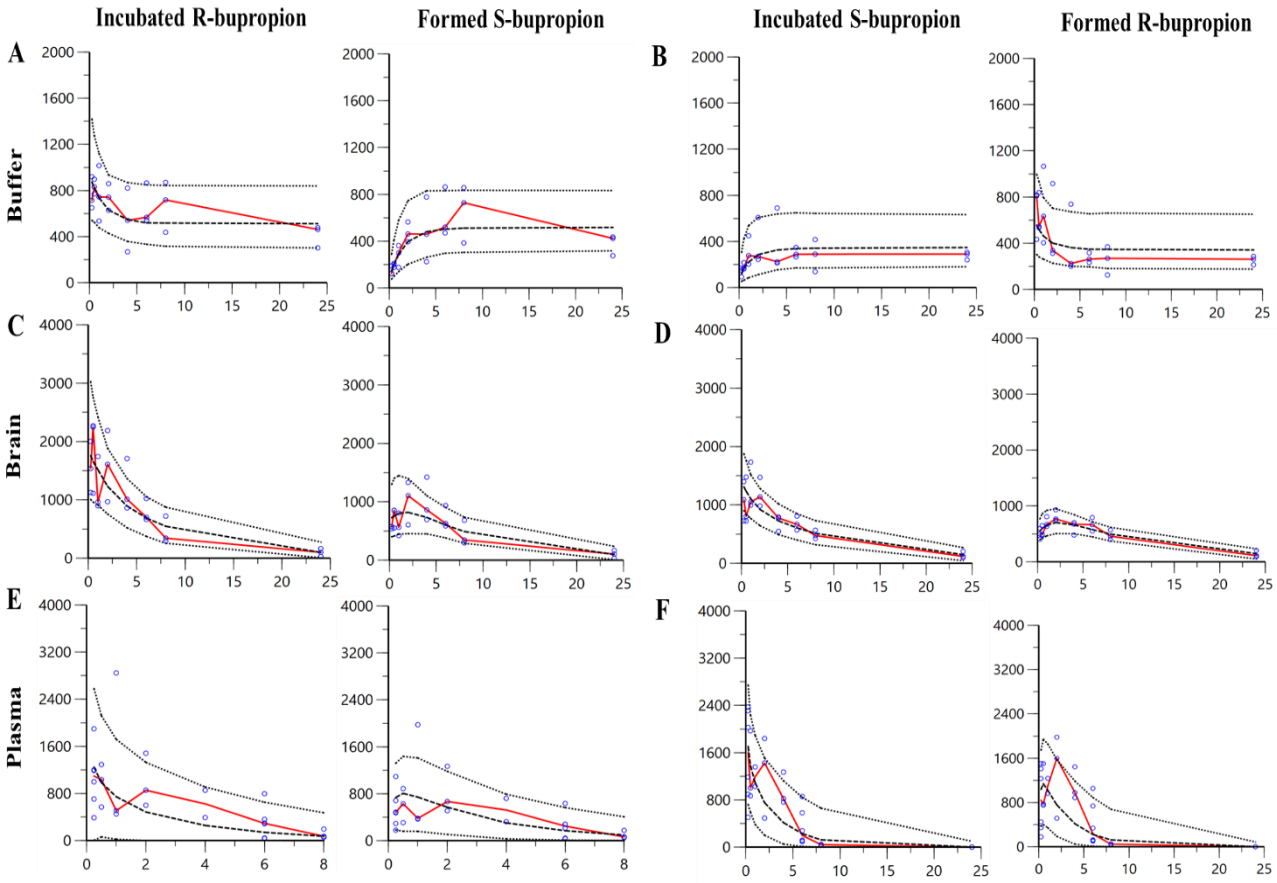


**Figure 4.6.** Visual predictive checks of bupropion enantiomers in 0.1 M phosphate pH 7.4 buffer (**Top panel, A** and **B**), rat brain homogenate (**Middle panel, C** and **D**) and rat plasma (**Bottom, E** and **F**). The red solid line in each plot represents the median of the observed concentrations, the black dashed line represents the median predicted concentrations, and the black dotted lines represent the 5% and 95% limits of the predicted 90% confidence intervals of the median. Individual observed concentrations are shown as the blue open circles.

**Table 4.6.** Summary of chiral inversion and degradation rates derived from population modeling in three matrices.

| Parameters | 0.1 M Phosphate buffer pH 7.4 | | Rat brain homogenate | | Rat plasma | |
|---|---|---|---|---|---|---|
| | R-BUP | S-BUP | R-BUP | S-BUP | R-BUP | S-BUP |
| Chiral inversion rate ($hr^{-1}$) | 0.318 | 0.392 | 0.217 | 0.312 | 0.813 | 1.23 |
| Chiral inversion half-life (hr) | 2.17 | 1.76 | 3.18 | 2.22 | 0.852 | 0.563 |
| Degradation rate ($hr^{-1}$) | - | - | 0.086 | 0.064 | 0.392 | 0.294 |
| Degradation half-life (hr) | - | - | 7.97 | 10.8 | 1.76 | 2.35 |
| Theoretical degradation/inversion rate ($hr^{-1}$) (from terminal phase of graphs) | 0.03 | 0.03 | 0.11 | 0.08 | 0.28 | 0.25 |
| Half-life (hr) | 24.75 | 20.38 | 6.42 | 8.25 | 2.46 | 2.82 |

BUP: Bupropion. Chiral inversion rate for an enantiomer in matrix was calculated from ratio of estimated inversion clearance over volume. Half-life = 0.693/rate.

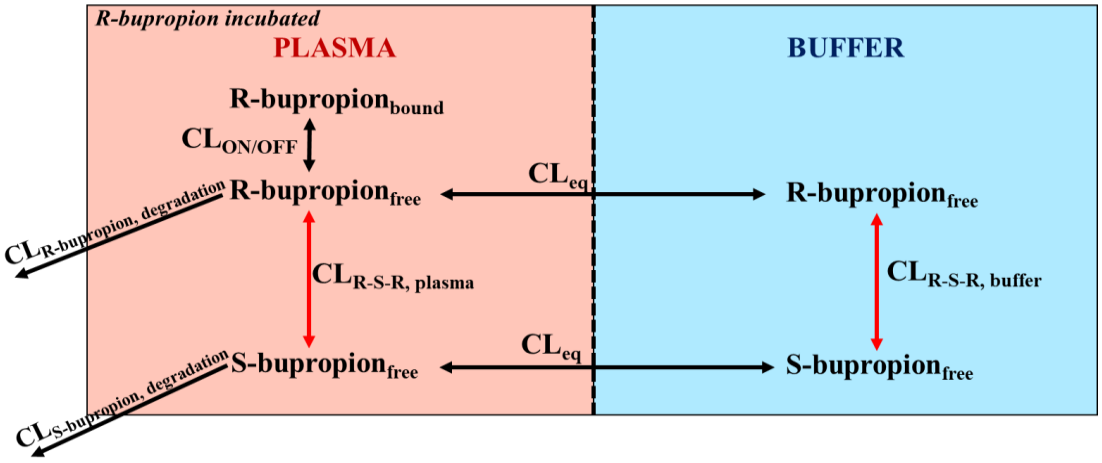


**Figure 4.7.** Diagrammatic representation of chiral inversion and degradation occurring in 96 well equilibrium dialysis apparatus (in each well) during plasma binding experiment.

$CL_{R\text{-}S\text{-}R}$ chiral inversion clearance; $CL_{R \text{ or } S\text{-bupropion degradation}}$ degradation clearance; $Cl_{eq}$ diffusional equilibrium, $CL_{ON/OFF}$: binding equilibrium --------- dialysis membrane

**Table 4.7.** Population pharmacokinetic parameter estimates of R-bupropion from rat brain binding experiment

| Parameter | Estimate (% CV) | Inter well variability (% CV) |
|---|---|---|
| R-bupropion incubated (brain) | | |
| $f_u$ brain, R-bupropion | 0.114 (36.5) | |
| $f_u$ brain, S-bupropion | 0.128 (67) | |
| V brain (mL) | 0.092 | |
| V buffer (mL) | 0.233 | 224 (100) |
| $CL_{R\text{-bupropion degradation, brain}}$ (mL/hr) | 0.008 | |
| $CL_{S\text{-bupropion degradation, brain}}$ (mL/hr) | 0.011 | |
| $CL_{R\text{-S-R, brain}}$ (mL/hr) | 0.02 | |
| $CL_{R\text{-S-R, buffer}}$ (mL/hr) | 0.074 | |
| $CL_{eq}$ (mL/hr) | 100 | |
| Residual error (proportional) | | |
| R-bupropion, brain | 0.369 (17.8) | |
| S-bupropion, brain | 0.619 (12.4) | |
| R-bupropion, buffer | 0.11 (66.2) | |
| S-bupropion, buffer | 0.062 (568) | |

$f_u$: unbound fraction; V: volume; $CL_{R\text{-S-R or S-R-S}}$: chiral inversion clearance; $CL_{R \text{ or } S\text{-bupropion degradation}}$ degradation clearance; $CL_{eq}$: diffusional equilibrium.

**Table 4.8.** Population pharmacokinetic parameter estimates of S-bupropion from rat brain binding experiment

| Parameter | Estimate (% CV) | Inter well variability (% CV) |
|---|---|---|
| S-bupropion incubated (brain) | | |
| $f_u$ brain, R-bupropion | 0.096 (11.3) | |
| $f_u$ brain, S-bupropion | 0.125 (13) | |
| V brain (mL) | 0.125 | |
| V buffer (mL) | 0.349 | 28.9 (10.2) |
| $CL_{R\text{-bupropion degradation, brain}}$ (mL/hr) | 0.011 | |
| $CL_{S\text{-bupropion degradation, brain}}$ (mL/hr) | 0.008 | |
| $CL_{S\text{-R-S, brain}}$(mL/hr) | 0.04 | |
| $CL_{S\text{-R-S, buffer}}$ (mL/hr) | 0.137 | |
| $CL_{eq}$ (mL/hr) | 100 | |
| Residual error (proportional) | | |
| R-bupropion, brain | 0.482 (7.67) | |
| S-bupropion, brain | 0.537 (38) | |
| R-bupropion, buffer | 0.002 (220) | |
| S-bupropion, buffer | 0.012 (21.6) | |

$f_u$: unbound fraction; V: volume; $CL_{R\text{-S-R or S-R-S}}$: chiral inversion clearance; $CL_{R \text{ or } S\text{-bupropion degradation}}$: degradation clearance; $CL_{eq}$: diffusional equilibrium.

**Table 4.9.** Population pharmacokinetic parameter estimates of R-bupropion from rat plasma protein binding experiment

| Parameter | Estimate (% CV) | Inter well variability (% CV) |
|---|---|---|
| R-bupropion incubated (plasma) | | |
| $f_u$ plasma, R-bupropion | 0.592 (5.13) | |
| $f_u$ plasma, S-bupropion | 0.606 (4.56) | |
| V plasma (mL) | 0.107 | |
| V buffer (mL) | 0.233 | |
| $CL_{R\text{-bupropion degradation, plasma}}$ (mL/hr) | 0.042 | 12.7 (3.6) |
| $CL_{S\text{-bupropion degradation, plasma}}$ (mL/hr) | 0.022 | 15 (3.53) |
| $CL_{R\text{-S-R, plasma}}$ (mL/hr) | 0.088 | |
| $CL_{R\text{-S-R, buffer}}$ (mL/hr) | 0.074 | |
| $CL_{eq}$ (mL/hr) | 100 | |
| Residual error (proportional) | | |
| R-bupropion, plasma | 0.361 (12.7) | |
| S-bupropion, plasma | 0.462 (8.09) | |
| R-bupropion, buffer | 0.008 (9.2) | |
| S-bupropion, buffer | 0.0029 (4.13) | |

$f_u$: unbound fraction; V: volume; $CL_{R\text{-S-R or S-R-S}}$: chiral inversion clearance; $CL_{R \text{ or } S\text{-bupropion degradation}}$: degradation clearance, $CL_{eq}$: diffusional equilibrium.

**Table 4.10**. Population pharmacokinetic parameter estimates of S-bupropion from rat plasma protein binding experiment

| Parameter | Estimate (% CV) | Inter well variability (% CV) |
|---|---|---|
| S-bupropion incubated (plasma) | | |
| $f_u$ plasma, R-bupropion | 0.572 (1.07) | |
| $f_u$ plasma, S-bupropion | 0.574 (0.647) | |
| V plasma (mL) | 0.078 | |
| V buffer (mL) | 0.349 | 40.3 (26.8) |
| $CL_{R\text{-bupropion degradation, plasma}}$ (mL/hr) | 0.019 | |
| $CL_{S\text{-bupropion degradation, plasma}}$ (mL/hr) | 0.023 | 49.2 (13.7) |
| $CL_{S\text{-R-S, plasma}}$ (mL/hr) | 0.096 | |
| $CL_{S\text{-R-S, buffer}}$ (mL/hr) | 0.137 | |
| $CL_{eq}$ (mL/hr) | 100 | |
| Residual error (proportional) | | |
| R-bupropion, plasma | 0.036 (42.5) | |
| S-bupropion, plasma | 0.007 (55.5) | |
| R-bupropion, buffer | 0.227 (18.6) | |
| S-bupropion, buffer | 0.225 (15) | |

$f_u$: unbound fraction; V: volume; $CL_{R\text{-S-R or S-R-S}}$: chiral inversion clearance; $CL_{R \text{ or } S\text{-bupropion degradation}}$: degradation clearance; $CL_{eq}$: diffusional equilibrium.

The buffer and plasma inversion and loss terms derived from Pop-PK model of individual matrix experiments were fixed while developing models to estimate unbound fractions of enantiomers in the plasma and brain binding studies. The diffusional equilibrium term ($CL_{eq}$), characterizing transfer of bupropion from plasma (or brain) to buffer through the dialysis membrane, was not determined experimentally, however, on varying values from 0.1-100 mL/hour, it was found that $CL_{eq}$ did not impact the model derived estimates of plasma or brain binding. Since $CL_{eq}$ is dependent on the physicochemical properties of the drug, this was assumed to be the same for plasma and brain binding models. The model derived fraction unbound values for both

enantiomers in the two matrices (**Tables 4.7-4.10**) were close to their respective experimentally determined values (**Table 4.1**).

## 4.4 Discussion

We incubated R and S-bupropion in rat plasma, brain homogenate, 0.1 M phosphate buffer pH 7.4 and used a population modeling approach to distinctly characterize chiral inversion and degradation rates of the enantiomers in these matrices. Model derived parameters (chiral inversion and degradation clearances) were subsequently used to estimate unbound fractions of bupropion enantiomers in two matrices (plasma and brain).

Model predicted degradation half-life of ~two hours (**Table 4.6**) in rat plasma suggests that after almost three half-lives, about 12.5 % (based on first order degradation kinetics) would be remaining in plasma, which is consistent with the low plasma stability of ~10 % observed at the end of the five-hour incubation in the plasma binding study (**Table 4.1**). The degradation rate constants from the brain model suggest that enantiomers are stable over the five-hour binding study in rat brain. In this case, the low stability observed in brain (25 % for R and 45% for S-bupropion) could possibly be explained by loss due to chiral inversion. The model derived chiral inversion half-life indicates that 50% of R-bupropion is converted to S-bupropion in two hours, and S is converted to R in three hours; therefore, by five hours about 25% of R-bupropion and 40% of S-bupropion would be remaining. The slightly slower (~two-fold) model derived degradation rate of S-bupropion than R-bupropion in rat brain is consistent with two-fold higher stability of S over R-bupropion observed at the end of the brain binding experiments (**Table 4.1**).

The three-fold slower degradation rate, from **Table 4.6**, in brain than plasma explains the three-fold higher stability observed in brain homogenate than plasma in the binding studies (**Table 4.1**). Chiral inversion and degradation could be low in brain relative to plasma, possibly because of higher binding of drug to brain than plasma, thus shielding an enantiomer from degradation and chiral inversion.

The model predicted volume in buffer was approximately two-fold higher than the experimental incubation volume of 0.1 mL. However, for both plasma and brain inversion and binding studies, the estimated volume was close to 0.1 mL. This discrepancy in volume estimates

could possibly be explained by potential loss due to adsorption in buffer, which is minimized by proteins/lipids in plasma and brain.

In this study, we observed bupropion enantiomers were not stable in rat plasma, which is consistent with known low stability in human plasma (Laizure & DeVane, 1985). However, the plasma stability half-lives in rat versus human plasma vary. Degradation half-life of bupropion enantiomers presently observed in rat plasma was about two hours, whereas its reported to be 11.4 hours (at 37 ºC) in human plasma (Laizure & DeVane, 1985). The crude analytical technique, using 1 M NaOH or concentrated phosphoric acid to treat human plasma may partly explain the differences in half-lives between the two species (Laizure & DeVane, 1985). An independent and unpublished work by Desta et al to determine binding of bupropion enantiomers and diastereomers in human plasma indicate about ~ 43 % stability (calculated from the ratio of five hour sample to zero time sample) of bupropion enantiomers at the end of a 5-hour incubation, which suggest bupropion is four-fold more stable in human plasma than rat plasma. However, this study did not use a chiral assay and percent stability could possibly be derived from the total of R-bupropion and S bupropion formed from R-bupropion due to chiral inversion.

The observed superior stability (over 24-hours) of bupropion enantiomers in buffer compared to other matrices was supported by population modeling which evaluated modeling structure without a degradation term to be a better model than with a degradation term and by a study which reported half-life of racemic bupropion at pH 7.4, phosphate buffer to be about 7-9 days over 30 ºC (Kiptoo et al., 2009; O'Byrne et al., 2010).

Another important finding from our study is that chiral inversion of bupropion is inevitable in any aqueous media and these rates vary in different matrices. The rat plasma chiral inversion rate is two-fold higher than that predicted in human plasma by Sager et al (Sager et al., 2016). We established from our study that two processes, inversion and degradation occur simultaneously in plasma and that rate of inversion is faster than degradation. The previous study by Sager et al did not delineate these two processes and the incubation experiments were done for only one hour (Sager et al., 2016).

The inversion half-life in 0.1 M phosphate buffer pH 7.4, predicted from our model is about two-fold higher than the reported racemization half-life of about 44 minutes in 0.1 M phosphate

buffer, pH 7.6 in a very early study by Musso et al (Musso et al., 1993). This could possibly be attributed to the pH difference between buffer, suggesting that, like its influence on stability, a higher pH may be one of the factors that could influence the rate of chiral inversion.

The model predicted unbound fractions were close to experimentally derived values; therefore, degradation and chiral inversion did not seem to impact the fraction unbound values. Possible reasons for this could be establishment of pseudo-steady state from attainment of chiral inversion and degradation equilibrium in three matrices by about 5 hours, the incubation period we used for the plasma/brain binding experiment. Also, being a small, moderately bound molecule, diffusional equilibrium was also assumed to be attained well within 5 hours. Hence, this model could be used for small, low to moderately bound molecules which undergo inversion and degradation, with the latter being the rate limiting step. If inversion occurred at a slower rate (rate limiting step) than degradation, then the fraction unbound value of the formed enantiomer could not be correctly predicted.

There are a few limitations with the present model. This model may not be applicable for highly bound drugs, where potential for incomplete diffusional equilibrium within 5-hours exists. Incomplete attainment of diffusional equilibrium could possibly lead to incorrect estimation of unbound fraction. Also, the present model may not be applicable to molecules which exhibit saturable binding and when degradant produced competes for binding to the active site. In such cases, further experiments on elucidating concentration dependent kinetics, determination of binding affinities may be necessary.

Overall, through this study, we have distinctly characterized two processes (inversion and degradation) occurring in parallel in plasma and brain. Although the degradation of bupropion did not impact the fraction unbound values, stability of bupropion has implications for its therapeutic use, formulation, pharmacokinetics and use during analysis and storage. Based on results from protein and brain binding experiments, and further corroborated by an independent study by Laizure et al (Laizure & DeVane, 1985), instability does not seem to be major concern for hydroxy metabolites and reductive metabolites. To obtain further insights into the mechanism of chiral inversion between bupropion enantiomers, further studies, such as performed to elucidate phthalidomides` mechanism of inversion, are needed (Reist, Carrupt, Francotte, & Testa, 1998).

Additional in vivo studies involving separate administration of the individual enantiomers followed by superposition with profiles of racemic bupropion administration are needed to account for the biological loss, not fully captured by in vitro studies. Also, understanding species differences (rats versus humans) regarding mechanism(s) of these processes in plasma and brain may ultimately help in understanding interindividual variability associated with bupropion use.

# CHAPTER 5. DEVELOPMENT OF PLASMA-BRAIN TRANSLATIONAL POPULATION-PHARMACOKINETIC MODEL OF BUPROPION AND S, S-HYDROXYBUPROPION

**Hypothesis 4.** Development of rat-to-human translational population-pharmacokinetic model that describes the central nervous system disposition of bupropion and its metabolite (S, S-hydroxybupropion) will advance our understanding of intersubject variability in human bupropion response.

**Specific aim 4.** Develop a translational population-pharmacokinetic model characterizing plasma-brain transfer (blood-brain-barrier transport) to predict bupropion and pharmacologically active metabolite S, S-hydroxybupropion exposures in human brain (target site), and their relationship to pharmacologic potency measures at the dopamine transporter (DAT) and the norepinephrine transporter (NET).

## 5.1 Introduction

Bupropion, despite its proven efficacy as an antidepressant and smoking cessation aid, is associated with wide intersubject variability (Benowitz et al., 2013; Connarn et al., 2017; Connarn et al., 2016; Golden, De Vane, et al., 1988; Hesse et al., 2004; Laizure et al., 1985; Woodcock et al., 2012; A. Z. X. Zhu et al., 2012; Andy Z. X. Zhu et al., 2014). Variability in metabolism is thought to be driving variability in response (Benowitz et al., 2013; Gufford et al., 2016; Hesse et al., 2004; Kharasch et al., 2008; Masters et al., 2016; A. Z. X. Zhu et al., 2012; Andy Z. X. Zhu et al., 2014). Species differences in metabolism of bupropion leading to differences in bupropion`s effect in models of depression support this hypothesis (Butz et al., 1982; Carroll et al., 2014; Suckow et al., 1986). Bupropion undergoes complex phase 1 and 2 stereoselective metabolism (Coles & Kharasch, 2008; Gufford et al., 2016; Kharasch et al., 2008; Masters et al., 2016; Sager et al., 2016). Its pharmacology is reported to be stereoselective and is not fully understood (Damaj et al., 2004). Its phase 1 metabolite S, S-hydroxybupropion is reported to be more potent than R, R-hydroxybupropion and bupropion at the norepinephrine transporter (NET) and nicotinic acetylcholine receptors, and almost as potent as bupropion at the dopamine transporter (DAT)

(Damaj et al., 2004). Animal studies suggest that bupropion has greater efficacy in mice versus rats in rodent models of depression (indicated by anti-tetrabenazine activity) (Suckow et al., 1986).

Our study in liver microsomes characterized stereoselective phase 1 metabolism of bupropion in three nonclinical species (mice, rats, non-human primates) in comparison to humans (Bhattacharya et al., 2019). This study revealed that formation of S, S-hydroxybupropion in mice is higher than rats. This difference provides reasonable explanation for the observed pharmacological difference in mice versus rats given the greater potency of S, S-hydroxybupropion than bupropion enantiomers at some of the pharmacologic targets (Damaj et al., 2004). Through comparison of stereoselective metabolism using hepatic microsomes in these four species, we demonstrated that non-human primates (NHPs) had metabolism closest to humans and would be the appropriate surrogate species to improve understanding of bupropion`s central nervous system (CNS) disposition in humans. However, the cost and limited pharmacokinetic (PK) and pharmacodynamic (PD) data in NHPs were insurmountable barriers to conducting in vivo studies in NHPs.

Comparison of rat versus mouse hepatic microsomal incubation study results to humans, determined that, compared to mice, rats produced quantifiable amounts of all the phase 1 metabolites (Bhattacharya et al., 2019). Reductive metabolites are important as they are thought to contribute to some of bupropion`s therapeutic efficacy (Ascher et al., 1995; Bondarev et al., 2003; Martin et al., 1990; Schroeder, May 1983). Also, there are substantial PK and PD information from prior studies in rats that would support development of PK and PK/PD models in this species. For example, there are several rat brain microdialysis studies of various neurotransmitters (Cremers et al., 2016; Li et al., 2002; Nomikos GG1, 1992 ; Yeniceli et al., 2011). However, few of these studies have measured unbound brain and or plasma concentrations of bupropion and or hydroxybupropion (Cremers et al., 2016; Yeniceli et al., 2011). The majority of these microdialysis studies have measured changes in neurotransmitter levels (such as dopamine and norepinephrine) and behavioral changes following bupropion administration (Li et al., 2002; Nomikos GG1, 1992 ). There are also studies that report potency measures (half-maximal inhibitory concentration-$IC_{50}$ values) of bupropion enantiomers and hydroxybupropion diastereomers in rat cortical synaptosomes (Damaj et al., 2004; Lukas et al., 2010). Based on the

above listed reasons, the next species of choice to characterize bupropion`s stereoselective CNS disposition and subsequent model development was the rat.

A study by Cremers et al in Sprague Dawley rats measured unbound brain and unbound plasma concentrations of bupropion and S, S-hydroxybupropion. Their findings suggested carrier dependent uptake transport as the cause of an observed net asymmetry at the blood-brain-barrier (BBB) (Cremers et al., 2016). The Cremers et al study did not use a chiral assay. In our present study we used the same dose, route of administration, formulation, animal species with similar weight range as did Cremers et al. We expanded on this previous study by using a chiral assay that enabled measurement of bupropion enantiomers and phase 1 diastereomers, and, instead of microdialysis, we used unbound whole brain measures (obtained by correcting for fraction unbound values through in vitro rat brain binding studies). We saw a similar time-dependent change in uptake clearance across the BBB of bupropion enantiomers and S, S-hydroxybupropion following administration of 10 mg/kg of racemic bupropion and 2 mg/kg preformed S, S-hydroxybupropion.

Translational PK approaches such as compartmental-population PK and physiologically based PK (PBPK) models have improved general understanding of disposition and pharmacology of drugs in the CNS (Badhan, Chenel, & Penny, 2014; Ball, Bouzom, Scherrmann, Walther, & Declèves, 2014; Gaohua, Neuhoff, Johnson, Rostami-Hodjegan, & Jamei, 2016; William Kielbasa et al., 2009; W. Kielbasa & Stratford, 2012; van Gaalen et al., 2019; Yamamoto et al., 2017). A bottom-up PBPK approach is data demanding, that is, it requires extensive in vitro studies, as well as knowledge of membrane transporters and metabolic enzymes to support model development (Jones & Rowland-Yeo, 2013; Miller, Reddy, Heikkinen, Lukacova, & Parrott, 2019). At present, lack of robust in vitro blood-barrier-models, limited information on brain transporters, their expression, abundance, or of brain metabolic enzymes in humans and other species, may not fully support development of a bottom up PBPK approach. Alternately, a top-down approach, such as population-based modeling, which uses data from multiple in vivo studies to support model development, as shown in the case of atomoxetine and duloxetine (William Kielbasa et al., 2009; W. Kielbasa & Stratford, 2012), may be used to characterize plasma-brain transfer of bupropion and S, S-hydroxybupropion.

The goal of the present study was to combine the former microdialysis study with another study (referred to henceforth as "present" or "2019" study) that used chiral analysis of bupropion and hydroxy-bupropion plasma and brain concentrations through a population-pk modeling approach. Through this effort, we hoped to improve understanding of BBB transport of these molecules, particularly with respect to time-dependent brain influx clearance ($CL_{in}$) implicated in the microdialysis study. Modeling BBB transport as bi-directional distributional clearance terms, we subsequently scaled rat parameters to human values using traditional allometric scaling to predict human brain concentrations of bupropion enantiomers and hydroxy-bupropion diastereomers. This approach allowed us to compare predicted human brain concentrations to pharmacologic potency measures of bupropion and hydroxybupropion at DAT and NET to create insight regarding the particular enantiomer (parent) and diastereomer (hydroxybupropion metabolite) inhibitory potentials at these two targets.

## 5.2 Methods

### 5.2.1 Pharmacokinetic study in animals.

Racemic bupropion (10 mg/kg) and S, S-hydroxybupropion (2 mg/kg) were administered subcutaneously to adult male Sprague Dawley rats (290–330 g, n = 24/compound). The experiments were approved by the Institutional Animal Care and Use Committee (IACUC, Indiana University School of Medicine). Brain and plasma were collected from rats (n = 3) at eight time points over a period of 6 hours and analyzed using a chiral LC-MS/MS method described in **Chapter 3**. Rat plasma protein and brain homogenate binding studies for R and S-bupropion, R, R- and S, S-hydroxybupropion were conducted to correct for unbound fraction in both matrices using a 96-well equilibrium dialysis method, as also described in **Chapter 3**. To support population PK analysis, this study was combined with a study published by Cremers et al in 2016 (Cremers et al., 2016). That study used microdialysis to measure unbound plasma and brain concentrations. Briefly, 10 mg/kg of racemic bupropion or 2 mg/kg of S, S-hydroxybupropion, each dissolved in 0.9% NaCl (2 mg/mL), were administered subcutaneously to 4-5 adult male Sprague Dawley rats (280-350 g). Dialysates from brain (probe in medial prefrontal cortex) and

jugular vein were collected every 30 minutes starting 1 hour prior to administration and continuing for 6 hours after administration. All the samples (from both studies) were stored at -80 ˚C until time of analysis by LC-MS/MS assay. This microdialysis study did not use a chiral assay.

### 5.2.2 Pharmacokinetic analysis

All Population PK analyses were conducted with Phoenix NLME 8.1 (Pharsight Corporation, Certara, L.P., Princeton NJ). Unbound hepatic clearances scaled from rat hepatic microsomal incubations of R and S-bupropion were different (0.29 L/hr and 0.04 L/hr respectively), but the apparent unbound plasma clearances (which are the sum of hepatic, renal and other clearance routes) of the enantiomers from the NCA analysis of the 2019 in vivo study were similar (2. 3 and 2.5 L/hr, respectively, as elaborated in **Chapter 3**). This suggested possible extrahepatic routes of disposition, which could be stereoselective. Since other clearance mechanisms and metabolites that could possibly explain the in vitro-in vivo discrepancy are at present not fully understood or characterized, we summed concentrations of R and S-bupropion measured in the 2019 study to get racemic bupropion concentrations in plasma and brain, and subsequently used these concentrations for population model development of the combined 2019 and 2016 (microdialysis) studies.

Unbound brain to unbound plasma exposure ratio ($K_{p,uu}$), both observed (AUC ratio) and predicted ($CL_{in}/CL_{out}$ ratio),was calculated using the below equation, where AUC is area under curve, $CL_{in}$ is brain influx clearance, $CL_{out}$ is brain efflux clearance, $CL_{passive}$ is passive permeability clearance, $CL_{active\ uptake}$ is clearance due to active uptake, $CL_{active\ efflux}$ is clearance due to active efflux, $CL_{metabolism}$ is clearance due to within brain metabolism and $CL_{bulk\ flow}$ is clearance due to bulk extracellular fluid flow draining to ventricles as CSF (Hammarlund-Udenaes et al., 2008; Andreas Reichel, 2015).

$$K_{p,uu} = \frac{AUC_{0-6hr,brain}}{AUC_{0-6hr,plasma}} \quad \text{.....Equation 5.1}$$

$$K_{p,uu} = \frac{CL_{in}}{CL_{out}}$$ .....Equation 5.2

$$K_{p,uu} = \frac{CL_{passive} + CL_{active\ uptake} - CL_{active\ efflux}}{Cl_{passive} + CL_{active\ efflux} - CL_{active\ uptake} + CL_{metabolism} + CL_{bulk\ flow}}$$ .....Equation 5.3

A population modeling approach similar to Cremers et al (Cremers et al., 2016) was used in this combined PK analysis of the two studies. Models in plasma, followed by plasma-brain models, were built for each administered compound (racemic bupropion and S, S hydroxybupropion). Model building for each of the dose groups proceeded initially using data from our present study (2019), and then combined with the microdialysis study (2016). Different plasma model structures were evaluated for each dose group. These included one and two compartment disposition, and zero order versus first order absorption, including with or without a time lag.

Experimentally obtained apparent unbound brain volume of distribution ($V_{u,brain}$) of bupropion and S, S-hydroxybupropion from the brain binding studies in rats reported in **Chapter 3** were found to be similar (around 8 mL/g). However, computationally derived values of 16 mL/g (28.8 mL) and 5 ml/g (9 mL) (for bupropion and S, S-hydroxybupropion, assuming brain weight of 1.8 g respectively), used by Cremers et al (Cremers et al., 2016), were adopted for the present analysis. This is because it has been shown that, unlike the brain slice technique, $V_{u,brain}$ from the brain homogenate method may not correctly capture brain distribution to that obtained through in vivo microdialysis, which is considered the gold standard for $V_{u,brain}$ determination (Fridén et al., 2007). Unfortunately, $V_{u,brain}$ was not determined in the 2016 study. Limitations associated with the brain homogenate technique have been noted (Fridén et al., 2007). Due to disruption of cell membranes in brain homogenate technique, it is not possible to differentiate between intra and extracellular distribution (Fridén et al., 2007).

Different bupropion and S, S-hydroxybupropion blood-brain-barrier dispositional model structures were evaluated. These were a single distributional clearance (Q), separate parameters for uptake ($CL_{in}$) and efflux ($CL_{out}$) distributional clearances, with or without time dependency on either uptake or efflux brain clearance or both.

After optimization of plasma or plasma-brain models of bupropion and preformed S, S-hydroxybupropion, plasma formation clearance ($CL_{f,\ SS\text{-}OHBUP}$) of S, S-hydroxybupropion was estimated after combining plasma bupropion (2019 and 2016 studies), preformed S,S-hydroxybupropion (2019 and 2016 studies), and formed S, S-hydroxybupropion (2019 study only). Following development of this combined plasma-brain model of bupropion and S, S-hydroxybupropion, the possibility of within-brain metabolism was also explored. Plasma and plasma-brain models of bupropion and S, S-hydroxybupropion that also included R, R-hydroxybupropion (formed metabolite from the present study) were also evaluated.

Due to limited sampling per animal (single plasma/brain sample per time point) from the present study, estimation of inter-animal variability was not feasible when modeling this study alone. However, after combining this study with the microdialysis study, between-animal variability regarding bupropion (combined enantiomers) and S, S-hydroxybupropion PK parameters was estimated. A log-normal distribution based on the exponential relationship, $P_i = P_{tv} \times \exp(\eta_i)$, where $P_i$ is the parameter estimate of clearance for the $i^{th}$ animal, $P_{tv}$ is the population typical value and $\eta_i$ is the deviation from the population value of the $i^{th}$ animal was assumed. Various residual error models were also evaluated. These were additive, proportional, and mixed additive – proportional. A proportional error model was eventually selected for the three matrices for bupropion and S,S-hydroxybupropion, based on $Y = F \times (1 + EPS(1))$, where Y is the observed dependent-variable, F is the corresponding individual specific model prediction and EPS is the residual error. For the two studies, there were 313 observations and 58 animals in the combined plasma-brain model of bupropion and S, S-hydroxybupropion (formed and pre-formed).

At all levels of model development, evaluation of model performance to predict observed concentrations was based on the objective function and precision of PK parameter estimates. In addition, visual inspection of goodness-of-fit plots (conditional weighted residual versus either population predicted or time after dose plots, as well as the observed versus individual predicted and population predicted concentration plots) was used. Upon expanding plasma models to include brain disposition predictions, stability of plasma parameter estimates was also used to support the final plasma-brain model structure. For the final model, a visual predictive check with 500 replicates was conducted.

***Human simulations***

The final rat plasma-brain model was scaled to predict steady-state human unbound brain exposure to bupropion and S, S-hydroxybupropion. Unbound brain fraction, and thereby $V_{u,brain}$, was assumed to be similar across species as suggested by Di et al (Di et al., 2011). A 150-mg dose of the extended-release (SR) bupropion product administered twice daily was selected based on studies of bupropion plasma PK using this formulation and dose frequency (J. A. Johnston et al., 2001; Learned-Coughlin et al., 2003). Bupropion plasma pharmacokinetic parameters used for the simulations were based on these studies and corrected for plasma protein binding of 85% (Jefferson, Pradko, & Muir, 2005). These were 1050 L/hr for CL/F and 12,400 liters for $V_D$/F. An absorption rate constant ($k_a$) of 0.6 $hr^{-1}$, which yielded a $t_{max}$ of 3 hours, the reported value for the SR formulation (Jefferson et al., 2005), was used. Consequently, bupropion steady-state plasma concentrations were between the reported average concentrations from the two multiple dose studies (J. Andrew Johnston et al., 2002). Both bupropion and hydroxybupropion pharmacokinetics are linear after long-term bupropion administration of 300–400 mg/d (Jefferson et al., 2005). Weight based allometric scaling of the rat plasma-brain distributional clearance (CL) and brain volume was used to derive the corresponding human brain parameters, using a rat brain weight of 2.45 g (1.8 g/250 g body weight (Davies & Morris, 1993)) and a human brain weight of 1.35 kg. The exponential factors were 0.75 for CL and 1.0 for brain distribution volume ($V_{u,brain}$). A total of 500 simulations was conducted. The rat to human formation clearance of S, S-hydroxybupropion, also obtained from allometric scaling, was 3.34 L/hr. This value is close to the hepatic formation clearance estimate of 4.4 L/hr derived from our published intrinsic formation clearance human hepatic microsome results (**Chapter 2**) (Bhattacharya et al., 2019). Further, the formation clearance calculated from the ratio of AUC of formed metabolite (S, S-hydroxybupropion $AUC_{0-\infty}$ 580 nM (Masters et al., 2016)) to parent (bupropion $AUC_{0-\infty}$ 1334 nM (Masters et al., 2016)), along with clearance of S, S-hydroxybupropion of 13.7 L/hr (Nora D. Volkow et al., 2005) from NCA analysis of digitized radafaxine (preformed S, S-hydroxybupropion) from a clinical trial, was 5.86 L/hr, which is close to the allometrically scaled value.

## 5.3 Results

Unbound plasma and brain exposure profiles of bupropion and preformed S, S-hydroxybupropion in rats from the 2019 and 2016 studies are shown in **Figure 5.1**.

**Figure 5.2** provides a summary of unbound brain to unbound plasma concentration ratio versus time profiles of bupropion, preformed S, S-hydroxybupropion from the 2019 and 2016 studies, and formed S, S-hydroxybupropion from the 2019 study.

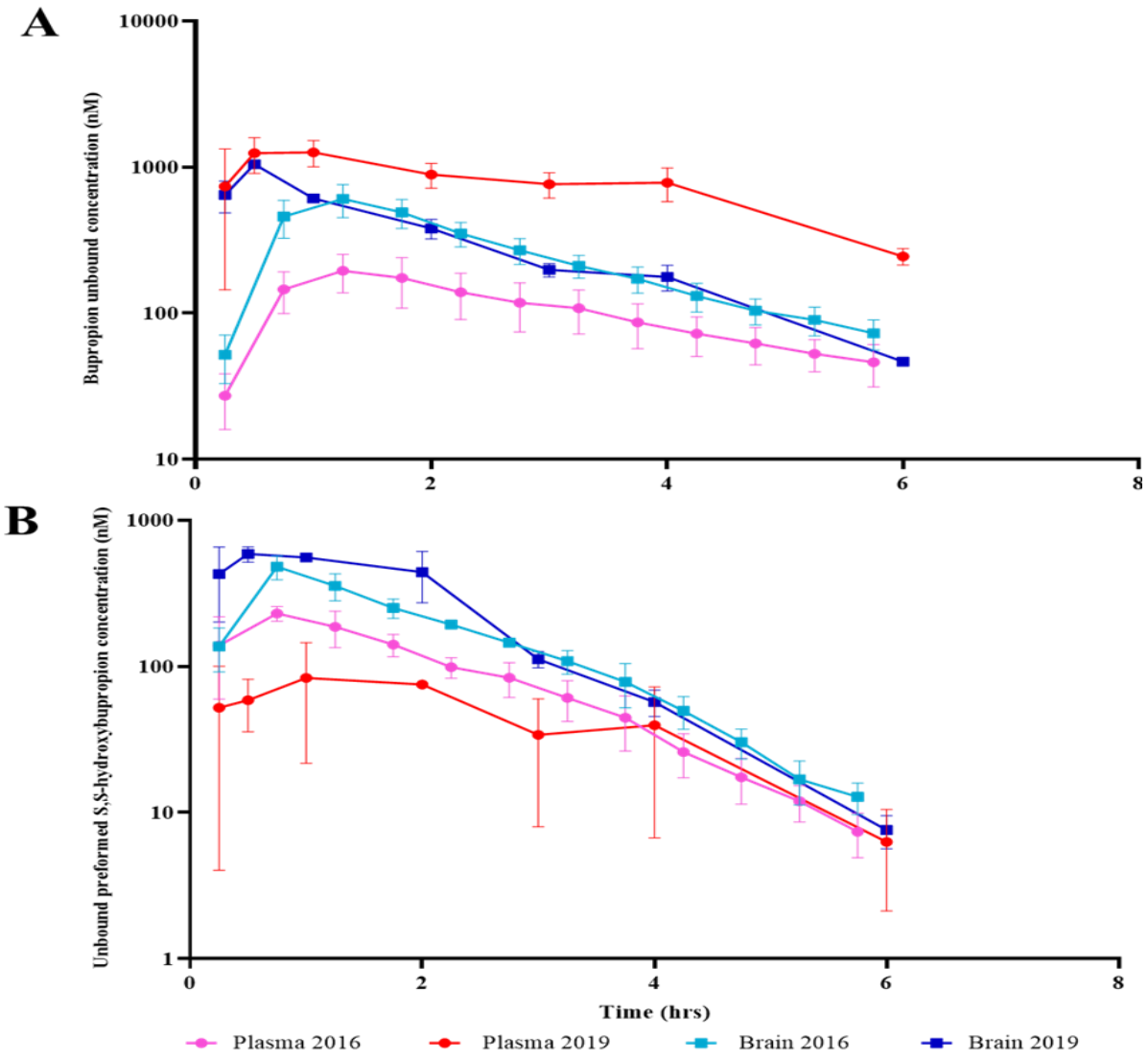


**Figure 5.1.** Mean unbound plasma and brain concentration time profiles of **A (Top)** bupropion and **B (Bottom)** preformed S, S-hydroxybupropion following subcutaneous administration of 10 mg/kg racemic bupropion and 2 mg/kg of preformed S, S-hydroxybupropion, respectively to adult male Sprague Dawley rats. Symbols and error bars denote observed means and standard deviation (n = 3 or 4 animals at each time point) respectively. Red and blue lines represent unbound plasma and brain profiles from the present study (corrected for unbound fraction through in vitro studies, 2019). Pink and light blue lines represent unbound plasma and brain profiles from the microdialysis study (2016).

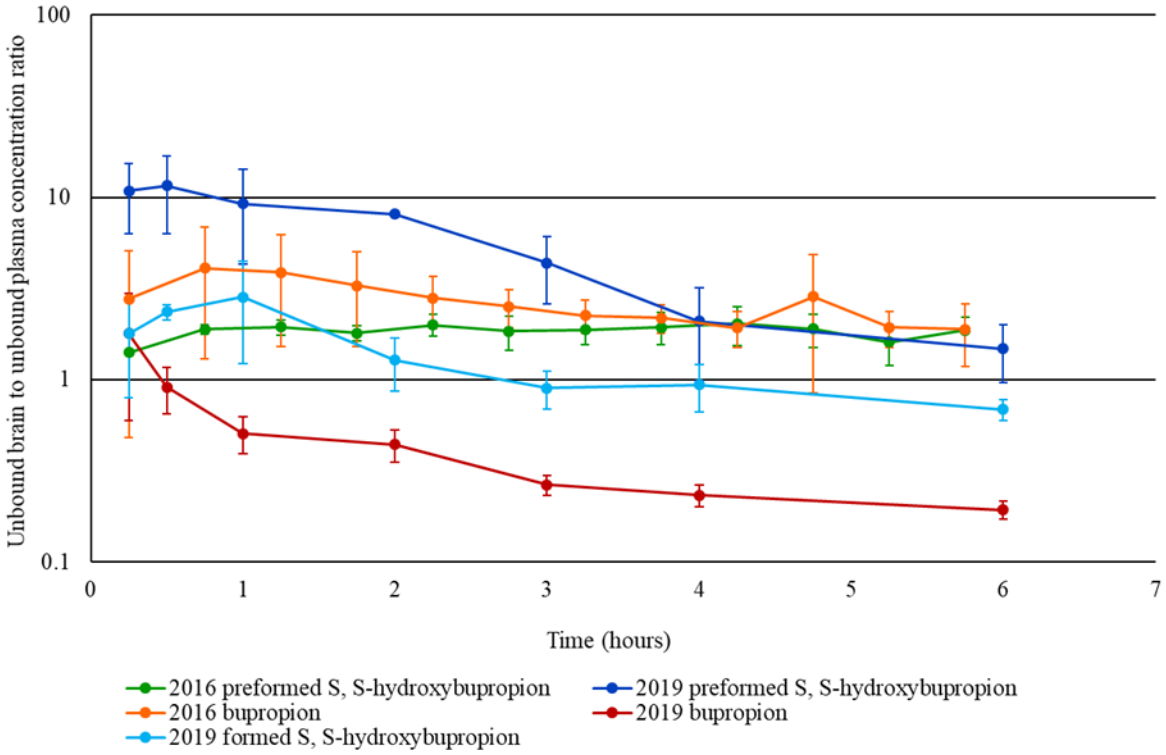


**Figure 5.2.** Mean unbound brain to unbound plasma concentration ratio time profiles of bupropion and S, S-hydroxybupropion (formed or preformed) following 10 mg/kg subcutaneous administration of racemic bupropion or 2 mg/kg preformed S, S-hydroxybupropion to adult male Sprague Dawley rats from two studies. Present study results indicated by "2019" represents unbound plasma and brain concentration derived after correcting for fraction unbound in plasma and brain through in vitro rat plasma and brain binding assay. Microdialysis study results which represent unbound plasma and unbound brain concentration are indicated by "2016" in figure legend. Symbols and error bars denote observed means and standard deviation (n=3 at each time point).

Results from non-compartmental analysis of unbound concentrations of bupropion, formed and preformed S, S-hydroxybupropion in rat plasma and brain are shown in **Table 5.1**.

**Table 5.1.** Observed unbound pharmacokinetic parameters from non-compartmental analysis. Results are shown for both rat plasma and brain after subcutaneous administration of 10 mg/kg of racemic bupropion or 2 mg/kg S, S-hydroxybupropion to adult male Sprague Dawley rats.

| | Rat pharmacokinetic parameters (unbound) | | | | | | |
|---|---|---|---|---|---|---|---|
| | Plasma | | | Brain | | | |
| Analyte | Half-life | $C_{max}$ | $AUC_{0-\infty}$ | Half-life | $C_{max}$ | $AUC_{0-\infty}$ | $K_{p,uu}$ |
| units | hours | nM | nM*h | hours | nM | nM*h | |
| BUP (present study, 2019) | 1.7 | 1262 | 5275 | 1.3 | 1049 | 1995 | 0.37 |
| BUP (microdialysis, 2016) | 2.2 | 198 | 770 | 1.8 | 607 | 1643.6 | 2.13 |
| Formed SS-OHBUP (present study, 2019) | 2.5 | 6.8 | 34.3 | 1.9 | 8.9 | 32.4 | 0.94 |
| Formed total OHBUP (present study, 2019) | 2.5 | 17 | 85.9 | 1.9 | 20.7 | 82.9 | 0.96 |
| Formed total OHBUP (microdialysis, 2016) | 1.7 | 15 | 44 | 1.6 | 23 | 70.8 | 1.61 |
| Preformed SS-OHBUP (present study, 2019) | 1.2 | 83.3 | 283. | 0.8 | 586.2 | 1396.8 | 4.93 |
| Preformed SS-OHBUP (microdialysis, 2016) | 0.8 | 175.2 | 497.2 | 0.8 | 479.7 | 941.1 | 1.89 |

BUP: bupropion; OHBUP: hydroxybupropion; $C_{max}$: maximum concentration; AUC: Area Under Curve; $K_{p,uu}$: Unbound brain $AUC_{0-\infty}$ to unbound plasma $AUC_{0-\infty}$ ratio.

As shown in **Table 5.1**, a 7-fold difference in unbound bupropion plasma AUC between the 2019 and the previous microdialysis study was observed. Since unbound extrapolated areas for plasma and brain were ≤ 25% for bupropion enantiomers, preformed S, S-hydroxybupropion and formed hydroxybupropion diastereomers (described in **Chapter 3**), we used $AUC_{0-\infty}$ for calculating $K_{p,uu}$ and for making comparisons across studies. From **Figure 5.1 (A)**, parallel plasma post-distribution kinetics (2-6 hours) suggest that the first order elimination rate constant, k, is similar, i.e, apparent volume of distribution and apparent oral clearance are similar between these two studies (k = Cl/V). Unlike plasma, the unbound brain AUCs for the two studies were similar (within two-fold). The time to peak concentration, $t_{max}$, for plasma and brain were similar within a given study. Slightly faster terminal phase decline in brain relative to plasma is also consistent for the two studies. From **Figure 5.1 (A)**, parallel plasma and brain terminal profiles (2-6 hours)

suggest distribution equilibrium was achieved in both the studies. Results from the microdialysis study suggested possible net uptake of bupropion at the blood-brain-barrier; whereas, in the present study, results suggest net bupropion efflux at the blood-brain-barrier.

From **Table 5.1** and **Figure 5.1 (B)**, we observed that the unbound plasma and brain exposures of preformed S, S-hydroxybupropion were similar (within 2-fold) between the two studies, both suggesting net uptake at the blood-brain barrier, more prominent with the present study results.

The discrepancy in bupropion unbound plasma exposures was hypothesized to be due to instability of bupropion in plasma, which is more likely to affect the magnitude of exposures rather than fractional elimination rate. Recoveries from the plasma microdialysis study were also not reported (Cremers et al., 2016). This hypothesis of markedly different bupropion plasma exposures for the two studies due to instability in plasma and different control of this between the studies was tested by a modeling approach. Unique relative bioavailability terms were assigned for the two studies to support simultaneous, population PK-based, estimation of study-independent apparent volume of distribution and clearance parameters. Based on precision of parameter estimates (**Table 5.2**) and graphical goodness-of-fit analyses, a good model was developed from this approach. Bioavailability of bupropion from the 2016 study was 10 % relative to the present study. The difference was attributed to post-sample collection instability of bupropion in the plasma from the 2016 study. Our stability studies of bupropion enantiomers in rat plasma, brain and buffer indicate bupropion is highly unstable in plasma (plasma degradation half-life of bupropion enantiomers is about 2 hours, as described in **Chapter 4**). S, S-hydroxybupropion was stable in rat plasma and brain from these stability studies. Therefore, we ascribe the difference in bupropion plasma exposures between the two studies to instability of bupropion in plasma following sample collection, possibly due prolonged storage at ambient temperature of collected microdialysate samples. Hence, plasma data of bupropion from the 2016 microdialysis study was excluded from the population PK modeling work.

**Figure 5.3** provides a summary of the population-pk model building approach used to develop the final combined plasma-brain model of bupropion and S, S-hydroxybupropion (preformed plus formed).

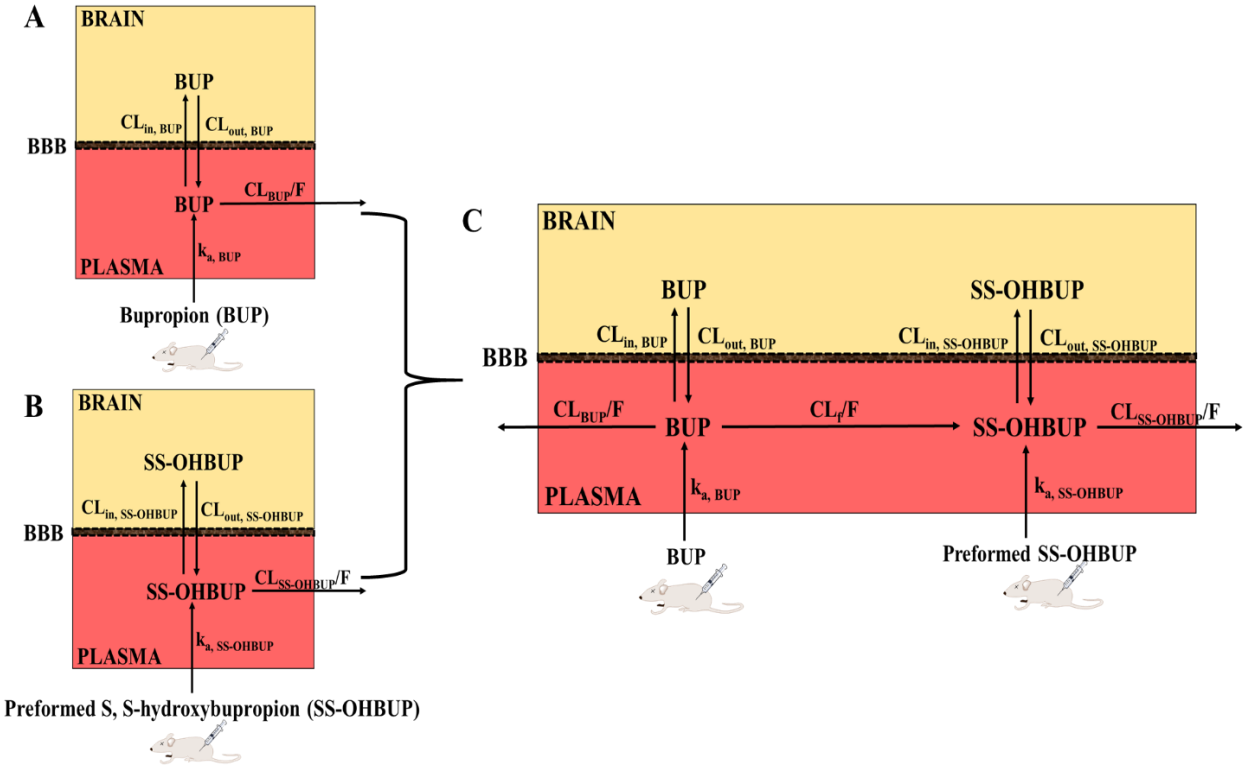


**Figure 5.3**. Plasma-brain compartmental pharmacokinetic model of bupropion, formed and preformed S, S-hydroxybupropion in rats. BUP: Bupropion; SS-OHBUP: S, S-hydroxybupropion; BBB: Blood-brain-barrier; $k_a$: absorption rate constant; $CL_{in}$: uptake clearance; $CL_{out}$: efflux clearance; CL/F: oral clearance; $CL_f/F$: formation clearance. **A (Top left)** represents plasma-brain model of racemic bupropion; **B (Bottom left)** represents plasma-brain model of preformed S, S-hydroxybupropion; **C (Right)** represents combined plasma-brain model of bupropion, formed and preformed S, S-hydroxybupropion.

For both bupropion and preformed S, S-hydroxybupropion, a one-compartment model provided the best description of the plasma concentration time courses, which is consistent with graphical observation of monoexponential decline in the respective profiles from the present study and the 2016 microdialysis study (**Figures 5.1 A** and **B**). Despite excluding bupropion plasma data from the 2016 microdialysis study, a model with unique absorption rate constants, ($k_a$ as covariate) fit the data better than a single $k_a$ value. This is in line with visual inspection of unbound brain profiles shown in **Figure 5.1 (A)** and not inconsistent with the hypothesis of plasma instability of bupropion. As the formulations were same for both studies (bupropion hydrochloride dissolved in

0.9% NaCl, 2 mg/mL), study specific absorption rate constants are attributed to different sampling methods, microdialysis sampling in 2016 study was over 30-minute window, versus discrete time points used in the present 2019 study. Bupropion, being a biopharmaceutical classification system (BCS) class 1 drug (Connarn et al., 2017) (high solubility, high permeability) and a small molecule (molecular weight of 239.74 g/mol), one would expect a rapid absorption (indicated by $k_a$) as seen in present study. It seems the timepoints in 2016 microdialysis study could not capture this rapid absorption.

For both bupropion and S, S-hydroxybupropion from the present study, and after combining with microdialysis data, a plasma-brain model with time dependency on $CL_{in}$ provided a superior fit than other model structures. The time-dependent component to $CL_{in}$ for bupropion or S, S-hydroxybupropion was expressed as $CL_{in}= CL_{in0}$-slope*time, where $CL_{in}$ decreases with time (slope) up to 3 hours and is constant thereafter. This model structure is consistent with that reported for bupropion from the microdialysis study (Cremers et al., 2016). In that previous study, time dependency was not reported for S, S-hydroxybupropion; however, in the present study, this time dependency on $CL_{in}$ fitted the data better.

**Tables 5.2** and **5.3** summarize plasma and brain bupropion and preformed S, S-hydroxybupropion specific population-pk model estimates, respectively, when combining the two studies. **Table 5.4** provides a summary of the plasma and brain unbound bupropion and S, S-hydroxybupropion PK parameters obtained in the final population PK model that combined both formed and pre-formed metabolite concentrations.

**Table 5.2.** Population pharmacokinetic parameter estimates of bupropion in rat plasma and brain.

| Parameter | Estimate (% CV) | Inter animal variability (% CV) | 2.5 % CI | 97.5 % CI |
|---|---|---|---|---|
| $k_{a\ BUP,\ 2016}$ ($hr^{-1}$) | 0.87 (14.89) | | 0.61 | 1.13 |
| $k_{a\ BUP,\ 2019}$ ($hr^{-1}$) | 3.62 (22.48) | | 2.01 | 5.23 |
| $V/F_{\ BUP}$ (L) | 7.33 (7.34) | | 6.27 | 8.40 |
| $CL/F_{\ BUP}$ (L/hr) | 2.52 (5.81) | 6.43 (1.61) | 2.23 | 2.82 |
| $V_{b,\ BUP}$ (L) | 0.01 (fixed) | | | |
| $CL_{in0,\ BUP}$ | 17.28 (5.98) | | 15.23 | 19.33 |
| $CL_{out,\ BUP}$ (L/hr) | 25.19 (17.57) | | 16.43 | 33.97 |
| slope | 3.86 (fixed) | | | |
| Residual error (proportional) | | | | |
| BUP, plasma | 0.31 (18.88) | | 0.20 | 0.43 |
| BUP, brain | 0.31 (10.86) | | 0.25 | 0.38 |

BUP: bupropion; CL/F: apparent elimination clearance; $k_a$: first-order rate constant for absorption; V/F: apparent systemic volume of distribution; $V_b$: apparent brain volume of distribution; $CL_{in0}$: apparent influx clearance at initial time; $CL_{out}$: apparent efflux clearance; slope: slope relating time-dependent change in $CL_{in}$; F: bioavailability fraction (1).

**Table 5.3.** Population pharmacokinetic parameter estimates of preformed S, S-hydroxybupropion in rat plasma and brain.

| Parameter | Estimate (% CV) | Inter animal variability (% CV) | 2.5 % CI | 97.5 % CI |
|---|---|---|---|---|
| $k_{a\ SS\text{-}OHBUP}$ ($hr^{-1}$) | 0.95 (3.46) | | 0.89 | 1.02 |
| $V/F_{\ SS\text{-}OHBUP}$ (L) | 4.66 (7.99) | 6.75 (2.01) | 3.93 | 5.40 |
| $CL/F_{\ SS\text{-}OHBUP}$ (L/hr) | 5.76 (7.20) | | 4.95 | 6.59 |
| $V_{b,\ SS\text{-}OHBUP}$ (L) | 0.005 (fixed) | | | |
| $CL_{in0,\ SS\text{-}OHBUP}$ | 20.58 (16.19) | | 13.99 | 27.18 |
| $CL_{out,\ SS\text{-}OHBUP}$ (L/hr) | 5.83 (31.92) | | 2.15 | 9.52 |
| slope | 3.86 (fixed) | | | |
| Residual error (proportional) | | | | |
| SS-OHBUP, plasma | 0.36 (14.14) | | 0.27 | 0.47 |
| SS-OHBUP, brain | 0.28 (12.97) | | 0.21 | 0.36 |

SS-OHBUP: S, S-hydroxybupropion; CL/F: apparent elimination clearance; $k_a$: first-order rate constant for absorption; V/F: apparent systemic volume of distribution; $V_b$: apparent brain volume of distribution; $CL_{in0}$: apparent influx clearance at initial time; $CL_{out}$ :apparent efflux clearance; slope: slope relating time-dependent change in $CL_{in}$; F: bioavailability fraction (1).

Attempts to estimate inter-individual variability in combined bupropion-S, S-hydroxybupropion (formed and preformed) model were unsuccessful. As the interindividual variability on apparent clearance or volume of distribution of bupropion or preformed S, S-hydroxybupropion models were small, ultimately a naïve-pooled approach was adopted for the final combined model.

**Table 5.4.** Population pharmacokinetic parameter estimates of bupropion and S, S-hydroxybupropion in rat plasma and brain from combined model analyses.

| Parameter | Estimate | CV% | 2.5 % CI | 97.5 % CI |
|---|---|---|---|---|
| $k_{a\ BUP,\ 2016}$ ($hr^{-1}$) | 0.87 | 33.39 | 0.29 | 1.44 |
| $k_{a\ BUP,\ 2019}$ ($hr^{-1}$) | 3.62 (fixed) | | | |
| $V/F_{\ BUP}$ (L) | 7.33 (fixed) | | | |
| $CL/F_{\ BUP}$ (L/hr) | 2.78 | 8.72 | 2.30 | 3.26 |
| $k_{a\ SS\text{-}OHBUP}$ ($hr^{-1}$) | 0.86 | 12.37 | 0.65 | 1.07 |
| $CL_f/F$ (L/hr) | 0.05 | 31.25 | 0.02 | 0.08 |
| $V/F_{SS\text{-}OHBUP}$ (L) | 5.70 (fixed) | | | |
| $CL/F_{SS\text{-}OHBUP}$ (L/hr) | 6.98 | 15.24 | 4.88 | 9.08 |
| Residual error (proportional) | | | | |
| BUP, plasma | 0.47 | 26.83 | 0.22 | 0.73 |
| SS-OHBUP, plasma | 0.75 | 33.80 | 0.25 | 1.26 |
| $V_{b,\ BUP}$ (L) | 0.01 (fixed) | | | |
| $CL_{in0,\ BUP}$ | 19.85 | 13.31 | 14.65 | 25.05 |
| $CL_{out,\ BUP}$ (L/hr) | 31.66 | 21.37 | 18.34 | 44.98 |
| $V_{b,SS\text{-}OHBUP}$ (L) | 0.005 (fixed) | | | |
| $CL_{in0,\ SS\text{-}OHBUP}$ | 21.31 | 19.05 | 13.32 | 29.30 |
| $CL_{out,SS\text{-}OHBUP}$ (L/hr) | 5.30 | 39.55 | 1.17 | 9.44 |
| slope | 3.86 | | | |
| Residual error (proportional) | | | | |
| BUP, brain | 0.38 | 10.04 | 0.31 | 0.46 |
| SS-OHBUP, brain | 0.42 | 11.36 | 0.33 | 0.52 |

BUP: bupropion; SS-OHBUP: S, S-hydroxybupropion; CL/F: apparent elimination clearance; $CL_f/F$ : S, S-hydroxybupropion formation clearance; $k_a$: first-order rate constant for absorption; V/F: apparent systemic volume of distribution; $V_b$: apparent brain volume of distribution; $CL_{in0}$: apparent influx clearance at initial time; $CL_{out}$ :apparent efflux clearance; slope: slope relating time-dependent change in $CL_{in}$; F: bioavailability fraction (1).

The ratio of S, S-hydroxybupropion formation clearance to total bupropion clearance from the compartmental model was 1.8 %. This value is close to 1.5 %, which is calculated from the AUC fractions of formed S, S-hydroxybupropion relative to bupropion. The model derived $K_{p,uu}$ was 0.26 ± 0.03 for bupropion and 1.83 ± 0.22 for S, S-hydroxybupropion, both in close agreement with AUC ratio estimates from NCA analysis in **Table 5.1**.

A model structure that incorporates within brain metabolism was also evaluated. However, this model did not improve model performance compared to a model without brain formation clearance.

**Figures 5.4** and **5.5** are graphical summaries of observed vs predicted, conditional weighted residuals in plasma and brain unbound concentrations of bupropion and preformed S, S-hydroxybupropion. **Figure 5.6** summarizes observed versus predicted unbound concentrations in plasma and brain from the final population PK model that combined bupropion, and both formed and pre-formed metabolite.

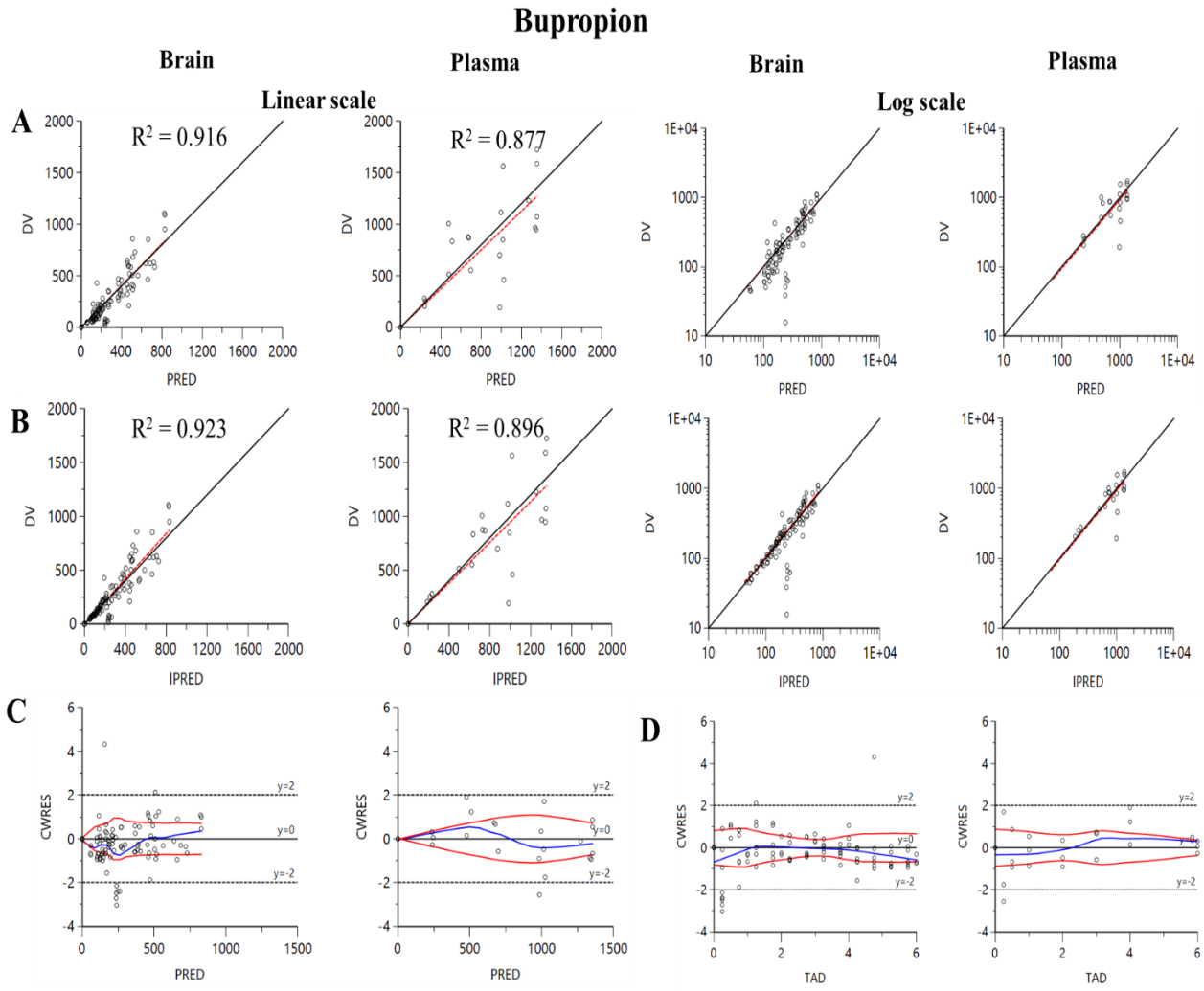


**Figure 5.4.** Model diagnostic plots for unbound bupropion concentrations in plasma and brain. **A (Top)**: Population predicted concentrations versus observed concentrations in brain and plasma (linear scale on LHS and log scale on RHS). **B (Middle panel)**: Individual predicted concentrations versus observed concentrations in brain and plasma (linear scale on LHS and log scale on RHS). The black solid line is the line of unity and the red-dashed line is the best fit line from linear regression. Shown above each figure is the associated linear regression correlation coefficient ($R^2$). **C (Bottom left panel)**: Conditional weighted residuals versus population predicted concentrations in brain and plasma. **D (Bottom right panel)**: CWRES, Conditional weighted residuals; DV observed concentration; IPRED, Individual predicted; PRED, Population predicted; TAD, Time After Dose. Units of concentration and time are nanomolar (nM) and hours respectively.

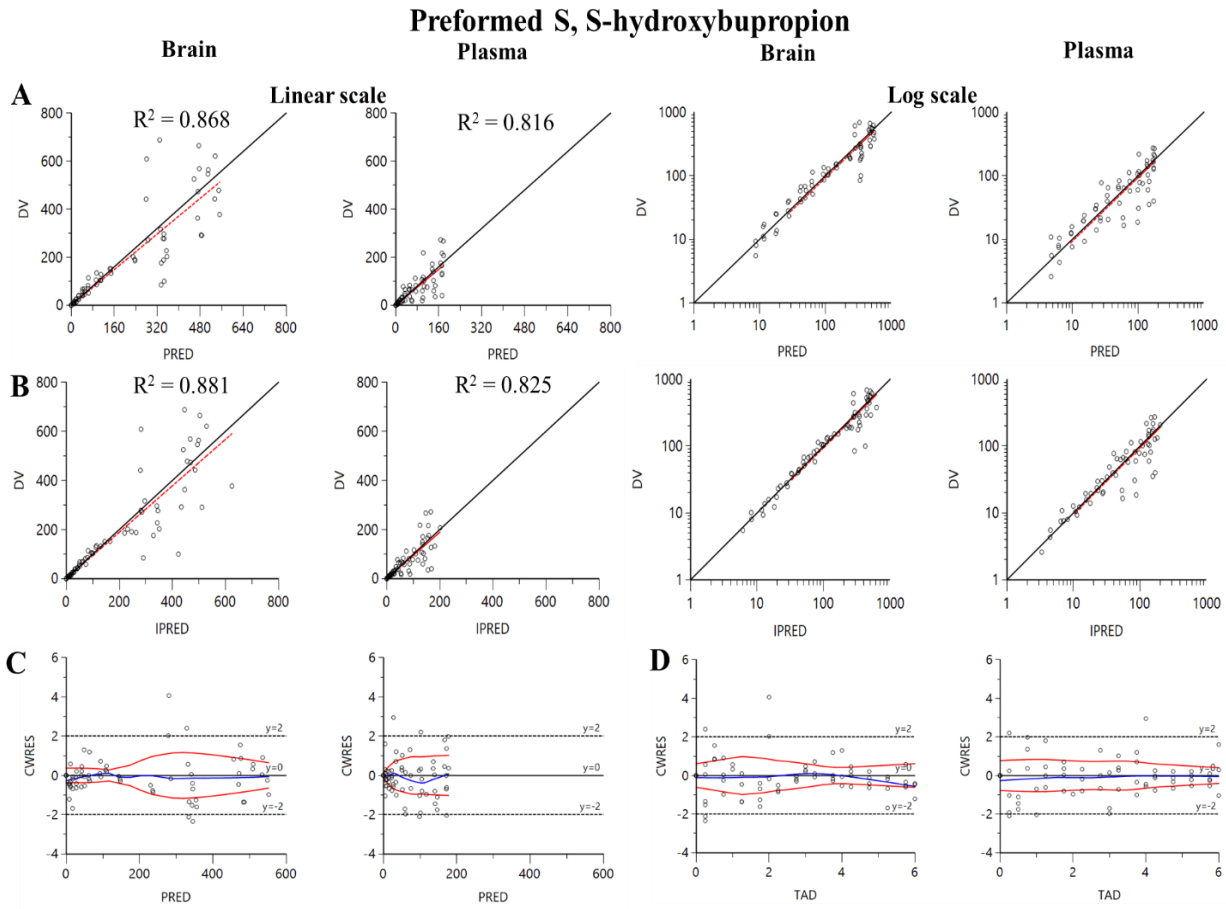


**Figure 5.5.** Model diagnostic plots for preformed S, S-hydroxybupropion concentrations in plasma and brain. **A (Top)**: Population predicted concentrations versus observed concentrations in brain and plasma (linear scale on LHS and log scale on RHS). **B (Middle panel)**: Individual predicted concentrations versus observed concentrations in brain and plasma (linear scale on LHS and log scale on RHS). The black solid line is the line of unity and the red-dashed line is the best fit line from linear regression. Shown above each figure is the associated linear regression correlation coefficient ($R^2$). **C (Bottom left panel)**: Conditional weighted residuals versus population predicted concentrations in brain and plasma. **D (Bottom right panel)**: CWRES: Conditional weighted residuals; DV: observed concentration; IPRED: Individual predicted; PRED: Population predicted; TAD: Time After Dose. Units of concentration and time are nanomolar (nM) and hours respectively.

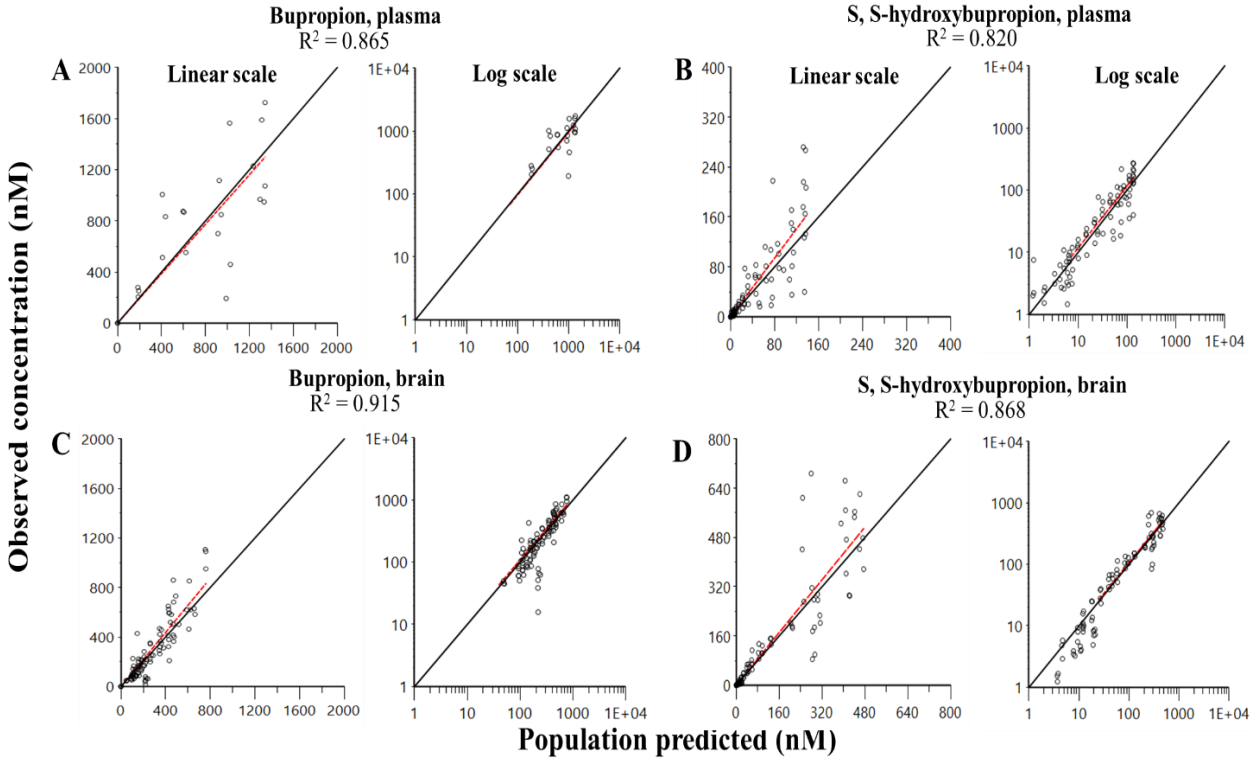


**Figure 5.6.** Model diagnostic plots from the final combined model for unbound bupropion and S, S-hydroxybupropion concentrations in plasma and brain. **A** and **B (Top first row):** Population predicted concentrations versus observed concentrations for bupropion and S, S-hydroxybupropion, respectively, in plasma. **C** and **D (Middle second row):** Population predicted concentrations versus observed concentrations for bupropion and S, S-hydroxybupropion, respectively, in brain. The solid black line is the line of unity, and the red-dashed line is the best fine from linear regression. Shown above each figure is the associated linear regression correlation coefficient ($R^2$).

**Figure 5.7** presents the visual predictive checks of the final combined bupropion, and S, S-hydroxybupropion (formed and preformed) model in plasma and brain along with pharmacological potency measures at DAT and NET.

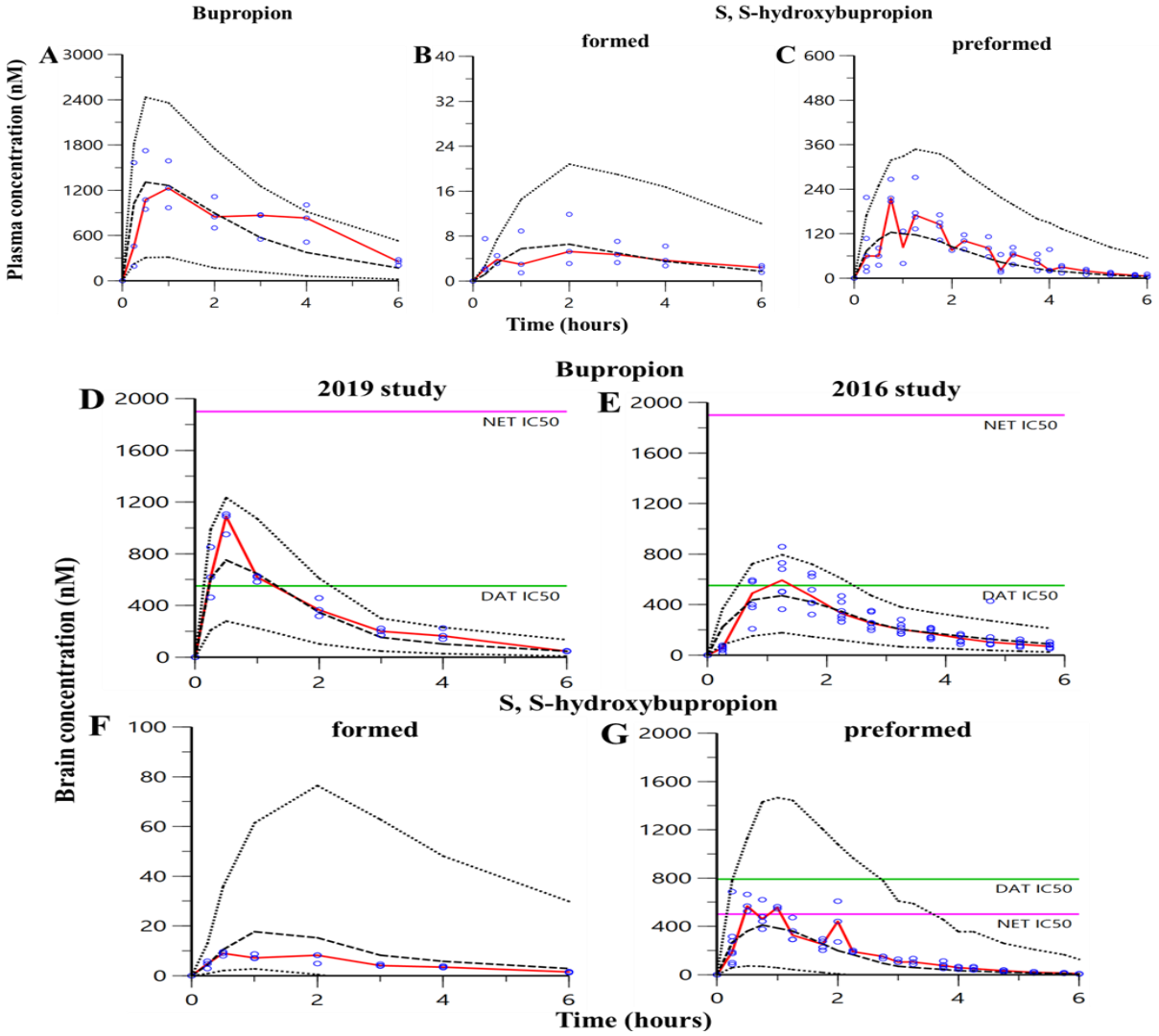


**Figure 5.7.** Visual predictive checks in plasma **(Top)** of **A:** bupropion, **B** and **C**: S, S-hydroxybupropion (formed and preformed respectively). Visual predictive checks in brain of bupropion **(D** and **E)** and S, S-hydroxybupropion **(F-formed** and **G- preformed)**. The red solid line in each plot represents the median of the observed concentrations, the black dashed line represents the median predicted concentrations, and the black dotted lines represent the 5% and 95% limits of the predicted 90% confidence intervals of the median predicted concentrations. Individual observed concentrations are shown as the blue circles. Due to the small values, the 5% limits of the predicted 90% confidence intervals of the median plasma predicted concentrations of pre-formed and formed S, S-hydroxybupropion cannot be seen **(B** and **C).** Green line refers to rat $IC_{50}$ value reported for dopamine transporter (DAT) and pink line refers to rat $IC_{50}$ value for norepinephrine transporter (NET). **B** and **F** represent formed S, S-hydroxybupropion concentrations from the present (2019) study. **G** represents unbound brain concentrations of preformed S, S-hydroxybupropion from the present (2019) and microdialysis studies (2016).

As shown in **Figures 5.7 (D)** and **5.7 (E)**, our rat model suggests that, following a 10 mg/kg dose of bupropion, brain exposures are similar to the $IC_{50}$ at DAT (550 nM) for up to 2 hours, and are below the $IC_{50}$ at NET (1900 nM) over the entire course. Formed S, S-hydroxybupropion brain levels **(Figure 5.7 F)** are below the DAT $IC_{50}$ (790 nM) and NET $IC_{50}$ (500 nM) (Lukas et al., 2010) for the entire time course. These findings offer an explanation as to why mice exhibit more pronounced antidepressant effects than rats in animal models of depression, that is, because of lower S, S-hydroxybupropion formation in rats (Bhattacharya et al., 2019; Damaj et al., 2004; Damaj et al., 2010; Grabus et al., 2012). Preformed S, S-hydroxybupropion brain exposures **(Figure 5.7 G)** were mostly below the NET $IC_{50}$ and were consistently below DAT $IC_{50}$ throughout the course of the study.

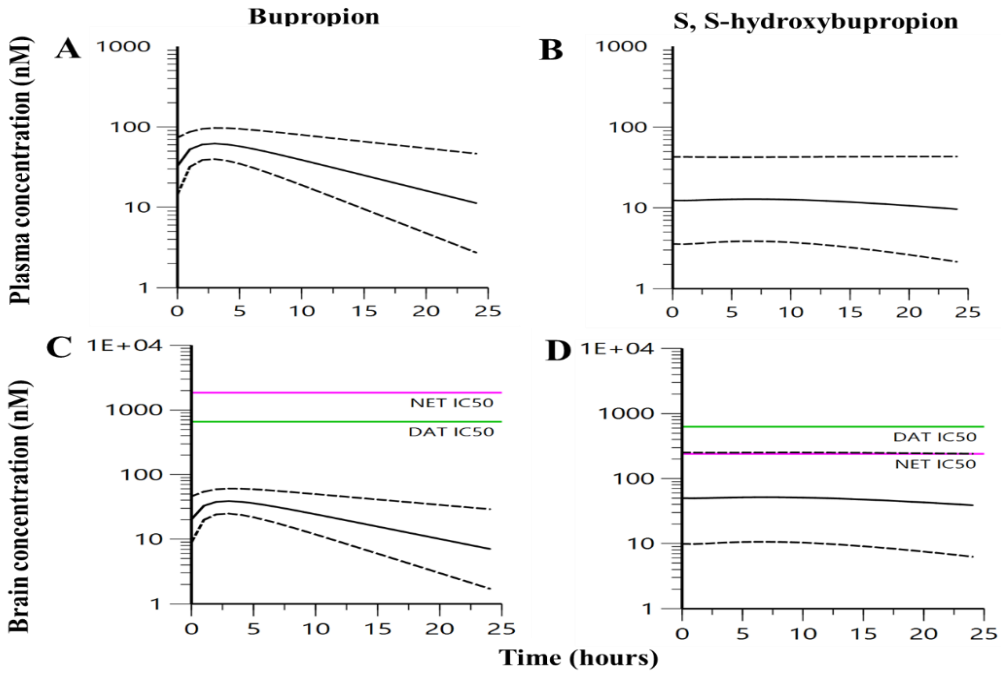


**Figure 5.8.** Simulated bupropion **(Left)** and S, S-hydroxybupropion **(Right)** concentrations over 12 hours in humans after multiple every-12-hour daily dosing of 150 mg of the bupropion SR formulation. The **top panel (A** and **B)** represents plasma unbound concentrations, and the **bottom panel (C** and **D)** represents unbound brain concentrations. The solid line describes the geometric mean predicted concentration, whereas the dotted lines represent the 5% and 95% predicted limits of the 90% confidence interval of the geometric mean concentrations. The green line in the brain plots refers to the human $IC_{50}$ value reported for the dopamine transporter (DAT), and the pink line refers to the $IC_{50}$ for norepinephrine transporter (NET).

From human simulations in **Figure 5.8**, the median maximum bupropion plasma concentration was 54 nM, occurring at 3 hours, which is the commonly observed peak time for the bupropion SR product (Jefferson et al., 2005). A comparison with reported $IC_{50}$ values for DAT and NET (Lukas et al., 2010) shows that unbound brain concentrations of S, S-hydroxybupropion after twice-daily administration of 150 mg bupropion SR are below its $IC_{50}$ values for DAT (630 nM) and NET (241 nM) over the entire time course, and bupropion concentrations were substantially lower than reported $IC_{50}$s for the two transporters (660 nM and 1850 nM, respectively) at all times.

An attempt was made to estimate plasma formation clearance of R, R-hydroxybupropion after incorporating it into the optimized combined plasma model of bupropion and S, S-hydroxybupropion (formed and preformed). Subsequently, estimation of brain $CL_{in}$ and $CL_{out}$ of R, R-hydroxybupropion was also made by freezing all plasma and brain related parameters of bupropion and S, S-hydroxybupropion. In this analysis, a BBB uptake asymmetry was not predicted for R, R-hydroxybupropion, which contrasts for S, S-hydroxybupropion and would be consistent with isomeric preference of a transporter. However, resolution regarding asymmetry at the blood-brain-barrier for R, R-hydroxybupropion would require a separate dose group. This is so because, after incorporation of brain R, R-hydroxybupropion data, predicted estimates of R, R-hydroxybupropion volume of distribution, clearance, formation clearance of R, R-hydroxybupropion varied with changing of initial estimates, indicating inability of the model to identify R, R-hydroxybupropion PK parameters. Estimation of formation clearance and structural parameters for S, S-hydroxybupropion was feasible because of administration of preformed S, S-hydroxybupropion dose group. Likewise, administration of R, R-hydroxybupropion dose group would likely have enabled estimation of these PK parameters. However, a separate pre-formed R, R-hydroxybupropion dose group was not included in our studies due to its much lower pharmacological potency than S, S-hydroxybupropion and bupropion at DAT and NET targets (Damaj et al., 2004; Damaj et al., 2010).

## 5.4 Discussion

In this study we used a population PK modeling approach to characterize plasma-brain disposition of bupropion and its pharmacologically active metabolite, S, S-hydroxybupropion following administration of 10 mg/kg racemic bupropion and 2 mg/kg of S, S-hydroxybupropion to adult male Sprague Dawley rats.

Incorporation into the model both plasma and brain data from a previous microdialysis study by Cremers et al (Cremers et al., 2016) was in part achieved. There were similarities in observations between the two studies. In both studies, formed and preformed S, S-hydroxybupropion half-life were similar in brain and plasma, and were similar to bupropion`s half-life in plasma and brain. These observations collectively suggest that disposition of S, S-hydroxybupropion follows formation rate-limited kinetics, that is, its disposition is rate-limited by bupropion`s kinetics in plasma and brain. The formation rate limited kinetics of S, S-hydroxybupropion observed in rats is similar to that observed in humans following administration of racemic bupropion (Masters et al., 2016).

On comparing bupropion`s disposition between the two studies, we noted similar (within 2-fold) unbound brain exposures derived from two different techniques. In the present study, unbound brain exposures were calculated after correcting for fraction unbound in brain homogenate, whereas microdialysis gave direct measures of extracellular fluid in rat prefrontal cortex. The unbound plasma and brain exposures from our present study were similar to Yenicelli et al (Yeniceli et al., 2011). However, a 7-fold difference in unbound bupropion plasma exposures between the present study and Cremers et al was observed. Additional comparative stability experiments in three matrices (rat plasma, brain and 0.1 M phosphate buffer pH 7.4, discussed in **Chapter 4**), indicated instability in plasma as a potential reason for the discrepancy in unbound plasma exposure levels between the microdialysis and present studies. This could have been due to incorrect plasma sample handling (prolonged storage at room temperature after microdialysis sampling). In our studies, we were careful to generate plasma from whole blood and store it within minutes of sample collection.

Naïve pooled approach was used for the final combined bupropion-S, S-hydroxybupropion model as the interindividual variability on V/F or CL/F in the individual bupropion or preformed

S, S-hydroxybupropion models were very small and inclusion of these additional omegas (interindividual variability) did not improve model performance.

Our present study results independently, and after combining data from Cremers et al, noted that both bupropion and S, S-hydroxybupropion exhibit changes in $K_{p,uu}$ over time in a pattern inconsistent with an expected increase over time to attain distributional equilibrium between plasma and brain, and thereafter a constant ratio. The profiles observed were adequately characterized by a model incorporating a time dependency on $CL_{in}$ for both bupropion and S, S-hydroxybupropion, in which this parameter decreased over time (Cremers et al., 2016). The model predicted bupropion $K_{p,uu}$ (0.26) derived from the ratio of $CL_{in}$ and $CL_{out}$ ($CL_{out} > CL_{in}$) and $K_{p,uu}$ (0.37) from NCA analysis, both values < 1 suggests that net efflux dominates the transport of bupropion at the BBB (Fridén et al., 2007). This is close to a CSF-plasma ratio of 0.43 reported in humans by Golden et al (Fridén et al., 2007; Golden, DeVane, et al., 1988). Inter-subject variations in efflux transporter expression, such as P-gp expression at the blood-brain-barrier, could possibly explain variability observed in individuals on bupropion therapy (O'Brien et al., 2012). The possibility of transporter involved in bupropion disposition has also been suggested by a study where bupropion administration significantly increased digoxin renal clearance in rats, possibly due to activation of OATP4C1 or P-gp mediated tubular secretion (He et al., 2014).

Possibility of within brain metabolism was also evaluated. Incorporation of a brain formation clearance term for S, S-hydroxybupropion did not improve model performance, suggesting that local (brain) formation of S, S-hydroxybupropion from bupropion has a negligible contribution to its overall brain clearance. However, there remains a possibility that bupropion may be metabolized locally to an uncharacterized metabolite. Unlike liver, expression of metabolic enzymes, such as CYP450, in brain, that could potentially contribute to local stereoselective bupropion metabolism, is lower and not well characterized, and, unlike hepatic microsomes, use of brain microsomes is not popular due to lower stability, lower yield and loss of cytochrome P450 during preparation (Vijayalakshmi Ravindranath & Anandatheerthavarada, 1990).

The transient overshoot in $K_{p,uu}$ of S, S-hydroxybupropion was more prominent in preformed S, S-hydroxybupropion than formed hydroxybupropion diastereomers. The discrepancy in $K_{p,uu}$ values of formed versus preformed S, S-hydroxybupropion could possibly be due to

competition between bupropion and this metabolite at the blood-brain-barrier. The relative exposure of S, S-hydroxybupropion to bupropion is much lower, which would enhance the ability of bupropion to compete with stereoselective carrier mediated transport of S, S-hydroxybupropion. Overshoot also implies involvement of a carrier-mediated uptake transporter, possibly the pH-dependent proton-coupled antiporter at the blood-brain-barrier as suggested in the study by Cremers et al (Cremers et al., 2016). This antiporter is thought to be involved in transport of weakly basic CNS drugs such as oxycodone, apomorphine, clonidine (André et al., 2009; Chapy, André, Declèves, Scherrmann, & Cisternino, 2015; Cremers et al., 2016; Okura et al., 2008; Okura et al., 2014; Sadiq et al., 2011). It is possible that the overshoot, modeled as time dependent distributional clearance, may have been due to eventual replacement of protons by bupropion or S, S-hydroxybupropion on the abluminal side (Cremers et al., 2016).

A model with further partitioning into the lysosomal compartment was not considered, as lysosomal volume is 0.5 % of total brain volume (Fridén et al., 2011). Also, similar (2-fold) unbound brain exposures from the present study and that derived from microdialysis studies suggest confinement to the extracellular compartment, which is also the site that bathes the targets, DAT and NET. The model did not include brain ECF bulk flow/CSF clearance (Szentistvanyi, Patlak, Ellis, & Cserr, 1984) since this is negligible (< 0.0001%) relative to $CL_{out}$ estimates and thus would not significantly contribute to overall brain clearance.

A dose group of R, R-hydroxybupropion was not included in our present study due to lower pharmacological potency compared to S, S-hydroxybupropion and bupropion (Damaj et al., 2004; Damaj et al., 2010). Modeling suggested possible lack of uptake symmetry for R, R-hydroxybupropion, which contrasts to S, S-hydroxybupropion. However, additional studies, including separate administration of R, R-hydroxybupropion, would be needed to explore this possibility.

Bupropion`s antidepressant and smoking cessation activity are thought to be due to its DAT and NET reuptake inhibiting activity (Stahl et al., 2004). Time to maximum concentrations (1 hour) in brain for bupropion enantiomers and hydroxybupropion diastereomers are close to peak dopamine and norepinephrine time (40-60 minutes) observed in studies employing microdialysis to measure these neurotransmitter levels in rats following administration of racemic bupropion (Li

et al., 2002; Nomikos GG1, 1992 ). Our model suggests that following a 10 mg/kg dose of bupropion unbound brain concentrations exceed its $IC_{50}$ at DAT for up to 1 hour but fall below its $IC_{50}$ at NET for the entire time course. For S, S-hydroxybupropion, its concentration in brain is above the NET-$IC_{50}$ up to 1 hour and several orders of magnitude below DAT $IC_{50}$. Overall, our rat models suggest animal studies in rats to understand bupropion`s antidepressant effect would need to be conducted at much higher bupropion doses in order to take into consideration the expected added effects of formed S, S-hydroxybupropion. An alternative approach would be to administer the pre-formed metabolite. Studies to investigate bupropion or hydroxybupropion antidepressant effects have so far been reported in mouse models of depression (forced swim test) (Damaj et al., 2004). Behavioral animal models to investigate the stimulus effects in a drug discrimination model using nicotine or amphetamine-trained rats of racemic bupropion and the two hydroxybupropion diastereoisomer metabolites (R, R and S, S-) administered as separate cohorts indicated that S, S-hydroxybupropion partially (66%) substituted for nicotine (Bondarev et al., 2003). In amphetamine-trained animals, S, S-hydroxybupropion ($ED_{50}$ = 4.4 mg/kg) generalized completely and was similar in potency to racemic bupropion ($ED_{50}$ = 5.4 mg/kg)(Bondarev et al., 2003). Furthermore, a study in marmosets demonstrated that S, S-hydroxybupropion, but not the R, R-hydroxybupropion, dose-dependently increased both locomotor activity and reversed motor disability in 1-methyl-4-phenyl-1,2,3,6-tetrahydropyridine-treated marmosets suggesting that S, S- hydroxybupropion may possess potential antiparkinsonian activity (Hansard et al., 2011). However, efforts to bring S, S-hydroxybupropion or its structural analogs to the clinic have met with limited success, implying that other metabolites may also contribute to bupropion's overall therapeutic activity (Deveaugh-Geiss et al., 2002; Nora D. Volkow et al., 2005). Translation of rat bupropion and S, S-hydroxybupropion plasma-brain distributional clearances to humans suggests bupropion`s antidepressant effect could possibly be due to dopamine and norepinephrine reuptake inhibition by S, S-hydroxybupropion. However, since the simulated human S, S-hydroxybupropion brain exposures were below their reported in vitro potencies at NET and DAT, our simulations suggest other pharmacological targets or mechanisms may be involved in bupropion`s efficacy. Also, receptor occupancy studies using PET or SPECT tracers specific for DAT and conducted at steady state based on bupropion multiple

dosing indicate occupancy of about 20% for about 24-hours in both patients with and without depression (Learned-Coughlin et al., 2003; J. H. Meyer et al., 2002). The low occupancy reported in these studies too suggest additional studies to investigate the mechanism of bupropion`s pharmacological action are needed.

Species differences regarding metabolism of bupropion and its implicated carrier-mediated transport at the BBB, limit the translational potential of our present model. Due to ethical and safety reasons, the human brain exposure-time profile of bupropion and metabolites are not available to validate the translational findings of the present study. A similar observation in a CNS model developed in non-human primates (due to its close genetic homology in humans) could have added gravitas to the translational potential of our present model. Additional studies such as in vitro transporter based assays (BBB), corroborated by in vivo studies in non-human primates, may further improve the understanding of disposition and pharmacology of bupropion, which may ultimately help in understanding the interindividual variability in efficacy and safety observed with bupropion.

# CHAPTER 6. DEVELOPMENT OF TRANSLATIONAL PBPK MODEL OF BUPROPION AND S, S-HYDROXYBUPROPION

**Hypothesis 5.** Development of rat-to-human translational physiologically-based pharmacokinetic model that describes the central nervous system disposition of bupropion and its metabolite (S, S-hydroxybupropion) will advance our understanding of intersubject variability in human bupropion response.

**Specific aim 5.** Develop a translational physiologically-based pharmacokinetic model to predict bupropion and pharmacologically active metabolite S, S-hydroxybupropion exposures in human brain (target site), and their relationship to pharmacologic potency measures at the dopamine transporter (DAT) and the norepinephrine transporter (NET).

## 6.1 Introduction

Bupropion therapy as an antidepressant and smoking cessation aid is associated with wide intersubject variability (Benowitz et al., 2013; Connarn et al., 2017; Connarn et al., 2016; Golden, De Vane, et al., 1988; Hesse et al., 2004; Laizure et al., 1985; Woodcock et al., 2012; A. Z. X. Zhu et al., 2012; Andy Z. X. Zhu et al., 2014). Variability in response is thought to be driven by variability in metabolism (Benowitz et al., 2013; Gufford et al., 2016; Hesse et al., 2004; Kharasch et al., 2008; Masters et al., 2016; A. Z. X. Zhu et al., 2012; Andy Z. X. Zhu et al., 2014). Species differences in metabolism of bupropion leading to differences in bupropion`s effect in models of depression support this hypothesis (Butz et al., 1982; Carroll et al., 2014; Suckow et al., 1986). Bupropion undergoes complex phase 1 and 2 stereoselective metabolism (Coles & Kharasch, 2008; Gufford et al., 2016; Kharasch et al., 2008; Masters et al., 2016; Sager et al., 2016). The pharmacology is reported to be stereoselective and is not fully understood (Damaj et al., 2004). Its phase 1 metabolite, S, S-hydroxybupropion, is reported to be more potent than R, R-hydroxybupropion and bupropion at the norepinephrine transporter (NET) and nicotinic acetylcholine receptors (nAChRs), and almost as potent as bupropion at the dopamine transporter (DAT) (Damaj et al., 2004). Animal studies indicate that bupropion has greater efficacy in mice

versus rats in rodent models of depression (indicated by anti-tetrabenazine activity) (Suckow et al., 1986).

Through comparison of phase 1 metabolism of bupropion in hepatic microsomes of four species (humans, mice, rat and non-human primates), we demonstrated that non-human primates (NHPs) would be the appropriate species to model bupropion`s disposition in CNS. However, cost was an insurmountable barrier to conducting in vivo studies in NHPs. Limited pharmacokinetic (PK) and pharmacodynamic (PD) data in NHPs was also problematic. In vitro microsomal studies also indicated that formation of S, S-hydroxybupropion in mice is higher than rats, thus providing a reasonable explanation for the observed pharmacological difference in mice versus rats given the greater potency of S, S-hydroxybupropion than racemic bupropion at some of the pharmacologic targets (Damaj et al., 2004). However, after considering multiple factors, such as the formation of reductive metabolites (higher in rats than mice), which are also thought to contribute to bupropion`s therapeutic efficacy, availability of microdialysis data measuring bupropion, and dopamine and norepinephrine neurotransmitter levels in brain extracellular fluid (ECF), as well as in vitro potency (DAT, NET $IC_{50}$ ) measures specific to rat, this species was chosen as the surrogate species to model bupropion`s disposition (Ascher et al., 1995; Bondarev et al., 2003; Martin et al., 1990; Schroeder, May 1983).

Translational PK/PD models have improved understanding of disposition and pharmacology of drugs acting in the central nervous system (CNS) (Badhan et al., 2014; Ball et al., 2014; Gaohua et al., 2016; William Kielbasa et al., 2009; W. Kielbasa & Stratford, 2012; van Gaalen et al., 2019; Yamamoto et al., 2017). Population-PK models use a “top-down” approach, that is, they are largely based on data from in vivo experiments to support model development. A challenge with this approach, as indicated by Ball et al, is that model estimated drug specific parameters, such as those characterizing brain disposition may not be truly translatable(Ball, Bouzom, Scherrmann, Walther, & Declèves, 2012). For example, blood-brain-barrier (BBB) distributional clearance parameters may depend on active transport, and physiological differences between species, such as surface expression of transporters, surface area, membrane composition and scaling based on simple allometric principles may be misleading (Ball et al., 2012, 2014). Alternatively, physiologically based pharmacokinetic (PBPK) models have been used to predict

concentration time profiles in multiple tissues based on physicochemical parameters, in vitro data and physiological parameters (Ball et al., 2012, 2014). The physiological structure of a PBPK model allows interspecies scaling of relevant species-specific parameters (Ball et al., 2012). Despite these advantages PBPK models offer over Population-PK, very few CNS-based PBPK models have been reported (Alqahtani & Kaddoumi, 2016; Badhan et al., 2014; Ball et al., 2012, 2014; Gaohua et al., 2016; Yamamoto et al., 2017; Zakaria & Badhan, 2018).

A major challenge in developing a PBPK model is that it requires many parameters such as organ volumes, organ specific bloods flows, membrane partition coefficients, in vitro data that may not be available (Ball et al., 2012). Also, the data from in vitro studies or preclinical species may not fully reflect human parameters. If human systemic pharmacokinetic profiles are available, the variables may be adjusted to improve model fit. However, this may not be the case for tissues which are not easily accessible, such as the brain. Limitations specific to CNS PBPK model development have been discussed by Ball et al (Ball et al., 2012). With respect to BBB transport, these limitations include differences in isolation procedures, culture conditions, cell type and origin, all of which can introduce interlaboratory variability in primary cultures of brain microvessel endothelial cells. Also, in vitro blood-brain-barrier models have questionable integrity and other non-blood-brain-barrier models such as the human colorectal adenocarcinoma cell line (Caco-2) and Madin-Darby canine kidney cells (MDCK), have phenotypic differences compared to the blood-brain-barrier. As examples, they do not capture the tightness of the blood-brain-barrier, nor efflux transporter expression profiles, and enzyme activity (Badhan et al., 2014; Garberg et al., 2005; Hakkarainen et al., 2010; Nicolazzo, Charman, & Charman, 2006; A. Reichel, Begley, & Abbott, 2003). It has also been reported that in vitro blood-brain-barrier models have higher P-glycoprotein (P-gp) expression than breast cancer resistant protein (BCRP), which is opposite to in vivo as reported by Uchida et al (Ball et al., 2012; Uchida et al., 2011). Possibility of introducing additional variability also applies to co-culture in vitro blood-brain-barrier models, which consist of endothelial cells grown with astrocytes, due to reported increased endothelial electrical resistance which could enhance P-gp functionality relative to in vivo (Ball et al., 2012). The above listed reasons, along with complexity of the blood brain-barrier structure, transporters which still have not been fully characterized, species differences in transporter expression and abundance,

may in part explain why there are few CNS PBPK models, and, ultimately, high attrition rates regarding CNS based drug discovery.

Cognizant of these challenges related to the development of a bupropion-specific brain PBPK model, that is, in the absence of all required in vitro BBB parameters, the objective of the present study was to develop an understanding of drug transfer characteristics of bupropion and its active metabolite S, S-hydroxybupropion across the BBB. This was achieved by including distinct terms for brain permeability clearance, brain active influx clearance, and brain active efflux clearance, that govern the net BBB transport within a physiological framework to ultimately support translation to human brain PK.

## 6.2 Methods

### 6.2.1 Pharmacokinetic study in animals

Racemic bupropion (10 mg/kg) and S, S-hydroxybupropion (2 mg/kg) were administered subcutaneously to adult male Sprague Dawley rats (290–330 g, n = 24/compound). Experiments were approved by the Institutional Animal Care and Use Committee (IACUC), Indiana University School of Medicine. Brain and plasma were collected from rats (n = 3) at eight time points over a period of 6 hours and analyzed using a chiral LC-MS/MS method described in **Chapter 3**. Rat plasma protein and brain homogenate binding studies for R and S-bupropion, R, R- and S, S-hydroxybupropion were conducted to correct for unbound fraction in both matrices using a 96-well equilibrium dialysis method as described in **Chapter 3**. Details of a microdialysis study also used to support model development, can be found in a study published by Cremers et al in 2016 (Cremers et al., 2016). Briefly, in that study, 10 mg/kg of racemic bupropion and 2mg/kg of S, S-hydroxybupropion dissolved in 0.9% NaCl (2 mg/mL) were administered subcutaneously to 4-5 Adult male Sprague Dawley rats (280-350 g). Dialysates from brain (probe in medial prefrontal cortex) and the jugular vein were collected every 30 minutes starting 1 hour prior to administration and continuing for 6 hours after administration. All the samples (from both studies) were stored at -80 ˚C until time of analysis by LC-MS/MS assay. The microdialysis study did not use a chiral assay.

### 6.2.2 PBPK model development for plasma

Simcyp® is a popular PBPK modeling software. However, the Simcyp® rat model (Simcyp® simulator, version 18, Certara®) currently lacks a full PBPK module to support analysis of formed metabolites in brain. Specific to bupropion, this limitation would prevent prediction of brain concentrations of bupropion, and its pharmacologically active metabolite S, S-hydroxybupropion. Accordingly, a bupropion-S, S,-hydroxybupropion PBPK parent-metabolite model was developed using the mrgsolve package in R (version 3.5.3) (Baron, 2019; Elmokadem, Riggs, & Baron, 2019; R Core Team, 2019; Wickham.). Graphs were built using the gglpot2 package in R (Wickham.). In vitro and physicochemical parameters supporting PBPK model development that were not experimentally generated through the present work were collated from the literature (references are provided in **Table 6.1**, **6.3**, **6.5**), or were optimized from rat in vivo data. Several optimization algorithms, such as local optimizer Newuoa (New unconstrained optimization) or Nelder Mead, and global optimizers, such as the Dividing Rectangles algorithm that uses maximum likelihood estimation, were evaluated (using the nonlinear optimization- nloptr package in R) (Johnson). These yielded similar results, which indicated the robustness of these estimates.

Structures of whole-body PBPK models have been recently reviewed (Jones & Rowland-Yeo, 2013). A common structure is shown in **Figure 6.1**. In this model, fourteen compartments were included, each representing an organ or tissue. The mass balance differential equations used in these models have been described and can be found in publications by Jones et al (Ball et al., 2012; Jones & Rowland-Yeo, 2013). All organs except the brain were considered to be homogeneous and well stirred with perfusion-limited uptake (Ball et al., 2012). The perfusion limited model assumes that, at steady state, the total drug concentration in the tissue is in equilibrium with the total drug concentration in the circulation, as determined by the specific tissue to plasma ratio ($K_p$). The time taken to reach steady state is determined by blood flow rate, tissue volume, and the $K_p$ value for the particular tissue (Jones & Rowland-Yeo, 2013). **Equation 6.1** below applies to each non-eliminating organ with perfusion limited uptake, where $dA_T/dt$ is the rate of change of the amount of drug in tissue, the subscript 'T' in the below equations denote tissue, $C_T$ is the concentration in a given tissue, $Q_T$ refers to the tissue blood flow rate, $C_{A,bl}$ and

$C_{V,bl,T}$ refer to the concentration in the arterial blood entering the tissue and the concentration in the venous blood leaving the tissue, respectively. $K_{p,T:bl}$ ,the drug concentration ratio between tissue and blood (tissue-to-blood partition coefficient), was predicted using the equations of Rodgers et al used in Simcyp® simulator, version 18, Certara® (Rodgers & Rowland, 2007). Briefly, the equations of Rodgers et al account for partitioning of unionized drug into neutral lipids and neutral phospholipids, dissolution of ionized and unionized drug in tissue water, electrostatic interactions between ionized drug and acidic phospholipids for strong ionized bases, and interactions with extracellular protein for neutrals, weak bases, and acids (Rodgers & Rowland, 2007).

$$\frac{dA_T}{dt} = Q_T \cdot \left(C_{A,bl} - C_{V,bl,T}\right) = Q_T \cdot \left(C_{A,bl} - \frac{C_T}{K_{p,T:bl}}\right) \quad \text{Equation 6.1}$$

For eliminating organs, such as liver and kidneys, an additional clearance (CL) term is added (**Equation 6.2**), where $CL_T$ could either be a first-order CL measured from in vivo data, or could be determined from scaling of in vitro metabolism intrinsic CL ($CL_{int,vitro}$) or kinetics ($V_{max}$ and $K_m$), determined in, for example, liver microsomes or hepatocytes, which are scaled up to intrinsic tissue CL, and then to an overall organ CL according to the well-stirred model (Ball et al., 2012).

$$\frac{dA_T}{dt} = Q_T \cdot \left(C_{A,bl} - C_{V,bl,T}\right) - CL_T \cdot C_T \quad \text{Equation 6.2}$$

Blood is split into two compartments representing arterial and venous blood separated by the lungs. Thus, the equations for the arterial and venous compartments are given below (**Equations 6.3** and **6.4**), where $dA_{A,bl}/dt$ is the rate of change of the amount of drug in arterial blood, $dA_{V,bl}/dt$ is the rate of change of the amount of drug in venous blood, $Q_{Ti}$ is blood flow rate of tissue i, $C_{V,bl,Ti}$ is the concentration in the venous blood leaving tissue i, and $Q_{cardiac}$ is cardiac output (80 mL/min in rats)(Ball et al., 2012).

$$\frac{dA_{A,bl}}{dt} = Q_{cardiac} \cdot (C_{V,bl,lung} - C_{A,bl})$$ .....Equation 6.3

$$\frac{dA_{V,bl}}{dt} = \sum_t^n (Q_{Ti} \cdot C_{A,bl,Tt} - Q_{cardiac} \cdot C_{V,bl})$$ .....Equation 6.4

The equation for the lung compartment is given below (**Equation 6.5**). Rat blood flows, and $K_p$ values for tissues can be found in **Appendix E**.

$$\frac{dA_{A,lung}}{dt} = Q_{cardiac}(C_{V,bl} - C_{V,bl,lung})$$ .....Equation 6.5

### 6.2.3 PBPK model development for brain

A permeability-limited brain model structure, adopted from Ball and Lu Gaohua, was used in our present work (Ball et al., 2012; Gaohua et al., 2016). Permeability across the BBB becomes the limiting process, that is, the time to reach equilibrium is dependent on the drug-specific permeability rather than the blood flow (Jones & Rowland-Yeo, 2013). Brain was divided into two separate compartments, namely the brain vasculature, and brain tissue, these separated by the BBB. The rate at which a drug crosses the BBB is determined by passive permeability along with transporter contributions (described below), protein binding and cerebral blood flow. In our model, active influx processes were grouped together as $CL_{active\ influx}$ and active efflux processes were grouped together as $CL_{active\ efflux}$ because of the lack of data for bupropion and S, S-hydroxybupropion from transporter-specific systems. (Andreas Reichel, 2010, 2014, 2015). $K_{p,uu}$ , the unbound brain to plasma ratio, which is independent of protein binding, reflects net transport equilibrium across the BBB. Mechanistically, as shown in **Equation 6.6**, $K_{p,uu}$ is determined by PS ($CL_{passive}$), the passive permeability-surface area product at the BBB, which describes the bidirectional passive drug transfer across blood-brain-barrier. $CL_{active\ uptake}$ is clearance due to

transporter-mediated uptake, $CL_{active\ efflux}$ is clearance due to efflux transporter(s), $CL_{metabolism}$ is clearance due to within brain metabolism, and $CL_{bulk\ flow}$ is clearance due to extracellular fluid bulk flow in brain (Hammarlund-Udenaes et al., 2008; Andreas Reichel, 2015). Due to prior prediction of negligible contribution of within brain metabolism to brain clearance from the population-PK model (**Chapter 5**), and absence of brain metabolism data, we assumed clearance due to brain metabolism was negligible and did not include this term in the model).

$$K_{p,uu} = \frac{PS + CL_{active\ uptake} - CL_{active\ efflux}}{PS + CL_{active\ efflux} - CL_{active\ uptake} + CL_{metabolism} + CL_{bulk\ flow}} \quad \text{.....Equation 6.6}$$

The general mass balance equations for brain tissue (brain) and brain vasculature (brain vasc) are given below in **Equations 6.7** and **6.8** (Ball et al., 2012; Gaohua et al., 2016).

$$\frac{dA_{brain\ vasc}}{dt} = Q_{brain} \cdot (C_{A,bl} - C_{V,brain\ vasc}) + PS \cdot (\lambda_{brain} \cdot fu_{brain} \cdot C_{brain} - \lambda_{brain\ vasc} \cdot fu_{plasma} \cdot C_{brain\ vasc}) + (CL_{active\ efflux} \cdot fu_{brain} \cdot C_{brain}) - (CL_{active\ uptake} \cdot fu_{plasma} \cdot C_{brain\ vasc}) \quad \text{.....Equation 6.7}$$

$$\frac{dA_{brain}}{dt} = PS \cdot (\lambda_{brain\ vasc} \cdot fu_{plasma} \cdot C_{brain\ vasc} - \lambda_{brain} \cdot fu_{brain} \cdot C_{brain}) - (CL_{active\ efflux} \cdot fu_{brain} \cdot C_{brain}) + (CL_{active\ uptake} \cdot fu_{plasma} \cdot C_{brain\ vasc}) \quad \text{.....Equation 6.8}$$

Lambda, λ, is the ionization coefficient and was determined using the Henderson-Hasselbach equation, which is dependent on compound charge type and its pKa, together with the matrix pH (7.12 for brain mass and 7.4 for plasma based on Simcyp® simulator, version 18, Certara®)(Gaohua et al., 2016).

Passive permeability clearance ($PS_{passive}$) was calculated using **Equation 6.9**, where $P_{app}$ is apparent permeability, S is in vivo brain vascular endothelial surface area (Ball et al., 2012).

$$PS_{passive} = P_{app} \cdot S \cdot Brainweight \quad \text{.....Equation 6.9}$$

Passive permeability clearance ($PS_{passive}$) was obtained from Simcyp®,which uses a QSAR based model (Juan & Eduardo, 2006), with molecular weight of 239.74 and log P of 3.21 for bupropion. The passive permeability surface area product for bupropion was 158.7 L/hr (44.03 mL/sec). $P_{app}$ was back calculated to 2 $x10^{-4}$ cm/sec using the above equation, with human brain weight of 1400 g and S of 157 $cm^2/g$ (Ball et al., 2012). This value is close to the brain permeability value reported by Summerfield et al of 1.68 x $10^{-4}$ cm/sec using a single-point in situ perfusion assay in rats (Summerfield et al., 2007). In absence of experimental data, we assumed this value of $P_{app}$ to be similar across species (Ball et al., 2012; Di et al., 2011). The apparent permeability reported for bupropion using the bovine in vitro BBB model was 5.5 $x10^{-5}$ cm/sec (Heymans, Sevin, Gosselet, Lundquist, & Culot, 2018), which is approximately 3-fold lower than the in situ perfusion value, thus exemplifying lack of reliance on in vitro blood-brain-barrier assays for developing CNS based PBPK models (Ball et al., 2012). Similarly, the human BBB $PS_{passive}$ for hydroxybupropion was predicted to be 35.9 L/hr using a molecular weight of 255.74 and log P of 1.9. The back calculated passive permeability of hydroxybupropion was 4.4 $x10^{-5}$ cm/sec. This value was used for development of S, S-hydroxybupropion PBPK model.

At present, efflux/uptake kinetic terms for bupropion and its metabolites for P-glycoprotein, BCRP, or other transporters are not available, which obstructs the development of CNS PBK model. To compensate for the absence of Michaelis–Menten parameters for carrier-mediated transport, the active efflux component of drug transport was described collectively by the term Efflux Ratio (ER) in the model, which is the difference in $P_{app,\ B:A}$ (basolateral to apical) and $P_{app,A:B}$ (apical to basolateral),as used by Ball et al (Ball et al., 2012). Transporter-mediated uptake clearance was collectively described by brain uptake clearance, $CL_{up}$. MPPGB is milligrams of protein per gram of brain (0.25 mg/g (Ball et al., 2012)) rat brain weight of 1.8 g was used in present model.

$$CL_{active\ efflux} = ER \cdot S \cdot Brainweight \quad \text{Equation 6.10}$$

$$CL_{active\ uptake} = CL_{up} \cdot MPPGB \cdot Brainweight \quad \text{Equation 6.11}$$

Different brain model structures, such as 1) flow limited structure using the brain to plasma ratio predicted by the Rodgers method (Rodgers & Rowland, 2007), 2) brain to plasma ratio based on our in vivo study, 3) only passive permeability clearance, and 4) passive permeability clearance plus $CL_{active\ efflux}$ and $CL_{active\ uptake}$ were evaluated for bupropion and S, S-hydroxybupropion.

### 6.2.4 PBPK model evaluation

Model evaluations of competing plasma-brain PBPK model structures were based on comparing predicted plasma and brain concentration profiles with the observed concentrations by visual inspection of concentration versus time profiles and by fold change in predicted versus observed PK parameters, area under the concentration versus time curve (AUC), and maximum concentration ($C_{max}$) for plasma and brain.

### 6.2.5 Model sensitivity analysis

The impact of variation in $fu_{plasma,}$ $fu_{brain,}$ blood-to-plasma ratio, absorption rate constant, renal clearance, hepatic clearance, passive clearance, and active influx and active efflux clearance, on plasma and brain exposures was conducted using sensitivity analysis available in the Flexible Modelling Environment (FME) package in R. FME is a package designed for inverse modelling, sensitivity and Monte Carlo analysis. It employs a Markov chain Monte Carlo estimator, to estimate parameter uncertainties (Soetaert & Petzoldt, 2010). Bupropion and S, S-hydroxybupropion $fu_{plasma,}$ $fu_{brain}$ and blood-to-plasma ratio (BP) was increased over the range of 0.1 to 0.8 in two-fold increments. Likewise, absorption rate constant was varied from 0.5 to 4 $hr^{-1}$, in two fold increments, and renal clearance was varied from 0.005 to 0.16 L/hr in two-fold increments. Intrinsic hepatic clearance was varied from 50 to 800 µL/min/mg protein for bupropion and 400 to 3200 µL/min/mg protein for S, S-hydroxybupropion, both in two-fold increments. Brain transport uptake clearance was varied from 10000 to 80000µL/min/mg brain, apparent permeability was varied from 0.0001 to 0.0008 cm/sec for bupropion and 0.00001 to 0.00008 cm/sec for S, S-hydroxybupropion, all in two-fold increments. Efflux term was varied from 0.01 to 0.08 cm/sec for bupropion and 0.001 to 0.008 cm/sec for S, S-hydroxybupropion,

both in two-fold increments. Sensitive parameters were then optimized using the nonlinear optimization- *nloptr* package to improve model fit (Johnson). Parameters were considered sensitive if they influenced plasma or brain exposure based on visual inspection of profiles from the sensitivity analysis. The ranges for sensitivity analysis were based on either physiological plausible ranges (0.1 to 0.8 for $fu_{plasma,}$ $fu_{brain}$, BP) or from preliminary assessment by varying the parameters over a 100-fold range with visual observation to narrow the range. Precision of estimates of the optimized parameter (% relative standard error-RSE) was determined using the hessian function in R (Hessian matrix is equal to the inverse of the covariance matrix) (Thacker, 1989).

### 6.2.6 Human simulations

The final rat brain model was scaled to predict steady-state human unbound brain exposure to bupropion and S, S-hydroxybupropion. Unbound brain fraction was assumed to be similar across species as suggested by Di et al (Di et al., 2011). Parameters based on drug physicochemical parameters (ionization constant, molecular weight, octanol: buffer partition coefficient) are species independent. Fraction unbound in microsomes was considered similar between species (Simcyp® simulator, version 18, Certara®). MPPGB was considered similar between species (Ball et al., 2012). For humans, microsomal protein per gram of liver (MPPGL) of 40 mg/g was used (Simcyp® simulator, version 18, Certara®). The brain transport parameters- $P_{app-}$ apparent permeability, ER- characterizing active efflux and $CL_{up}$ were considered species independent and were scaled to humans using brain vascular surface area S of 157 $cm^2/g$ and brain weight of 1400 g (Ball et al., 2012). Human tissue to plasma concentration ratios were calculated using the Rodgers et al method in Simcyp® (Simcyp® simulator, version 18, Certara®), which were largely comparable to rat values (Rodgers & Rowland, 2007). Bupropion plasma pharmacokinetics were corrected for human plasma protein binding of 85% (Jefferson et al., 2005). An absorption rate constant ($k_a$) of 0.6 $hr^{-1}$, the reported value for the SR formulation in humans, was used (Jefferson et al., 2005). Bupropion metabolism is the major route of its elimination in humans, with <1% excreted unchanged in urine (Welch et al., 1987). Consequently, renal clearance for bupropion was assigned

a value of 1 L/hr, and the remainder was assumed to be eliminated through metabolism with an hepatic clearance value of 147 L/hr (Dash et al., 2018; Masters et al., 2016).

For S, S-hydroxybupropion, the total apparent clearance determined from non-compartmental analysis (NCA) of digitized data from a radafaxine clinical trial (40 mg S, S-hydroxybupropion administered orally) was 13.4 L/hr (Nora D. Volkow et al., 2005). The intrinsic hepatic formation clearance of this metabolite (0.93 µl/min/mg of microsomal protein) was derived from our published in vitro human liver microsomal assay results (**Chapter 2**) (Bhattacharya et al., 2019). In this work, the Michaelis-Menten parameters ($V_{max}$ and $K_m$) were not determined, nor were they from a study that used the S9 liver fraction by Sager et al (Sager et al., 2016). The hepatic formation clearance of 4.4 L/hr was scaled from an intrinsic microsomal clearance of 0.93 µl/min/mg of microsomal protein , which is similar to 7 L/hr reported by Sager et al (Sager et al., 2016). Furthermore, the formation clearance calculated from the ratio of AUC of formed metabolite (S, S-hydroxybupropion $AUC_{0-\infty}$ 580 nM (Masters et al., 2016) to bupropion $AUC_{0-\infty}$ 1334 nM (Masters et al., 2016), which is 0.44), multiplied by clearance of S, S hydroxybupropion of 13.4 L/hr (Nora D. Volkow et al., 2005) (from NCA analysis of digitized radafaxine, that is, preformed S, S-hydroxybupropion from a clinical trial), was 5.86 L/hr, which is close to the hepatic clearance scaled from our in vitro microsomal clearance study (Bhattacharya et al., 2019). Renal clearance of 1.28 L/hr was taken from a study by Desta et al, and was calculated as the ratio of the cumulative amount excreted in the urine by 48 hours to the area under the plasma concentration-time curve during the same interval (Masters et al., 2016). Total clearance of 13.4 L/hr was partitioned to 1.28 for renal clearance (Masters et al., 2016) and the remainder 12.5 L was assumed to be hepatically eliminated. Unbound plasma fraction in humans for S, S-hydroxybupropion was 0.23 (Cremers et al., 2016; J. Andrew Johnston et al., 2002).

## 6.3 Results

The schematic of the parent and pharmacologically active metabolite (bupropion-S, S-hydroxybupropion) PBPK model structure is shown in **Figure 6.1**. Typically, drug administered via the subcutaneous route is absorbed directly into blood or enters blood indirectly following absorption first into the lymphatic circulation (Richter & Jacobsen, 2014). Both the enzymes and

species differences in pre-systemic catabolism, or lymphatic pathways for bupropion leading to incomplete bioavailability are not fully understood or available (Richter & Jacobsen, 2014). Further, the lipid composition for the subcutaneous compartment to determine the $K_p$ (based on partitioning of unionized drug into neutral lipids and neutral phospholipids, dissolution of ionized and unionized drug in subcutaneous tissue) was not available for the rat. So, for development of a rat PBPK model we dosed into the oral compartment, assuming the absorption rates (indicated by $k_a$) were similar for the oral and subcutaneous compartments, and the overall exposures or clearance were not impacted. The similarity in $k_a$s supports this assumption ($k_a$ for preformed S, S-hydroxybupropion from the population-pk model, **Chapter 5**, was 0.95 $hr^{-1}$ and that from the PBPK model was 1.5 $hr^{-1}$. $k_a$ for bupropion from the population-pk model was 0.87-3.6 $hr^{-1}$ and that from PBPK model was 1.5 $hr^{-1}$). The absolute oral bioavailability for bupropion in rats in a study by Butz et al is reported to be 10% (Butz et al., 1982). However, with known low stability of bupropion (Laizure & DeVane, 1985; O'Byrne et al., 2010; Suma et al., 2006) and the crude analytical technique used in earlier analysis of bupropion, skepticism lingers around this estimate values; hence, we did not incorporate bioavailability in the present model, and assumed that oral and subcutaneous bioavailabilities were similar.

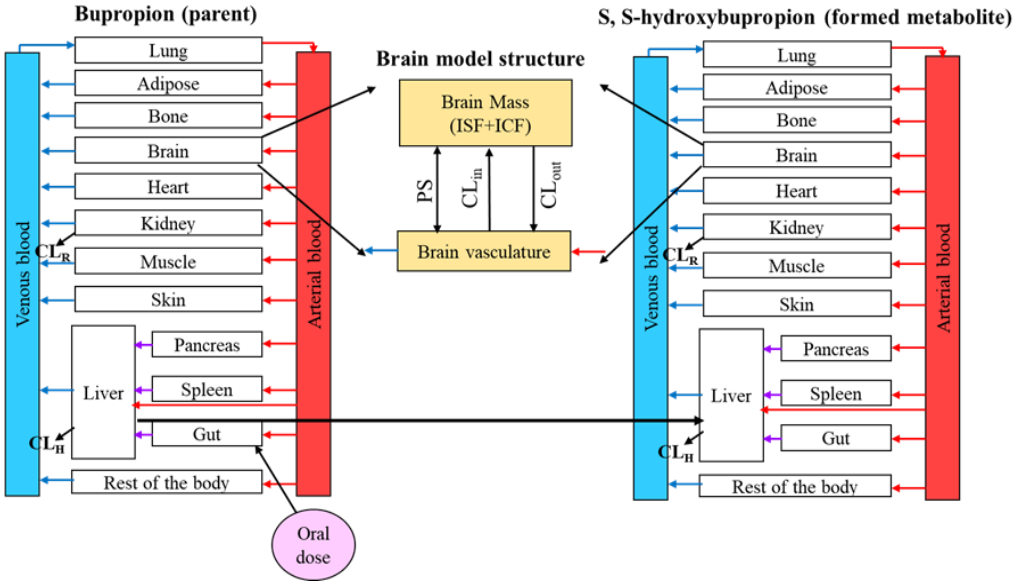


**Figure 6.1.** Parent (bupropion)-metabolite (S, S-hydroxybupropion) physiologically-based pharmacokinetic (PBPK) model structure for rat and humans. ISF: Interstitial fluid; ICF: Intracellular; PS: Passive permeability-surface area product on blood-brain-barrier; $CL_{in}$: influx clearance, $CL_{out}$: efflux clearance; $CL_R$:renal clearance; $CL_H$:hepatic clearance.

The drug related parameters for bupropion, preformed and formed S, S-hydroxybupropion used in the final rat-specific model are shown in **Tables 6.1, 6.3** and **6.5,** respectively.

Comparison of model independent and PBPK model derived unbound plasma and brain pharmacokinetic parameters of bupropion, preformed and formed S, S-hydroxybupropion used in the final rat model are shown in **Tables 6.2, 6.4**, **6.6,** respectively.

The predicted versus observed rat plasma unbound concentration-time profiles of bupropion, preformed and formed S, S-hydroxybupropion are shown in **Figures 6.3, 6.7** and **6.11**, respectively. Comparison of predictions from various brain model structures for bupropion preformed and formed S, S-hydroxybupropion are shown in **Figures 6.4, 6.8, 6.12** respectively. The predicted versus observed rat brain (final model structure) unbound concentration-time profiles of bupropion, preformed S, S-hydroxybupropion and formed S, S-hydroxybupropion are shown in **Figures 6.5** (bupropion)**, 6.9** (preformed metabolite) and **6.13** (formed metabolite), respectively.

Results from sensitivity analysis evaluating the impact of various parameters on bupropion, preformed and formed S, S-hydroxybupropion`s plasma and brain exposures in rat are shown in **Figure 6.2, 6.6, 6.10,** respectively.

**Figure 6.2.** Sensitivity analysis to evaluate the impact of parameters on unbound plasma **(Left)** and unbound brain **(Right)** exposures of bupropion. Mean observed data are shown in pink filled circles. Impact of varying unbound plasma fraction from 0.1 to 0.8 (observed data unbound plasma fraction=0.5) on bupropion plasma exposures (**A**) and brain exposures (**B**). Impact of varying unbound brain fraction from 0.1 to 0.8 (observed data unbound brain fraction = 0.13) on bupropion plasma exposures (**C**) and brain exposures (**D**). Impact of varying blood to plasma ratio (BP) from 0.1 to 0.8 (observed data BP = 0.42) on bupropion plasma exposures (**E**) and brain exposures (**F**). Impact of varying oral absorption rate constant from 0.5 to 4 (observed data ka=1.5 $hr^{-1}$) on bupropion plasma exposures (**G**) and brain exposures (**H**). Impact of varying renal clearance from 0.005 to 0.16 (observed data renal clearance=0.018 L/hr) on bupropion plasma exposures (**I**) and brain exposures (**J**). Impact of varying intrinsic hepatic clearance from 50 to 800 µL/min/mg protein (observed data intrinsic hepatic clearance = 190 µL/min/mg protein) on bupropion plasma exposures (**K**) and brain exposures (**L**). Impact of varying BBB permeability surface area product from 0.0001 to 0.0008 (observed data BBB permeability surface area product = 0.00016 cm/sec) on bupropion plasma exposures (**M**) and brain exposures (**N**). Impact of varying BBB efflux 0.01 to 0.16 (observed data BBB permeability surface area product =0.03 cm/sec) on bupropion plasma exposures (**O**) and brain exposures (**P**). Impact of varying brain uptake clearance (observed data brain uptake clearance=14237 µL/min/mg brain protein) on bupropion plasma exposures (**Q**) and brain exposures (**R**)

Figure 6.2 continued

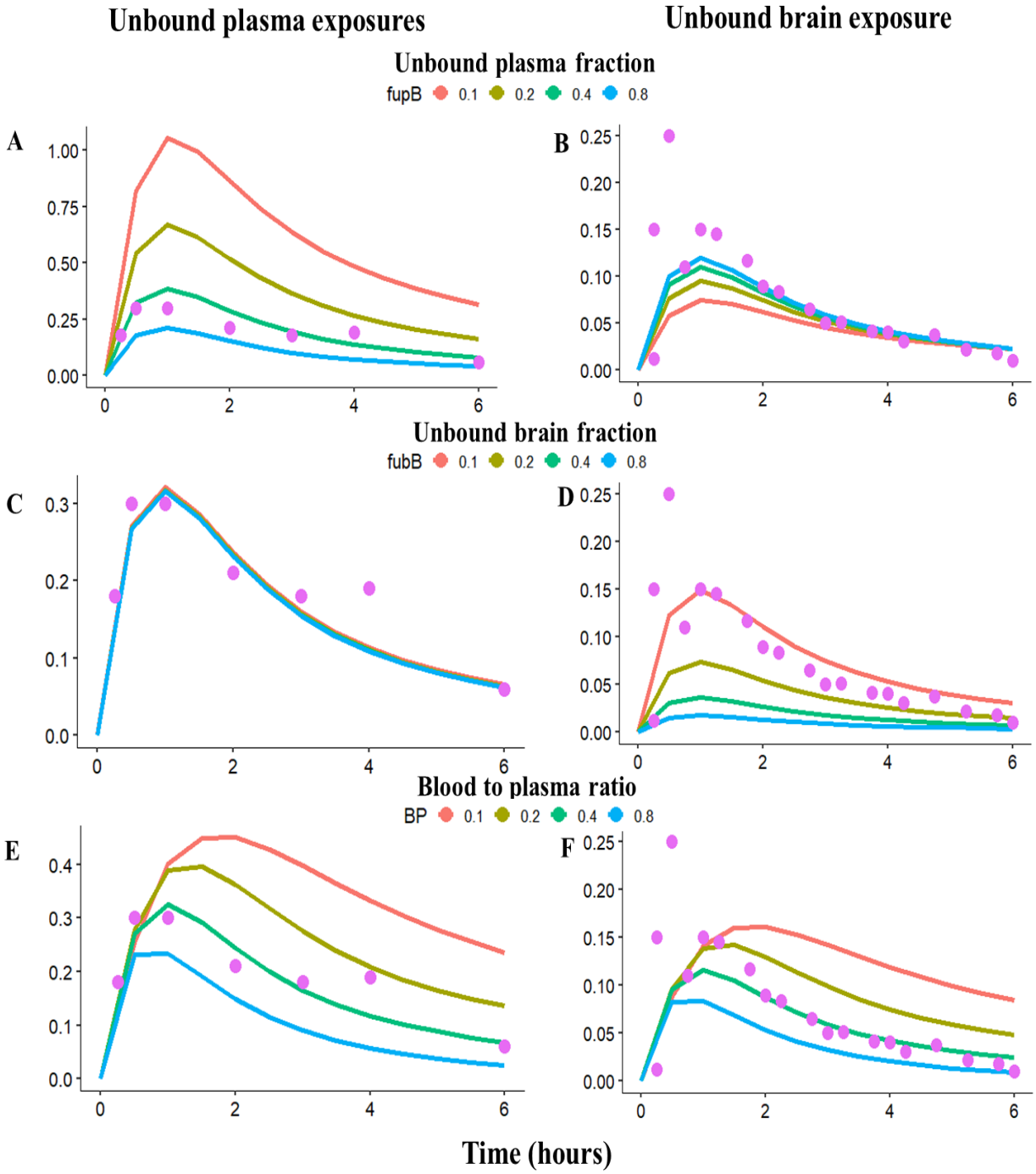

Figure 6.2 continued

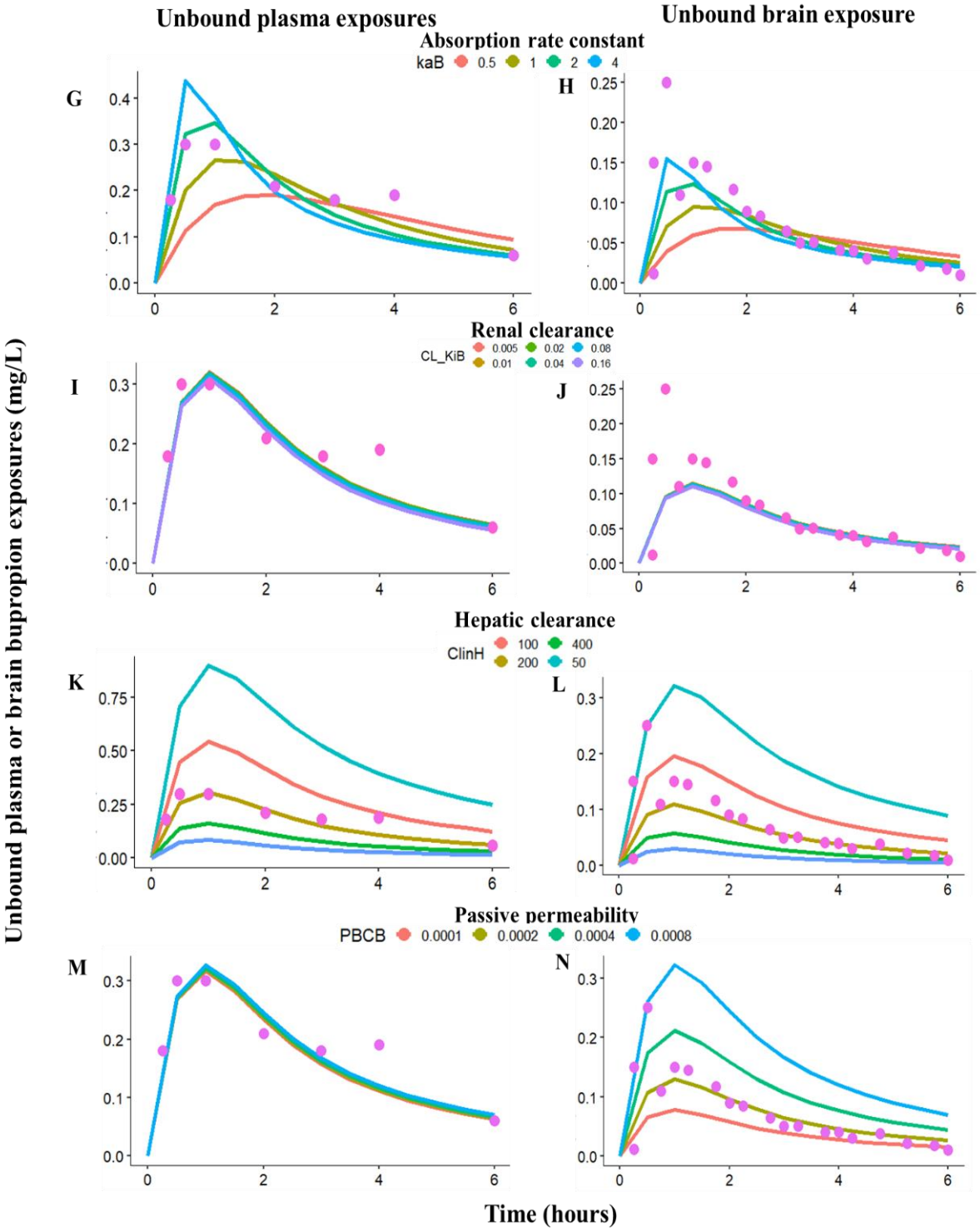

Figure 6.2 continued

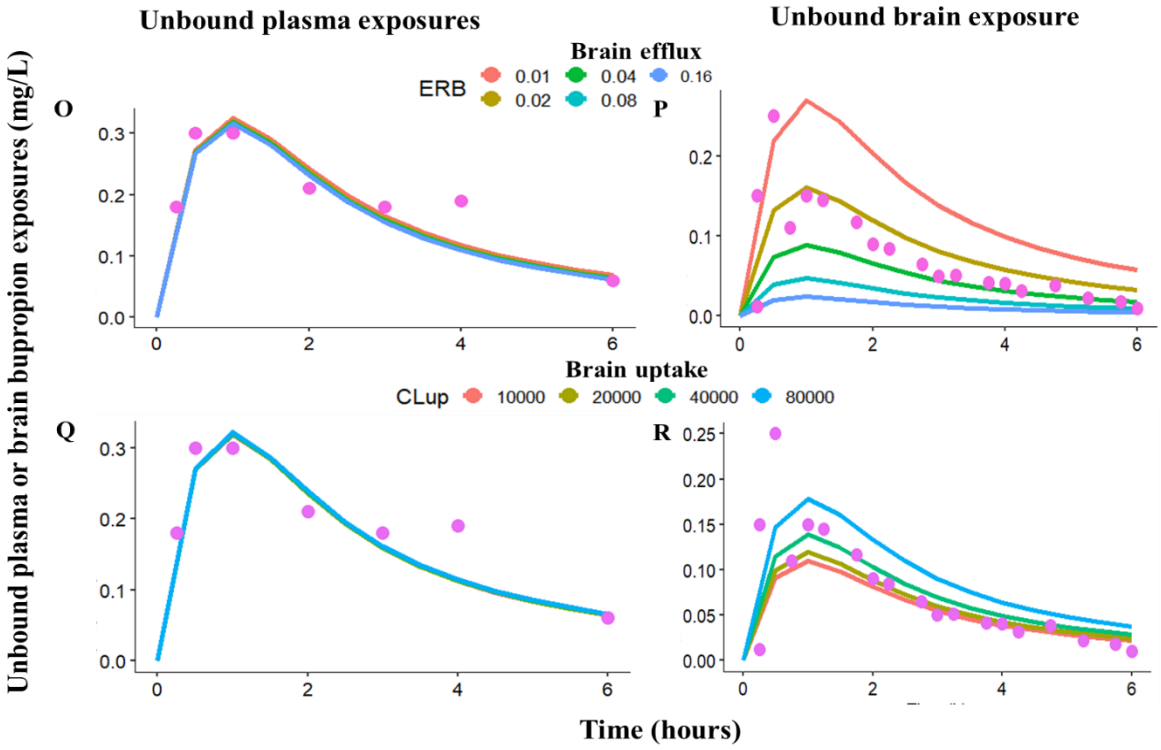


.

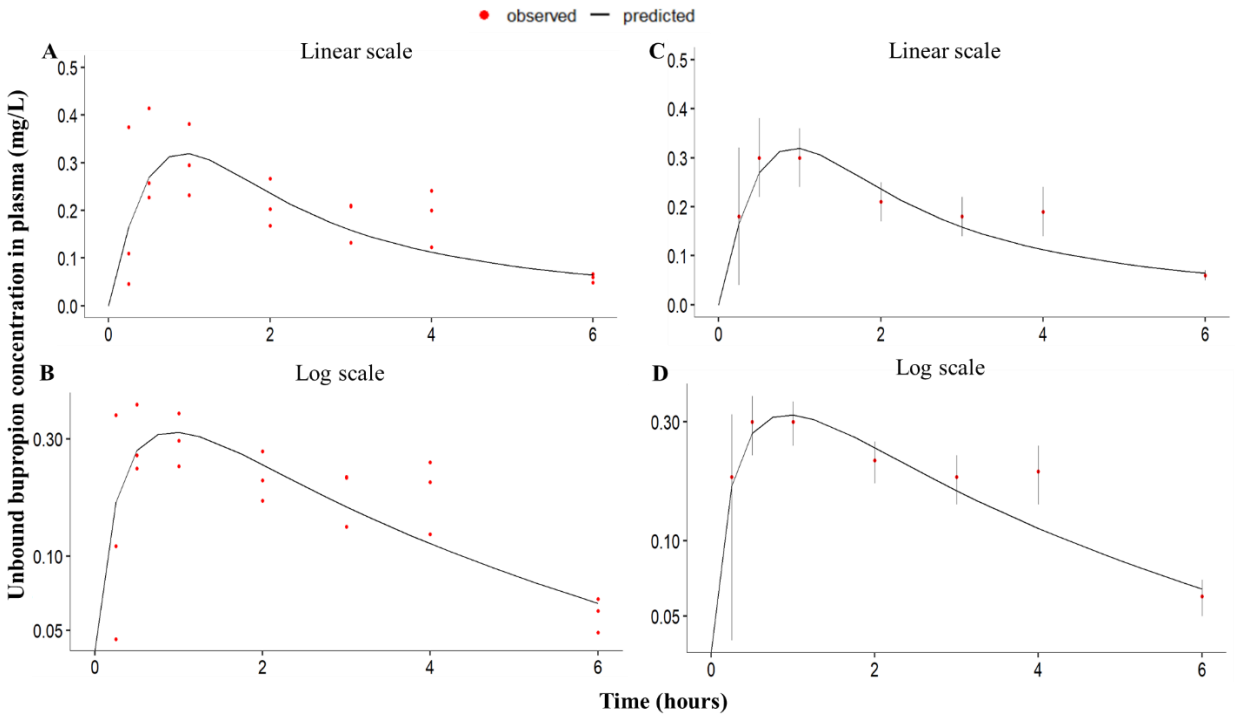


**Figure 6.3.** Predicted versus observed unbound plasma bupropion concentration time profiles in rats after 10 mg/kg extravascular bupropion administration. **A** and **B** represent mean predicted (solid line) and individual observed plasma concentrations (red filled circles). **C** and **D** represent mean predicted (black solid line) and red filled circles and error bars denote observed means and standard deviation (n = 3 animals), respectively. The observed unbound plasma data is from the present study, where total plasma concentration was corrected for unbound fraction through in vitro studies.

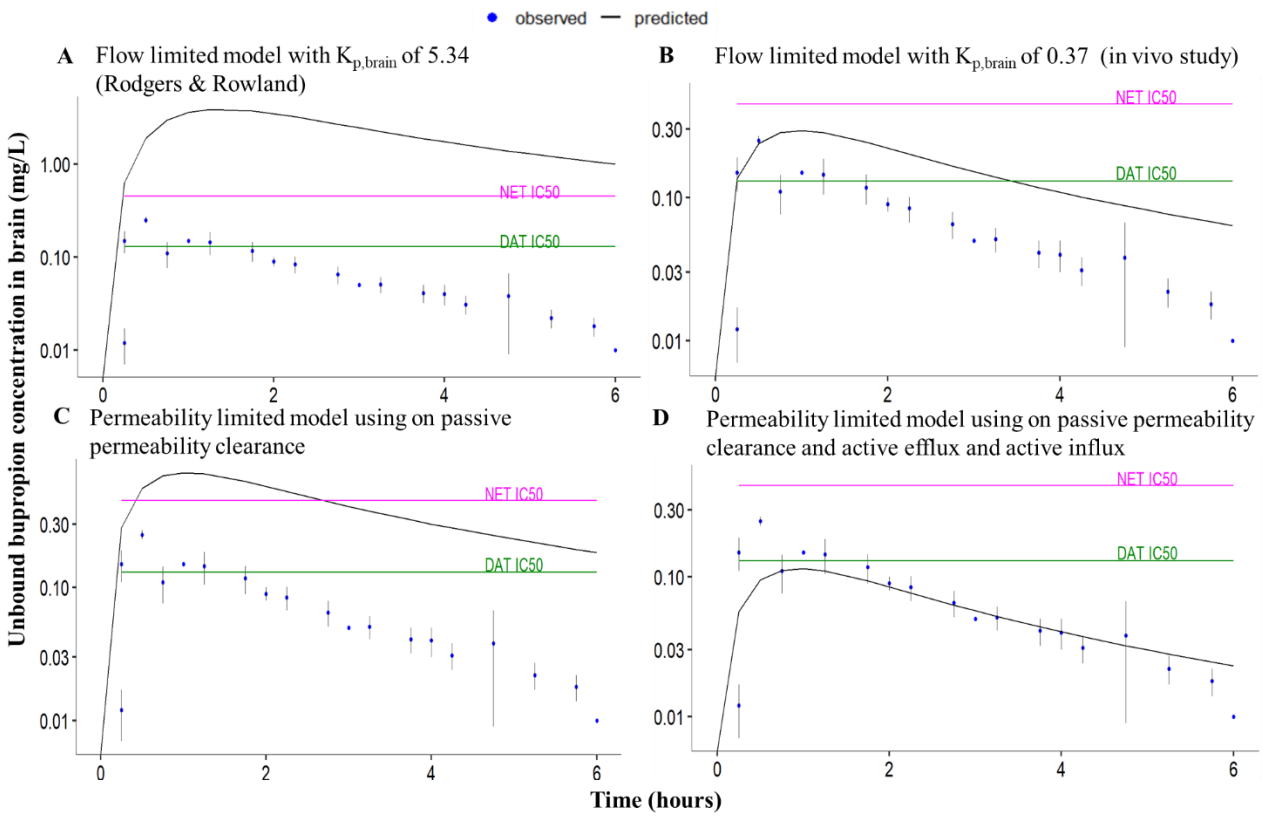


**Figure 6.4.** Predicted (black solid line) versus observed ± SD (blue filled circles) unbound mean brain bupropion log-concentration time profiles in rats after 10 mg/kg extravascular bupropion administration. Blue filled circles and error bars denote observed means and standard deviation (n = 3 from 2019 study or 4 animals from 2016 microdialysis study at each time point), respectively. The observed means comprise data from 2016 microdialysis study which directly measured unbound brain extracellular fluid concentrations and present/2019 study where whole brain homogenate measures were corrected for unbound fraction through in vitro brain binding assay. **A** represents flow limited brain model structure with brain to plasma ratio of 5.34 calculated based on the Rodgers and Rowland method. **B** represents flow limited brain model structure with brain to plasma ratio of 0.37 calculated using in vivo study (Chapter 3). **C** represents permeability limited model structure using passive surface area product/ passive clearance. **D** represents permeability limited brain model structure with passive surface area product plus influx and efflux clearances. Green line refers to rat $IC_{50}$ value 0.13 mg/L reported for dopamine transporter (DAT) and pink line refers to rat $IC_{50}$ value of 0.45 mg/L for norepinephrine transporter (NET).

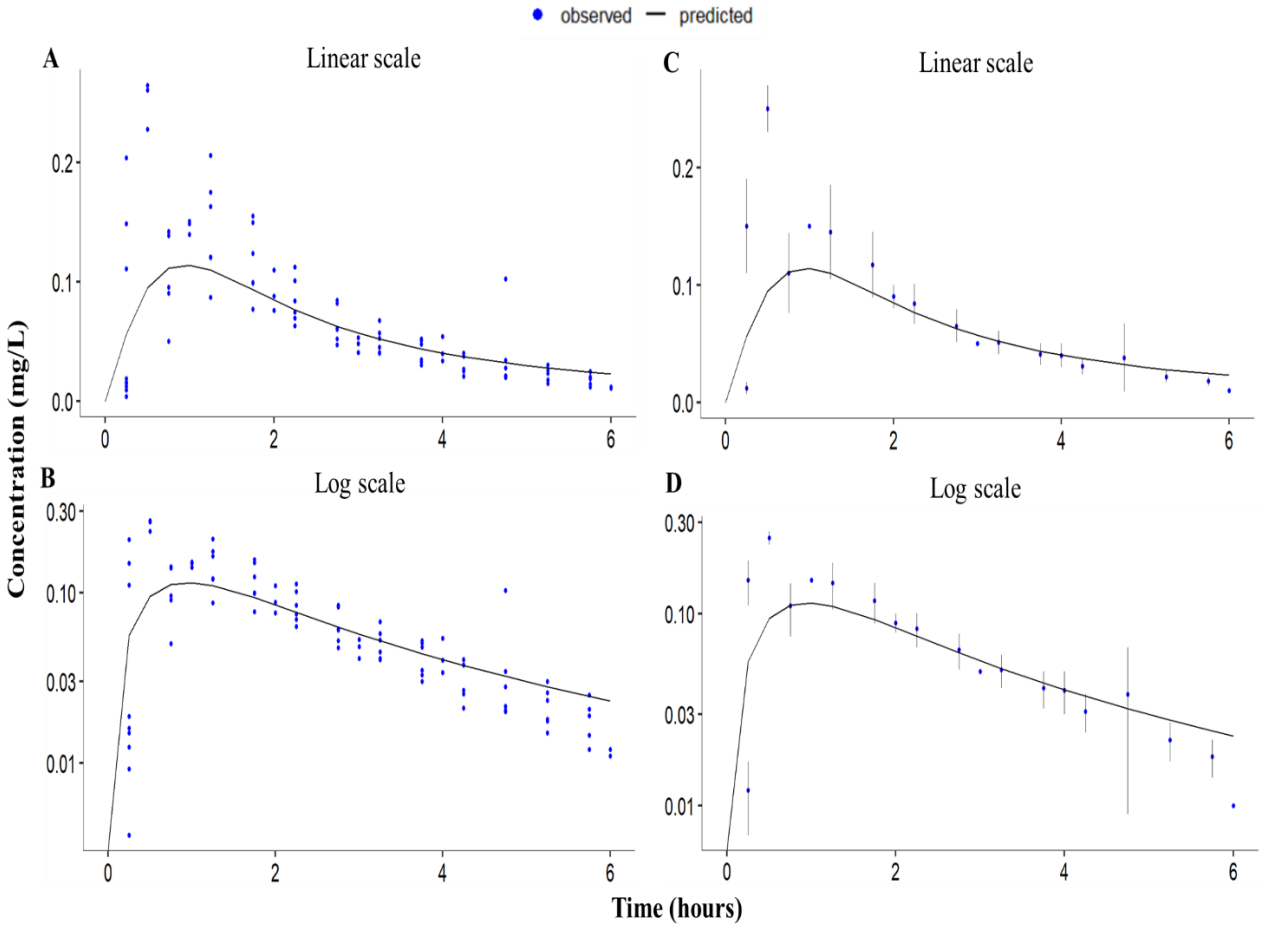


**Figure 6.5.** Predicted versus observed unbound brain bupropion concentration time profiles in rats after 10 mg/kg extravascular bupropion administration. This represents final-brain model structure, which is a permeability limited structure comprising of passive permeability clearance, active brain efflux and active influx terms. **A** and **B** represent mean predicted (solid line) and individual observed brain concentrations (red filled circles). **C** and **D** represent mean predicted (black solid line) and blue filled circles and error bars denote observed means and standard deviation (n = 3 from 2019 or n = 3 or 4 from 2016 microdialysis study each time point), respectively. The observed means comprise data from 2016 microdialysis study which directly measured unbound brain extracellular fluid concentrations and present/2019 study where whole brain homogenate measures were corrected for unbound fraction through in vitro brain binding assay.

**Table 6.1.** Drug related parameters used for bupropion rat PBPK model

| Parameter | Description | Value | Reference/Note |
|---|---|---|---|
| MW (g/mol) | Molecular weight of bupropion | 239.74 | Simcyp® |
| logP | Octanol: buffer partition coefficient | 3.27 | Simcyp® |
| pKa | Acid dissociation constant (base) | 8.22 | Simcyp® |
| BP | Blood-to-plasma partition ratio | 0.42 | (Sager et al., 2016) |
| $fu_p$ | Fraction unbound in plasma | 0.5 | Experimental |
| **Absorption** | | | |
| $k_a$ (1/hr) | Absorption rate constant | 1.5 | Sensitivity analysis |
| **Distribution** | | | |
| $K_p$ | Tissue to plasma ratios | | Simcyp® |
| **Elimination** | | | |
| $CL_{inH}$ (µL/min/mg protein) | Liver microsomal protein in vitro intrinsic clearance | 191 | Parameter estimation % RSE=26.2, CI(95%)= 161-202 |
| $CL_R$ (L/h) | Renal clearance | 0.018 | (Masters et al., 2016) allometric scaling from human data |
| MPPGL (mg/g)) | Microsomal protein per gram of liver | 46 | Simcyp® (rat) |
| $fu_{mic}$ | Fraction unbound in microsomes | 0.58 | Simcyp® for 0.5 mg/mL microsome concentration |
| **Brain transport** | | | |
| PS (L/hr) | Passive permeability clearance | 0.16 | Simcyp®, QSAR model Apparent permeability 0.000168 cm/sec |
| $\lambda_{bm}$ | Ionization coefficient at brain mass | 31 | Henderson–Hasselbalch equation |
| $\lambda_{bb}$ | Ionization coefficient at BBB | 17 | brain mass pH = 7.12, plasma pH =7.4 |
| $CL_{uptake}$ (L/h) | Influx clearance at BBB | 0.36 | Sensitivity analysis Adjusted to 15000 µL/min/mg to fit data |
| $CL_{efflux}$ (L/hr) | Efflux clearance at BBB | 19.44 | Sensitivity analysis/parameter estimation $0.03 \times 10^{-6}$ cm/sec, % RSE=22.5 , CI(95%)=0.0164-0.0392 |
| $fu_b$ | Fraction unbound in brain | 0.13 | experimental |
| MPPGB (mg/g) | Milligrams of protein per gram of brain | 0.25 | (Ball et al., 2012) |

RSE: relative standard error; CI: Confidence interval

**Table 6.2.** Mean unbound pharmacokinetic parameters of bupropion in plasma and brain. Observed values are from model independent analysis and predicted values are from the final PBPK model following administration of 10 MPK subcutaneous bupropion.

| Matrix | Unbound PK parameters | Observed (O) (2019) | Observed (O) (2016) | Predicted (P) | % Relative error (% RE) | | Fold error (P/O) | |
|---|---|---|---|---|---|---|---|---|
| | | | | | 2019 | 2016 | 2019 | 2016 |
| Plasma | $AUC_{0-\infty}$ (mg*hr/L) | 1.30 | - | 1.28 | 1.53 | - | 0.98 | - |
| | $C_{max}$ (mg/L) | 0.3 | - | 0.32 | 6.66 | - | 1.06 | - |
| | $t_{max}$ (hr) | 0.5 | - | 1 | 100 | - | 2 | - |
| Brain | $AUC_{0-\infty}$ (mg*hr/L) | 0.47 | 0.40 | 0.46 | 2.12 | 15 | 0.97 | 1.15 |
| | $C_{max}$ (mg/L) | 0.25 | 0.15 | 0.12 | 52 | 20 | 0.48 | 0.80 |
| | $t_{max}$ (hr) | 0.5 | 1.25 | 1 | 100 | 20 | 2 | 0.80 |

AUC: Area under curve, $C_{max}$: Maximum concentration, $t_{max}$: time to maximum concentration
The above observed data represents mean unbound brain values from four rats in 2016 microdialysis study, which directly measured unbound brain extracellular fluid concentration, and 2019 brain homogenate study from twenty-four rats (three rat brains per time point),where whole brain measures were corrected for unbound fraction using in vitro brain binding study.
% Relative error was calculated using 100 · (observed - predicted)/observed

**Figure 6.6.** Sensitivity analysis to evaluate the impact of parameters on unbound plasma **(Left)** and unbound brain **(Right)** exposures of preformed S, S-hydroxybupropion. Mean observed data are shown in pink filled circles. Impact of varying unbound plasma fraction from 0.1 to 0.8 (observed data unbound plasma fraction=0.7) on S, S-hydroxybupropion plasma exposures (**A**) and brain exposures (**B**). Impact of varying unbound brain fraction from 0.1 to 0.8 (observed data unbound brain fraction=0.14) on S, S-hydroxybupropion plasma exposures (**C**) and brain exposures (**D**). Impact of varying blood to plasma ratio (BP) from 0.1 to 0.8 (observed data BP=0.42) on S, S-hydroxybupropion plasma exposures (**E**) and brain exposures (**Figure F**). Impact of varying oral absorption rate constant from 0.5 to 4 (observed data ka=1.5 $hr^{-1}$) on S, S-hydroxybupropion plasma exposures (**G**) and brain exposures (**H**). Impact of varying renal clearance from 0.005 to 0.16 (observed data renal clearance=0.012 L/hr) on S, S-hydroxybupropion plasma exposures **(I**) and brain exposures (**J**). Impact of varying intrinsic hepatic clearance from 100 to 1600 µL/min/mg protein (observed data intrinsic hepatic clearance=590 µL/min/mg protein) on S, S-hydroxybupropion plasma exposures (**K**) and brain exposures (**L**). Impact of varying BBB permeability surface area product from 0.00001 to 0.00008 (observed data BBB permeability surface area product =0.00004 cm/sec) on S, S-hydroxybupropion plasma exposures (**M**) and brain exposures (**N**). Impact of varying BBB efflux 0.0001 to 0.0008 (observed data efflux term=0.0007 cm/sec) on S, S-hydroxybupropion plasma exposures (**O**) and brain exposures (**P**). Impact of varying brain uptake clearance from 10000 to 80000 (observed data brain uptake clearance=13500 µL/min/mg brain protein) on S, S-hydroxybupropion plasma exposures (**Q**) and brain exposures (**R**).

Figure 6.6 continued

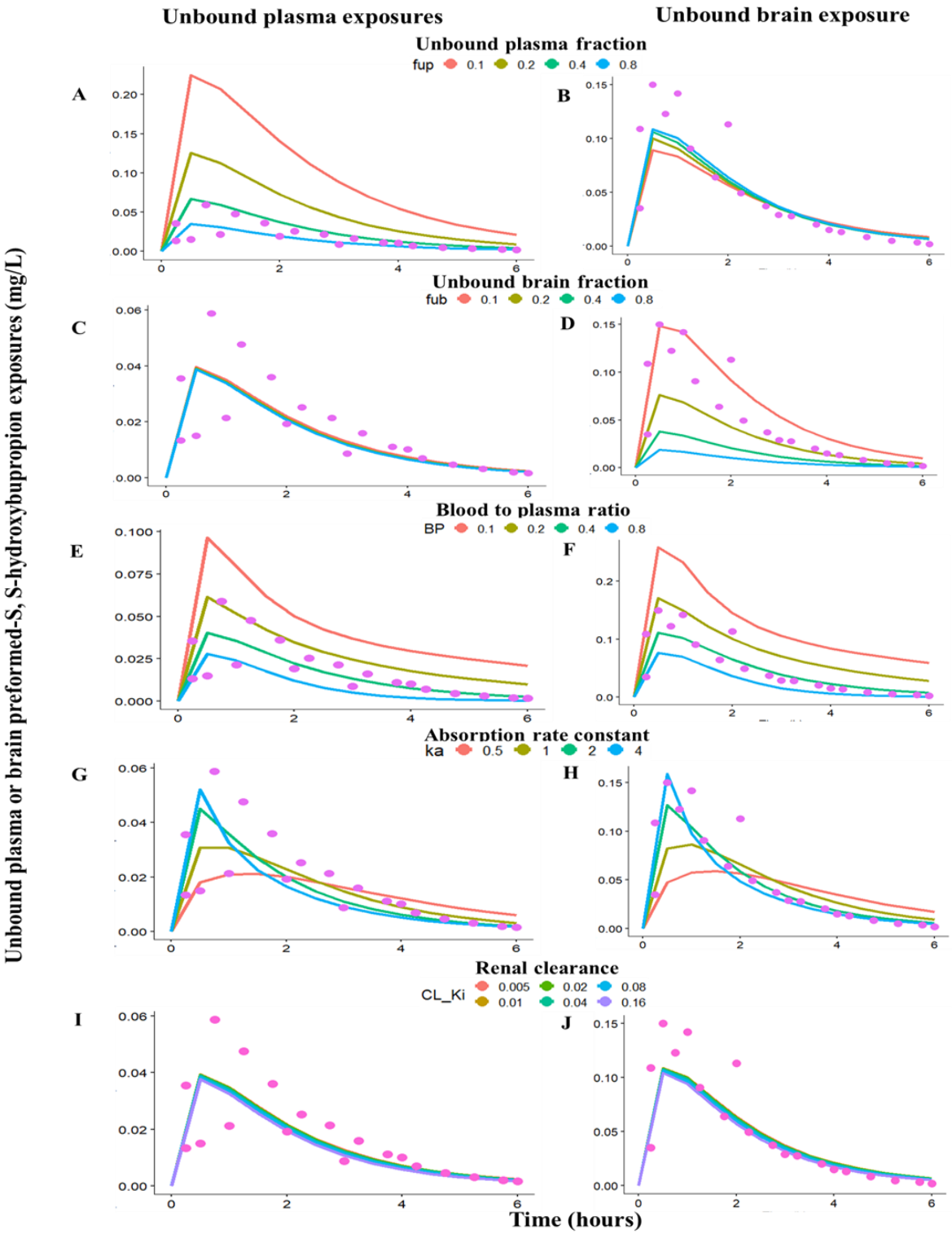

Figure 6.6 continued

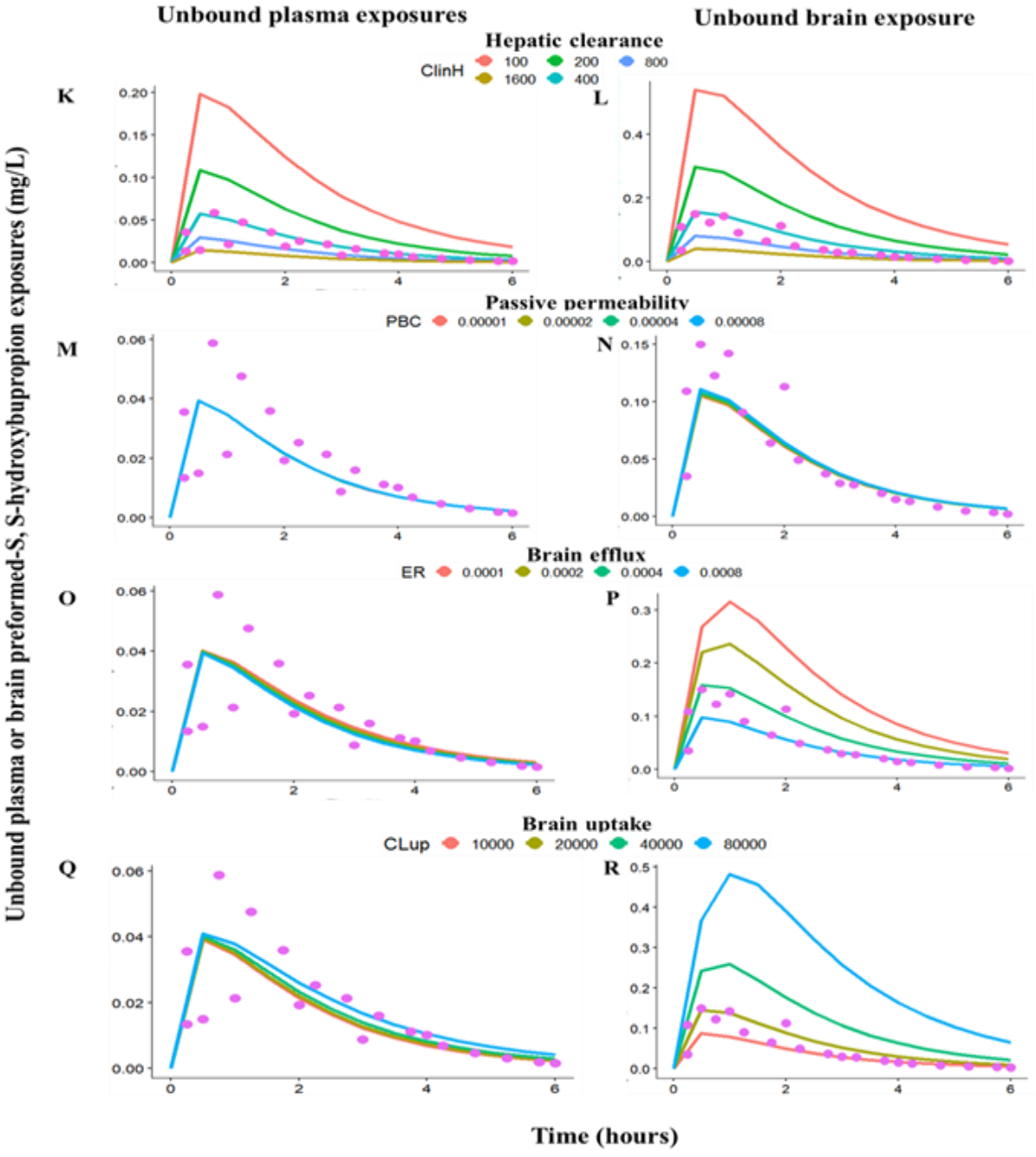

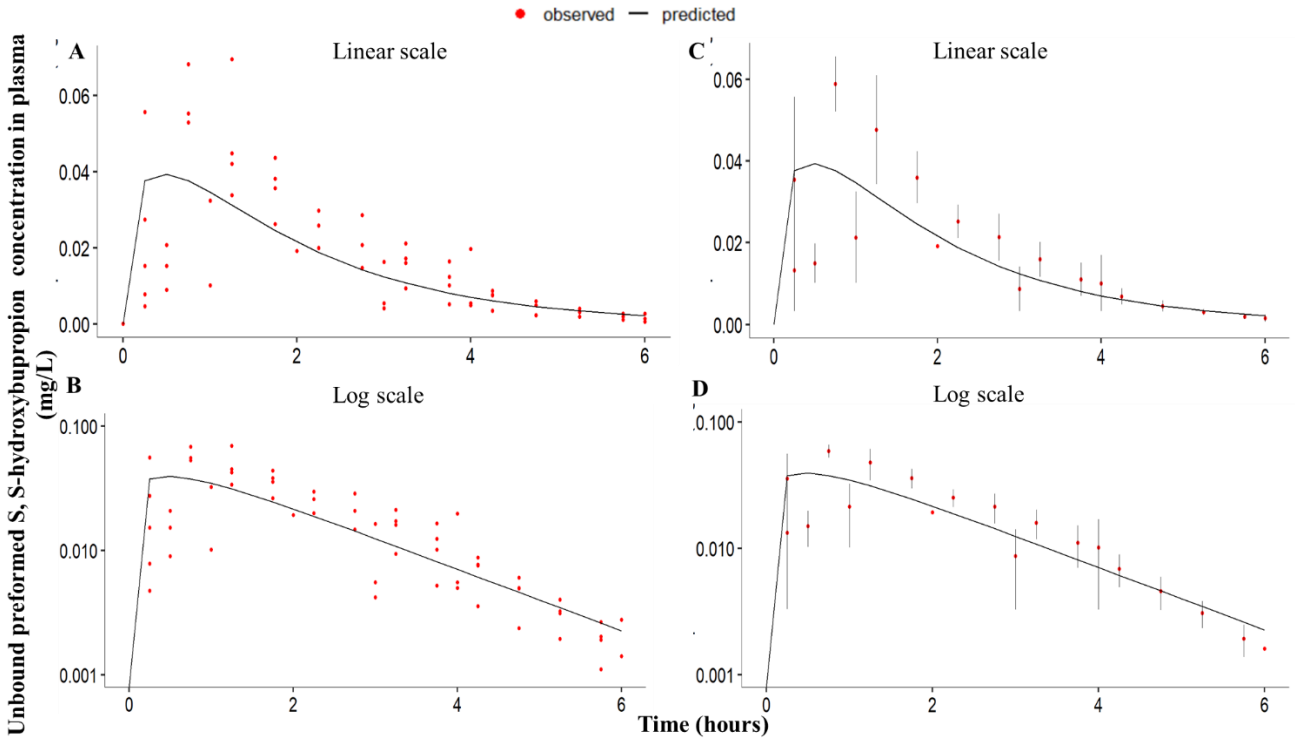


**Figure 6.7.** Predicted versus observed unbound plasma preformed S, S-hydroxybupropion concentration time profiles in rats after 2 mg/kg extravascular S, S-hydroxybupropion administration. **A** and **B** represent mean predicted (solid line) and individual observed plasma concentrations (red filled circles). **C** and **D** represent mean predicted concentrations (solid line) and red filled circles and error bars denote observed means and standard deviation (n = 3 from 2019 study or 3 or 4 animals from 2016 microdialysis study at each time point), respectively. The observed means comprise data from 2016 microdialysis study, which directly measured unbound plasma and present/2019 study, where total plasma concentrations were corrected for unbound fraction through in vitro plasma binding assay.

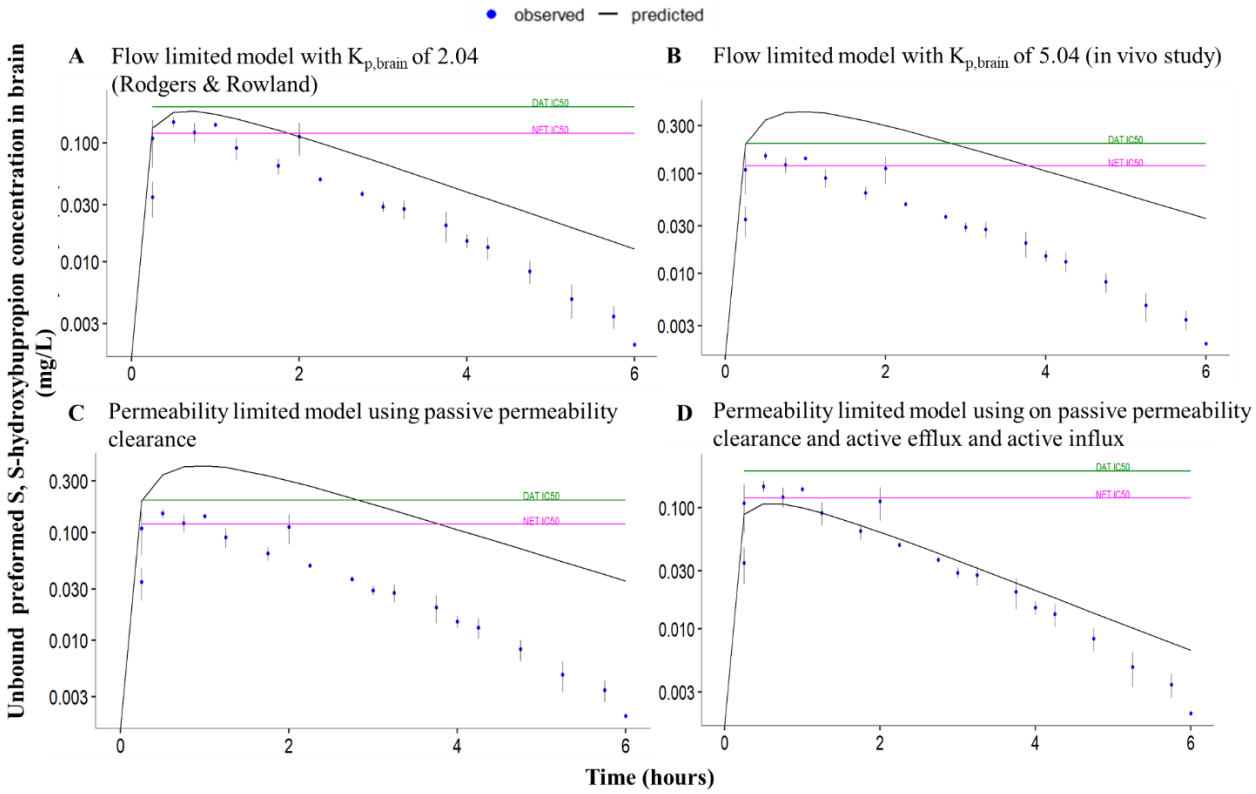


**Figure 6.8.** Predicted (black solid line) versus observed ± SD (blue filled circles) unbound mean brain preformed S, S hydroxybupropion log-concentration time profiles in rats after 2 mg/kg extravascular S, S-hydroxybupropion administration. Blue filled circles and error bars denote observed means and standard deviation (n = 3 animals from 2019 study or 3 or 4 animals from 2016 microdialysis study at each time point), respectively. The observed means comprise data from 2016 microdialysis study which directly measured unbound brain extracellular fluid concentrations and present/2019 study where whole brain homogenate measures were corrected for unbound fraction through in vitro brain binding assay. **A** represents flow limited brain model structure with brain to plasma ratio of 2.04 calculated using Rodgers and Rowland method. **B** represents flow limited brain model structure with brain to plasma ratio of 5.04 calculated using in vivo study. **C** represents permeability limited model structure using on passive surface area product/ passive clearance. **D** represents permeability limited brain model structure with passive surface area product with influx and efflux clearance. Green line refers to rat $IC_{50}$ value 0.2 mg/L reported for dopamine transporter (DAT) and pink line refers to rat $IC_{50}$ value of 0.12 mg/L for norepinephrine transporter (NET).

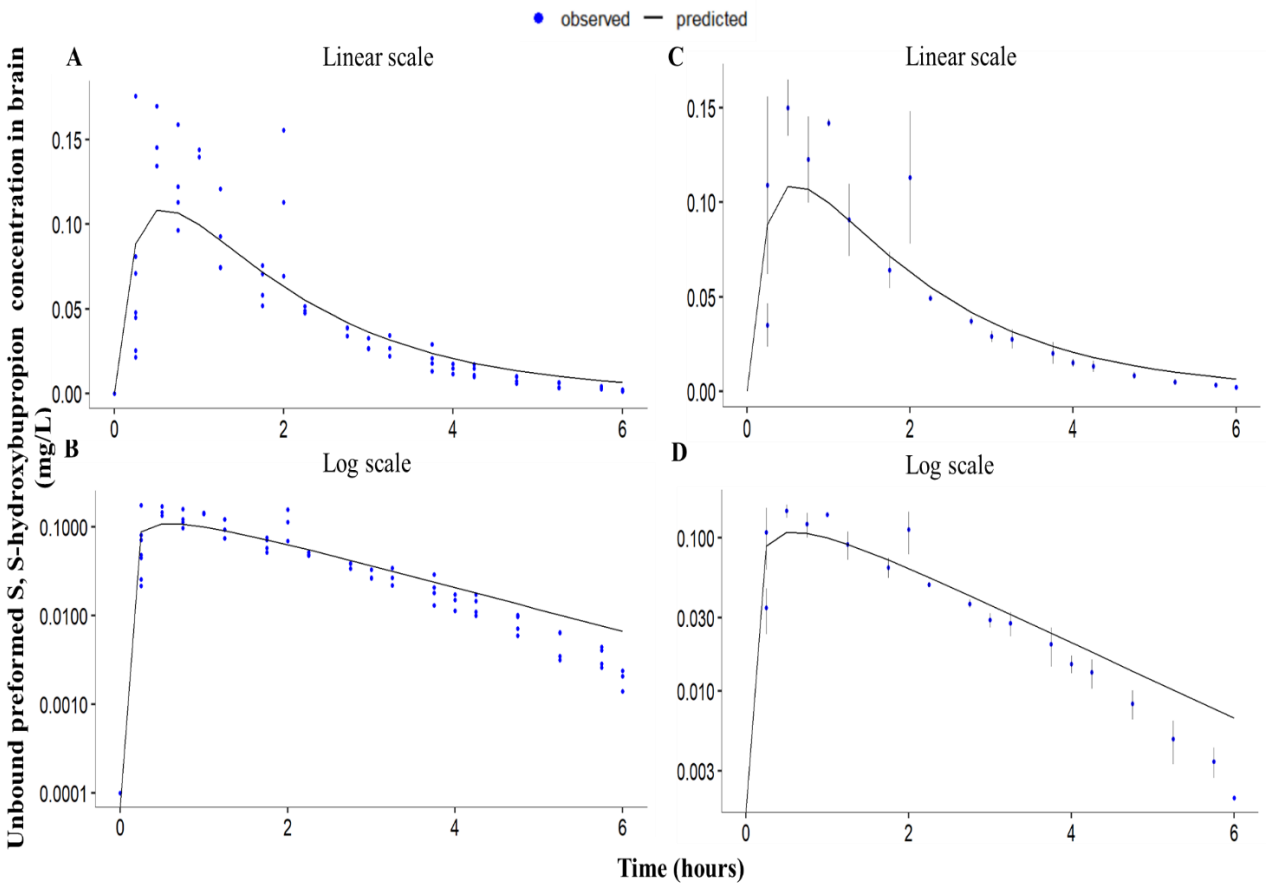


**Figure 6.9.** Predicted versus observed unbound brain preformed S, S-hydroxybupropion log-concentration time profiles in rats after 2 mg/kg extravascular S, S-hydroxybupropion administration. This represents final-brain model structure, which is a permeability limited structure comprising of passive permeability clearance, brain efflux and influx terms. **A** and **B** represent mean predicted (solid line) and individual observed brain concentrations (blue filled circles). **C** and **D** represent mean predicted (black solid line) and blue filled circles and error bars denote observed means and standard deviation (n = 3 animals from 2019 study or 3 or 4 animals from 2016 microdialysis study at each time point) respectively. The observed means comprise data from 2016 microdialysis study which directly measured unbound brain extracellular fluid concentrations and present/2019 study where whole brain homogenate measures were corrected for unbound fraction through in vitro brain binding assay.

**Table 6.3.** Drug related parameters used for preformed S, S-hydroxybupropion rat PBPK model.

| Parameter | Description | Value | Reference/Notes |
|---|---|---|---|
| MW (g/mol) | Molecular weight of hydroxybupropion | 255.74 | Simcyp® |
| logP | Octanol: buffer partition coefficient | 1.9 | Simcyp® |
| pKa | Acid dissociation constant (base) | 7.65 | Simcyp® |
| BP | Blood-to-plasma partition ratio | 0.42 | (Sager et al., 2016) |
| $fu_p$ | Fraction unbound in plasma | 0.7 | Experimental |
| **Absorption** | | | |
| $k_a$ (1/hr) | Absorption rate constant | 1.5 | Sensitivity analysis |
| **Distribution** | | | |
| $K_p$ | Tissue to plasma ratios | | Simcyp® |
| **Elimination** | | | |
| $CL_{inH}$ (µL/min/mg protein) | Liver microsomal protein in vitro intrinsic clearance | 590 | % RSE=29.4, CI (95%)= 336-1040 |
| $CL_R$(L/h) | Renal clearance | 0.012 | (Masters et al., 2016) |
| MPPGL (mg/g) | Microsomal protein per gram of liver | 46 | Simcyp® (rat) |
| $fu_{mic}$ | Fraction unbound in microsomes | 0.9 | Simcyp® for 0.5 mg/mL microsome concentration |
| **Brain transport** | | | |
| PS (L/hr) | Passive permeability clearance | 0.043 | Simcyp®, QSAR model Apparent permeability 0.0000443 cm/sec |
| $\lambda_{bm}$ | Ionization coefficient at brain mass | 4.4 | Henderson–Hasselbalch equation |
| $\lambda_{bb}$ | Ionization coefficient at blood-brain | 2.8 | brain mass pH = 7.12, plasma pH =7.4 |
| $CL_{uptake}$(L/h) | Influx clearance at BBB | 0.36 | parameter estimation 12000 µL/min/mg protein % RSE=10.6 , CI(95%)=9720-14700 |
| $CL_{efflux}$(L/h) | Efflux clearance at BBB | 0.68 | parameter estimation 0.0007 x $10^{-6}$ cm/sec, % RSE=39.6 , CI(95%)=0.00035-0.00156 |
| $fu_b$ | Fraction unbound in brain | 0.14 | experimental |
| MPPGB (mg/g) | Milligrams of protein per gram of brain | 0.25 | (Ball et al., 2012) |

RSE: relative standard error; CI: Confidence interval

**Table 6.4.** Mean unbound pharmacokinetic parameters of preformed S, S-hydroxybupropion in plasma and brain from model independent analysis (observed) and PBPK model (predicted) following extravascular administration of 2 mg/kg of preformed S, S-hydroxybupropion.

| Matrix | Unbound PK parameters | Observed (O) (2019) | Observed (O) (2016) | Predicted (P) | % Relative error (% RE) | | Fold error (P/O) | |
|---|---|---|---|---|---|---|---|---|
| | | | | | 2019 | 2016 | 2019 | 2016 |
| Plasma | $AUC_{0-\infty}$ (mg*hr/L) | 0.07 | 0.13 | 0.10 | 42.8 | 23 | 1.42 | 0.76 |
| | $C_{max}$ (mg/L) | 0.02 | 0.06 | 0.04 | 100 | 33.3 | 2 | 0.66 |
| | $t_{max}$ (hr) | 1 | 0.75 | 0.5 | 50 | 33.3 | 0.5 | 0.66 |
| Brain | $AUC_{0-\infty}$ (mg*hr/L) | 0.36 | 0.24 | 0.28 | 22.2 | 16.6 | 0.77 | 1.16 |
| | $C_{max}$ (mg/L) | 0.15 | 0.12 | 0.11 | 26.6 | 8.3 | 0.73 | 0.91 |
| | $t_{max}$ (hr) | 0.5 | 0.75 | 0.5 | 0 | 33.3 | 1 | 0.66 |

AUC: Area under curve, $C_{max}$: Maximum concentration, $t_{max}$: time to maximum concentration.
The above observed data represents mean unbound plasma and brain values from four rats in 2016 microdialysis study, which directly measured unbound brain extracellular fluid concentration and 2019 brain homogenate study from twenty-four rats (three rat brains per time point), where whole brain measures were corrected for unbound fraction using in vitro brain binding study.
% Relative error was calculated using 100 · (observed - predicted)/observed

**Figure 6.10.** Sensitivity analysis to evaluate the impact of parameters on unbound plasma **(Left)** and unbound brain **(Right)** exposures of formed S, S-hydroxybupropion. Mean observed data are shown in pink filled circles. Impact of varying unbound plasma fraction from 0.1 to 0.8 (observed data unbound plasma fraction=0.7) on S, S-hydroxybupropion plasma exposures (**A**) and brain exposures (**B**). Impact of varying unbound brain fraction from 0.1 to 0.8 (observed data unbound brain fraction=0.14) on S, S-hydroxybupropion plasma exposures (**C**) and brain exposures (**D**). Impact of varying blood to plasma ratio (BP) from 0.1 to 0.8 (observed data BP=0.42) on S, S-hydroxybupropion plasma exposures (**E**) and brain exposures (**F**). Impact of varying renal clearance from 0.005 to 0.16 (observed data renal clearance=0.012 L/hr) on S, S-hydroxybupropion plasma exposures **(G**) and brain exposures (**H**). Impact of varying intrinsic hepatic clearance from 100 to 1600 µL/min/mg protein (observed data intrinsic hepatic clearance=777 µL/min/mg protein) on S, S-hydroxybupropion plasma exposures (**I**) and brain exposures (**J**). Impact of varying BBB permeability surface area product from 0.00001 to 0.00008 (observed data BBB permeability surface area product =0.00004 cm/sec) on S, S-hydroxybupropion plasma exposures (**K**) and brain exposures (**L**). Impact of varying BBB efflux 0.0001 to 0.0008 (observed data efflux term=0.002 cm/sec) on S, S-hydroxybupropion plasma exposures (**M**) and brain exposures (**N**). Impact of varying brain uptake clearance from 10000 to 80000 (observed data brain uptake clearance=12000 µL/min/mg brain protein) on S, S-hydroxybupropion plasma exposures (**O**) and brain exposures (**P**).

Figure 6.10 continued

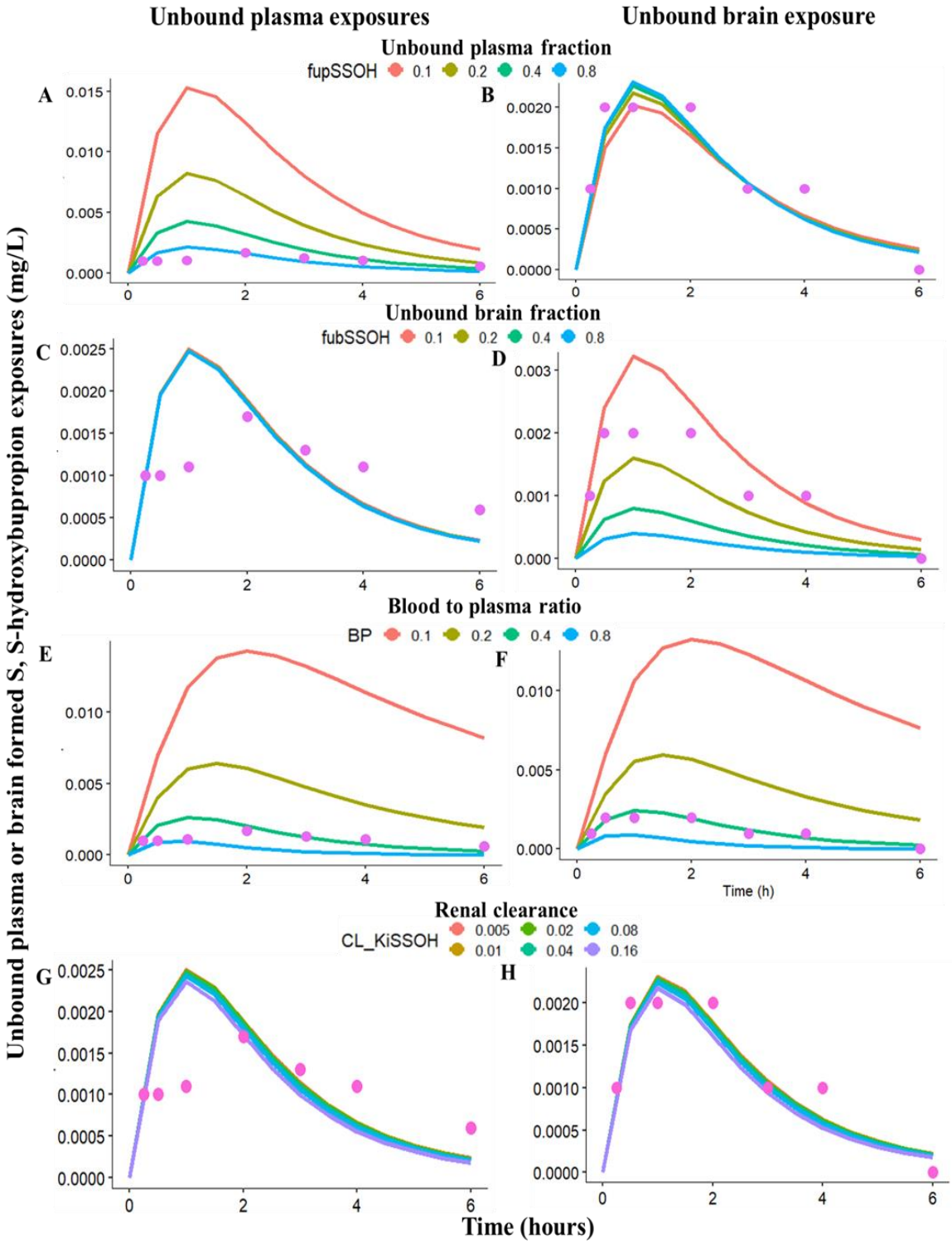

Figure 6.10 continued

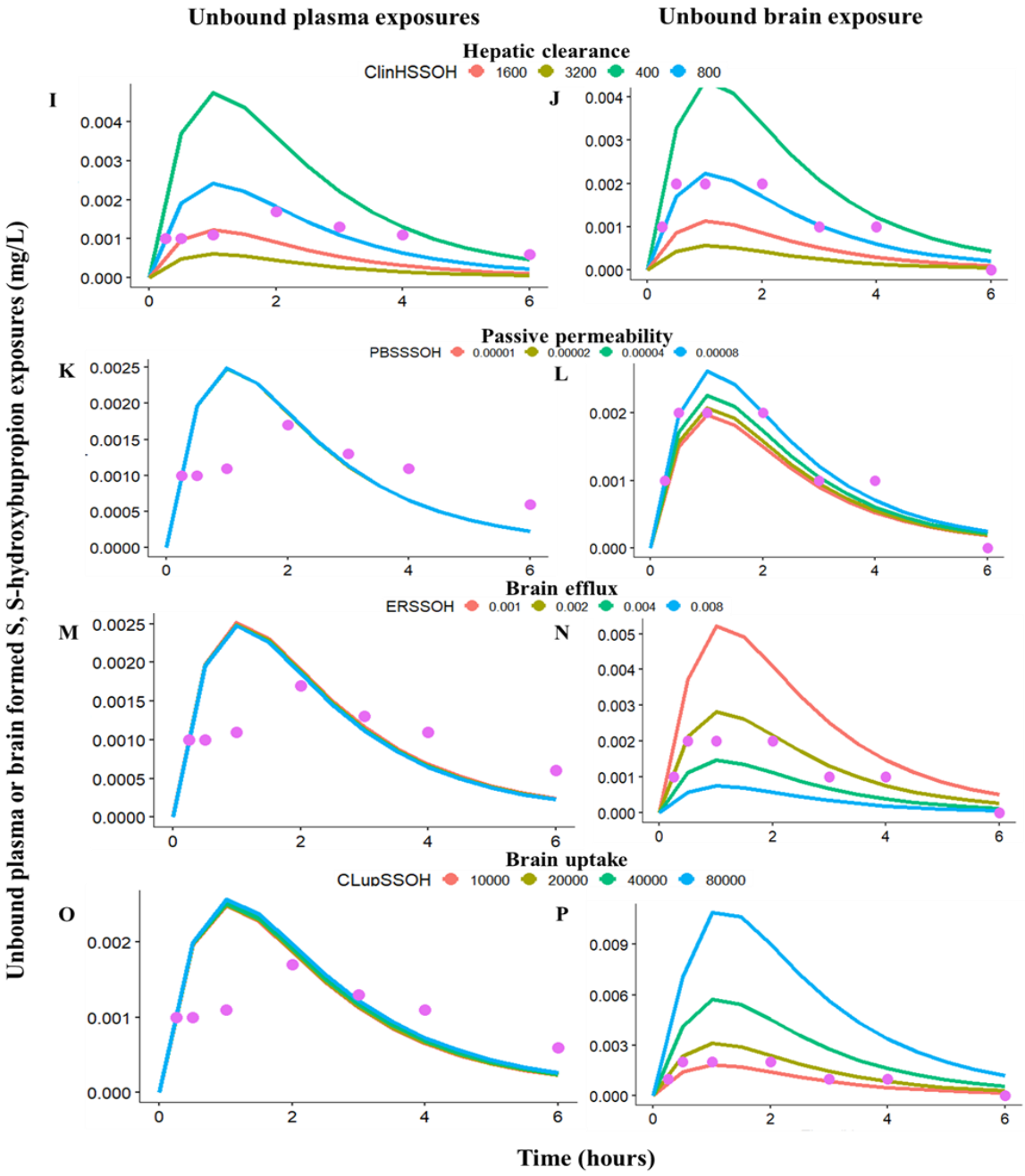

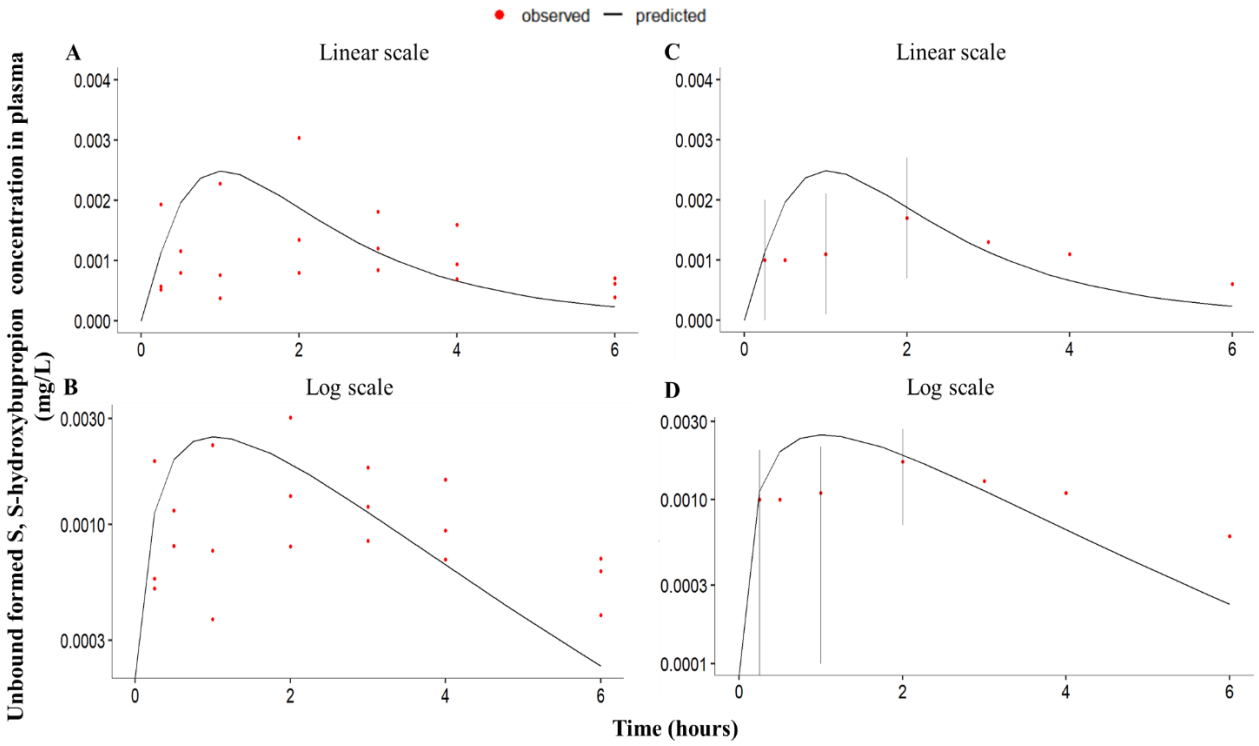


**Figure 6.11.** Predicted versus observed unbound plasma formed S, S-hydroxybupropion concentration time profiles in rats after 10 mg/kg extravascular bupropion administration. **A** and **B** represent mean predicted (solid line) and individual observed plasma concentrations (red filled circles). **C** and **D** represent mean predicted (black solid line) and red filled circles and error bars denote observed means and standard deviation (n = 3 animals), respectively. The observed unbound plasma data is from the present study, where total plasma concentration was corrected for unbound fraction through in vitro studies.

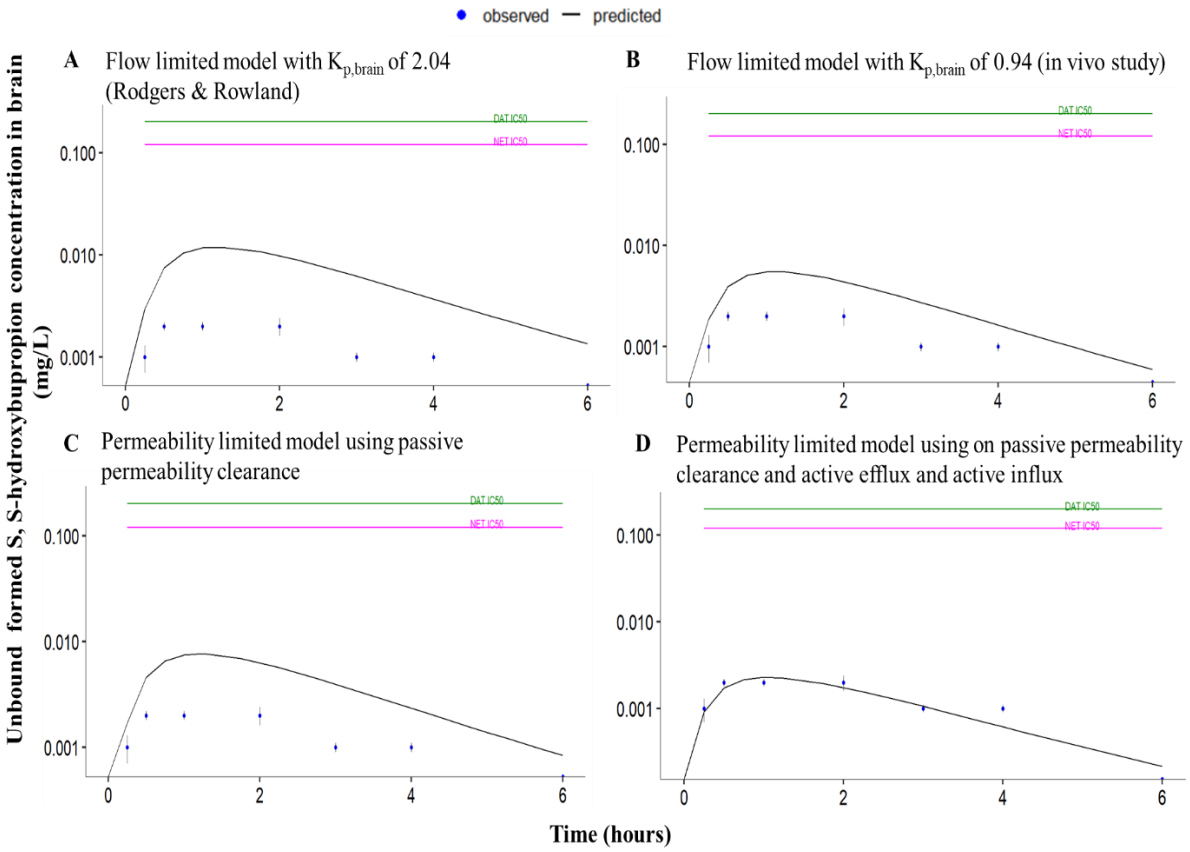


**Figure 6.12.** Predicted (black solid line) versus observed ± SD (blue filled circles) unbound mean brain formed S, S hydroxybupropion concentration time profiles in rats after 10 mg/kg extravascular bupropion administration. Blue filled circles and error bars denote observed means and standard deviation (n = 3 animals at each time point) respectively. The observed means comprise data from present/2019 study where whole brain homogenate measures were corrected for unbound fraction through in vitro brain binding assay. **A** represents flow limited brain model structure with brain to plasma ratio of 2.04 calculated using Rodgers and Rowland method. **B** represents flow limited brain model structure with brain to plasma ratio of 0.94 calculated from in vivo study. **C** represents permeability limited model structure using on passive surface area product/ passive clearance. **D** represents permeability limited brain model structure with passive surface area product with influx and efflux clearance. Green line refers to rat $IC_{50}$ value 0.2 mg/L reported for dopamine transporter (DAT) and pink line refers to rat $IC_{50}$ value of 0.12 mg/L for norepinephrine transporter (NET).

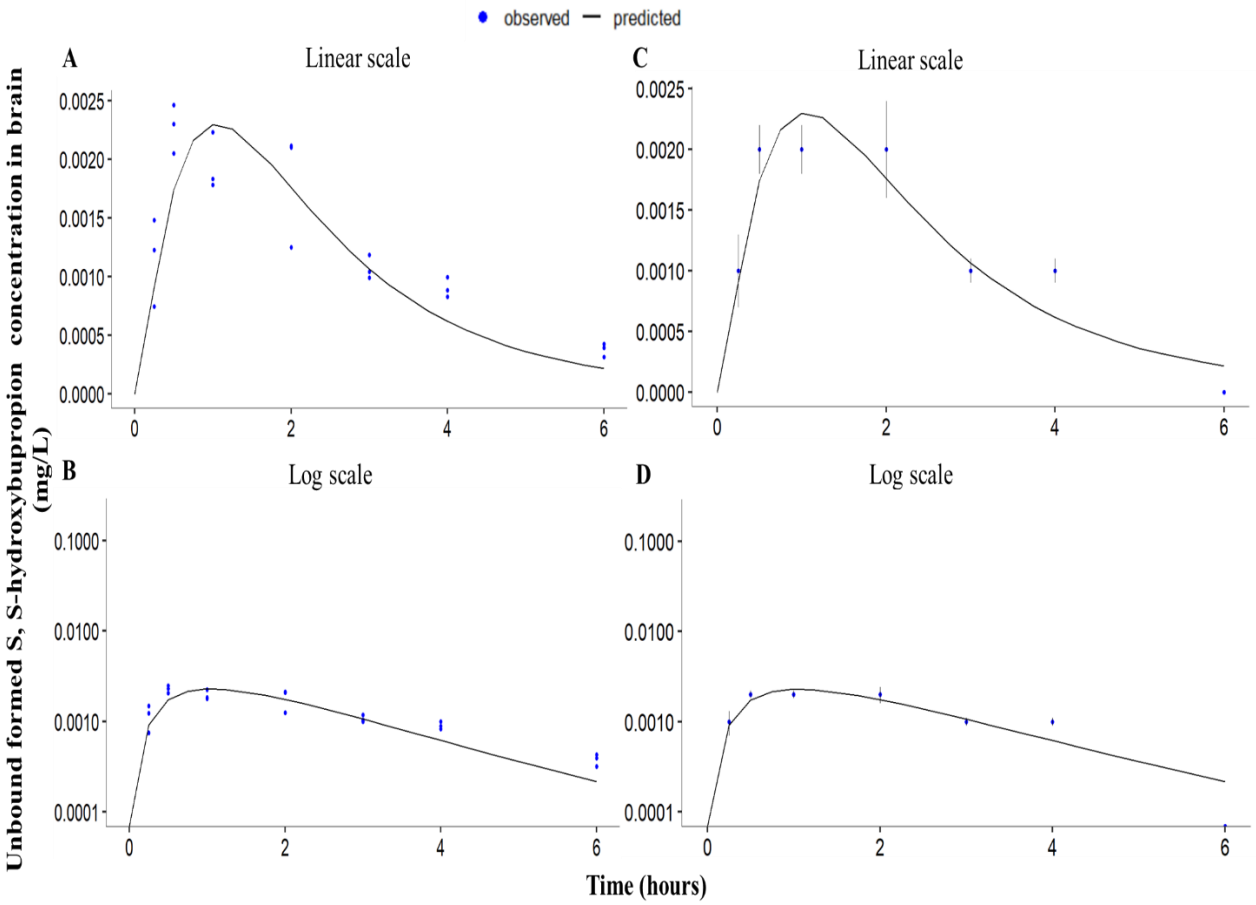


**Figure 6.13.** Predicted versus observed unbound brain formed S, S-hydroxybupropion log-concentration time profiles in rats after 10 mg/kg extravascular bupropion administration. This represents final-brain model structure, which is a permeability limited structure comprising of passive permeability clearance, active brain efflux and active influx terms. **A** and **B** represent mean predicted (solid line) and individual observed brain concentrations (blue filled circles). **C** and **D** represent mean predicted (black solid line) and blue filled circles and error bars denote observed means and standard deviation (n = 3 animals at each time point), respectively. The observed means comprise data from present/2019 study where whole brain homogenate measures were corrected for unbound fraction through in vitro brain binding assay.

**Table 6.5.** Drug related parameters used for formed S, S-hydroxybupropion rat PBPK model.

| Parameter | Description | Value | Reference/Notes |
|---|---|---|---|
| MW (g/mol) | Molecular weight of hydroxybupropion | 255.74 | Simcyp® |
| logP | Octanol: buffer partition coefficient | 1.9 | Simcyp® |
| pKa | Acid dissociation constant (base) | 7.65 | Simcyp® |
| BP | Blood-to-plasma partition ratio | 0.42 | (Sager et al., 2016) |
| $fu_p$ | Fraction unbound in plasma | 0.7 | Experimental |
| **Distribution** | | | |
| $K_p$ | Tissue to plasma ratios | | Rodgers and Rowland (Simcyp®) |
| **Elimination** | | | |
| $V_{max}$ (pmol/min/mg microsomal protein) | Maximum rate of metabolite formation | 8.38 | Hepatic microsomal incubation experiment |
| $K_m$ (μM) | Michaelis Menten constant | 19.85 | (Masters et al., 2016) |
| $CL_{inH}$ (μL/min/mg protein) | Liver microsomal protein in vitro intrinsic clearance | 777 | parameter estimation % RSE=22.4, CI (95%)= 504-1200 |
| $CL_R$(L/h) | Renal clearance | 0.0120 | allometric scaling from human data (Masters et al., 2016) allometric scaling from human data |
| **Brain transport** | | | |
| PS (L/hr) | Passive permeability clearance | 0.043 | Simcyp®, QSAR model Apparent permeability 0.0000443 cm/sec |
| $\lambda_{bm}$ | Ionization coefficient at brain mass | 4.4 | Henderson–Hasselbalch equation |
| $\lambda_{bb}$ | Ionization coefficient at blood-brain | 2.8 | brain mass pH = 7.12, plasma pH =7.4 |
| $CL_{uptake}$ (L/h) | Influx clearance at BBB | 0.36 | Sensitivity analysis and Preformed S, S-hydroxybupropion |
| $CL_{efflux}$ (L/h) | Efflux clearance at BBB | 0.68 | Sensitivity analysis/ 0.0025 x $10^{-6}$ cm/sec. Adjusted to fit data |
| $fu_b$ | Fraction unbound in brain | 0.14 | experimental |
| MPPGB (mg/g) | Milligrams of protein per gram of brain | 0.25 | (Ball et al., 2012) |

RSE: relative standard error; CI: Confidence interval

**Table 6.6.** Mean unbound pharmacokinetic parameters of formed S, S-hydroxybupropion in plasma and brain following 10 mg/kg administration of racemic bupropion. Observed values are from model independent analysis and predicted values are from the final PBPK model.

| Matrix | Unbound PK parameters | Observed (O) | Predicted (P) | % Relative error (% RE) | Fold error (P/O) |
|---|---|---|---|---|---|
| Plasma | $AUC_{0-\infty}$ (mg*hr/L) | 0.008 | 0.007 | 12.5 | 0.87 |
| | $C_{max}$ (mg/L) | 0.002 | 0.002 | - | 1 |
| | $t_{max}$ (hr) | 2 | 1 | 50 | 0.5 |
| Brain | $AUC_{0-\infty}$ (mg*hr/L) | 0.008 | 0.007 | 12.5 | 0.87 |
| | $C_{max}$ (mg/L) | 0.002 | 0.002 | - | 1 |
| | $t_{max}$ (hr) | 0.5 | 1 | 100 | 2 |

AUC: Area under curve, $C_{max}$: Maximum concentration, $t_{max}$: time to maximum concentration.
The above observed data represents mean unbound plasma and brain values from 2019 brain homogenate study from twenty-four rats (three rat brains per time point), where whole brain measures were corrected for unbound fraction using in vitro plasma and brain binding study.
% Relative error was calculated using 100 · (observed - predicted)/observed

From sensitivity analysis, as one would intuitively expect, increased $fu_{plasma,}$, hepatic clearance and blood-plasma ratio resulted in decreased plasma exposures for both bupropion and S, S-hydroxybupropion. Fraction unbound in brain ($fu_{brain}$), passive apparent permeability, efflux and uptake clearances, were key parameters influencing brain exposures of bupropion and S, S-hydroxybupropion. Experimentally derived values of unbound rat plasma, brain fraction, blood to plasma ratio of bupropion and S, S-hydroxybupropion, which also seemed to fit the data well from graphical sensitivity analysis, were used in the final model. Simcyp® based values of BBB passive permeability clearance of 0.16 L/hr and 0.043 L/hr were used for bupropion and S, S-hydroxybupropion, respectively. Optimization based on the maximum likelihood estimation method were employed (using the nonlinear optimization- nloptr package (Johnson)) to optimize hepatic clearance, BBB ER, and active influx across the BBB to fit the data. The optimized BBB efflux term for bupropion was ER: 0.03 x $10^{-6}$ cm/sec (% RSE=22.5, CI 95% =0.0164-0.0392). The estimated value of brain uptake term was 36387 µL/min/mg protein, but had >30% RSE, so

it was adjusted to value of 15000 to fit the data. The optimized intrinsic hepatic clearance of bupropion was 191 µL/min/mg protein (% RSE=26.2, CI 95% = 161-202). The intrinsic hepatic clearance of preformed S, S-hydroxybupropion was 590 µL/min/mg protein (% RSE=29.4, 95% CI = 336-1040). The optimized BBB efflux term for preformed S, S-hydroxybupropion was 0.0007 x $10^{-6}$ cm/sec, % RSE=39.6, CI (95%) = 0.00035-0.00156) and brain uptake term was 12000 µL/min/mg protein (% RSE=10.6, 95% CI 95% = 9720-14700). The formed S, S-hydroxybupropion`s intrinsic hepatic clearance was 777 µL/min/mg protein (% RSE=22.4, 95% CI 95%= 504-1200). The formed S, S-hydroxybupropion` brain efflux and uptake terms could not be precisely estimated, possibly because of few data points and high variability in the data. So graphical sensitivity analysis was used to fit the brain formed S, S-hydroxybupropion data. The brain uptake term of 12000 µL/min/mg protein was used for the formed S, S-hydroxybupropion as well (from graphical sensitivity analysis). However, the efflux had to be adjusted to a value of 0.0024 x $10^{-6}$ cm/sec to fit the data. This three-fold difference in efflux between formed versus preformed S, S-hydroxybupropion could possibly be due to competition between bupropion and this metabolite at the blood-brain-barrier. The relative exposure of S, S-hydroxybupropion to bupropion is much lower, which would enhance the ability of bupropion to compete with stereoselective carrier mediated transport of S, S-hydroxybupropion.

Parameters characterizing brain transport (apparent brain permeability, brain efflux and uptake) did not influence unbound plasma exposures of bupropion and S, S-hydroxybupropion (formed and preformed). This could be attributed to much larger systemic volumes of distribution relative to brain. We had a similar observation during plasma-brain population model development of individual and combined bupropion-S, S-hydroxybupropion. We saw plasma estimates were stable after addition of the brain component. Renal clearance had no influence on plasma and brain exposures of bupropion and S, S-hydroxybupropion. This is consistent with reported route of elimination, as bupropion is primarily eliminated through metabolism, with only <0.1% of parent drug excreted unchanged in urine in humans and rats (Suckow et al., 1986; Welch et al., 1987).

In vivo derived $K_{p,uu}$ failed to capture brain exposures of bupropion, formed and preformed S,S-hydroxybupropion. Use of passive permeability clearance values alone overpredicted bupropion, preformed and formed S, S-hydroxybupropion brain exposures. Adding efflux and

influx clearance terms improved model fit for the three entities. **Figures 6.3**, **6.5**, **6.7**, **6.9**, **6.11**, **6.13** show that the mean predicted plasma and brain concentrations were similar to observations; namely, predicted PK parameters were within 2-fold of the mean observed data.

Simulations of human plasma and brain concentrations following 150 mg SR bupropion dose are shown below in **Figure 6.14**.

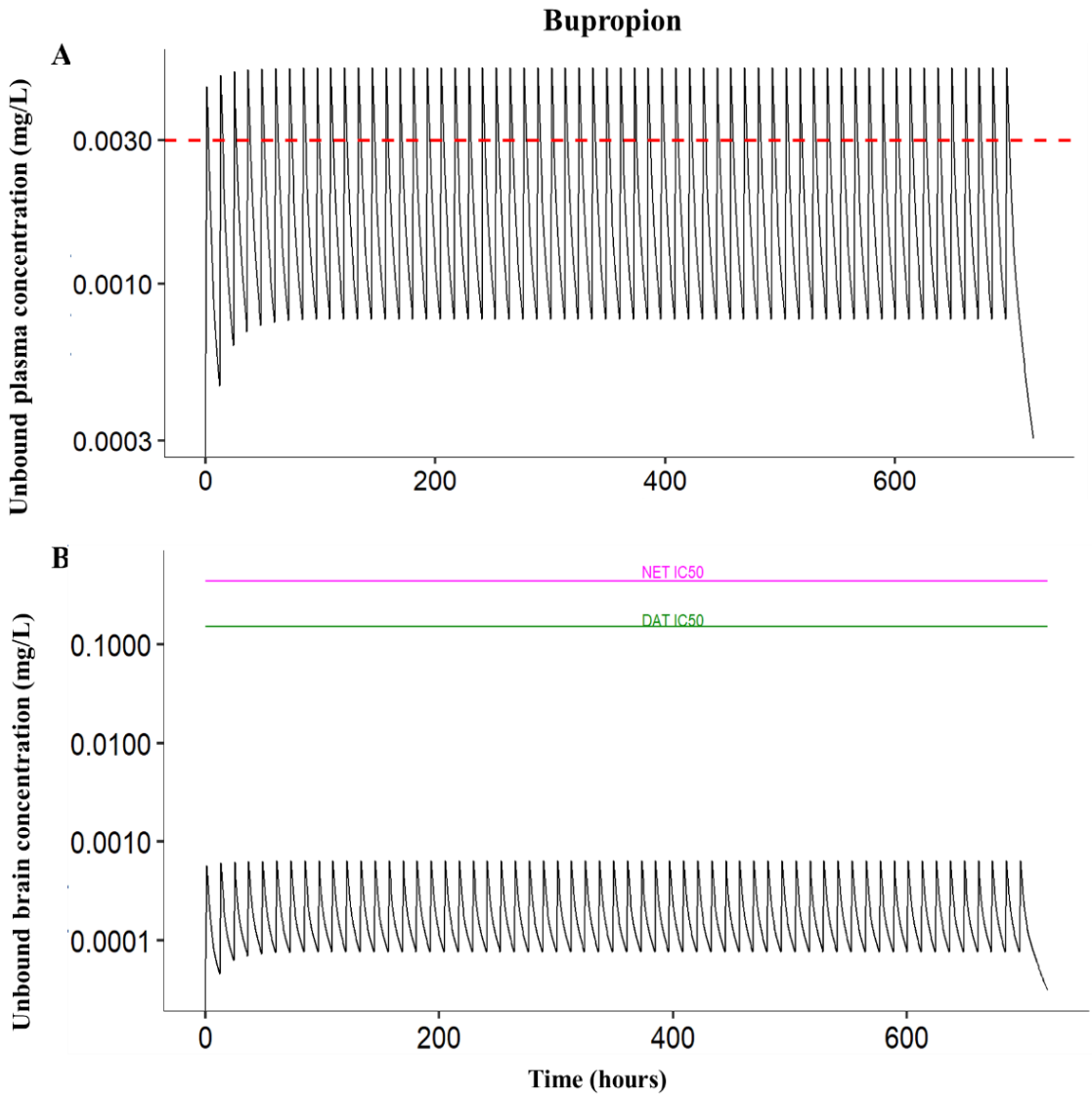


**Figure 6.14.** Simulated bupropion and formed S, S-hydroxybupropion concentrations over 30 days in humans after multiple every-12-hour daily dosing of 150 mg of the bupropion SR formulation. **A** and **B** represent unbound plasma and brain bupropion concentrations, respectively. **C** and **D** represent unbound plasma and brain S, S-hydroxybupropion concentrations, respectively. The green line in the brain plots refers to the human $IC_{50}$ value reported for the dopamine transporter (DAT), and the pink line refers to the $IC_{50}$ for norepinephrine transporter (NET). The red dashed line is the steady stae unbound plasma concentration from Johnston et al (J. A. Johnston et al., 2001).

Figure 6.14 continued

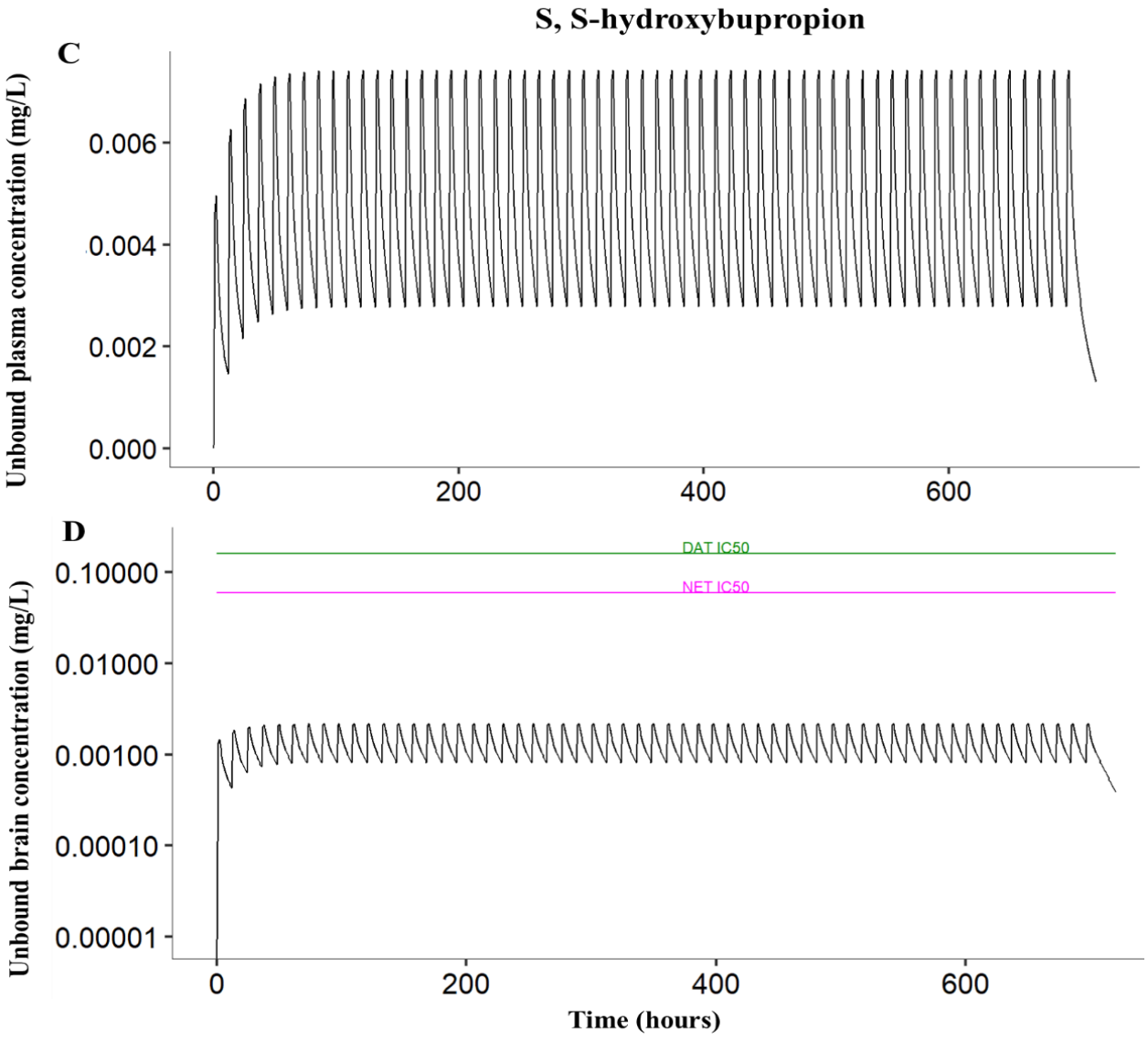


.

Predicted S, S-hydroxybupropion human unbound plasma exposures ($AUC_{0-\infty}$= 0.04 mg·hr/L, $C_{max}$ = 0.003 mg/L, $t_{max}$ = 2 hr), when corrected for unbound fraction and absorption rate constant of 0.8 $hr^{-1}$, are similar to those from a 100 mg immediate release formulation single dose reported by Desta et al ($AUC_{0-\infty}$ = 0.034 mg·hr/L, $C_{max}$ = 0.002 mg/L, $t_{max}$ = 2.5 hr) (Masters et al., 2016). The predicted unbound bupropion human plasma exposure ($AUC_{0-\infty}$= 0.02 mg·hr/L, $C_{max}$ = 0.004 mg/L, $t_{max}$ = 1 hr) was slightly lower compared to that study ($AUC_{0-\infty}$= 0.04 mg·hr/L, $C_{max}$ = 0.01 mg/L, $t_{max}$ = 1 hr), but was the same as compared to a study by Findlay et al ($AUC_{0-\infty}$= 0.02 mg·hr/L, $C_{max}$ = 0.004 mg/L, $t_{max}$ = 1 hr) (Butz et al., 1982). A PBPK model was previously developed by Xue et al, however that model predicted only total systemic plasma concentrations (Xue et al., 2018).

## 6.4 Discussion

We developed a parent-metabolite whole-body rat PBPK model of bupropion and S, S-hydroxybupropion using in vitro parameters, where available, and scaled it to predict human brain exposures and their relationship to in vitro potency measures at DAT and NET.

Generally, unlike a population-PK model, a preformed dose group may not be required for development of a parent-metabolite PBPK model, provided reliable in vitro data characterizing the disposition of metabolite are available. This was the case for bupropion and its pharmacologically active metabolite, S, S-hydroxybupropion. Unlike a population-PK modeling approach, incorporation of a preformed dose group for the active metabolite, S, S-hydroxybupropion, was not required to predict from a PBPK model its formation from bupropion administration. As PBPK model development relies on parameters from in vitro studies, we incorporated Michaelis-Menten parameters from a prior in vitro hepatic microsomal incubation study (**Chapter 2**) (Bhattacharya et al., 2019). Model-derived estimates of elimination clearance associated with formed and preformed S, S-hydroxybupropion were similar (within two-fold) in the PBPK model. The elimination clearance of the formed S, S-hydroxybupropion was adjusted/optimized to fit the data. PBPK model development can become quite challenging when all the required in vitro data are not available. Specific to bupropion in vitro brain carrier-mediated transport, (efflux and influx clearance), data were not available to support plasma and brain exposure predictions using this

approach. For translation to humans, in vitro parameters from our human hepatic microsomal study (**Chapter 2**) (Bhattacharya et al., 2019), and apparent clearance from a radafaxine trial (Nora D. Volkow et al., 2005) were used. Overall a mixed in vitro-in vivo (middle-out) approach was used to develop this plasma-brain PBPK model.

Population model-based predicted rat formation clearance of S, S-hydroxybupropion (discussed in **Chapter 5**) was three to four-fold higher than the scaled rat hepatic formation clearance from the in vitro microsomal incubation study (**Chapter 2**) (Bhattacharya et al., 2019). The rat hepatic microsomal systems were not fully saturated in our previous study, that is, S, S-hydroxybupropion formation (shown in **Chapter 2**) from bupropion begins to take the shape of a classic Michaelis-Menten-parabolic curve at the used concentration range, but is not fully saturated, which could possibly lead to inaccurate estimates of $K_m$ and $V_{max}$, ultimately leading to poor estimation (in this case under estimation) of hepatic clearance from our in vitro experiment.

Consistent with our findings from the plasma-brain population PK model of bupropion and S, S-hydroxybupropion, we learned that a flow-limited brain model structure, or a structure incorporating only passive permeability brain clearance did not fit the observed brain data. Active efflux and uptake processes had to be incorporated in the model to fit the brain concentration-time profiles for both parent and metabolite. The disconnect between brain clearance values for population PK (bupropion $CL_{in}$ 19.85 L/hr and $CL_{out}$ 31.66 L/hr; S, S-hydroxybupropion $CL_{in}$ 21.31and $CL_{out}$ 5.3 L/hr) versus PBPK approaches (bupropion $CL_{in}$ 0.36 L/hr and $CL_{out}$ 19.44 L/hr; S, S-hydroxybupropion $CL_{in}$ 0.36 and $CL_{out}$ 0.68 L/hr) could possibly be due to different modeling structures in population-PK versus PBPK models. A slope term was used in the population model to capture a time dependent component in the uptake clearance of bupropion and S, S-hydroxybupropion. Traditionally, PBPK based brain clearance parameters depend on passive and active transport, surface expression of carrier protein, transporters, surface area, membrane composition. In our present PBPK model, we have grouped carrier mediated uptake and efflux clearances as one term, that is, multiple uptake and multiple efflux transporters may participate, and these were grouped together respective of each transport direction as the experimental values from in vitro systems supporting the two transport directions are not available. The population-PK based approach we used also does not separate these processes from passive transport. Additional

studies, such as in vitro assays expressing putative transporters are needed to corroborate the model findings with respect to functional role of uptake and efflux transporters at the BBB. Difference in units (mg/L in PBPK modeling versus nM in population modeling) makes it difficult to compare with population modeling results. Further modeling work is necessary to correct for the units. Also, rat PBPK model with subcutaneous route shall be developed. Uptake and efflux clearance parameters derived from additional in vitro BBB transporter based assays may throw further light into the observed discrepancies between relative unbound brain exposure difference. However, despite the differences, both population and PBPK models indicate that at a 10 mg/kg bupropion dose, both bupropion and S, S-hydroxybupropion brain exposures are below their respective DAT and NET $IC_{50}$ estimates for these transporters specific to rat (Damaj et al., 2004).

A model with further partitioning into the lysosomal compartment was not considered, as lysosomal volume is 0.5 % of total brain volume (Fridén et al., 2011). Also, similar (2-fold) unbound brain exposures from the present study and that derived from microdialysis studies suggest rapid distribution of unbound drug between intracellular and extracellular fluid (ECF) brain compartments. The model did not include brain ECF bulk flow component as a brain clearance pathway (Szentistvanyi et al., 1984) since this is negligible (<0.0001%) relative to $CL_{out}$ estimates and thus would not significantly contribute to overall brain clearance. These interpretations regarding model structure that best inform determinants of observed exposures are the same as we concluded for the population PK model.

The hepatic formation clearance of R, R-hydroxybupropion from the in vitro rat liver microsome based assay (**Chapter 2**) was 8-fold higher compared to S, S-hydroxybupropion (Bhattacharya et al., 2019). The Michaelis-Menten parameters, $V_{max}$ and $K_m$, estimated from the rat hepatic microsome incubations could not be estimated as the system was not saturated. However, the rat in vivo systemic exposure (AUC) of R, R-hydroxybupropion was only 1.5-fold higher than S, S-hydroxybupropion. This in vitro-in vivo discrepancy could be due to other disposition routes for the R, R-hydroxybupropion metabolite. Furthermore, results from in vitro human hepatic microsomal studies indicate that the formation clearance of R, R-hydroxybupropion is 3 to 4-fold higher than S, S-hydroxybupropion **(Chapter 2**) (Bhattacharya et al., 2019). However, the plasma exposure of R, R-hydroxybupropion was over 60-fold higher than S, S-

hydroxybupropion following administration of 100 mg IR dose of bupropion (Masters et al., 2016). In vitro hepatic microsomal based systems clearly do not explain this vast difference. As well, the renal clearance of S, S-hydroxybupropion is only 10-fold higher than R, R-hydroxybupropion. Both rodent and human studies indicate that additional studies with separate administration of R, R-hydroxybupropion may be necessary to understand its clearance mechanism before undertaking further PBPK modeling. Though R, R-hydroxybupropion was not included in the present study, as it is less potent than S, S-hydroxybupropion, it is possible that due to its higher exposure (30-fold) than bupropion it might achieve exposures approximating its in vitro DAT and NET $IC_{50}$ potency values (Damaj et al., 2004).

Obviously, human brain concentration time profiles of bupropion and S, S-hydroxybupropion to support model predictions regarding brain exposure are not available to validate the model predictions. Generally, estimates of $fu_{brain}$ measured in vitro by equilibrium dialysis of rat and human brain homogenates have been reported to be similar, primarily because of species independent nonspecific binding to tissue components (Ball et al., 2012; Di et al., 2011). In contrast, the intrinsic rate of drug transfer across the BBB is the net effect of passive clearances, and carrier-mediated efflux and influx clearances. Processes such as carrier-mediated transport depend on transporter abundance and specificity, both of which could be highly species dependent. At present, due to lack of availability of data, carrier-mediated uptake and efflux processes were grouped together as $CL_{uptake,active}$ and $CL_{efflux,active}$ that is, multiple uptake and multiple efflux transporters may participate, and these were grouped together respective of each transport direction. however, passive clearance can be considered to be conserved across species, based on assumptions of similar BBB tight junction development and endothelial to brain tissue surface area preservation (Ball et al., 2012).

Similar to our observation from human simulations using a population-PK approach, we noted that human-brain exposure predictions using the PBPK approach too suggested that bupropion and S, S-hydroxybupropion concentrations are below the reported DAT and NET $IC_{50}$ estimates for the human transporters. This suggests that other pharmacological targets or mechanisms may be involved in bupropion`s efficacy. In a [$^{11}$C] raclopride PET study to determine whether bupropion administration increased extracellular dopamine levels in the rat and human

striatum, bupropion administration decreased striatal [$^{11}$C] raclopride specific binding in rat, consistent with observed increased in extracellular dopamine concentrations resulting from inhibition of dopamine reuptake (Egerton et al., 2010). However, when this approach was translated to humans by assigning a cognitive task to stimulate dopamine release, no significant decreases in striatal [$^{11}$C] raclopride specific binding were observed, indicating that extracellular dopamine levels were not increased to levels detectable using this approach (Egerton et al., 2010). It is possible that at doses administered to rats, though significant increase in dopamine levels compared to baseline are known to be observed, dopamine levels may not hit the reported $IC_{50}$ potency measures. To our knowledge, studies that measured change in dopamine levels using microdialysis did not simultaneously measure bupropion levels in ECF and vice versa. Further microdialysis studies with a wider range of bupropion doses and measuring simultaneously dopamine and bupropion would be useful. Overall, these results indicate that, in man, bupropion's therapeutic efficacy is unlikely to be solely due to an increase in striatal dopaminergic transmission. Also, receptor occupancy studies using PET or SPECT tracers specific for DAT and conducted at steady state based on bupropion multiple dosing indicate occupancy of about 20% for about 24-hours in both patients with and without depression (Learned-Coughlin et al., 2003; J. H. Meyer et al., 2002). Altogether, these findings suggest additional studies to investigate the mechanism of bupropion`s pharmacological action are needed.

The present model, though termed "physiological", represents a structurally simplified version of complicated brain structure. Furthermore, the influence of disease conditions or age (Bors et al., 2018), including specifically on permeability across the BBB (de Vries et al., 2012; Nicolas, 2015), or of species differences in BBB transporter activity (Nicolas, 2015; Syvänen et al., 2009) are not fully understood, and, accordingly, were not factored into the present model. Nevertheless, our findings and interpretations identify opportunities for model refinement as more data on brain transporter expression and abundance is gained through additional studies that will ultimately improve the translational potential of the model.

# CHAPTER 7. SUMMARY AND CONCLUSIONS

Bupropion therapy is associated with wide intersubject variability, which is thought to be driven by variability in metabolism. Much of bupropion`s therapeutic activity is attributed to its active metabolites, especially S, S-hydroxybupropion. There have been extensive efforts to elucidate bupropion`s metabolic profile though plasma and urinary pharmacokinetic studies in humans. However, understanding its stereoselective disposition at its target site, that is the brain, and its potential contribution to bupropion`s high intersubject variability regarding its efficacious versus adverse/intolerability effects is limited by ethical and safety concerns. Our approach to better understand this variability was to conduct detailed non-clinical studies using animal models that would enable stereoselective measurement of bupropion and metabolite disposition in brain. Armed with this detailed information, the objective was to use modelling and translational simulations to predict human brain disposition of these molecular entities and thereby gain insight regarding key determinants responsible for bupropion's wide inter-subject variability in its pharmacologic and toxicologic effects. To accomplish this overarching objective, the following hypotheses and associated specific aims were developed and investigated.

## 7.1 Hypothesis and Specific aim 1

Our first step was to identify a surrogate non-clinical species that demonstrated similar metabolic profile to humans through in vitro hepatic microsomal incubation studies. We hypothesized that due to close genetic homology to humans, marmoset monkeys would have a metabolic profile similar to humans. In absence of any preliminary in vivo data in nonhumans primates it was imperative to confirm through in vitro studies that marmoset monkeys formed key metabolites in quantifiable amount before investing resources (time and money) in vivo studies.

Our findings from comparison of stereospecific formation kinetics of bupropion metabolites in liver microsomes of three animal species (rat, mouse, nonhuman primate-NHPs) to humans indicated that phase 1 metabolism in NHPs best approximated that observed in humans, thereby supporting, based on similarity of stereoselective metabolite formation patterns alone,

preferential use of this species to extend our understanding of stereoselective bupropion CNS disposition. Since the goal of the study was primarily to see if animals had a metabolic profile similar to humans and formed metabolites in quantifiable amounts, we did not saturate the systems; thus, Michealis Menten parameters ($V_{max}$ and $K_m$) for all phase 1 metabolites in all species were not be estimated.

However, the cost and limited pharmacokinetic and pharmacodynamic data in NHPs were insurmountable barriers to conducting in vivo studies in NHPs. After considering multiple factors, such as the formation of reductive metabolites (higher in rats than mice), which are also thought to contribute to bupropion`s therapeutic efficacy, availability of microdialysis data measuring bupropion and dopamine, norepinephrine levels in brain extracellular fluid (ECF) and several in vitro studies measuring potency in rats, this species was chosen as the surrogate species to model bupropion`s disposition.

### 7.2 Hypothesis and Specific aim 2

Next, we hypothesized that plasma exposure of bupropion and its metabolites in rat (chosen surrogate species) was not a good indicator for brain exposure. So, we measured bupropion enantiomers and their corresponding phase 1 metabolites in rat plasma and brain.

In absence of microdialysis, unbound concentrations in plasma and brain were determined by correcting total concentrations in these two matrices via unbound fraction measurements made by in vitro plasma and brain homogenate binding assays. Results from in vitro rat plasma and brain homogenate binding assays of bupropion enantiomers and diastereomers indicated that overall the rat plasma unbound fractions were five-fold higher than their corresponding brain unbound fractions. Amongst the enantiomeric or diastereomeric pairs, for plasma or brain unbound fractions, we noted that only unbound plasma fraction of S, S-hydroxybupropion to be different than R, R-hydroxybupropion (1.5-fold higher). We also observed that bupropion enantiomers had low stability and recoveries in plasma (stability < 10 %, recovery > 450 %) and brain (stability < 45 %).

## 7.3 Hypothesis and Specific aim 3

Next, we hypothesized that instability of bupropion enantiomers exists and may be different in the three matrices (rat plasma, brain and 0.1 M phosphate buffer pH 7.4) used for determination of fraction unbound determination. Consequently, we hypothesized that both instability and inversion of bupropion enantiomers alters in vitro unbound fraction estimates for plasma and brain.

To evaluate the potential impact of low stability and inversion on estimates of unbound fraction measures in rat plasma and brain, we conducted additional experiments to characterize 24-hour degradation and chiral inversion profile of the bupropion enantiomers in three matrices, rat plasma, brain homogenate and phosphate buffer pH 7.4. These studies indicated that chiral inversion occurred in all three matrices. In plasma and brain, we saw degradation and inversion occurred simultaneously. Through subsequent population modeling efforts, we were able to delineate and estimate the rates of these two processes (inversion and degradation) in the three matrices. The matrix specific models (plasma and brain) indicated that the rate of inversion between the enantiomers was faster than their degradation rates. Applying matrix specific model estimates of inversion and degradation to protein binding results (plasma and brain), we demonstrated that the model predicted unbound fractions of bupropion enantiomers in both matrices (plasma and brain) were close to experimentally derived values; therefore, we concluded that, despite being clearly measurable and quantifiable, degradation and chiral inversion did not impact the fraction unbound values. This is due to establishment of pseudo-steady state from attainment of chiral inversion and degradation equilibrium in the three matrices within 5 hours, the incubation period we used for the plasma/brain binding experiment.

Based on results from protein and brain binding experiments, instability was not a concern for hydroxy and reductive-metabolites. Additional in vivo studies involving separate administration of the individual enantiomers followed by superposition with profiles of racemic bupropion administration are needed to account for loss due to inversion and metabolism, not fully captured by our in vitro studies conducted using achiral chromatography. Also, understanding species differences (rats versus humans) regarding relative rates of inversion and degradation in

plasma and brain may ultimately help in understanding interindividual variability associated with bupropion use.

Unlike humans, we did not see marked stereoselective disposition of the enantiomers or phase 1 metabolite diastereomers in rats, that is, the unbound concentrations of bupropion enantiomers and reductive diastereomeric pairs in rat plasma or brain were similar. The unbound R, R-hydroxybupropion exposure was 1.5-fold times higher than S, S-hydroxybupropion in plasma and brain. The unbound brain to unbound plasma ratio $K_{p,uu}$ (derived from $AUC_{0\text{-}6hr}$ in each matrix) of bupropion enantiomers were < 1 suggesting net efflux at BBB, and that of formed metabolites were almost equal to 1 suggesting net passive transport at BBB. The preformed S, S-hydroxybupropion dose group had a $K_{p,uu}$ of 5, suggesting net uptake at BBB.

### 7.4 Hypothesis and Specific aim 4 and 5

Next, we hypothesized that development of rat-to-human translational population-pharmacokinetic or physiologically-based pharmacokinetic models describing the central nervous system disposition of bupropion and its metabolite (S, S-hydroxybupropion) would advance our understanding of intersubject variability in human bupropion response.

A population-PK modeling approach enabled parameterization of $K_{p,uu}$ into influx brain clearance ($CL_{in}$) and efflux brain clearance ($CL_{out}$). Since we did not observe a significant difference in clearance or exposures of bupropion enantiomers in plasma and brain, we summed up concentrations of R and S-bupropion to get total bupropion concentrations in each matrix. Further, we also clubbed data from a prior microdialysis study which used same route, dose, formulation strength, species as the present study. For both bupropion and S, S-hydroxybupropion, a model structure with time dependent change in brain influx clearance was required to adequately characterize the BBB transport. Our model suggests involvement of carrier-mediated transport involved in bupropion and S, S-hydroxybupropion CNS disposition. Using a physiologically-based pharmacokinetic model (PBPK) approach too, incorporation of efflux and influx terms in addition to passive permeability was necessary to adequately characterize brain disposition of bupropion and S, S-hydroxybupropion. Later, on incorporation of DAT and NET $IC_{50}$ potency

measures in population-PK and PBPK models indicated that at the administered dose (10 mg/kg), brain exposures were below their respective DAT and NET $IC_{50}$.

Both modeling approaches (population-PK and PBPK) when translated to humans indicated that the predicted human brain exposures fell below the reported DAT and NET $IC_{50}$ measures of bupropion and S. S-hydroxybupropion, suggesting other CNS targets or mechanisms could be involved in bupropion`s mechanism of action.

In conclusion, these results demonstrated carrier-mediated process such as uptake and efflux are involved in bupropion`s disposition. Species differences regarding metabolism of bupropion and its implicated carrier-mediated transport at the BBB, limit the translational potential of our present model. A similar observation in a CNS model developed in non-human primates (due to its close genetic homology in humans) could have added gravitas to the translational potential of our present model. Additional studies such as in vitro transporter based assays (BBB), corroborated by in vivo studies in non-human primates, may further improve the understanding of disposition and pharmacology of bupropion, which may ultimately help in understanding the interindividual variability in efficacy and safety observed with bupropion. Also, an additional dose group of preformed R, R-hydroxybupropion may further improve our understanding of bupropion`s disposition, as it is also possible in humans, due to its higher exposure, despite its lower potency, R, R-hydroxybupropion might reach pharmacologically relevant levels.

In summary, pharmacokinetic models (population PK and PBPK) predicting bupropion and S, S-hydroxybupropion concentrations in brain of rats were developed. The models suggest that active efflux transport and/or carrier-mediated uptake contributes to the BBB transport of both compounds. The model predicted bupropion and S, S-hydroxybupropion concentrations in human brains were below their respective $IC_{50}$ measures at DAT and NET, and this is in line with reported low DAT occupancy in human brain. Additional studies investigating mechanisms of action of bupropion and transporters are further needed to understand potential factors associated with the high intersubject variability of this important drug. Overall, such a translational Population-PK or PBPK approach along with appropriate in vitro Ki values (unbound inhibitor concentration), may be used as a tool early in CNS drug discovery to help understand the potential impact of BBB

efflux or uptake inhibition on CNS drug exposure and response, which could ultimately help with design of clinical studies.

# APPENDIX A. MICROSOMAL INCUBATION STUDY COPYRIGHT CLEARANCE TO USE IN THESIS

SPRINGER NATURE LICENSE
TERMS AND CONDITIONS

May 11, 2020

---

This Agreement between Purdue University -- Chandrali Bhattacharya ("You") and Springer Nature ("Springer Nature") consists of your license details and the terms and conditions provided by Springer Nature and Copyright Clearance Center.

| | |
|---|---|
| License Number | 4826070682241 |
| License date | May 11, 2020 |
| Licensed Content Publisher | Springer Nature |
| Licensed Content Publication | European Journal of Drug Metabolism and Pharmacokinetics |
| Licensed Content Title | Comparison of In Vitro Stereoselective Metabolism of Bupropion in Human, Monkey, Rat, and Mouse Liver Microsomes |
| Licensed Content Author | Chandrali Bhattacharya et al |
| Licensed Content Date | Oct 8, 2018 |
| Type of Use | Thesis/Dissertation |
| Requestor type | academic/university or research institute |
| Format | electronic |
| Portion | full article/chapter |

| | |
|---|---|
| Will you be translating? | no |
| Circulation/distribution | 1 - 29 |
| Author of this Springer Nature content | yes |
| Title | Measurement of stereoselective bupropion disposition in rat brain to support translational PBPK/PD model development and application |
| Institution name | Purdue UNiversity |
| Expected presentation date | Jun 2020 |
| Requestor Location | Purdue University<br>910 W 10th Street<br>Apt 1324D<br><br>INDIANAPOLIS, IN 46202<br>United States<br>Attn: Purdue University |
| Total | 0.00 USD |

# APPENDIX B. IACUC PROTOCOL APPROVAL

Version 7.2016
Updated: 4.2.2018

**Indiana University School of Medicine**
**Institutional Animal Care and Use Committee (IACUC) Animal Protocol Form**

| For IACUC Office Use Only | | | |
|---|---|---|---|
| Protocol Number: | 18091 MD/R | Old Protocol Number: | |
| Approval Date: | 10/05/2018 | 3-Year Expiration Date: | 10/05/2021 |
| Amendment #: | | Amendment Approval Date: | |

**Section A**
**General Information**

**THIS FORM MUST BE SUBMITTED AS A WORD FILE VIA EMAIL TO: somiacuc@iupui.edu**

- The Core and Supplement-Protocol Associate (PA) are required for all applications.
- For specific animal procedures, you will need to check item(s) in the Procedures Check List then complete the corresponding Animal Procedure section(s) as a separate file(s). Submit the necessary appendices with your submission.
- A variety of supplemental information to assist investigators with completing this protocol application, including IACUC policies and guidelines, can be found at the SOM IACUC website http://researchcompliance.iu.edu/iacuc/iupui/index.html

**Section A01: Principal Investigator and General Information**

| Title of Project: | Development of a PK/PD translational model to predict stereoselective bupropion disposition in the brain |
|---|---|

| Principal Investigator: | Robert E Stratford | Degree(s): | PhD |
|---|---|---|---|
| Campus Address: | 950 W Walnut Street | Department: | Department of Medicine |
| Campus Phone: | 317-274-2822 | IU e-mail address: | robstrat@iu.edu |
| Note: As PI you need to be listed in the protocol associate form. | | | |

| CO- Principal Investigator: | | Degree(s): | |
|---|---|---|---|
| Campus Address: | | Department: | |
| Campus Phone: | | IU e-mail address: | |

| Protocol Type - Check all that apply | | | | |
|---|---|---|---|---|
| ✓ | Research Protocol | | Teaching Protocol | |
| | Pilot Protocol | | Protocol Other (Explain) | |
| | Replacement Protocol: Please provide the expiring protocol number this will replace | | | |
| | Amendment: Proceed to the "Amendment Summary of Changes" section below | | | |

**Amendment Summary of Changes**

In the text box below; please summarize all proposed changes to the protocol and follow these guidelines:

1. If changes are not showing as tracked, please contact the IACUC office at somiacuc@iupui.edu.
2. **Do not delete prior text** from this amendment summary. Place new text for the amendment summary below any previous amendment text.
3. Include the amendment number (i.e. A1, A2) to distinguish from previous approved amendments.
4. Update the Procedures Check List as needed and update/complete corresponding subsection of the protocol.
5. The Purpose, Goals, and Hypothesis section should be updated with the added amendment changes.
6. If a new procedure is added which may cause pain or distress, a new literature search for the consideration of alternatives for painful procedures (Section G) is required.
7. If you are requesting additional animals, ensure the additional number of required animals in Section B.
8. If you are requesting a new strain or genotype of animal, please be sure to provide the rationale on why the new strain/genotype has been requested. Please make sure the stain name is consistent with the nomenclature used during animal ordering processes.

**Current Funding**

This section is required because the Institution/IACUC must implement a process for ensuring that sponsored program support is consistent with the approved activities involving animals.

| Funding Sources | Grant Title(s) | Name of PI(s) on Grant |
|---|---|---|
| Start-up funds | | |
| | | |
| | | |
| | | |
| | | |

**Note: *If funded by VA*, you must complete the VA section D15 and submitted it with this form.**

## Section A02: Procedure Check List

**This Checklist is part of your application.**

**for New Protocols:**

- The "Core Sections" (B, C, E, F, G, H) and Protocol Associates Supplement are required for all protocols.
- For Section D, "Procedures", place an X next to each procedure to be performed in the protocol and complete the corresponding supplemental sections to be included in this application.
- Complete the necessary appendices and submit them with the application.

**for Amendments:**

- List which of the following section(s) is being modified in the "Amendment Summary" section, above. If you are adding a procedure, make sure to complete the supplemental section(s) and submit with the amendment.
- The IACUC Staff will insert the additional sections into the amendment document at the time of submission. As the PI, you do not need to combine the documents.

| | | | |
|---|---|---|---|
| **B: Summary, Experimental Design, Rational, and Animal Numbers** | | | |
| **C: Research Sites** | | | |
| **D: Procedures (Check all that apply)** | | | |
| | | | D01: Breeding, Weaning, and Genotyping |
| | | | D02: Anesthesia, Sedation, Analgesia |
| | | | Appendix 2: Anesthetic/Sedation (if D02 is selected and you are using Anesthetic/Sedation, you will need to submit Appendix 2 with your application) |
| | | | Appendix 3: Analgesia, (if D02 is selected and you are using Analgesia, you will need to submit Appendix 3 with your application) |
| | | | D03: Surgical Procedures |
| | | | Non-survival Surgery |
| | | | Single Survival Surgery |
| | | | Multiple Survival Surgery |
| | x | | D04: Agent Administration |
| | | ✓ | Non-Hazardous |
| | | | Hazardous |

| | | |
|---|---|---|
| | | D05: Irradiation, Imaging with Ionizing Radiation, and Other Radioisotope Administration |
| | ✓ | D06: Body Fluid, Tissue and Device Collection / Blood Sampling |
| | | D07: Behavioral Testing/Adverse Stimuli |
| | | D08: Special Caging, Husbandry, Food/Water Deprivation/Restriction |
| | | D09: Immunization |
| | | D10: Hybridoma |
| | | D11: Physical Restraint |
| | | D12: Laser Use |
| | | D13: Satellite Housing |
| | | D14: Animal Identification/Marking |
| | | D15: VA Supplemental Documentation – ACORP questions and certifications |
| | | D16: Controlled Substances |
| **E: Expected Experimental Complications and Emergency Management Plan** | | |
| **F: Disposition and Euthanasia** | | |
| **G: Justification for the Use of Animals, Unnecessary Duplication & The 3 R's** | | |
| **H: Principal Investigator Assurance** | | |
| **Protocol Associates Supplement** | | |

## Section B
## Summary, Experimental Design, Rationale, and Animal Numbers

### Section B01: Abbreviations

| Please list all abbreviations/acronyms used throughout the protocol in alphabetical order and include their definition. |
|---|
| BBB: blood brain barrier<br>CNS: central nervous system<br>ISV: inter subject variability<br>LC: Liquid Chromatography<br>SC: subcutaneous<br>MPK: milligram per kilogram<br>MS: Mass Spectrometry<br>NaCl: Sodium Chloride<br>PK: Pharmacokinetic<br>PD: Pharmacodynamic |


| Go to Beginning of Document | Go to Procedures Check List |
|---|---|


### Section B02: Non-Technical (Lay) Summary

| **Relevance of the proposed project to human/animal health and summary of animal work**<br>**Non-Technical** (Lay) **Summary**<br>This section will be evaluated by non-scientists. Avoid the use of terms that would be unfamiliar to non-scientists. Please define technical terms in language the general public would understand. |
|---|
| Describe how the proposed research addresses an underlying medical or scientific problem and how it will advance human and/or animal health, or scientific knowledge, for the good of society. |
| Bupropion, a known antidepressant and smoking cessation aid is known to produce wide inter-subject variability (ISV) ranging from no therapeutic effect to serious side effect like seizures. It has complex pharmacokinetic (what body does to a drug) and pharmacodynamic (what drug does to the body) profiles. The presence of biological targets and metabolic enzymes in the brain, makes it a potential source contributing to ISV. A way to understand contribution of brain to ISV is to conduct experiments in surrogate animal species and develop a model to make predictions for human brain. This study would allow us to make prediction of human brain concentration of bupropion and its metabolites using appropriate scaling techniques from rodents. This would provide insight to dosing adjustments in humans to improve safety and efficacy with regard to bupropion use. |
| Please list the major procedures and the possible animal welfare implications that may occur with each procedure. |
| Literature reports no observable distress to animals on administration of bupropion (10 MPK, SC) and hydroxybupropion (2MPK, SC). However, an increase in locomotor activity is known to be observed at 10 MPK dose of bupropion. However, this is more pronounced at higher doses, which is not in the scope of the current study. |
| Describe potential complications that can arise from the experiments and what efforts will be done to minimize pain and distress. |
| Bupropion at doses ≥ 10MPK, is known to produce an increase in locomotor activity. This could possibly lead to injury to animal during blood sample collection. Though this increase in locomotor activity is more pronounced at higher doses |

Bupropion at doses ≥ 10MPK, is known to produce an increase in locomotor activity. This could possibly lead to injury to animal during blood sample collection. Though this increase in locomotor activity is more pronounced at higher doses (20 MPK, not included in this study), any complications, if observed will be managed upon notification and we will work with the veterinary staff to minimize pain and distress of the animal.

Go to Beginning of Document | Go to Procedures Check List

## Section B03: Scientific Rational & Hypotheses

**Please provide the scientific rationale and hypotheses for your research**.
(This section is to be more scientifically specific compared to the "Non-Technical Summary" above)

**Note: Do not exceed 1 page**

This section will help the IACUC understand the scientific justification for the proposed research. Please address the following areas when completing this section.

1) State the global hypothesis or central hypotheses of the proposed research hypotheses that will be tested and a brief rationale for each.
2) If there is a direct relationship with a grant, you can add the specific aims or objectives in this section.

**Global hypothesis**: Development of a rodent model that describes the CNS disposition of bupropion enantiomers and their respective metabolites will advance our understanding of intersubject variability in human bupropion response.
**Proposed research hypothesis**: Transport of bupropion and S,S-hydroxybupropion across the BBB and their metabolism within brain contribute to intersubject variability in bupropion response.

Go to Beginning of Document | Go to Procedures Check List

## Section B04: Experimental Design, Groups and Timelines

**Experimental Design Groups and Timelines**

Explain the experimental design and all animal procedures. This description should allow the IACUC to understand the experimental course of what happens to an animal from its entry into the experiment to the animal's endpoint.

For **each** separate experiment, provide

1) the specific objective/hypothesis to be tested including the main outcome or experimental variables to be evaluated
2) the experimental groups and their size (n/group) **NOTE: the statistical justification for group sizes is requested in a subsequent section.**
3) a simple sequential list of all procedures performed on animals beginning with procurement/acclimation and ending with final disposition
4) a very brief statement of why any procedure is being done and provide a summary of animal numbers for each experiment (details of the procedures should be described in Section D)
5) **The breeding schemes are to be explained in Section D01, <u>not</u> in the experimental timeline.**

If new studies are proposed in an amendment, they should be added here, with the amendment number and new text at the top of the box.

Please see the example protocol found on the following webpage (http://researchcompliance.iu.edu/iacuc/iupui/iacuc_forms.html) on how to write the experimental timeline.

**Specific objective:** To measure exposures of bupropion and metabolites in rat plasma and brain following administration of racemic bupropion (10 MPK) and S,S-hydroxybupropion (2 MPK)
**Major outcomes for experiments:** Measurement of bupropion (R and S enantiomer), their metabolites hydroxybupropion, (R,R and S,S), threohydrobupropion (R,R and S,S-), and erythrohydrobupropion (S,R and R,S) in plasma and brain following bupropion (racemic) administration. S,S-hydroxybupropion concentration in plasma and brain would be measured following separate administration of S,S-hydroxybupropion.
**Experimental groups and their size (n/group): Total animals:48 (2 groups, 24 animals/group): Group A: animals (N) =24 animals**. **Racemic bupropion** would be administered (SC) to 24 animals. In a course of 6 hrs (total 8 timepoints), at each timepoint, n=3 animals, blood samples would be collected via tail vein and brains would be harvested, which would be further processed to measure concentration in plasma and brain homogenate. **Group B: Total animals (N) = 24 animals**. S,S-hydroxybupropion would be administered(SC) to 24 animals. In a course of 6 hrs (total 8 timepoints), at each timepoint, n=3 animals, blood samples animals would be collected via tail vein and brains would be harvested which would be further processed to measure concentration in plasma and brain homogenate.

**Summary of experimental plan**

| | GROUP A | GROUP B |
|---|---|---|
| Drug | Racemic bupropion | S,S-hydroxybupropion |
| Dose (10 mpk) | 10 | 2 |
| Total animals (24+ 24=48) | 24 | 24 |
| Total time points | 8 (0, 15 min, 30 min, 1 hr,2 hr, 3 hr, 4 hr, 6 hr) | 8 (0, 15 min, 30 min, 1 hr, 2 hr, 3 hr, 4 hr, 6 hr ) |
| Number of animals sacrificed at each time point. | 3 | 3 |
| Samples collected at each time point | blood, brain | blood, brain |
| Blood collection | Please see section D06 | Please see section D06 |
| Brain harvestation | Carbon dioxide | Carbon dioxide |
| Formulation | Bupropion in 0.9% NaCl | S,S-hydroxybupropion in 0.9% NaCl. |

Sequential list of procedures:

- Acquisition from vendor
- Acclimation at IUSM for minimum of 7 days.
- Random assignment to 2 groups.
- Subcutaneous administration of racemic bupropion to Group A and S,S-hydroxybupropion to Group B.
- Blood withdrawal and brain harvestation at predefined time points for both the groups.
- Analysis of samples by chiral LC-MS/MS

| | |
|---|---|
| **List the total number of animals requested for all experiments described above.** If more than 1 species, list total for each species. You do not need to list your breeding animals in this section unless they are used for experiments. | 48 |

**Species and Number of Animals**

Provide the information requested in the table below. See the IACUC policy on Assigning Animals to USDA Pain & Distress Categories for further guidance.

**Category B:** Animals being held, bred, or conditioned for use in teaching, experiments, research or surgery, but not yet used for such purposes.

**Examples:**

- Holding protocol
- Animal breeding, pregnancy, parturition or lactation (note: if tail snips or other tissue is collected, Category B is not appropriate)
- Observation of animal behavior in the wild without manipulating the animal or it's environment
- Euthanasia of animals on a holding protocol following AVMA-acceptable methods (2013 guidelines)

**Category C:** Animals that are subject to procedures that cause no pain or distress, or only momentary or slight pain or distress and do not require the use of pain-relieving drugs.

**Examples:**

Provide the information requested in the table below. See the IACUC policy on Assigning Animals to USDA Pain & Distress Categories for further guidance.

**Category B:** Animals being held, bred, or conditioned for use in teaching, experiments, research or surgery, but not yet used for such purposes.

**Examples:**
- Holding protocol
- Animal breeding, pregnancy, parturition or lactation (note: if tail snips or other tissue is collected, Category B is not appropriate)
- Observation of animal behavior in the wild without manipulating the animal or it's environment
- Euthanasia of animals on a holding protocol following AVMA-acceptable methods (2013 guidelines)

**Category C:** Animals that are subject to procedures that cause no pain or distress, or only momentary or slight pain or distress and do not require the use of pain-relieving drugs.

**Examples:**
- Physical or chemical restraint and husbandry procedures, such as applying identification tags, ear notching/punching, tattoos, etc.
- Routine agricultural husbandry procedures approved by the IACUC in a protocol
- Holding or weighing animals in teaching, demonstration or research activities
- Observation of animal behavior in the lab
- Peripheral injections, blood collection or catheter implantation
- Gastric gavage
- Feed studies, which do not result in clinical health problems
- Live trapping
- Positive reward training or research
- Exposure to alteration in environmental conditions (not extreme) with appropriate conditioning and microenvironment
- Food restriction that reduces the animals weight by no more than 20% of normal age matched controls
- tail snips or other tissue is collected

**Category D:** Animals subjected to potentially painful or stressful procedures for which they receive appropriate anesthetics, analgesics and/or tranquilizer drugs.

**Examples:**
- Diagnostic procedures such as laparoscopy or needle biopsies
- Non-survival surgical procedures
- Survival surgical procedures
- Post-operative pain or distress w/ analgesics
- Retro-orbital blood collection
- Surgical catheter implantation
- Induced infections or antibody production
- Genetically engineered phenotype that causes pain or distress that will be alleviated
- Tumor induction or implantation if alleviation of pain/distress
- Terminal cardiac blood collection
- Anesthetize and release (i.e. for blood sampling) of wildlife
- Studies that involve special housing requests which are exceptions to the *Guide* such as: housing rodents on wire bottom cages; cages that do not conform to space and height recommendations; requests to house animals outside recommended temperatures
- Exsanguination with anesthesia

**Category E:** Animals subjected to potentially painful or stressful procedures that are not relieved with anesthetics, analgesics and/or tranquilizer drugs. Withholding anesthesia/analgesia must be scientifically justified in writing and approved by the IACUC. If you list animals in this category, you must provide a detailed justification.

**Examples:**
- Toxicological or microbiological or infectious disease research that requires continuation after clinical symptoms are evident without medical relief or require death as an endpoint.
- Ocular or skin irritancy testing
- Water deprivation beyond what is necessary for ordinary pre-surgical preparation where stress or physiologic impairment is a concern
- Food restriction which reduces the animals weight by more than 20% of normal age matched controls
- Application of noxious stimuli that the animal cannot avoid/escape
- Any procedure for which needed analgesics, tranquilizers, sedatives, or anesthetics must be withheld for justifiable study purposes

| Species | Strain/ Nomenclature/ Genotype | *Tg/KO/KI (check all that apply) | | | Weight or Age | Source ("LARC Vendor" is acceptable) | Total Number of Animals per Category | | | |
|---|---|---|---|---|---|---|---|---|---|---|
| | | Tg | KO | KI | | | B | C | D | E** |
| rat | Adult male Sprague-Dawley rats | | | | Adult | LARC Vendor | | 48 | | |
| | | | | | | | | | | |
| | | | | | | | | | | |
| | | | | | | | | | | |
| | | | | | | Total Numbers of Animals | | 48 | | |

NOTE: These totals should match the number of animals needed for experiments and those generated from breeding (used and not used from the breeding table in the breeding Section D01)

* Tg = transgenic animal; KO = Knockout animal; KI = Knock-in animal

**Do you have an IBC approved protocol for the Tg/KO/KI animals listed above?**

| | |
|---|---|
| | Yes. Please provide the IBC protocol # |
| | No. Please contact the IBC http://researchcompliance.iu.edu/ibc/bio_contacts.html |

****FOR CATEGORY E ANIMALS ONLY**

Please complete this section for any Category E animals and provide scientific justification to explain any of the applicable conditions:

**Category E Conditions (Check all that apply):**

| | |
|---|---|
| | Use of anesthetics, analgesics, sedatives or tranquilizers during and/or following painful or distressing procedures is contraindicated due to study design. |
| | The nature of the study involves potentially significant pain or distress that may not be fully relieved even if anesthetics, analgesics, sedatives or tranquilizers would be given. |
| | Death is an endpoint and animals may not be euthanized early due to study design. |
| | Prolonged restraint or other adverse environmental conditions will be in use. |
| | Other: |

Provide Scientific Justification for each of the selections above:

Go to Beginning of Document | Go to Procedures Check List

## Section B05: Animal Number Justification

**Address each species individually by copying/pasting this table**

Note: The *Guide* strongly recommends statistical estimates (power analysis) when possible. The IACUC believes that a power analysis should be used for justification in the majority of animal research protocols.

Species: Adult male Sprague-Dawley rats

The number of animals requested for this protocol is based on the following (select/complete all that apply):

| | |
|---|---|
| | A statistical estimate (power analysis) is used to estimate the number of animals and experimental groups. Please provide the justification, calculations, and details below. |
| | |
| X | The estimated minimum number necessary to achieve the goals of the research in the absence of a statistical estimate. Explain: |

PK study requires sampling up to at-least 3.5 half-lives, which in rats is 3.5*1.6 = 6 hrs. The exploratory nature of this study, precludes setting up a definite effect size. However, as most data publication requires replicate experiments, either as journal policy or due to data analysis, samples would be collected from n=3 animals at each time point, for total of 8 time points for both groups. Thus 3 (animals)* 8 (timepoints) * 2 (groups) = 48 animals.

| | |
|---|---|
| | The number necessary to obtain sufficient tissue or other material for testing or analysis, i.e. collection of cells for in vitro experiments. Explain: |
| | |
| | The number required to provide sufficient technical training or practice for the number of trainees expected. Explain: |
| | |
| | Other. Explain: |

## Section C
## Research Sites/Use Areas

| | |
|---|---|
| **Where will animals be housed?** | |
| X | LARC |
| | Methodist Research Institute (MRI) |
| | Other. Please specify the animal facility: |
| **For other institutions, have you submitted an IACUC form to those campuses?** | |
| | Yes |
| | No |

| | |
|---|---|
| **VA (Veterans Administration) Research** | |
| Will live animals be on RLR VAMC (VA) property during this research? | |
| | Yes |
| | No |
| Will VA space be utilized for live animal research? | |
| | Yes |
| | No |
| Will VA resources be utilized at the VA, IU, or LARC specifically for live animal research? | |
| | Yes |
| | No |
| Will VA paid staff (VA employees, or non-VA employee where IU salary is paid by VA funds) be working with the live animals during this research project? | |
| | Yes |
| | No |
| If **"yes"** is indicated to any of the above questions, approval is required from the Veterans Administration Research & Development Committee) | |

| | |
|---|---|
| **Will live animals be used or transported outside LARC**? | |
| | **Yes** |
| | **Note**:<br>• If you are requesting rodents and lower species (such as fish) to be kept outside of LARC for **more than 24 hours**, you must complete this section and **D13: Satellite Housing**<br>• USDA-regulated mammals that are kept outside of LARC is discouraged. If housing outside of LARC is needed for **more than 12 hours**, the Principal Investigator must consult with the Attending Veterinarian and/or IACUC Chair before planning any experiments. This includes hamsters, gerbils or guinea pigs that would require housing the animals outside LARC more than 12 hours. |
| ✓ | **No** |

| **Please select procedures below and complete the table as appropriate.**<br>**Note: Column 1 and 2 are required to be completed.** | | | |
|---|---|---|---|
| **Column 1** | **Column 2** | **Column 3** | **Column 4** |
| **Procedure** | **Building and Room number where <u>Records will be kept</u>** (if in LARC, indicate "LARC" below) | **Building and Room Number where the Procedure will take place, <u>if outside of LARC</u>** | **Length of Time <u>outside of LARC</u>**<br>**Note:** Time over 24 hours for rodents or 12 hours for USDA, you will need to complete Section D13 |
| Breeding, Weaning, and Genotyping (D01) | | | |
| Anesthesia, Sedation, Analgesia (D02 and Appendix 2 and/or 3) | | | |
| Non-survival Surgery (D03) | | | |

| | | | | |
|---|---|---|---|---|
| | Single Survival Surgery (D03 and Appendix 4) | | | |
| | Multiple Survival Surgery (D03 and Appendix 4) | | | |
| X | Agent Administration (D04) | R4 324 | | |
| | Irradiation (D05) | | | |
| | Imaging (D05) | | | |
| | Imaging with Ionizing Radiation (D05) | | | |
| | Other Radioisotope Administration (D05) | | | |
| X | Body Fluid, Tissue and Devise Collections and Blood Sampling (D06) | LARC | | |
| | Behavioral Testing or Adverse Stimuli (D07) | | | |
| | Special Caging/Husbandry (D08) | | | |
| | Food/Water Deprivation/Restriction (D08) | | | |
| | Immunization (D09) | | | |
| | Hybridoma (D10) | | | |
| | Physical Restraint (D11) | | | |
| | Laser Use (D12) | | | |
| | Satellite Housing (D13) | | | |
| X | Animal Identification (D14) | LARC | | |
| X | Euthanasia | | | |
| | X $CO_2$ with flow meter | LARC | | |
| | Other Method: | | | |
| | Other Non-surgical procedures: | | | |
| | Other: | | | |
| | Other: | | | |

| **Is your research being conducted under Food and Drug Administration (FDA) Good Laboratory Practices (GLP) regulations (21 CFR Part 58) to support applications for research or marketing permits for products regulated by FDA?** | |
|---|---|
| | Yes |
| ✓ | No |


| Go to Beginning of Document | Go to Procedures Check List |
|---|---|


## Section D
## Procedures

### Section D04: Agent Administration

**NOTE: if any of the below agents are controlled substances, you need to complete Section D16.**

| **Chemical Agents** |
|---|
| **Compliance with pharmaceutical grade agents**. Investigators are expected to use pharmaceutical-grade agents whenever possible. Note that per federal guidelines the use of non-pharmaceutical grade agents requires justification, even for acute procedures. Please consult the IACUC Policy on the Use of Non-Pharmaceutical grade Chemicals/Compounds in Laboratory Animals to be aware of recent clarifications to this policy. |

| **Non-Hazardous Compounds** | | | | | |
|---|---|---|---|---|---|
| Is this a Pharmaceutical grade agent? (yes or no) | Agent Name | Route of Administration (IP, PO, SQ, etc.) | Max Dose (mg/kg, gm, etc.) | Max Volume (uL, ml, etc.) | Frequency / Duration |
| Yes | Bupropion | SQ | 10 mg/kg | 10mL/kg | Single injection |

| | | | | | |
|---|---|---|---|---|---|
| Yes | S,S-hydroxybupropion | SQ | 2 mg/kg | 10mL/kg | Single injection |

Please provide **justification for using any Non-Pharmaceutical Grade Chemicals / Compounds** listed in the above table and indicate if you will or will not be following the IACUC policy for Non-Pharmaceutical grade substances.

| **Hazardous Compounds (including carcinogens, toxins, teratogens, etc.)** | | | | | | |
|---|---|---|---|---|---|---|
| Agent Name | Type of agent | Route of Administration (IP, PO, SQ, etc.) | Max Dose (mg/kg, gm, ml, etc.) | Max Volume (uL, ml, etc.) | Frequency / Duration | Route of excretion |
| | | | | | | |
| | | | | | | |
| | | | | | | |

**Biologic agents / Biohazard agents**
**(biological toxins, blood, body fluids, human cells, animal cells, neoplastic tissues or cells, recombinant DNA, etc.)**

Protocols using biohazard agents will not receive IACUC approval until the Investigator provides evidence of approval from the Institutional Biosafety Committee (IBC). If you are unsure, please contact the IBC office.

**Do you have an IBC approved protocol for the work using biohazard agents described in this** protocol**?**

| | | |
|---|---|---|
| | Yes. Please provide the IBC protocol # | |
| | No. | |

| Agent Name | ABS Level; 1, 2, 2+3 Precautions, or 3 | Route of Administration, Volume, Dosing & Frequency | Is the agent infectious to humans? | Is the agent infectious to animals? | Is the agent shed in feces, urine, or body secretions? |
|---|---|---|---|---|---|
| | | | | | |
| | | | | | |

**If you are using Biologic or Biohazard agents, you must read and certify, by checking the below box, you understand the following statement.**

| | |
|---|---|
| | By checking this box, As PI, I understand that my lab staff and/or I are required to notify the LARC ABSL-2 veterinary staff at LARChaz@iupui.edu 3 business days prior to any work with biohazard or other hazardous agents. **Work cannot begin without proper signage posted to the animal housing room and cage.** |

**Safety Procedures for Animal Handlers - (LARC Personnel and Laboratory Personnel)**

| **Who has the potential to be exposed to this material?** | | x | **LARC Personnel** | ✓ | **Laboratory Personnel** |
|---|---|---|---|---|---|
| **Personal Protection** (indicate personal protective apparel/procedures to be used): | | | | | |
| **x** | Hair cover | **x** | Gown | ✓ | Lab coat | | Booties |
| | Waterproof boots | **x** | Safety glasses | | Goggles | | Face shield |
| | Film Badges | | | | | | |
| **x** | Respiratory mask (type: choose dust mist or respirator) | | Dust mask or N95 | | Gloves (type: choose latex and/or nitrile): | | latex |

| **Materials Handling:** | | | |
|---|---|---|---|
| | In cabinet (indicate type): | | |
| | Chemical Fume Hood | | Biosafety cabinet |
| Decontamination of area after use: | | | |
| Surveys performed required? | | Yes, if "yes," all areas less than 200 cpm/100 $cm^2$ (must be to be released) | No |
| Procedures: | | | |
| Building for each hood used: | | | |

| **Waste Disposal:** | | | |
|---|---|---|---|
| | Bedding/excreta radioactive: | | Duration: (days) | |
| Indicate disposal method: | | | |
| | Incinerate | | Autoclave |
| | Bedding/excreta disposed as normal | | Bedding/excreta disposed through Radiation Safety Office |
| | Decontaminate cage before washing: | | |

## Section D06: Body Fluid, Tissue and Device Collection

**Other Body Fluid, Tissue and Device Collection**

List each body fluid, tissue, or device to be collected and complete the table below to indicate the nature of the collection.

| Body Fluid, Tissue, or Device to be Collected | Collected After Euthanasia? (Y/N) | Collection Before Euthanasia? (Y/N) | | |
|---|---|---|---|---|
| | | Blood Collection Associated with Antibody Production | Collected as Part of a Surgical Procedure | Other Collection from Live Animals |
| Brain | Y | N | N | N |
| | | | | |

**Blood Sampling**

Please use ranges when completing the table below.

| Species | Describe the method of withdrawal | Volume of each withdrawal (e.g. ml | Total number of withdrawals per animal | Interval between withdrawals |
|---|---|---|---|---|
| Adult male Sprague Dawley rats | Tail vein via butterfly needle | 0.2 mL | 1 | NA |
| Adult male Sprague Dawley rats | Cardiac puncture post-euthanasia | 1.0 mL | 1 | NA |

If you are performing longitudinal studies, please list the number of times and time intervals this procedure will be performed below. (e.g. – Glucose tolerance test and pharmacokinetics)

Go to Beginning of Document | Go to Procedures Check List

## Section E
## Expected Experimental Complications and Emergency Management Plan

Consult a LARC Veterinarian if needed

**Can the animals be euthanized for health reasons before completion of the research?**

| | |
|---|---|
| | **No** Please provide a scientific justification of why early euthanasia (humane endpoints) cannot be used for this research. |
| ✓ | **Yes** Please answer the following questions. |

Describe any expected complications/symptoms. Include induced disease condition including animal phenotypes from breeding and/or complications from surgeries.

None

Describe how the animals will be monitored for the development of these complications/symptoms. Include the frequency of monitoring.

**For general health issues -** We will monitor the rats daily and determine weight and general appearance. Both the body weight and loss of body condition will be used to assess animal health. If >2 of the assesments are met below and /or there is rapid loss of body weight, rats will be euthanized immediately. The following assessments will be evaluated: rapid loss of 15-20% body weight (rats will be weighed weekly); inactivity with hunched posture; lesions that interfere with ability to eat and drink; evidence of self-mutilation, lesions with major ulcerating surfaces (ulcerations that are at least 5mm in diamater); loss of righting reflex and inability to maintain upright posture; loss of general body condition with spine becoming visible; loss of the ability to move freely because of tumor growth; dehiscence of wounds and/or evidence of infection not responsive to veterinary treatment.

How will the complications/symptoms be managed/treated prior to euthanasia?

For any ulcerations or wounds triple antibiotic cream will be applied. Wet food can also be provided to prevent dehydration.

| |
|---|
| For any ulcerations or wounds triple antibiotic cream will be applied. Wet food can also be provided to prevent dehydration. |
| **Describe the criteria that will be used in this protocol to determine if and when animals will be euthanized humanely prior to the planned termination of the experiment.** |
| Both the body weight and loss of body condition will be used to assess animal health. If >2 of the assesmentsare met below and /or there is rapid loss of body weight, rats will be euthanized immediately. The following assessments will be evaluated: rapid loss of 15-20% body weight (rats will be weighed weekly); inactivity with hunched posture; lesions that interfere with ability to eat and drink; evidence of self-mutilation, lesions with major ulcerating surfaces (ulcerations that are at least 5mm in diamater); loss of righting reflex and inability to maintain upright posture; loss of general body condition with spine becoming visible; loss of the ability to move freely because of tumor growth; dehiscence of wounds and/or evidence of infection not responsive to veterinary treatment. |
| If emergency veterinary care is required, are there any classes of drugs that cannot be used due to potential for interference with research results? If yes, please provide the types of drugs that must be avoided. |

| | |
|---|---|
| X | **No** Any type of emergency drugs may be used based on veterinary discretion. |
| | **Yes.** Please describe which drugs must be avoided below. |
| | |

Go to Beginning of Document | Go to Procedures Check List

## Section F
## Disposition and Euthanasia

| Final Disposition of Animal | |
|---|---|
| ✓ | Euthanasia. If checked, please complete the questions below. |
| | Return to Colony |
| | Transfer to a Different Protocol (following IACUC and LARC procedures to transfer animals) |
| | Other: |

**Select Primary Method of Euthanasia**

Euthanasia shall be in accordance with methods approved by the American Veterinary Medical Association (AVMA) guidelines. The *AVMA Guidelines for the Euthanasia of Animals* (2013) is available from: https://www.avma.org/KB/Policies/Documents/euthanasia.pdf.

A primary method of euthanasia is used to create rapid loss of consciousness followed by cardiac or respiratory arrest and loss of brain function. A secondary (confirmatory) method of euthanasia is required to ensure death.

- Physical methods of euthanasia (decapitation, thoracotomy, exsanguination, cervical dislocation) may be used when scientifically justified and generally only under general anesthesia.
- Carbon dioxide must be delivered from a compressed gas cylinder (no dry ice) and must be delivered very slowly to a chamber that has not been pre-filled.
- Perfusion and exsanguination can be considered euthanasia methods, distinct from non-survival surgery, only if no other significant procedures are occurring in association. See the IUSM Euthanasia policy http://www.researchcompliance.iu.edu/iacuc/iupui/iacuc_policies.html for further details.

**Place an "X" to indicate which technique(s) may be used.**
Alternatively, use the "other" text box to describe the methods to be used. Documentation of training specific to the method(s) used is required.

| Technique Used | Species | Agent or Mechanism | Method Description |
|---|---|---|---|

| | | | |
|---|---|---|---|
| ✓ | Mice or Rats | Anesthetic Overdose | • Carbon Dioxide: Inhalation overdose delivered using a gas cylinder, flow meter/regulator, and induction chamber. 100% $CO_2$ delivered at a rate such that 20-30% of the volume of the chamber is displaced per minute.<br>• Isoflurane (5% inhaled): Inhalation overdose with waste gas scavenging. Using an induction chamber or face mask and anesthetic machine with vaporizer to deliver the gas; alternatively, using the method of delivery whereby the rodent is placed into an induction chamber containing a small amount of liquid isoflurane (kept separate from the liquid by a physical barrier).<br>• Pentobarbital sodium: ≥ 120 mg/kg by IP or IV injection using commercially available formulations (examples: Beuthanasia-D®, Euthasol®, Fatal-Plus®, Nembutal®, Socumb®)<br>• Ketamine-Xylazine: Ketamine ≥ 500mg/kg + Xylazine ≥ 25 mg/kg IP |
| | Mice or Rats | Intracardiac exsanguination under general anesthesia (closed-chest only): | • Anesthetic agents and their proper use are described under Section D02. Under deep plane of surgical anesthesia, the full recoverable amount of circulating blood will be removed by performing a cardiac stick through a closed chest wall using a syringe-needle set. |
| | Mice, Rats, Rabbit, Dog, Swine | Perfusion under general anesthesia | • Anesthetic agents and their proper use are **described under Section D02.**<br>• Agents administered for the perfusion (e.g. saline, paraformaldehyde) **must be included in Section D04.** |
| | **Details of where/how any incisions will be made, how the perfusion will occur, and the approximate length of time for the procedure must be described below:** | | |
| | | | |
| | Mice, Rats, Rabbit, Dog, Swine | Exsanguination under general anesthesia | • Anesthetic agents and their proper use are described under Section D02. Under deep plane of surgical anesthesia, the full recoverable amount of circulating blood will be removed. |
| | **Details of where/how any incisions will be made, how the blood collection will occur, and the approximate length of time for the procedure must be described below:** | | |
| | | | |
| | Rabbit, Dog, Swine | Pentobarbital sodium | • ≥ 120 mg/kg by IP or IV injection using commercially available formulations (examples: Beuthanasia-D®, Euthasol®, Fatal-Plus®, Nembutal®, Socumb®) |
| | Rabbit, Dog, Swine | Potassium chloride under general anesthesia | • Anesthetic agents to be used are described under Section D02. ≥ 2 mEq K+/kg (≥ 75 to 150 mg/kg) potassium chloride is given by rapid IV or intracardiac injection under deep surgical plane general anesthesia. |

**Secondary Method of Euthanasia**

Performing a secondary means of euthanasia is required as a confirmatory step. After the primary method is performed, the animal is assessed to verify the absence of consciousness, respiration, cardiac function, reflexes, and muscle tone. A secondary method is then carried out, usually using a physical method.

Place an "X" to indicate which technique(s) may be used. Alternatively, use the "other secondary method" text box to describe the methods to be used. Documentation of training specific to the method(s) used is required.

NOTE: Cervical dislocation cannot be used in rats > 200 g body weight as it is not effective.

| Technique Used | Species | Method |
|---|---|---|

| | | |
|---|---|---|
| | Mouse | One or more of the following will be used: Cervical dislocation, bilateral pneumothorax, decapitation, exsanguination, heart removal |
| ✓ | Rat | One or more of the following will be used: Bilateral pneumothorax, decapitation, exsanguination, heart removal |
| | Rabbit, Dog, Swine | One or more of the following will be used: Bilateral pneumothorax, exsanguination, heart removal |

**Other secondary method: If different species or methods will be used please describe.**

**Alternative Method of Euthanasia: Physical Method Alone**

If a physical method of euthanasia such as cervical dislocation or decapitation **is used without** sedation or anesthesia, scientific justification is required. Please provide a detailed description of the proposed method(s) and the justification for why sedation or anesthesia cannot be used.

**Please note:** If LARC Personnel are requested to perform euthanasia, a written request specifying the animal(s) and date to perform such euthanasia must be signed by the principal investigator, co-investigator, faculty sponsor or responsible technician.

Go to Beginning of Document | Go to Procedures Check List

## Section G
## Justification for the Use of Animals, Unnecessary Duplication & The 3 R's (Replacement, Refinement, Reduction)

**Animal Justification**

The justification for using live vertebrate animals rather than alternative means of achieving the research goal is: (check all that apply)

✓ The complexity of the processes being studied cannot be duplicated or modeled in simpler systems because:

In-vitro BBB models developed so far do not fully represent the tightness of the BBB, transporters and enzymes. All these are potential factors contributing to the stereoselective disposition of bupropion in brain. Further, to truly understand brain`s contribution to ISV, it necessitates measurement of plasma PK profile in the same in vivo system to ultimately calculate brain to plasma exposure ratio. Given the complex PK profile and potential sources contributing to ISV, and lack of an in-vitro system to capture this complexity in plasma and brain, there is a compelling need for an in-vivo study.

☐ There is not enough information known about all the processes being studied to design nonliving models. (explain):

☐ Other (explain):

**Species Justification**

Address each species individually by copying and pasting this table for each species

Species: Adult Male Sprague-Dawley rats

This species was selected for the research because of the following attributes (select all that apply):

✓ A large database exists allowing comparisons with previous data. (explain):

There have been studies conducted in this species, investigating the PK (plasma and brain concentration time profile) and the PD (neurotransmitter levels, behavioral studies) changes after administration of racemic bupropion. However, the studies conducted so far have not investigated the stereoselective PK and PD of bupropion and its metabolites in plasma and brain of rodents. This is important as the parent and the metabolites are thought to have stereoselective PK and PD, which may have clinical implications.

☐ The anatomy or physiology is uniquely suited to the research proposed. (explain):

☐ This is the lowest species on the phylogenetic scale that is suitable for the proposed research. (explain):

| | |
|---|---|
| | Other attributes (details required): |
| | |

| **Duplication**<br>Animal welfare regulations do not allow **unnecessary** duplication of previous experiments. | |
|---|---|
| Do any of the studies proposed duplicate previous experiments? | |
| ✓ | No |
| | Yes. Please explain why it is **scientifically necessary** to replicate the/these experiments: |
| | |
| | NA. This is a teaching activity involving different student groups. |

| **Painful Procedures – non-USDA species**<br>Note: The IACUC recommends the use of this site if you need assistance: http://iupui.campusguides.com/iacuc | |
|---|---|
| | For all pain category D (anesthesia / analgesia provided to relieve potential pain) and pain category E (pain not relieved by anesthesia / analgesia) animals use procedures, **by checking this box,** I certify that I have reviewed the pertinent scientific literature and the sources and/or databases and found no scientifically acceptable alternative to any of those procedures that would result in less pain or distress. **Note:** Keep a copy of the search, but you do not need to send the search with your IACUC protocol. The IACUC may ask to see the search during the semi-annual inspections. |

**Painful Procedures –USDA species only**
**(Rodents are not considered a USDA covered species)**
**Pain Category C, D or E**

This table need to be complete **only if** you are using **USDA covered species**
in pain category C, D or E as designated in the Species and Number of Animals table above

**Note:** Keep a copy of the search, but you do not need to send the search with your IACUC protocol. The IACUC may ask to see the search during the semi-annual inspections.

| Place an X in the checkboxes that apply to indicate which databases were used: | | | | | | | | | |
|---|---|---|---|---|---|---|---|---|---|
| | Ovid Medline | | PubMed Medline | | EMBASE | | Scopus | | Other |

| | |
|---|---|
| Date(s) the database search was performed: | |
| Years covered by the search *(e.g., 1985 to present):* | |
| Keywords used in the search: | |

| Did the literature search reveal less painful alternatives to the potentially painful procedures that were proposed? | |
|---|---|
| | No alternatives were found |
| | Yes, but they cannot replace the procedures that were proposed for the following reason(s): |

| Potentially Painful Procedures in this Protocol (match to keywords used) | Write a BRIEF explanation why the alternatives found to this potentially painful procedure were not acceptable alternatives. |
|---|---|
| | |
| | |

Go to Beginning of Document | Go to Procedures Check List

## Section H
## Principal Investigator Assurance

Review each statement and check each box to indicate agreement. Completion of the checkboxes and the signing of this form are the responsibility of the Principal Investigator. Completion of the approval process will fulfill Public Health Service and USDA requirements under the federal Animal Welfare Act, and will serve as documentation for the users and the public of Indiana University School of Medicine's commitment to the humane care and use of animals.

| I certify that: | |
|---|---|
| ✓ | These studies will be conducted in compliance with Public Health Service (PHS) policy, The Animal Welfare Act, "The Guide for the Care and Use of Laboratory Animals", and other applicable University policies and procedures. |
| ✓ | All individuals listed on the protocol will read and understand the appropriate sections of the protocol, will enroll in the occupational health program, and will receive appropriate training in the procedures that they will be conducting prior to participating in the research. |

| | |
|---|---|
| ✓ | The IACUC and the appropriate LARC Veterinary Personnel will be notified regarding any unexpected research results that impact the welfare of the animals and any unanticipated pain or distress, morbidity, or mortality as soon as possible. |
| ✓ | All procedures, treatments, anesthetic and analgesic regiments will be adhered to as outlined in this protocol and any changes to these studies will be submitted to the IACUC via an amendment form and not initiated until approved by the IACUC. |
| ✓ | The proposed work will utilize pharmaceutical grade compounds whenever possible, as is consistent with PHS policy and the use of non-pharmaceutical grade materials, when necessary, will be carried out in accordance with policies of the Indiana School of Medicine IACUC. |
| ✓ | The proposed work is congruent with the scope of any grants or external funding arrangements listed in the funding section of this protocol. |
| ✓ | Any use of videos or photos is consistent with the LARC policy. |
| ✓ | I understand approval for this IACUC protocol will be strictly limited to a length of 3 years per PHS Policy and that in order to continue similar research beyond this time, a new protocol must be submitted to the IACUC and approved before the present protocol expires. In order to continue animal work without interruption, I understand that it is strongly recommended that I submit any replacement protocols a minimum of **3 months** in advance of the expiration date so as to allow sufficient time for the IACUC review process. I understand that failure to have an approved IACUC protocol in place means I will be unable to conduct work with animals and in many cases may be unable to use NIH grant money to pay for animal housing during the period of time my protocol is expired. |
| ✓ | I will alert the LARC ABSL-2 veterinary staff at ***LARChaz@iupui.edu*** 3 business days before starting any animal work with a biohazard, chemical hazard, or other hazardous agent. This ensures that LARC staff can prepare the animal housing room adequately for the proposed hazard. |

| I acknowledge responsibility for this protocol. | |
|---|---|
| Robert Stratford | 06 September-2018 |
| **Typed Name or Electronic Signature of PI** | **Date** |

## Supplement - Protocol Associates

| | | | | | | | |
|---|---|---|---|---|---|---|---|
| **Name of Protocol Associate (PA) (first, middle Initial, last):** | Robert E. Stratford – having no contact with any live animal | | | | | | |
| **PA IU E-mail:** | robstrat@iu.edu | | | | | | |
| **Emergency Contact:** This person is responsible for performing the monitoring and managing the complications. | | | Yes | | No | | |
| **Campus Phone:** | 317-274-2822 | **Emergency Phone:** | | | | | |

| | **Procedures this PA will perform:** | **Species** | **Years of Experience** | **Training Received and by Whom or To be Provided and by Whom** |
|---|---|---|---|---|
| | Breeding, Weaning, and Genotyping | | | |
| | Anesthesia | | | |
| | If performing Gas Anesthesia, has the PA completed the IU required waste anesthetic training? For more information, click on the following link: https://protect.iu.edu/environmental-health/occupational-health/anesthetic-gas.html | | | |
| | Sedation | | | |
| | Analgesia | | | |
| | Non-survival Surgery | | | |
| | Surgery: | | | |
| | Surgery: | | | |
| | Single Survival Surgery | | | |
| | Surgery: | | | |
| | Surgery: | | | |
| | Multiple Survival Surgery: | | | |
| | Surgery: | | | |
| | Surgery: | | | |
| | Agent Administration | | | |
| | Irradiation | | | |
| | Imaging | | | |
| | Blood Sampling | | | |
| | Behavioral Testing | | | |
| | Immunization | | | |
| | Hybridoma | | | |
| | Physical Restraint | | | |
| | Laser Use | | | |
| | Animal Identification | | | |
| | Euthanasia | | | |
| | $CO_2$ with flow meter | | | |
| | Other Method: | | | |
| | Other Non-surgical procedures | | | |
| | Other: | | | |
| | Other: | | | |

| | | | | | | | |
|---|---|---|---|---|---|---|---|
| **Name of Protocol Associate (PA) (first, middle Initial, last):** | Anthony L Sinn | | | | | | |
| **PA IU E-mail:** | alsinn@iupui.edu | | | | | | |
| **Emergency Contact:** This person is responsible for performing the monitoring and managing the complications. | | X | Yes | | No | | |
| **Campus Phone:** | 4-8811 | **Emergency Phone:** | 317-260-0952 | | | | |

| | **Procedures this PA will perform:** | **Species** | **Years of Experience** | **Training Received and by Whom or To be Provided and by Whom** |
|---|---|---|---|---|
| | Breeding, Weaning, and Genotyping | | | |
| | Anesthesia | | | |

| | | | | | | | | |
|---|---|---|---|---|---|---|---|---|
| | If performing Gas Anesthesia, has the PA completed the IU required waste anesthetic training? For more information, click on the following link: https://protect.iu.edu/environmental-health/occupational-health/anesthetic-gas.html | | | | | Yes | | No |
| | Sedation | | | | | | | |
| | Analgesia | | | | | | | |
| | Non-survival Surgery | | | | | | | |
| | Surgery: | | | | | | | |
| | Surgery: | | | | | | | |
| | Single Survival Surgery | | | | | | | |
| | Surgery: | | | | | | | |
| | Surgery: | | | | | | | |
| | Multiple Survival Surgery: | | | | | | | |
| | Surgery: | | | | | | | |
| | Surgery: | | | | | | | |
| X | Agent Administration | | Rat | 17 | faculty supervisor IUSM, Eli Lilly, BAS | | | |
| | Irradiation | | | | | | | |
| | Imaging | | | | | | | |
| X | Blood Sampling | | Rat | 17 | faculty supervisor IUSM, Eli Lilly, BAS | | | |
| | Behavioral Testing | | | | | | | |
| | Immunization | | | | | | | |
| | Hybridoma | | | | | | | |
| | Physical Restraint | | | | | | | |
| | Laser Use | | | | | | | |
| | Animal Identification | | | | | | | |
| X | Euthanasia | | | | | | | |
| | X | $CO_2$ with flow meter | Rat | 17 | faculty supervisor IUSM, Eli Lilly, BAS | | | |
| | | Other Method: | | | | | | |
| X | Other Non-surgical procedures necropsy | | Rat | 17 | faculty supervisor IUSM, Eli Lilly, BAS | | | |
| | X | Other: blood collection via tail prick | Rat | 17 | faculty supervisor IUSM, Eli Lilly, BAS | | | |
| | | Other: | | | | | | |

| | | | | | | | | |
|---|---|---|---|---|---|---|---|---|
| **Name of Protocol Associate (PA) (first, middle Initial, last):** | Dawn Bullock | | | | | | | |
| **PA IU E-mail:** | bullock@iu.edu | | | | | | | |
| **Emergency Contact:** This person is responsible for performing the monitoring and managing the complications. | | | | | | X | Yes | No |
| **Campus Phone:** | 4-8811 | | **Emergency Phone:** | 317-431-2060 | | | | |
| **Procedures this PA will perform:** | | | **Species** | **Years of Experience** | **Training Received and by Whom or To be Provided and by Whom** | | | |
| | Breeding, Weaning, and Genotyping | | | | | | | |
| | Anesthesia | | | | | | | |
| | If performing Gas Anesthesia, has the PA completed the IU required waste anesthetic training? For more information, click on the following link: https://protect.iu.edu/environmental-health/occupational-health/anesthetic-gas.html | | | | | | Yes | No |
| | Sedation | | | | | | | |
| | Analgesia | | | | | | | |
| | Non-survival Surgery | | | | | | | |
| | Surgery: | | | | | | | |
| | Surgery: | | | | | | | |
| | Single Survival Surgery | | | | | | | |
| | Surgery: | | | | | | | |
| | Surgery: | | | | | | | |
| | Multiple Survival Surgery: | | | | | | | |
| | Surgery: | | | | | | | |

| | | | | | |
|---|---|---|---|---|---|
| | Surgery: | | | | |
| X | Agent Administration | | Rat | 15 | Eli Lilly |
| | Irradiation | | | | |
| | Imaging | | | | |
| X | Blood Sampling | | Rat | 15 | Eli Lilly |
| | Behavioral Testing | | | | |
| | Immunization | | | | |
| | Hybridoma | | | | |
| | Physical Restraint | | | | |
| | Laser Use | | | | |
| | Animal Identification | | | | |
| X | Euthanasia | | | | |
| | X | $CO_2$ with flow meter | Rat | 15 | Eli Lilly |
| | | Other Method: | | | |
| X | Other Non-surgical procedures | | | | |
| | X | Other necropsy | Rat | 15 | Eli Lilly |
| | X | Other: blood collection via tail prick | Rat | 15 | Eli Lilly |

| | | | | |
|---|---|---|---|---|
| **Name of Protocol Associate (PA) (first, middle Initial, last):** | Melissa A. Trowbridge | | | |
| **PA IU E-mail:** | mtrowbri@iu.edu | | | |
| **Emergency Contact:** This person is responsible for performing the monitoring and managing the complications. | X | Yes | | No |
| **Campus Phone:** 4-8811 | **Emergency Phone:** 317-796-9651 | | | |

| | **Procedures this PA will perform:** | **Species** | **Years of Experience** | **Training Received and by Whom or To be Provided and by Whom** |
|---|---|---|---|---|
| | Breeding, Weaning, and Genotyping | | | |
| | Anesthesia | | | |
| | If performing Gas Anesthesia, has the PA completed the IU required waste anesthetic training? For more information, click on the following link: https://protect.iu.edu/environmental-health/occupational-health/anesthetic-gas.html | | Yes / No | |
| | Sedation | | | |
| | Analgesia | | | |
| | Non-survival Surgery | | | |
| | Surgery: | | | |
| | Surgery: | | | |
| | Single Survival Surgery | | | |
| | Surgery: | | | |
| | Surgery: | | | |
| | Multiple Survival Surgery: | | | |
| | Surgery: | | | |
| | Surgery: | | | |
| X | Agent Administration | Rat | 15 | Eli Lilly/Covance/CrownBio |
| | Irradiation | | | |
| | Imaging | | | |
| X | Blood Sampling | Rat | 15 | Eli Lilly/Covance/CrownBio |
| | Behavioral Testing | | | |
| | Immunization | | | |
| | Hybridoma | | | |
| | Physical Restraint | | | |
| | Laser Use | | | |
| | Animal Identification | | | |
| X | Euthanasia | | | |
| | X $CO_2$ with flow meter | Rat | 15 | Eli Lilly/Covance/CrownBio |
| | Other Method: | | | |

| | | | | | |
|---|---|---|---|---|---|
| X | Other Non-surgical procedures | | | | |
| | X | Other: necropsy | Rat | 15 | Eli Lilly/Covance/CrownBio |
| | | Other: blood collection via tail prick | Rat | 15 | Eli Lilly/Covance/CrownBio |

# APPENDIX C. CHAPTER 4 CHIRAL INVERSION/DEGRADATION POPULATION MODEL CODES

**R-bupropion buffer population inversion/stability model**

```
deriv(ARBUPBu = (CLRSRBUPBu * CSBUPBu) - (CLRSRBUPBu * CRBUPBu))
deriv(ASBUPBu = - (CLRSRBUPP * CSBUPP) + (CLRSRBUPBu * CRBUPBu))
dosepoint(ARBUPBu)
dosepoint(ASBUPBu)
CRBUPBu = ARBUPBu/ Vc
CSBUPBu = ASBUPBu / Vc
error(CEpsRBUPBu = 0.284)
observe(CObsRBUPBu = CRBUPBu * (1 + CEpsRBUPBu))
error(CEpsSBUPBu = 0.311)
observe(CObsSBUPBu = CSBUPBu * (1 + CEpsSBUPBu))
stparm(Vc = tvVc* exp(nVc))
stparm(CLRSRBUPBu = tvCLRSRBUPBu)
fixef(tvVc = c(, 0.1, ))
fixef(tvCLRSRBUPBu = c(, 0.1, ))
ranef(diag(nVc) = c(1))
```

**R-bupropion plasma population inversion/stability model**

```
deriv(ASBUPP = - (CLRSRBUPP * CSBUPP) + (CLRSRBUPP * CRBUPP) - (CLSBUPP
* CSBUPP))
deriv(ARBUPP = - (CLRBUPP * CRBUPP) + (CLRSRBUPP * CSBUPP)- (CLRSRBUPP
* CRBUPP))
dosepoint(ARBUPP)
dosepoint(ASBUPP)
CRBUPP = ARBUPP / Vc
CSBUPP = ASBUPP / Vc
error(CEpsSBUPP = 0.685057)
observe(CObsSBUPP = CSBUPP * (1 + CEpsSBUPP))
error(CEpsRBUPP = 0.702833)
observe(CObsRBUPP = CRBUPP * (1 + CEpsRBUPP))
stparm(Vc = tvVc)
stparm(CLRBUPP = tvCLRBUPP * exp(nCLRBUPP))
stparm(CLSBUPP = tvCLSBUPP)
stparm(CLRSRBUPP = tvCLRSRBUPP)
fixef(tvVc= c(, 0.114994, ))
fixef(tvCLRBUPP = c(, 0.0195318, ))
fixef(tvCLSBUPP = c(, 0.0340937, ))
fixef(tvCLRSRBUPP= c(, 0.055356, ))
```

```
ranef(diag(nCLRBUPP) = c(1))
```

**R-bupropion brain population inversion/stability model**

```
deriv(ASBUPB = - (CLSBUPB * CSBUPB) - (CLRSRBUPB * CSBUPB) + (CLRSRBUPB * CRBUPB))
deriv(ARBUPB = - (CLRBUPB * CRBUPB) + (CLRSRBUPB * CSBUPB)- (CLRSRBUPB * CRBUPB))
  dosepoint(ARBUPB)
deriv(ASBUPB = - (CLSBUPB * CSBUPB) - (CLRSRBUPB * CSBUPB) + (CLRSRBUPB * CRBUPB))
deriv(ARBUPB = - (CLRBUPB * CRBUPB) + (CLRSRBUPB * CSBUPB)- (CLRSRBUPB * CRBUPB))
  dosepoint(ARBUPB)
dosepoint(ASBUPB)
CRBUPB = ARBUPB / Vc
CSBUPB = ASBUPB / Vc
error(CEpsSBUPB = 0.369399)
observe(CObsSBUPB = CSBUPB * (1 + CEpsSBUPB))
error(CEpsRBUPB = 0.387344)
observe(CObsRBUPB = CRBUPB * (1 + CEpsRBUPB))
stparm(Vc = tvVc*exp(nVc))
stparm(CLRBUPB = tvCLRBUPB * exp(nCLRBUPB))
stparm(CLSBUPB = tvCLSBUPB * exp(nCLSBUPB))
stparm(CLRSRBUPB = tvCLRSRBUPB*exp(nCLRSRBUPB))
fixef(tvVc= c(, 0.0947913, ))
fixef(tvCLRBUPB = c(, 0.00922878, ))
fixef(tvCLSBUPB = c(, 0.00979925, ))
fixef(tvCLRSRBUPB= c(, 0.0184995, ))
ranef(diag(nVc, nCLRBUPB, nCLSBUPB, nCLRSRBUPB) = c(1,1,1,1))
```

**R-bupropion plasma binding population model**

```
deriv(ASBUPPT = -(CLSBUPP / fus * CSBUPPU) - (CLRSRBUPP / fus * CSBUPPU) + (CLRSRBUPP  / fur * CRBUPPU) - (CLSRBUPeq*CSBUPPU) + (CLSRBUPeq*CSBUPBu))
deriv(ARBUPPT = - (CLRBUPP / fur * CRBUPPU) + (CLRSRBUPP / fus * CSBUPPU) - (CLRSRBUPP / fur * CRBUPPU) - (CLSRBUPeq*CRBUPPU) + (CLSRBUPeq*CRBUPBu))
deriv(ASBUPBu = - (CLRSRBUPBu * CSBUPBu)+(CLRSRBUPBu * CRBUPBu)+(CLSRBUPeq*CSBUPPU)-(CLSRBUPeq*CSBUPBu))
deriv(ARBUPBu = (CLRSRBUPBu * CSBUPBu)-(CLRSRBUPBu * CRBUPBu)+(CLSRBUPeq*CRBUPPU)-(CLSRBUPeq*CRBUPBu))
CRBUPPT = ARBUPPT / VcP
CSBUPPT = ASBUPPT / VcP
CSBUPPU = CSBUPPT * fus
CRBUPPU = CRBUPPT * fur
CSBUPBu = ASBUPBu / VcBu
CRBUPBu = ARBUPBu / VcBu
dosepoint(ASBUPPT)
dosepoint(ARBUPPT)
error(CEpsSBUPPT = 0.461795)
```

```
        observe(CObsSBUPPT = CSBUPPT * (1 + CEpsSBUPPT))
        error(CEpsRBUPPT = 0.300823)
        observe(CObsRBUPPT = CRBUPPT * (1 + CEpsRBUPPT))
        error(CEpsSBUPBu = 0.00359569)
        observe(CObsSBUPBu = CSBUPBu * (1 + CEpsSBUPBu))
        error(CEpsRBUPBu = 0.00931914)
        observe(CObsRBUPBu = CRBUPBu * (1 + CEpsRBUPBu))
        stparm(VcP = tvVcP)
        stparm(VcBu = tvVcBu * exp(nVcBu))
        stparm(fus = tvfus)
        stparm(fur = tvfur)
        stparm(CLRBUPP = tvCLRBUPP * exp(nCLRBUPP))
        stparm(CLSBUPP = tvCLSBUPP * exp(nCLSBUPP))
        stparm(CLRSRBUPP = tvCLRSRBUPP)
        stparm(CLRSRBUPBu = tvCLRSRBUPBu)
        stparm(CLSRBUPeq = tvCLSRBUPeq)
        fixef(tvfus = c(, 0.6, ))
        fixef(tvfur = c(, 0.5, ))
        fixef(tvVcP(freeze) = c(, 0.107, ))
    fixef(tvVcBu(freeze) = c(, 0.233, ))
        fixef(tvCLRBUPP(freeze) = c(, 0.042, ))
        fixef(tvCLSBUPP(freeze) = c(, 0.022, ))
        fixef(tvCLRSRBUPP(freeze) = c(, 0.088, ))
        fixef(tvCLRSRBUPBu(freeze) = c(, 0.074, ))
        fixef(tvCLSRBUPeq(freeze)= c(,100,))
        ranef(diag(nVcBu, nCLRBUPP, nCLSBUPP) = c(1,1,1))
```

**R-bupropion brain binding population model**

```
        deriv(ASBUPBT = - (CLSBUPB / fus * CSBUPBU) - (CLRSRBUPB / fus * CSBUPBU)
+ (CLRSRBUPB  / fur * CRBUPBU) - (CLSRBUPeq*CSBUPBU) + (CLSRBUPeq*CSBUPBu))

        deriv(ARBUPBT = - (CLRBUPB / fur * CRBUPBU) + (CLRSRBUPB / fus * CSBUPBU)
- (CLRSRBUPB / fur * CRBUPBU) - (CLSRBUPeq*CRBUPBU) + (CLSRBUPeq*CRBUPBu))
        deriv(ASBUPBu = - (CLRSRBUPBu * CSBUPBu)+(CLRSRBUPBu *
CRBUPBu)+(CLSRBUPeq*CSBUPBU)-(CLSRBUPeq*CSBUPBu))
        deriv(ARBUPBu = (CLRSRBUPBu * CSBUPBu)-(CLRSRBUPBu *
CRBUPBu)+(CLSRBUPeq*CRBUPBU)-(CLSRBUPeq*CRBUPBu))
        CRBUPBT = ARBUPBT / VcB
        CSBUPBT = ASBUPBT / VcB
        CSBUPBU = CSBUPBT * fus
        CRBUPBU = CRBUPBT * fur
        CSBUPBu = ASBUPBu / VcBu
        CRBUPBu = ARBUPBu / VcBu
```

```
        dosepoint(ASBUPBT)
        dosepoint(ARBUPBT)
        error(CEpsSBUPBT = 0.70221)
        observe(CObsSBUPBT = CSBUPBT * (1 + CEpsSBUPBT))
        error(CEpsRBUPBT = 0.437103)
        observe(CObsRBUPBT = CRBUPBT * (1 + CEpsRBUPBT))
        error(CEpsSBUPBu = 0.403886)
        observe(CObsSBUPBu = CSBUPBu * (1 + CEpsSBUPBu))
        error(CEpsRBUPBu = 0.354436)
        observe(CObsRBUPBu = CRBUPBu * (1 + CEpsRBUPBu))
        stparm(VcB = tvVcB)
        stparm(VcBu = tvVcBu * exp(nVcBu))
        stparm(fus = tvfus)
        stparm(fur = tvfur)
        stparm(CLRBUPB = tvCLRBUPB)
        stparm(CLSBUPB = tvCLSBUPB)
        stparm(CLRSRBUPB = tvCLRSRBUPB)
        stparm(CLRSRBUPBu = tvCLRSRBUPBu)
        stparm(CLSRBUPeq=tvCLSRBUPeq)
        fixef(tvfus = c(, 0.181157, ))
        fixef(tvfur = c(, 0.173595, ))
        fixef(tvVcB(freeze) = c(, 0.092, ))
    fixef(tvVcBu(freeze) = c(, 0.233, ))
        fixef(tvCLRBUPB(freeze) = c(, 0.0085, ))
        fixef(tvCLSBUPB(freeze) = c(, 0.0111, ))
        fixef(tvCLRSRBUPB(freeze) = c(, 0.0204, ))
        fixef(tvCLRSRBUPBu(freeze) = c(, 0.074, ))
        fixef(tvCLSRBUPeq(freeze) = c(,100,))
        ranef(diag(nVcBu) = c(1))
        secondary(fusbrain= 0.33/((1/tvfus-1)+0.33))
        secondary(furbrain= 0.33/((1/tvfur-1)+0.33))
```

**S-bupropion buffer population inversion/stability model**

```
        deriv(ARBUPP = - (CLSRSBUPP * CRBUPP) + (CLSRSBUPP * CSBUPP))
        deriv(ASBUPP = (CLSRSBUPP * CRBUPP)- (CLSRSBUPP * CSBUPP))
        dosepoint(ASBUPP)
    dosepoint(ARBUPP)
        CRBUPP = ARBUPP / Vc
        CSBUPP = ASBUPP / Vc
        error(CEpsSBUPP = 0.116387)
        observe(CObsSBUPP = CSBUPP * (1 + CEpsSBUPP))
        error(CEpsRBUPP = 0.00274078)
        observe(CObsRBUPP = CRBUPP * (1 + CEpsRBUPP))
        stparm(Vc = tvVc * exp(nVc))
```

```
        stparm(CLSRSBUPP = tvCLSRSBUPP * exp(nCLSRSBUPP))
        fixef(tvVc = c(, 0.349198, ))
        fixef(tvCLSRSBUPP = c(, 0.137186, ))
        ranef(diag(nVc, nCLSRSBUPP) = c(0.14392838,0.20455851))
```

**S-bupropion plasma population inversion/stability model**

```
        deriv(ARBUPP = - (CLSRSBUPP * CRBUPP) + (CLSRSBUPP * CSBUPP) - (CLRBUPP
* CRBUPP))
        deriv(ASBUPP = - (CLSBUPP * CSBUPP) + (CLSRSBUPP * CRBUPP)- (CLSRSBUPP
* CSBUPP))
        dosepoint(ASBUPP)
        dosepoint(ARBUPP)
        CRBUPP = ARBUPP / Vc
        CSBUPP = ASBUPP / Vc
        error(CEpsSBUPP = 0.693063)
        observe(CObsSBUPP = CSBUPP * (1 + CEpsSBUPP))
        error(CEpsRBUPP = 0.856812)
        observe(CObsRBUPP = CRBUPP * (1 + CEpsRBUPP))
        stparm(Vc = tvVc)
        stparm(CLSBUPP = tvCLSBUPP * exp(nCLSBUPP))
        stparm(CLRBUPP = tvCLRBUPP * exp(nCLRBUPP))
        stparm(CLSRSBUPP = tvCLSRSBUPP * exp(nCLSRSBUPP))
        fixef(tvVc = c(, 0.0652926, ))
        fixef(tvCLSBUPP = c(, 0.021199, ))
        fixef(tvCLRBUPP = c(, 0.019048, ))
        fixef(tvCLSRSBUPP = c(, 0.0195009, ))
        ranef(diag(nCLSBUPP, nCLRBUPP, nCLSRSBUPP) = c(1,1,1))
```

**S- bupropion brain population inversion/stability model**

```
        deriv(ARBUPB = - (CLRBUPB * CRBUPB) - (CLSRSBUPB * CRBUPB) +
(CLSRSBUPB * CSBUPB))
        deriv(ASBUPB = - (CLSBUPB * CSBUPB) + (CLSRSBUPB * CRBUPB) -
(CLSRSBUPB * CSBUPB))
        dosepoint(ASBUPB)
    dosepoint(ARBUPB)
        CRBUPB = ARBUPB / Vc
        CSBUPB = ASBUPB / Vc
        error(CEpsSBUPB = 0.145734)
        observe(CObsSBUPB = CSBUPB * (1 + CEpsSBUPB))
        error(CEpsRBUPB = 0.00858328)
        observe(CObsRBUPB = CRBUPB * (1 + CEpsRBUPB))
        stparm(Vc = tvVc * exp(nVc))
        stparm(CLSBUPB = tvCLSBUPB * exp(nCLSBUPB))
        stparm(CLRBUPB = tvCLRBUPB)
```

```
stparm(CLSRSBUPB = tvCLSRSBUPB)
fixef(tvVc = c(, 0.125416, ))
fixef(tvCLSBUPB = c(, 0.00800994, ))
fixef(tvCLRBUPB = c(, 0.011174, ))
fixef(tvCLSRSBUPB = c(, 0.0399063, ))
ranef(diag(nVc, nCLSBUPB) = c(0.034435557,0.2428362))
```

**S-bupropion plasma binding population model**

```
deriv(ARBUPPT = - (CLRBUPP / fur * CRBUPPU) - (CLSRSBUPP / fur * CRBUPPU)
+ (CLSRSBUPP  / fus * CSBUPPU) - (CLSRBUPeq*CRBUPPU) + (CLSRBUPeq*CRBUPBu))
deriv(ASBUPPT = - (CLSBUPP / fus * CSBUPPU) + (CLSRSBUPP / fur * CRBUPPU)
- (CLSRSBUPP / fus * CSBUPPU) - (CLSRBUPeq*CSBUPPU) + (CLSRBUPeq*CSBUPBu))
deriv(ARBUPBu = - (CLSRSBUPBu * CRBUPBu)+(CLSRSBUPBu *
CSBUPBu)+(CLSRBUPeq*CRBUPPU)-(CLSRBUPeq*CRBUPBu))
deriv(ASBUPBu = (CLSRSBUPBu * CRBUPBu)-(CLSRSBUPBu *
CSBUPBu)+(CLSRBUPeq*CSBUPPU)-(CLSRBUPeq*CSBUPBu))
CRBUPPT = ARBUPPT / VcP
CSBUPPT = ASBUPPT / VcP
CSBUPPU = CSBUPPT * fus
CRBUPPU = CRBUPPT * fur
CSBUPBu = ASBUPBu / VcBu
CRBUPBu = ARBUPBu / VcBu
dosepoint(ASBUPPT)
dosepoint(ARBUPPT)
error(CEpsSBUPPT = 0.0022739)
observe(CObsSBUPPT = CSBUPPT * (1 + CEpsSBUPPT))
error(CEpsRBUPPT = 0.0350654)
observe(CObsRBUPPT = CRBUPPT * (1 + CEpsRBUPPT))
error(CEpsSBUPBu = 0.219084)
observe(CObsSBUPBu = CSBUPBu * (1 + CEpsSBUPBu))
error(CEpsRBUPBu = 0.267401)
observe(CObsRBUPBu = CRBUPBu * (1 + CEpsRBUPBu))
stparm(VcP = tvVcP * exp(nVcP))
stparm(VcBu = tvVcBu * exp(nVcBu))
stparm(fus = tvfus)
stparm(fur = tvfur)
stparm(CLSBUPP = tvCLSBUPP * exp(nCLSBUPP))
stparm(CLRBUPP = tvCLRBUPP)
stparm(CLSRSBUPP = tvCLSRSBUPP)
stparm(CLSRSBUPBu = tvCLSRSBUPBu)
stparm(CLSRBUPeq=tvCLSRBUPeq)
fixef(tvfus = c(, 0.574276, ))
fixef(tvfur = c(, 0.573606, ))
```

```
        fixef(tvVcP(freeze) = c(, 0.0787, ))
    fixef(tvVcBu(freeze) = c(, 0.349, ))
        fixef(tvCLSBUPP(freeze) = c(, 0.0231, ))
        fixef(tvCLRBUPP(freeze) = c(, 0.0194, ))
        fixef(tvCLSRSBUPP(freeze) = c(, 0.096, ))
        fixef(tvCLSRSBUPBu(freeze) = c(, 0.137, ))
        fixef(tvCLSRBUPeq(freeze) = c(,100,))
        ranef(diag(nVcP, nVcBu, nCLSBUPP) = c(3.0671399,0.66549748,0.51366299))
```

**S-bupropion binding population model**

```
deriv(ARBUPBT = - (CLRBUPB / fur * CRBUPBU) - (CLSRSBUPB / fur * CRBUPBU) +
(CLSRSBUPB  / fus * CSBUPBU) - (CLSRBUPeq*CRBUPBU) + (CLSRBUPeq*CRBUPBu))
        deriv(ASBUPBT = - (CLSBUPB / fus * CSBUPBU) + (CLSRSBUPB / fur * CRBUPBU)
- (CLSRSBUPB / fus * CSBUPBU) - (CLSRBUPeq*CSBUPBU) + (CLSRBUPeq*CSBUPBu))
        deriv(ARBUPBu = - (CLSRSBUPBu * CRBUPBu)+(CLSRSBUPBu *
CSBUPBu)+(CLSRBUPeq*CRBUPBU)-(CLSRBUPeq*CRBUPBu))
        deriv(ASBUPBu = (CLSRSBUPBu * CRBUPBu)-(CLSRSBUPBu *
CSBUPBu)+(CLSRBUPeq*CSBUPBU)-(CLSRBUPeq*CSBUPBu))
        CRBUPBT = ARBUPBT / VcB
        CSBUPBT = ASBUPBT / VcB
        CSBUPBU = CSBUPBT * fus
        CRBUPBU = CRBUPBT * fur
        CSBUPBu = ASBUPBu / VcBu
        CRBUPBu = ARBUPBu / VcBu
        dosepoint(ASBUPBT)
        dosepoint(ARBUPBT)
        error(CEpsSBUPBT = 0.365318)
        observe(CObsSBUPBT = CSBUPBT * (1 + CEpsSBUPBT))
        error(CEpsRBUPBT = 0.50483)
        observe(CObsRBUPBT = CRBUPBT * (1 + CEpsRBUPBT))
        error(CEpsSBUPBu = 0.013418)
        observe(CObsSBUPBu = CSBUPBu * (1 + CEpsSBUPBu))
        error(CEpsRBUPBu = 0.00201464)
        observe(CObsRBUPBu = CRBUPBu * (1 + CEpsRBUPBu))
        stparm(VcB = tvVcB)
        stparm(VcBu = tvVcBu * exp(nVcBu))
        stparm(fus = tvfus)
        stparm(fur = tvfur)
        stparm(CLSBUPB = tvCLSBUPB)
        stparm(CLRBUPB = tvCLRBUPB)
        stparm(CLSRSBUPB = tvCLSRSBUPB)
        stparm(CLSRSBUPBu = tvCLSRSBUPBu)
        stparm(CLSRBUPeq = tvCLSRBUPeq)
        fixef(tvfus = c(, 0.290724, ))
```

```
        fixef(tvfur = c(, 0.235917, ))
        fixef(tvVcB (freeze)= c(, 0.125, ))
fixef(tvVcBu (freeze)= c(, 0.349, ))
        fixef(tvCLSBUPB(freeze)= c(, 0.008, ))
        fixef(tvCLRBUPB(freeze)= c(, 0.011, ))
        fixef(tvCLSRSBUPB(freeze) = c(, 0.04, ))
        fixef(tvCLSRSBUPBu(freeze) = c(, 0.137, ))
        fixef(tvCLSRBUPeq(freeze)= c(,100,))
        ranef(diag(nVcBu) = c(1))
        secondary(fusbrain= 0.33/((1/tvfus-1)+0.33))
        secondary(furbrain= 0.33/((1/tvfur-1)+0.33))
```

# APPENDIX D. CHAPTER 5 PLASMA-BRAIN POPULATION MODEL CODES

```
deriv(Abup = - (ClbupP * CbupP) + (Aabup * Kabup) - (Clfssohbup * CbupP)-(Clinbup * CbupP) +(Cloutbup*CbupB))
deriv(AbupB= (Clinbup * CbupP) -(Cloutbup*CbupB))
deriv(Assohbup = - (ClssohbupP * CssohbupP)+ (Aassohbup * KaSSOH) + (Clfssohbup * CbupP)-(Clinssohbup * CssohbupP)+(Cloutssohbup*CssohbupB))
deriv(AssohbupB = (Clinssohbup * CssohbupP) -(Cloutssohbup*CssohbupB))
dosepoint(Aabup,bioavail = (Fbup),idosevar=AabupDose)
dosepoint(Aassohbup,bioavail = (Fssohbup),idosevar=AassohbupDose)
deriv(Aabup = - (Aabup * Kabup))
deriv(Aassohbup = - (Aassohbup * KaSSOH))
CbupP = Abup / VbupP
CbupB = AbupB /VbupB
CssohbupP = Assohbup / VssohbupP
CssohbupB = AssohbupB / VssohbupB
observe(CObsbupP = CbupP * (1 + CEpsbupP))
observe(CObsbupB = CbupB * (1 + CEpsbupB))
observe(CObssohbupP = CssohbupP * (1 + CEpsssohbupP))
observe(CObssohbupB = CssohbupB * (1 + CEpsssohbupB))
error(CEpsbupP = 0.484265747524648)
error(CEpsbupB = 0.387907948253321)
error(CEpsssohbupP = 0.734683496615348)
error(CEpsssohbupB = 0.429551011699051)
fcovariate(Dose_Group())
fcovariate(flag())
Kabup=tvKabup019*flag + tvKabup016*(1-flag)
Clinbup=(t<=3?Clinbup0 - slp*t:Clinbup0 - slp*3)
Clinssohbup=(t<=3?Clinssohbup0 - slp*t:Clinssohbup0 - slp*3)
stparm(Clfssohbup = tvClfssohbup)
stparm(Clinbup0 = tvClinbup0)
stparm(Cloutbup = tvCloutbup)
stparm(Clinssohbup0 = tvClinssohbup0 * exp(nClinssohbup0))
stparm(Cloutssohbup = tvCloutssohbup)
stparm(VbupB=tvVbupB)
stparm(VbupP=tvVbupP)
stparm(VssohbupB = tvVssohbupB)
stparm(VssohbupP =tvVssohbupP)
stparm(ClbupP = tvClbupP * exp(nClbupP))
stparm(Kabup016 = tvKabup016)
stparm(Kabup019 = tvKabup019)
```

```
        stparm(KaSSOH = tvKaSSOH)
        stparm(ClssohbupP = tvClssohbupP * exp(nClssohbupP))
        fixef(tvClfssohbup = c(, 0.0530947292551691, ))
        fixef(tvKabup016 = c(, 0.877061130160696, ))
        fixef(tvKabup019(freeze) = c(,3.66558713628573, ))
        fixef(tvKaSSOH = c(, 0.9, ))
        fixef(tvVbupP(freeze)= c(, 7.33, ))
        fixef(tvVbupB(freeze)= c(, 0.01, ))
        fixef(tvVssohbupP (freeze) = c(, 5.7, ))
        fixef(tvVssohbupB (freeze) = c(, 0.005, ))
        fixef(tvClbupP = c(, 2.79873250802894, ))
        fixef(tvClssohbupP  = c(, 6.75396275568425, ))
        fixef(tvClinbup0 = c(, 19.9652587640822, ))
        fixef(tvCloutbup = c(, 31.9042567127378, ))
        fixef(tvClinssohbup0 = c(, 21.8718830392132, ))
        fixef(tvCloutssohbup = c(,5.70024519393509, ))
        fixef(Fssohbup(freeze)= c(, 1, ))
        fixef(Fbup(freeze)= c(, 1, ))
        fixef(slp (freeze) = c(, 3.86, ))
        ranef(diag(nClbupP,nClssohbupP,nClinssohbup0)
= c(0.082807152,0.29967791,0.28349065))
```

# APPENDIX E. CHAPTER 6 PBPK MODEL CODES

**Bupropion and S, S-hydroxybupropion rat PBPK model**

```
[PARAM]
  //Tissue volumes for rat (L);
  Vad = 0.021//adipose
  Vbo = 0.02//bone
  Vbr = 0.0018 //brain
  Vbrvas = 0.00006 // brain va ulature (L)
  VguWall = 0.00619 //gut wall
  VguLumen = 0.0025 //gut lumen
  Vhe = 0.00134//heart
  Vki = 0.0028//kidneys
  Vli = 0.0109//liver
  Vpa= 0.0013 // pancreas
  Vlu = 0.00158//lungs
  Vmu = 0.148 //muscle
  Vsk = 0.03941//skin
  Vsp = 0.0007//spleen
  Vbl = 0.01724//blood =RBC volume+plasma volume
  Vsc=0.0016 // subcutaneous depot

  //Tissue blood flows (L/h); Cardiac output = 80(mL/min)or 0.08( L/min);
  Qad = 0.059*0.08*60//adipose
  Qbo = 0.101*0.08*60//bone
  Qbr = 0.015*0.08*60//brain
  Qgu = 0.138*0.08*60 // gut
  Qhe = 0.04*0.08*60 // heart
  Qki = 0.145*0.08*60//kidneys
  Qmu = 0.237*0.08*60//muscle
  Qsk= 0.051*0.08*60//skin
  Qsp = 0.008*0.08*60//spleen
  Qpa = 0.00625*0.08*60//pancreas
  Qha = 0.016*0.08*60//hepatic artery
  Qlu = 0.08*60//same as cardiac output
  Qsc = 0.0015*0.08*60// subcutaneous depot

  //partition coefficients estimated by Rodgers and Rowland for bupropion (Simcyp)

 KpadB = 9.9//adipose:plasma
 KpmuB = 2.31//muscle:plasma
 KpskB= 7.41//skin:plasma
```

```
 KpbrB= 0.4// brain: plasma
 KpguB = 18.3//gut:plasma
 KpreB = 2// assumed remaining
 KpliB = 3.25//liver:plasma
 KpspB = 2.16//spleen:plasma
 KpboB = 2.48//bone:plasma
 KpheB = 2.73 //heart:plasma
 KpkiB = 2.96 //kidney:plasma
 KpluB = 3.67//lungs:plasma
 KppaB=2 //pancreas/plasma
 KpscB= 2 // subcutaneous (assumed)

//partition coefficients estimated by Rodgers and Rowland for S, S-hydroxybupropion (Simcyp)
  KpadSSOH = 1.45//adipose:plasma
  KpbrSSOH= 2.04// brain
  KpboSSOH = 1.05//bone:plasma
  KpguSSOH = 1.93//gut:plasma
  KpheSSOH = 1.40 //heart:plasma
  KpkiSSOH = 1.46 //kidney:plasma
  KpliSSOH = 1.58//liver:plasma
  KpluSSOH = 1.58//lungs:plasma
  KpmuSSOH = 1.45//muscle:plasma
  KpskSSOH= 2.09//skin:plasma
  KpspSSOH = 1.41//spleen:plasma
  KppaSSOH= 2 //pancreas/plasma assumed
  KpreSSOH = 1 //assumed remaining

 //other parameters
  Weight = 0.31 //(kg)
  fupB = 0.5 //fraction of unbound drug in plasma measured
  ClinH = 190// uL/min/mg protein
  BP = 0.42//blood:plasma ratio
  kaB = 1.5//bupropion absorption rate constant (L/hr)
 CL_KiB = 0.018 //(L/hr) bupropion renal clearance
 fupSSOH = 0.7 //fraction of unbound drug in plasma measured
 CL_KiSSOH = 0.012 //(L/hr) S, S-hydroxybupropion renal clearance

//common  brain related parameters
S = 150 // CM2/g brain surface area
BRW = 1.8 //brain weight
MPPGB =0.25 // mg Protein/g Brain

// Bupropion brain related parameters
fubB = 0.13 // fraction unbound in brain homogenate
```

```
UIBbmB = 31 // bupropion Unionization coefficient in brain mass
UIBbbB = 17 // bupropion ionization coefficient in blood-brain
PBCB = 0.000168// bupropion brain permeability cm/sec
ERB = 0.03// efflux bupropion
CLup = 15000 // uptake bupropion

// S, S-hydroxybupropion brain related parameters
PBSSSOH =0.0000443 // permeability clearance
fubSSOH= 0.14 // fraction unbound in brain homogenate
UIbmSSOH = 4.4 // S, S-hydroxybupropion ionization coefficient in brain mass
UIbbSSOH = 2.8 // S, S-hydroxybupropion ionization coefficient in BB
ERSSOH = 0.0025// efflux
CLupSSOH= 13500 // brain uptake clearance (uL/min/mg brain protein)

//in vitro hepatic clearance parameters
fumicB = 0.58 ;//fraction of unbound drug in microsomes
  ClinHSSOH = 777;// uL/min/mg protein
MPPGLOH = 46 ;//rat mg microsomal protein per g liver (mg/g)
fumicOH = 0.88 ;//fraction of unbound drug in microsomes
VmaxHSSOHF = 8.38;// formation
KmHSSOHF = 19.85;// formation

[CMT]
  GUTLUMENB GUTB ADIPOSEB BRAINB BRAINvasB HEARTB BONEB
  KIDNEYB LIVERB LUNGB MUSCLEB SKINB SPLEENB PANCREASB RESTB
  ARTB VENB SCB GUTSSOH ADIPOSESSOH BRAINSSOH BRAINvasSSOH
HEARTSSOH BONESSOH KIDNEYSSOH LIVERSSOH LUNGSSOH MUSCLESSOH
SKINSSOH SPLEENSSOH PANCREASSSOH RESTSSOH ARTSSOH VENSSOH

[MAIN]
  //additional volume derivations
  double Vve = 0.70*Vbl; //venous blood
  double Var = 0.3*Vbl; //arterial blood
  doubleVre=Weight-
(Vli+Vki+Vsp+Vpa+Vhe+Vlu+Vbo+Vbr+Vbrvas+Vmu+Vsk+Vad+VguWall+VguLumen+Vbl
+Vsc); //volume of rest of the body compartment

  //additional blood flow derivation
  double Qli = Qgu + Qsp + Qpa+Qha;
  double Qre = Qlu - (Qli + Qki + Qbo + Qhe + Qmu + Qsk+Qad + Qbr+Qsc);

//intrinsic hepatic clearance calculation
  double CL_LiB = (ClinH*MPPGLB*Vli*1000*60*1e-6)/ fumicB; //(L/hr) hepatic clearance
double CL_LiSSOH = (ClinHSSOH*MPPGLOH*Vli*1000*60*1e-6) / fumicOH;
```

```
double CL_LiSSOHF = ((VmaxHSSOHF/KmHSSOHF)*MPPGLOH*Vli*1000*60*1e-6) / fumicOH;

// BRAIN CLEARANCE
double PSB = PBCB*S*BRW*3.6;//l/h BUPROPION brain permeabilty l/h
double CLBout = ERB*S*BRW*3.6;//efflux bupropion
double CLBin = CLup*MPPGB*BRW*60*1e-6; // uptake bupropion (L/hr)
double PSSSOH = PBSSSOH*S*BRW*3.6;//l/h SSOHBUP passive clearance l/h
double CLSSOHout = ERSSOH*S*BRW*3.6;//efflux ssohbup
double CLSSOHin = CLupSSOH*MPPGB*BRW*60*1e-6; // influx (L/hr)ssohbup


[ODE]
  //Calculation of tissue drug concentrations for Bupropion(mg/L)
  double CadiposeB = ADIPOSEB/Vad;
  double CboneB = BONEB/Vbo;
  double CbrainB = BRAINB/Vbr;
  double CbrvasB = BRAINvasB/Vbrvas;
  double CheartB = HEARTB/Vhe;
  double CkidneyB = KIDNEYB/Vki;
  double CliverB = LIVERB/Vli;
  double ClungB = LUNGB/Vlu;
  double CmuscleB = MUSCLEB/Vmu;
  double CskinB= SKINB/Vsk;
  double CspleenB = SPLEENB/Vsp;
  double CpancreasB=PANCREASB/Vpa;
  double CrestB = RESTB/Vre;
  double CarterialB = ARTB/Var;
  double CvenousB = VENB/Vve;
  double CgutLumenB = GUTLUMENB/VguLumen;
  double CgutB = GUTB/VguWall;
  double CscB = SCB/Vsc;

//Calculation of tissue drug concentrations for S, S-hydroxybupropion (mg/L)

  double CadiposeSSOH = ADIPOSESSOH/Vad;
  double CboneSSOH = BONESSOH/Vbo;
  double CbrainSSOH = BRAINSSOH/Vbr;
  double CbrvasSSOH = BRAINvasSSOH/Vbrvas;
  double CheartSSOH = HEARTSSOH/Vhe;
  double CkidneySSOH = KIDNEYSSOH/Vki;
  double CliverSSOH = LIVERSSOH/Vli;
  double ClungSSOH = LUNGSSOH/Vlu;
  double CmuscleSSOH = MUSCLESSOH/Vmu;
```

```
  double CskinSSOH= SKINSSOH/Vsk;
  double CspleenSSOH = SPLEENSSOH/Vsp;
  double CpancreasSSOH=PANCREASSSOH/Vpa;
  double CrestSSOH = RESTSSOH/Vre;
  double CarterialSSOH = ARTSSOH/Var;
  double CvenousSSOH = VENSSOH/Vve;
  double CgutSSOH = GUTSSOH/VguWall;


  //ODEs bupropion
  dxdt_GUTLUMENB = -kaB*GUTLUMENB;
  dxdt_GUTB = kaB*GUTLUMENB + Qgu*(CarterialB - CgutB/(KpguB/BP));
  dxdt_ADIPOSEB = Qad*(CarterialB - CadiposeB/(KpadB/BP));
  dxdt_BRAINvasB=Qbr*(CarterialB-CbrvasB)+PSB*((UIBbmB*fubB*CbrainB)-
(UIBbbB*fupB*CbrvasB))-(CLBin*fupB*CbrvasB)+(CLBout*fubB*CbrainB);
dxdt_BRAINB=PSB*((UIBbbB*fupB*CbrvasB)-
(UIBbmB*fubB*CbrainB))+(CLBin*fupB*CbrvasB)-(CLBout*fubB*CbrainB);
  dxdt_HEARTB = Qhe*(CarterialB - CheartB/(KpheB/BP));
  dxdt_KIDNEYB=Qki*(CarterialB-CkidneyB/(KpkiB/BP))-
CL_KiB*(fupB*CkidneyB/(KpkiB/BP));
  dxdt_LIVERB=Qgu*(CgutB/(KpguB/BP))+Qsp*(CspleenB/(KpspB/BP))+
Qpa*(CpancreasB/(KppaB/BP)) + Qha*(CarterialB) - Qli*(CliverB/(KpliB/BP)) -
    CL_LiB*(fupB*CliverB/(KpliB/BP))-(CL_LiSSOHF*CliverB);
  dxdt_LUNGB = Qlu*(CvenousB - ClungB/(KpluB/BP));
  dxdt_MUSCLEB = Qmu*(CarterialB - CmuscleB/(KpmuB/BP));
  dxdt_SKINB = Qsk*(CarterialB - CskinB/(KpskB/BP));
  dxdt_SPLEENB = Qsp*(CarterialB - CspleenB/(KpspB/BP));
  dxdt_PANCREASB = Qpa*(CarterialB - CpancreasB/(KppaB/BP));
  dxdt_BONEB = Qbo*(CarterialB - CboneB/(KpboB/BP));
  dxdt_RESTB = Qre*(CarterialB - CrestB/(KpreB/BP));
  dxdt_SCB =  Qsc*(CarterialB - CscB/(KpscB/BP));
  dxdt_VENB = Qad*(CadiposeB/(KpadB/BP)) + Qbr*(CbrainB/(KpbrB/BP)) +
    Qhe*(CheartB/(KpheB/BP)) + Qki*(CkidneyB/(KpkiB/BP)) + Qli*(CliverB/(KpliB/BP)) +
    Qmu*(CmuscleB/(KpmuB/BP))     +Qsk*(CskinB/(KpskB/BP))     +     Qsc*(CarterialB     -
CscB/(KpscB/BP))+
+Qbo*(CboneB/(KpboB/BP)) + Qre*(CrestB/(KpreB/BP)) - Qlu*CvenousB;
  dxdt_ARTB = Qlu*(ClungB/(KpluB/BP) - CarterialB);

//ODEs S, S-hydroxybupropion

  dxdt_GUTSSOH = Qgu*(CarterialSSOH - CgutSSOH/(KpguSSOH/BP));
  dxdt_ADIPOSESSOH = Qad*(CarterialSSOH - CadiposeSSOH/(KpadSSOH/BP));
```

```
  dxdt_BRAINvasSSOH=Qbr*(CarterialSSOH-CbrvasSSOH)+
PSSSOH*((UIbmSSOH*fubSSOH*CbrainSSOH)-(UIbbSSOH*fupSSOH*CbrvasSSOH))-
(CLSSOHin*fupSSOH*CbrvasSSOH)+(CLSSOHout*fubSSOH*CbrainSSOH);
dxdt_BRAINSSOH=PSSSOH*((UIbbSSOH*fupSSOH*CbrvasSSOH)-
(UIbmSSOH*fubSSOH*CbrainSSOH))+(CLSSOHin*fupSSOH*CbrvasSSOH)-
(CLSSOHout*fubSSOH*CbrainSSOH);
  dxdt_HEARTSSOH = Qhe*(CarterialSSOH - CheartSSOH/(KpheSSOH/BP));
  dxdt_KIDNEYSSOH=Qki*(CarterialSSOH-CkidneySSOH/(KpkiSSOH/BP))-
CL_KiSSOH*(fupSSOH*CkidneySSOH/(KpkiSSOH/BP));
  dxdt_LIVERSSOH=(CL_LiSSOHF*CliverB)+(Qgu*(CgutSSOH/(KpguSSOH/BP))+
Qsp*(CspleenSSOH/(KpspSSOH/BP))+Qpa*(CpancreasSSOH/(KppaSSOH/BP))+
Qha*(CarterialSSOH) - Qli*(CliverSSOH/(KpliSSOH/BP)) -
    CL_LiSSOH*(fupSSOH*CliverSSOH/(KpliSSOH/BP)));
  dxdt_LUNGSSOH = Qlu*(CvenousSSOH - ClungSSOH/(KpluSSOH/BP));
  dxdt_MUSCLESSOH = Qmu*(CarterialSSOH - CmuscleSSOH/(KpmuSSOH/BP));
  dxdt_SKINSSOH = Qsk*(CarterialSSOH - CskinSSOH/(KpskSSOH/BP));
  dxdt_SPLEENSSOH = Qsp*(CarterialSSOH - CspleenSSOH/(KpspSSOH/BP));
  dxdt_PANCREASSSOH = Qpa*(CarterialSSOH - CpancreasSSOH/(KppaSSOH/BP));
  dxdt_BONESSOH = Qbo*(CarterialSSOH - CboneSSOH/(KpboSSOH/BP));
  dxdt_RESTSSOH = Qre*(CarterialSSOH - CrestSSOH/(KpreSSOH/BP));
  dxdt_VENSSOH=Qad*(CadiposeSSOH/(KpadSSOH/BP))+
Qbr*(CbrainSSOH/(KpbrSSOH/BP)) +
    Qhe*(CheartSSOH/(KpheSSOH/BP))+Qki*(CkidneySSOH/(KpkiSSOH/BP))+
Qli*(CliverSSOH/(KpliSSOH/BP))+Qmu*(CmuscleSSOH/(KpmuSSOH/BP))
+Qsk*(CskinSSOH/(KpskSSOH/BP))
+Qbo*(CboneSSOH/(KpboSSOH/BP))+Qre*(CrestSSOH/(KpreSSOH/BP))-
Qlu*CvenousSSOH;
  dxdt_ARTSSOH = Qlu*(ClungSSOH/(KpluSSOH/BP) - CarterialSSOH);


[TABLE]

  capture CBB = CbrainB/BP ;
  capture CPB= CvenousB/BP;
  capture CBSSOH = CbrainSSOH/BP ;
  capture CPSSOH= CvenousSSOH/BP;
```

# REFERENCES


Agarwal, V., Kommaddi, R. P., Valli, K., Ryder, D., Hyde, T. M., Kleinman, J. E., . . . Ravindranath, V. (2008). Drug Metabolism in Human Brain: High Levels of Cytochrome P4503A43 in Brain and Metabolism of Anti-Anxiety Drug Alprazolam to Its Active Metabolite. *PLoS ONE, 3*(6), e2337. doi:10.1371/journal.pone.0002337

Alqahtani, S., & Kaddoumi, A. (2016). Development of a Physiologically Based Pharmacokinetic/Pharmacodynamic Model to Predict the Impact of Genetic Polymorphisms on the Pharmacokinetics and Pharmacodynamics Represented by Receptor/Transporter Occupancy of Central Nervous System Drugs. *Clinical Pharmacokinetics, 55*(8), 957-969. doi:10.1007/s40262-016-0367-6

André, P., Debray, M., Scherrmann, J.-M., & Cisternino, S. (2009). Clonidine Transport at the Mouse Blood—Brain Barrier by a New H+ Antiporter that Interacts with Addictive Drugs. *Journal of Cerebral Blood Flow & Metabolism, 29*(7), 1293-1304. doi:10.1038/jcbfm.2009.54

Apovian, C. M. (2015). Naltrexone/bupropion for the treatment of obesity and obesity with Type 2 diabetes. *Future Cardiology, 12*(2), 129-138. doi:10.2217/fca.15.79

Apovian, C. M., Aronne, L., Rubino, D., Still, C., Wyatt, H., Burns, C., . . . Group, C.-I. S. (2013). A randomized, phase 3 trial of naltrexone SR/bupropion SR on weight and obesity-related risk factors (COR-II). *Obesity (Silver Spring, Md.), 21*(5), 935-943. doi:10.1002/oby.20309

Árgyelán, M., Szabó, Z., Kanyó, B., Tanács, A., Kovács, Z., Janka, Z., & Pávics, L. (2005). Dopamine transporter availability in medication free and in bupropion treated depression: A 99mTc-TRODAT-1 SPECT study. *Journal of Affective Disorders, 89*(1), 115-123. doi:https://doi.org/10.1016/j.jad.2005.08.016

Ascher, J. A., Cole, J. O., Colin, J.-N., Feighner, J. P., Ferris, R. M., Fibiger, H. C., . . . Richelson, E. (1995). Bupropion: A review of its mechanism of antidepressant activity. *The Journal of Clinical Psychiatry, 56*(9), 395-401.

Avdeef, A. (2012). Permeability:Blood-Brain Barrier *Absorption and drug development solubility, permeability, and charge state* (2nd ed.. ed., pp. 595). Hoboken, N.J.: Hoboken, N.J. : John Wiley & Sons.

Badhan, R. K. S., Chenel, M., & Penny, J. I. (2014). Development of a Physiologically-Based Pharmacokinetic Model of the Rat Central Nervous System. *Pharmaceutics, 6*(1), 97-136.

Ball, K., Bouzom, F., Scherrmann, J.-M., Walther, B., & Declèves, X. (2012). Development of a Physiologically Based Pharmacokinetic Model for the Rat Central Nervous System and Determination of an In Vitro–In Vivo Scaling Methodology for the Blood–Brain Barrier Permeability of Two Transporter Substrates, Morphine and Oxycodone. *Journal of Pharmaceutical Sciences, 101*(11), 4277-4292. doi:10.1002/jps.23266

Ball, K., Bouzom, F., Scherrmann, J.-M., Walther, B., & Declèves, X. (2014). Comparing translational population-PBPK modelling of brain microdialysis with bottom-up prediction of brain-to-plasma distribution in rat and human. *Biopharmaceutics & Drug Disposition, 35*(8), 485-499. doi:10.1002/bdd.1908

Banks, M. L., Smith, D. A., & Blough, B. E. (2016). Methamphetamine-like discriminative stimulus effects of bupropion and its two hydroxy metabolites in male rhesus monkeys. *Behavioural Pharmacology, 27*(2-3 Spec Iss), 196-203. doi:10.1097/FBP.0000000000000224

Baron, K. T. (2019). mrgsolve: Simulate from ODE-Based Models. R package version 0.9.0. https://CRAN.R-project.org/package=mrgsolve.

Benowitz, N. L., Zhu, A. Z. X., Tyndale, R. F., Dempsey, D., & Jacob, P. (2013). Influence of CYP2B6 genetic variants on plasma and urine concentrations of bupropion and metabolites at steady state. *Pharmacogenetics and genomics, 23*(3), 135-141. doi:10.1097/FPC.0b013e32835d9ab0

Berigan, T. R. (2002). The Many Uses of Bupropion and Bupropion Sustained Release (SR) in Adults. *Primary Care Companion to The Journal of Clinical Psychiatry, 4*(1), 30-32.

Beyens, M.-N., Guy, C., Mounier, G., Laporte, S., & Ollagnier, M. (2008). Serious adverse reactions of bupropion for smoking cessation: analysis of the French Pharmacovigilance Database from 2001 to 2004. *Drug Safety, 31*(11), 1017-1026.

Bhasker, C. R., McKinnon, W., Stone, A. L., Angus CTa; Kubota, Takahirob; Ishizaki, Takashic; Miners, & O, J. (2000). Genetic polymorphism of UDP-glucuronosyltransferase 2B7 (UGT2B7) at amino acid 268: ethnic diversity of alleles and potential clinical significance. *Pharmacogenetics and genomics, 10*(8), 679-685.

Bhattacharya, C., Kirby, D., Van Stipdonk, M., & Stratford, R. E. (2019). Comparison of In Vitro Stereoselective Metabolism of Bupropion in Human, Monkey, Rat, and Mouse Liver Microsomes. *European Journal of Drug Metabolism and Pharmacokinetics, 44*(2), 261-274. doi:10.1007/s13318-018-0516-4

Bondarev, M. L., Bondareva, T. S., Young, R., & Glennon, R. A. (2003). Behavioral and biochemical investigations of bupropion metabolites. *European Journal of Pharmacology, 474*(1), 85-93. doi:https://doi.org/10.1016/S0014-2999(03)02010-7

Bors, L., Tóth, K., Tóth, E. Z., Bajza, Á., Csorba, A., Szigeti, K., . . . Erdő, F. (2018). Age-dependent changes at the blood-brain barrier. A Comparative structural and functional study in young adult and middle aged rats. *Brain Research Bulletin, 139*, 269-277. doi:https://doi.org/10.1016/j.brainresbull.2018.03.001

Bruijnzeel, A. W., & Markou, A. (2003). Characterization of the effects of bupropion on the reinforcing properties of nicotine and food in rats. *Synapse, 50*(1), 20-28. doi:10.1002/syn.10242

Butz, R. F., Schroeder, D. H., Welch, R. M., Mehta, N. B., Phillips, A. P., & Findlay, J. W. (1981). Radioimmunoassay and pharmacokinetic profile of bupropion in the dog. *Journal of Pharmacology and Experimental Therapeutics, 217*(3), 602.

Butz, R. F., Welch, R. M., & Findlay, J. W. (1982). Relationship between bupropion disposition and dopamine uptake inhibition in rats and mice. *Journal of Pharmacology and Experimental Therapeutics, 221*(3), 676.

Carroll, F. I., Blough, B. E., Mascarella, S. W., Navarro, H. A., Lukas, R. J., & Damaj, M. I. (2014). Chapter Five - Bupropion and Bupropion Analogs as Treatments for CNS Disorders. In P. D. Linda (Ed.), *Advances in Pharmacology* (Vol. Volume 69, pp. 177-216): Academic Press.

Chapy, H., André, P., Declèves, X., Scherrmann, J.-M., & Cisternino, S. (2015). A polyspecific drug/proton antiporter mediates diphenhydramine and clonidine transport at the mouse blood-retinal barrier. *British Journal of Pharmacology, 172*(19), 4714-4725. doi:10.1111/bph.13246

Coles, R., & Kharasch, E. D. (2008). Stereoselective Metabolism of Bupropion by Cytochrome P4502B6 (CYP2B6) and Human Liver Microsomes. *Pharmaceutical Research, 25*(6), 1405-1411. doi:10.1007/s11095-008-9535-1

Connarn, J. N., Flowers, S., Kelly, M., Luo, R., Ward, K. M., Harrington, G., . . . Sun, D. (2017). Pharmacokinetics and Pharmacogenomics of Bupropion in Three Different Formulations with Different Release Kinetics in Healthy Human Volunteers. *The AAPS Journal, 19*(5), 1513-1522. doi:10.1208/s12248-017-0102-8

Connarn, J. N., Luo, R., Windak, J., Zhang, X., Babiskin, A., Kelly, M., . . . Sun, D. (2016). Identification of non-reported bupropion metabolites in human plasma. *Biopharmaceutics & Drug Disposition, 37*(9), 550-560. doi:10.1002/bdd.2046

Connarn, J. N., Zhang, X., Babiskin, A., & Sun, D. (2015). Metabolism of Bupropion by Carbonyl Reductases in Liver and Intestine. *Drug Metabolism and Disposition, 43*(7), 1019-1027. doi:10.1124/dmd.115.063107

Cooper, B. R., Wang, C. M., Cox, R. F., Norton, R., Shea, V., & Ferris, R. M. (1994). Evidence that the Acute Behavioral and Electrophysiological Effects of Bupropion (Wellbutrin®) Are Mediated by a Noradrenergic Mechanism. *Neuropsychopharmacology, 11*(2), 133-141. doi:10.1038/npp.1994.43

Cremers, T. I. F. H., Flik, G., Folgering, J. H. A., Rollema, H., & Stratford, R. E. (2016). Development of a Rat Plasma and Brain Extracellular Fluid Pharmacokinetic Model for Bupropion and Hydroxybupropion Based on Microdialysis Sampling, and Application to Predict Human Brain Concentrations. *Drug Metabolism and Disposition, 44*(5), 624-633. doi:10.1124/dmd.115.068932

Dalgaard, L. (2015). Comparison of minipig, dog, monkey and human drug metabolism and disposition. *Journal of Pharmacological and Toxicological Methods, 74*, 80-92. doi:https://doi.org/10.1016/j.vascn.2014.12.005

Damaj, M. I., Carroll, F. I., Eaton, J. B., Navarro, H. A., Blough, B. E., Mirza, S., . . . Martin, B. R. (2004). Enantioselective Effects of Hydroxy Metabolites of Bupropion on Behavior and on Function of Monoamine Transporters and Nicotinic Receptors. *Molecular Pharmacology, 66*(3), 675.

Damaj, M. I., Grabus, S. D., Navarro, H. A., Vann, R. E., Warner, J. A., King, L. S., . . . Carroll, F. I. (2010). Effects of Hydroxymetabolites of Bupropion on Nicotine Dependence Behavior in Mice. *The Journal of Pharmacology and Experimental Therapeutics, 334*(3), 1087-1095. doi:10.1124/jpet.110.166850

Dash, R. P., Rais, R., & Srinivas, N. R. (2018). Chirality and neuropsychiatric drugs: an update on stereoselective disposition and clinical pharmacokinetics of bupropion. *Xenobiotica, 48*(9), 945-957. doi:10.1080/00498254.2017.1376765

Davidson, J. (1990). Seizures and bupropion: a review. *Journal of Clinical Psychopharmacology, 10*(1), 60-62.

Davies, B., & Morris, T. (1993). Physiological parameters in laboratory animals and humans. *Pharm Res, 10*. doi:10.1023/a:1018943613122

de Vries, H. E., Kooij, G., Frenkel, D., Georgopoulos, S., Monsonego, A., & Janigro, D. (2012). Inflammatory events at blood-brain barrier in neuroinflammatory and neurodegenerative disorders: implications for clinical disease. *Epilepsia, 53 Suppl 6*(Suppl 6), 45-52. doi:10.1111/j.1528-1167.2012.03702.x

Deveaugh-Geiss, J., Conners, C. K., Sarkis, E. H., Winner, P. K., Ginsberg, L. D., Hemphill, J. M., . . . Asgharnejad, M. (2002). GW320659 for the Treatment of Attention-Deficit/Hyperactivity Disorder in Children. *Journal of the American Academy of Child & Adolescent Psychiatry, 41*(8), 914-920. doi:https://doi.org/10.1097/00004583-200208000-00009

Di, L., Umland, J. P., Chang, G., Huang, Y., Lin, Z., Scott, D. O., . . . Liston, T. E. (2011). Species Independence in Brain Tissue Binding Using Brain Homogenates. *Drug Metabolism and Disposition, 39*(7), 1270. doi:10.1124/dmd.111.038778

Dunner, D. L., Zisook, S., Billow, A. A., Batey, S. R., Johnston, J. A., & Ascher, J. A. (1998). A prospective safety surveillance study for bupropion sustained-release in the treatment of depression. *J Clin Psychiatry, 59*(7), 366-373. doi:10.4088/jcp.v59n0705

Dunner DL, Z. S., and Billow AA. et al. (1998). A prospective safety surveillance study for bupropion sustained-release in the treatment of depression. *J Clin Psychiatry., 59*, 366–373.

Egerton, A., Shotbolt, J. P., Stokes, P. R. A., Hirani, E., Ahmad, R., Lappin, J. M., . . . Grasby, P. M. (2010). Acute effect of the anti-addiction drug bupropion on extracellular dopamine concentrations in the human striatum: An [11C]raclopride PET study. *NeuroImage, 50*(1), 260-266. doi:https://doi.org/10.1016/j.neuroimage.2009.11.077

Elmokadem, A., Riggs, M. M., & Baron, K. T. (2019). Quantitative Systems Pharmacology and Physiologically-Based Pharmacokinetic Modeling With mrgsolve: A Hands-On Tutorial. *CPT: pharmacometrics & systems pharmacology, 8*(12), 883-893. doi:10.1002/psp4.12467

Fabre J., Louis, F., & McLendon, D. M. (1978). Double-blind placebo-controlled study of bupropion hydrochloride (Wellbutrin®) in the treatment of depressed in-patients. *Current Therapeutic Research, 23*(3), 393.

Fang, Q. K., Han, Z., Grover, P., Kessler, D., Senanayake*, C. H., & Wald, S. A. (2000). Rapid access to enantiopure bupropion and its major metabolite by stereospecific nucleophilic substitution on an α-ketotriflate. *Tetrahedron: Asymmetry, 11*(18), 3659-3663. doi:https://doi.org/10.1016/S0957-4166(00)00349-9

Faucette, S. R., Hawke, R. L., Lecluyse, E. L., Shord, S. S., Yan, B., Laethem, R. M., & Lindley, C. M. (2000). Validation of Bupropion Hydroxylation as a Selective Marker of Human Cytochrome P450 2B6 Catalytic Activity. *Drug Metabolism and Disposition, 28*(10), 1222-1230.

Fava, M., Rush, A. J., Thase, M. E., Clayton, A., Stahl, S. M., Pradko, J. F., & Johnston, J. A. (2005). 15 Years of Clinical Experience With Bupropion HCl: From Bupropion to Bupropion SR to Bupropion XL. *Primary Care Companion to The Journal of Clinical Psychiatry, 7*(3), 106-113.

Ferguson, C. S., & Tyndale, R. F. (2011). Cytochromes P450 in the brain: Emerging evidence for biological significance. *Trends in Pharmacological Sciences, 32*(12), 708-714. doi:10.1016/j.tips.2011.08.005

Ferris, R. M., Cooper, B. R., & Maxwell, R. A. (1983). Studies of bupropion's mechanism of antidepressant activity. *J Clin Psychiatry, 44*(5 Pt 2), 74-78.

Fridén, M., Bergström, F., Wan, H., Rehngren, M., Ahlin, G., Hammarlund-Udenaes, M., & Bredberg, U. (2011). Measurement of Unbound Drug Exposure in Brain: Modeling of pH Partitioning Explains Diverging Results between the Brain Slice and Brain Homogenate Methods. *Drug Metabolism and Disposition, 39*(3), 353. doi:10.1124/dmd.110.035998

Fridén, M., Gupta, A., Antonsson, M., Bredberg, U., & Hammarlund-Udenaes, M. (2007). In Vitro Methods for Estimating Unbound Drug Concentrations in the Brain Interstitial and Intracellular Fluids. *Drug Metabolism and Disposition, 35*(9), 1711.

Gaohua, L., Neuhoff, S., Johnson, T. N., Rostami-Hodjegan, A., & Jamei, M. (2016). Development of a permeability-limited model of the human brain and cerebrospinal fluid (CSF) to integrate known physiological and biological knowledge: Estimating time varying CSF drug concentrations and their variability using in vitro data. *Drug Metabolism and Pharmacokinetics, 31*(3), 224-233. doi:https://doi.org/10.1016/j.dmpk.2016.03.005

Garberg, P., Ball, M., Borg, N., Cecchelli, R., Fenart, L., Hurst, R. D., . . . Osterberg, T. (2005). In vitro models for the blood-brain barrier. *Toxicol In Vitro, 19*(3), 299-334. doi:10.1016/j.tiv.2004.06.011

GlaxoSmithKline. WELLBUTRIN SR (bupropion hydrochloride) sustained-release tablets for oral use. https://www.accessdata.fda.gov/drugsatfda_docs/label/2019/020358s061lbl.pdf

Golden, R. N., De Vane, C. L., Laizure, S. C., Rudorfer, M. V., Sherer, M. A., & Potter, W. Z. (1988). Bupropion in depression. II. The role of metabolites in clinical outcome. *Arch Gen Psychiatry, 45*(2), 145-149. doi:10.1001/archpsyc.1988.01800260055007

Golden, R. N., DeVane, C., Laizure, S., Rudorfer, M. V., Sherer, M. A., & Potter, W. Z. (1988). Bupropion in depression: Ii. the role of metabolites in clinical outcome. *Archives of General Psychiatry, 45*(2), 145-149. doi:10.1001/archpsyc.1988.01800260055007

Grabus, S. D., Carroll, F. I., & Damaj, M. I. (2012). Bupropion and its Main Metabolite Reverse Nicotine Chronic Tolerance in the Mouse. *Nicotine & Tobacco Research, 14*(11), 1356-1361. doi:10.1093/ntr/nts088

Grandas, F., & López-Manzanares, L. (2007). Bupropion-induced parkinsonism. *Movement Disorders, 22*(12), 1830-1831. doi:10.1002/mds.21425

Gufford, B. T., Lu, J. B. L., Metzger, I. F., Jones, D. R., & Desta, Z. (2016). Stereoselective Glucuronidation of Bupropion Metabolites In Vitro and In Vivo. *Drug Metabolism and Disposition, 44*(4), 544-553. doi:10.1124/dmd.115.068908

Hakkarainen, J. J., Jalkanen, A. J., Kääriäinen, T. M., Keski-Rahkonen, P., Venäläinen, T., Hokkanen, J., . . . Forsberg, M. M. (2010). Comparison of in vitro cell models in predicting in vivo brain entry of drugs. *Int J Pharm, 402*(1-2), 27-36. doi:10.1016/j.ijpharm.2010.09.016

Hamedi, M., Mohammdi, M., Ghaleiha, A., Keshavarzi, Z., Jafarnia, M., Keramatfar, R., . . . Akhondzadeh, S. (2014). Bupropion in adults with Attention-Deficit/Hyperactivity Disorder: a randomized, double-blind study. *Acta Medica Iranica*, 6.

Hammarlund-Udenaes, M., Fridén, M., Syvänen, S., & Gupta, A. (2008). On the rate and extent of drug delivery to the brain. *Pharmaceutical Research, 25*(8), 1737-1750. doi:10.1007/s11095-007-9502-2

Hansard, M. J., Jackson, M. J., Smith, L. A., Rose, S., & Jenner, P. (2011). A major metabolite of bupropion reverses motor deficits in 1-methyl-4-phenyl-1,2,3,6-tetrahydropyridine-treated common marmosets. *Behavioural Pharmacology, 22*(3), 269-274. doi:10.1097/FBP.0b013e328345ca37

He, J., Yu, Y., Prasad, B., Chen, X., & Unadkat, J. D. (2014). Mechanism of an unusual, but clinically significant, digoxin–bupropion drug interaction. *Biopharmaceutics & Drug Disposition, 35*(5), 253-263. doi:10.1002/bdd.1890

Hesse, L. M., He, P., Krishnaswamy, S., Hao, Q., Hogan, K., Moltke, L. L., . . . Court, M. H. (2004). Pharmacogenetic determinants of interindividual variability in bupropion hydroxylation by cytochrome P450 2B6 in human liver microsomes. *Pharmacogenetics and genomics, 14*(4), 225-238.

Heymans, M., Sevin, E., Gosselet, F., Lundquist, S., & Culot, M. (2018). Mimicking brain tissue binding in an in vitro model of the blood-brain barrier illustrates differences between in vitro and in vivo methods for assessing the rate of brain penetration. *European Journal of Pharmaceutics and Biopharmaceutics, 127*, 453-461. doi:https://doi.org/10.1016/j.ejpb.2018.03.007

Jefferson, J. W., Pradko, J. F., & Muir, K. T. (2005). Bupropion for major depressive disorder: Pharmacokinetic and formulation considerations. *Clinical Therapeutics, 27*(11), 1685-1695. doi:http://dx.doi.org/10.1016/j.clinthera.2005.11.011

Johnson, S. G. The NLopt nonlinear-optimization package, http://ab-initio.mit.edu/nlopt.

Johnston, J. A., Ascher, J., Leadbetter, R., Schmith, V. D., Patel, D. K., Durcan, M., & Bentley, B. (2002). Pharmacokinetic Optimisation of Sustained-Release Bupropion for Smoking Cessation. *Drugs, 62*(2), 11-24. doi:10.2165/00003495-200262002-00002

Johnston, J. A., Fiedler-Kelly, J., Glover, E. D., Sachs, D. P., Grasela, T. H., & DeVeaugh-Geiss, J. (2001). Relationship between drug exposure and the efficacy and safety of bupropion sustained release for smoking cessation. *Nicotine Tob Res, 3*(2), 131-140. doi:10.1080/14622200110042852

Johnston JA, L. C., and Ascher JA. et al. . (1991 ). A 102-center prospective study of seizure in association with bupropion. *J Clin Psychiatry, 52*, 450–456.

Jones, H., & Rowland-Yeo, K. (2013). Basic concepts in physiologically based pharmacokinetic modeling in drug discovery and development. *CPT: pharmacometrics & systems pharmacology, 2*(8), e63-e63. doi:10.1038/psp.2013.41

Juan, M. L., & Eduardo, M. (2006). QSAR Studies on Blood-Brain Barrier Permeation. *Current Computer-Aided Drug Design, 2*(1), 31-55. doi:http://dx.doi.org/10.2174/157340906776056437

Kalvass, J. C., Maurer, T. S., & Pollack, G. M. (2007). Use of Plasma and Brain Unbound Fractions to Assess the Extent of Brain Distribution of 34 Drugs: Comparison of Unbound Concentration Ratios to in Vivo P-Glycoprotein Efflux Ratios. *Drug Metabolism and Disposition, 35*(4), 660. doi:10.1124/dmd.106.012294

Kharasch, E. D., Mitchell, D., & Coles, R. (2008). Stereoselective Bupropion Hydroxylation as an In Vivo Phenotypic Probe for Cytochrome P4502B6 (CYP2B6) Activity. *The Journal of Clinical Pharmacology, 48*(4), 464-474. doi:10.1177/0091270008314254

Kharasch, E. D., Neiner, A., Kraus, K., Blood, J., Stevens, A., Schweiger, J., . . . Lenze, E. J. (2019). Bioequivalence and Therapeutic Equivalence of Generic and Brand Bupropion in Adults With Major Depression: A Randomized Clinical Trial. *Clinical pharmacology and therapeutics, 105*(5), 1164-1174. doi:10.1002/cpt.1309

Khokhar, J. Y., Miksys, S. L., & Tyndale, R. F. (2010). Rat brain CYP2B induction by nicotine is persistent and does not involve nicotinic acetylcholine receptors. *Brain Research, 1348*, 1-9. doi:https://doi.org/10.1016/j.brainres.2010.06.035

Khokhar, J. Y., & Tyndale, R. F. (2011). Drug Metabolism within the Brain Changes Drug Response: Selective Manipulation of Brain CYP2B Alters Propofol Effects. *Neuropsychopharmacology, 36*(3), 692-700. doi:10.1038/npp.2010.202

Kielbasa, W., Kalvass, J. C., & Stratford, R. (2009). Microdialysis Evaluation of Atomoxetine Brain Penetration and Central Nervous System Pharmacokinetics in Rats. *Drug Metabolism and Disposition, 37*(1), 137-142. doi:10.1124/dmd.108.023119

Kielbasa, W., & Stratford, R. E. (2012). Exploratory Translational Modeling Approach in Drug Development to Predict Human Brain Pharmacokinetics and Pharmacologically Relevant Clinical Doses. *Drug Metabolism and Disposition, 40*(5), 877-883. doi:10.1124/dmd.111.043554

Kiptoo, P. K., Paudel, K. S., Hammell, D. C., Pinninti, R. R., Chen, J., Crooks, P. A., & Stinchcomb, A. L. (2009). Transdermal delivery of bupropion and its active metabolite, hydroxybupropion: a prodrug strategy as an alternative approach. *Journal of Pharmaceutical Sciences, 98*(2), 583-594. doi:10.1002/jps.21463

Kirby, B. J., Collier, A. C., Kharasch, E. D., Dixit, V., Desai, P., Whittington, D., . . . Unadkat, J. D. (2011). Complex Drug Interactions of HIV Protease Inhibitors 2: In Vivo Induction and In Vitro to In Vivo Correlation of Induction of Cytochrome P450 1A2, 2B6, and 2C9 by Ritonavir or Nelfinavir. *Drug Metabolism and Disposition, 39*(12), 2329. doi:10.1124/dmd.111.038646

Kirby, B. J., Collier, A. C., Kharasch, E. D., Whittington, D., Thummel, K. E., & Unadkat, J. D. (2012). Complex Drug Interactions of the HIV Protease Inhibitors 3: Effect of Simultaneous or Staggered Dosing of Digoxin and Ritonavir, Nelfinavir, Rifampin, or Bupropion. *Drug Metabolism and Disposition, 40*(3), 610. doi:10.1124/dmd.111.042705

Laizure, S. C., & DeVane, C. L. (1985). Stability of Bupropion and its Major Metabolites in Human Plasma. *Therapeutic Drug Monitoring, 7*(4), 447-450.

Laizure, S. C., DeVane, C. L., Stewart, J. T., Dommisse, C. S., & Lai, A. A. (1985). Pharmacokinetics of bupropion and its major basic metabolites in normal subjects after a single dose. *Clinical Pharmacology & Therapeutics, 38*(5), 586-589. doi:10.1038/clpt.1985.228

Learned-Coughlin, S., Bergström, M., Savitcheva, I., Ascher, J., Schmith, V., & Langstrom, B. (2003). In vivo activity of bupropion at the human dopamine transporter as measured by positron emission tomography. *Biological Psychiatry, 54*, 800-805. doi:10.1016/S0006-3223(02)01834-6

Li, S. X.-M., Perry, K. W., & Wong, D. T. (2002). Influence of fluoxetine on the ability of bupropion to modulate extracellular dopamine and norepinephrine concentrations in three mesocorticolimbic areas of rats. *Neuropharmacology, 42*(2), 181-190. doi:https://doi.org/10.1016/S0028-3908(01)00160-5

Liu, X., & Chen, C. (2015). Free Drug Hypothesis for CNS Drug Candidates *Blood-Brain Barrier in Drug Discovery* (pp. 42-65).

Luissint, A.-C., Artus, C., Glacial, F., Ganeshamoorthy, K., & Couraud, P.-O. (2012). Tight junctions at the blood brain barrier: physiological architecture and disease-associated dysregulation. *Fluids and Barriers of the CNS*, *9*, 23-23. doi:10.1186/2045-8118-9-23

Lukas, R. J., Muresan, A. Z., Damaj, M. I., Blough, B. E., Huang, X., Navarro, H. A., . . . Carroll, F. I. (2010). Synthesis and characterization of in vitro and in vivo profiles of hydroxybupropion analogues: aids to smoking cessation. *Journal of Medicinal Chemistry*, *53*(12), 4731-4748. doi:10.1021/jm1003232

Martin, P., Massol, J., Colin, J. N., Lacomblez, L., & Puech, A. J. (1990). Antidepressant Profile of Bupropion and three Metabolites in Mice. *Pharmacopsychiatry, 23*(04), 187-194. doi:10.1055/s-2007-1014505

Masters, A. R., Gufford, B. T., Lu, J. B. L., Metzger, I. F., Jones, D. R., & Desta, Z. (2016). Chiral Plasma Pharmacokinetics and Urinary Excretion of Bupropion and Metabolites in Healthy Volunteers. *Journal of Pharmacology and Experimental Therapeutics*, *358*(2), 230-238. doi:10.1124/jpet.116.232876

Masters, A. R., McCoy, M., Jones, D. R., & Desta, Z. Stereoselective method to quantify bupropion and its three major metabolites, hydroxybupropion, erythro-dihydrobupropion, and threo-dihydrobupropion using HPLC-MS/MS. *Journal of Chromatography B*. doi:http://dx.doi.org/10.1016/j.jchromb.2016.02.018

Meyer, A., Vuorinen, A., Zielinska, A. E., Strajhar, P., Lavery, G. G., Schuster, D., & Odermatt, A. (2013). Formation of Threohydrobupropion from Bupropion Is Dependent on 11β-Hydroxysteroid Dehydrogenase 1. *Drug Metabolism and Disposition*, *41*(9), 1671-1678. doi:10.1124/dmd.113.052936

Meyer, J. H., Goulding, V. S., Wilson, A. A., Hussey, D., Christensen, B. K., & Houle, S. (2002). Bupropion occupancy of the dopamine transporter is low during clinical treatment. *Psychopharmacology*, *163*(1), 102-105. doi:10.1007/s00213-002-1166-3

Miksys, S., Lerman, C., Shields, P. G., Mash, D. C., & Tyndale, R. F. (2003). Smoking, alcoholism and genetic polymorphisms alter CYP2B6 levels in human brain. *Neuropharmacology*, *45*(1), 122-132. doi:https://doi.org/10.1016/S0028-3908(03)00136-9

Miksys, S., & Tyndale, R. F. (2004). The Unique Regulation of Brain Cytochrome P450 2 (CYP2) Family Enzymes by Drugs and Genetics. *Drug metabolism reviews*, *36*(2), 313-333. doi:10.1081/DMR-120034149

Miller, N. A., Reddy, M. B., Heikkinen, A. T., Lukacova, V., & Parrott, N. (2019). Physiologically Based Pharmacokinetic Modelling for First-In-Human Predictions: An Updated Model Building Strategy Illustrated with Challenging Industry Case Studies. *Clinical Pharmacokinetics*, *58*(6), 727-746. doi:10.1007/s40262-019-00741-9

Musso, D. L., Mehta, N. B., Soroko, F. E., Ferris, R. M., Hollingsworth, E. B., & Kenney, B. T. (1993). Synthesis and evaluation of the antidepressant activity of the enantiomers of bupropion. *Chirality*, *5*(7), 495-500. doi:10.1002/chir.530050704

Nainggolan, L. (September 10, 2014). FDA Approves Bupropion/Naltrexone (Contrave) for Obesity. Retrieved from http://www.medscape.com/viewarticle/831513

National Center for Biotechnology Information. PubChem Database. m-Chlorohippuric acid, CID=448, https://pubchem.ncbi.nlm.nih.gov/compound/m-Chlorohippuric-acid (accessed on May 20, 2020).

Newton, T. F., Roache, J. D., De La Garza, R., Fong, T., Wallace, C. L., Li, S.-H., . . . Kahn, R. (2006). Bupropion Reduces Methamphetamine-Induced Subjective Effects and Cue-Induced Craving. *Neuropsychopharmacology, 31*(7), 1537-1544. doi:10.1038/sj.npp.1300979

Nicolas, J. M. (2015). Species Differences and Impact of Disease State on BBB *Blood-Brain Barrier in Drug Discovery* (pp. 66-93).

Nicolazzo, J. A., Charman, S. A., & Charman, W. N. (2006). Methods to assess drug permeability across the blood-brain barrier. *J Pharm Pharmacol, 58*(3), 281-293. doi:10.1211/jpp.58.3.0001

Nomikos GG1, D. G., Wenkstern D, Fibiger HC. ( 1992 ). Effects of chronic bupropion on interstitial concentrations of dopamine in rat nucleus accumbens and striatum. *Neuropsychopharmacology., 7*(1), 7-14.

O'Brien, F. E., Dinan, T. G., Griffin, B. T., & Cryan, J. F. (2012). Interactions between antidepressants and P-glycoprotein at the blood-brain barrier: clinical significance of in vitro and in vivo findings. *British Journal of Pharmacology, 165*(2), 289-312. doi:10.1111/j.1476-5381.2011.01557.x

O'Byrne, P. M., Williams, R., Walsh, J. J., & Gilmer, J. F. (2010). The aqueous stability of bupropion. *Journal of Pharmaceutical and Biomedical Analysis, 53*(3), 376-381. doi:https://doi.org/10.1016/j.jpba.2010.04.024

Okura, T., Hattori, A., Takano, Y., Sato, T., Hammarlund-Udenaes, M., Terasaki, T., & Deguchi, Y. (2008). Involvement of the Pyrilamine Transporter, a Putative Organic Cation Transporter, in Blood-Brain Barrier Transport of Oxycodone. *Drug Metabolism and Disposition, 36*(10), 2005-2013. doi:10.1124/dmd.108.022087

Okura, T., Higuchi, K., Kitamura, A., & Deguchi, Y. (2014). Proton-Coupled Organic Cation Antiporter-Mediated Uptake of Apomorphine Enantiomers in Human Brain Capillary Endothelial Cell Line hCMEC/D3. *Biological and Pharmaceutical Bulletin, 37*(2), 286-291. doi:10.1248/bpb.b13-00773

Ornellas, T., & Chavez, B. (2011). Naltrexone SR/Bupropion SR (Contrave): A New Approach to Weight Loss in Obese Adults. *Pharmacy and Therapeutics, 36*(5), 255-262.

Poling, J., Oliveto, A., Petry, N., Sofuoglu, M., Gonsai, K., Gonzalez, G., . . . Kosten, T. R. (2006). Six-Month Trial of Bupropion With Contingency Management for Cocaine Dependence in a Methadone-Maintained Population. *Archives of General Psychiatry, 63*(2), 219-228. doi:10.1001/archpsyc.63.2.219

R Core Team, R. F. f. S. C. (2019). R: A language and environment for statistical computing. . Vienna, Austria. Retrieved from https://www.R-project.org/

Ravindranath, V., & Anandatheerthavarada, H. K. (1990). Preparation of brain microsomes with cytochrome P450 activity using calcium aggregation method. *Analytical Biochemistry, 187*(2), 310-313. doi:https://doi.org/10.1016/0003-2697(90)90461-H

Ravindranath, V., Kommaddi, R. P., & Pai, H. V. (2006, 2006//). *Unique cytochromes P450 in human brain: implication in disease pathogenesis.* Paper presented at the Parkinson's Disease and Related Disorders, Vienna.

Reichel, A. (2010). The Blood-Brain Barrier and CNS Penetration: a Drug Discovery Point of View. *Frontiers in Pharmacology, 1*. doi:10.3389/conf.fphar.2010.02.00028

Reichel, A. (2014). Integrated Approach to Optimizing CNS Penetration in Drug Discovery: From the Old to the New Paradigm and Assessment of Drug–Transporter Interactions. In M. Hammarlund-Udenaes, C. M. E. de Lange, & G. R. Thorne (Eds.), *Drug Delivery to the Brain: Physiological Concepts, Methodologies and Approaches* (pp. 339-374). New York, NY: Springer New York.

Reichel, A. (2015). Pharmacokinetics of CNS Penetration *Blood-Brain Barrier in Drug Discovery* (pp. 5-41).

Reichel, A., Begley, D. J., & Abbott, N. J. (2003). An overview of in vitro techniques for blood-brain barrier studies. *Methods Mol Med, 89*, 307-324. doi:10.1385/1-59259-419-0:307

Reimherr, F. W., Hedges, D. W., Strong, R. E., Marchant, B. K., & Williams, E. D. (2005). Bupropion SR in adults with ADHD: a short-term, placebo-controlled trial. *Neuropsychiatric Disease and Treatment, 1*(3), 245-251.

Reist, M., Carrupt, P.-A., Francotte, E., & Testa, B. (1998). Chiral Inversion and Hydrolysis of Thalidomide: Mechanisms and Catalysis by Bases and Serum Albumin, and Chiral Stability of Teratogenic Metabolites. *Chemical Research in Toxicology, 11*(12), 1521-1528. doi:10.1021/tx9801817

Richter, W. F., & Jacobsen, B. (2014). Subcutaneous Absorption of Biotherapeutics: Knowns and Unknowns. *Drug Metabolism and Disposition, 42*(11), 1881. doi:10.1124/dmd.114.059238

Rodgers, T., & Rowland, M. (2007). Mechanistic Approaches to Volume of Distribution Predictions: Understanding the Processes. *Pharmaceutical Research, 24*(5), 918-933. doi:10.1007/s11095-006-9210-3

Sadiq, M. W., Borgs, A., Okura, T., Shimomura, K., Kato, S., Deguchi, Y., . . . Hammarlund-udenaes, M. (2011). Diphenhydramine Active Uptake at the Blood–Brain Barrier and Its Interaction with Oxycodone in vitro and in Vivo. *Journal of Pharmaceutical Sciences, 100*(9), 3912-3923. doi:http://dx.doi.org/10.1002/jps.22567

Sager, J. E., Price, L. S. L., & Isoherranen, N. (2016). Stereoselective Metabolism of Bupropion to OH-bupropion, Threohydrobupropion, Erythrohydrobupropion, and 4′-OH-bupropion in vitro. *Drug Metabolism and Disposition, 44*(10), 1709-1719. doi:10.1124/dmd.116.072363

Schindler, C. W., Gilman, J. P., Panlilio, L. V., McCann, D. J., & Goldberg, S. R. (2011). Comparison of the effects of methamphetamine, bupropion and methylphenidate on the self-administration of methamphetamine by rhesus monkeys. *Experimental and Clinical Psychopharmacology, 19*(1), 1-10. doi:10.1037/a0022432

Schroeder, D. H. (May 1983). Metabolism and kinetics of bupropion. *J Clin Psychiatry., 44*((5 Pt 2)), 79-81.

Sharon, M., & Tyndale, R. F. (2009). Brain Drug-Metabolizing Cytochrome P450 Enzymes are Active In Vivo, Demonstrated by Mechanism-Based Enzyme Inhibition. *Neuropsychopharmacology : official publication of the American College of Neuropsychopharmacology, 34*(3), 634-640. doi:10.1038/npp.2008.110

Shen, Y., Yu, Y., Lai, W., Li, S., Xu, Z., Jin, J., . . . Hong, K. (2018). Evaluation of a Potential Clinical Significant Drug-Drug Interaction between Digoxin and Bupropion in Cynomolgus Monkeys. *Pharmaceutical Research, 36*(1), 1. doi:10.1007/s11095-018-2525-z

Silverstone, P. H., Williams, R., McMahon, L., Fleming, R., & Fogarty, S. (2008). Convulsive liability of bupropion hydrochloride metabolites in Swiss albino mice. *Annals of General Psychiatry, 7*, 19-19. doi:10.1186/1744-859X-7-19

Skarydova, L., Tomanova, R., Havlikova, L., Stambergova, H., Solich, P., & Wsol, V. (2014). Deeper Insight into the Reducing Biotransformation of Bupropion in the Human Liver. *Drug Metabolism and Pharmacokinetics, 29*(2), 177-184. doi:https://doi.org/10.2133/dmpk.DMPK-13-RG-051

Slemmer, J. E., Martin, B. R., & Damaj, M. I. (2000). Bupropion Is a Nicotinic Antagonist. *Journal of Pharmacology and Experimental Therapeutics, 295*(1), 321-327.

Soetaert, K., & Petzoldt, T. (2010). Inverse Modelling, Sensitivity and Monte Carlo Analysis in R Using Package FME. *2010, 33*(3), 28. doi:10.18637/jss.v033.i03

Soroko, F. E., Mehta, N. B., Maxwell, R. A., Ferris, R. M., & Schroeder, D. H. (1977). Bupropion hydrochloride ((+/-) alpha-t-butylamino-3-chloropropiophenone HCl): a novel antidepressant agent. *J Pharm Pharmacol, 29*(12), 767-770. doi:10.1111/j.2042-7158.1977.tb11460.x

Spraggs CF, P. S., Dow D, Douglas C, McCarthy L, Manasco PK, Stubbins M, Roses AD. (2005). Pharmacogenetics and obesity: common gene variants influence weight loss response of the norepinephrine/dopamine transporter inhibitor GW320659 in obese subjects. . *Pharmacogenetics and genomics, 15*(12), 883–889.

Stahl, S. M., Pradko, J. F., Haight, B. R., Modell, J. G., Rockett, C. B., & Learned-Coughlin, S. (2004). A Review of the Neuropharmacology of Bupropion, a Dual Norepinephrine and Dopamine Reuptake Inhibitor. *Primary Care Companion to The Journal of Clinical Psychiatry, 6*(4), 159-166.

Stingl, J. C., Brockmoller, J., & Viviani, R. (2013). Genetic variability of drug-metabolizing enzymes: the dual impact on psychiatric therapy and regulation of brain function. *Mol Psychiatry, 18*(3), 273-287.

Suckow, R. F., Smith, T. M., Perumal, A. S., & Cooper, T. B. (1986). Pharmacokinetics of bupropion and metabolites in plasma and brain of rats, mice, and guinea pigs. *Drug Metabolism and Disposition, 14*(6), 692-697.

Suma, R., Kosanam, H., & Sai Prakash, P. K. (2006). Stability study of bupropion and olanzapine in formaldehyde solutions. *Rapid Communications in Mass Spectrometry, 20*(8), 1390-1394. doi:10.1002/rcm.2458

Summerfield, S. G., Read, K., Begley, D. J., Obradovic, T., Hidalgo, I. J., Coggon, S., . . . Jeffrey, P. (2007). Central Nervous System Drug Disposition: The Relationship between in Situ Brain Permeability and Brain Free Fraction. *Journal of Pharmacology and Experimental Therapeutics, 322*(1), 205. doi:10.1124/jpet.107.121525

Swan, G. E., Valdes, A. M., Ring, H. Z., Khroyan, T. V., Jack, L. M., Ton, C. C., . . . McAfee, T. (2004). Dopamine receptor DRD2 genotype and smoking cessation outcome following treatment with bupropion SR. *The Pharmacogenomics Journal, 5*, 21. doi:10.1038/sj.tpj.6500281

Syvänen, S., Lindhe, Ö., Palner, M., Kornum, B. R., Rahman, O., Långström, B., . . . Hammarlund-Udenaes, M. (2009). Species Differences in Blood-Brain Barrier Transport of Three Positron Emission Tomography Radioligands with Emphasis on P-Glycoprotein Transport. *Drug Metabolism and Disposition, 37*(3), 635. doi:10.1124/dmd.108.024745

Szentistvanyi, I., Patlak, C. S., Ellis, R. A., & Cserr, H. F. (1984). Drainage of interstitial fluid from different regions of rat brain. *American Journal of Physiology-Renal Physiology, 246*(6), F835-F844. doi:10.1152/ajprenal.1984.246.6.F835

Thacker, W. C. (1989). The role of the Hessian matrix in fitting models to measurements. *Journal of Geophysical Research: Oceans, 94*(C5), 6177-6196. doi:10.1029/JC094iC05p06177

Timothy E. Wilens, M.D. ,, Thomas J. Spencer, M.D. ,, Joseph Biederman, M.D. ,, Kristine Girard, M.D. ,, Robert Doyle, M.D. ,, Jefferson Prince, M.D. ,, . . . Asha Parekh, M.D. (2001). A Controlled Clinical Trial of Bupropion for Attention Deficit Hyperactivity Disorder in Adults. *American Journal of Psychiatry, 158*(2), 282-288. doi:10.1176/appi.ajp.158.2.282

Toselli, F., Dodd, P. R., & Gillam, E. M. J. (2016). Emerging roles for brain drug-metabolizing cytochrome P450 enzymes in neuropsychiatric conditions and responses to drugs. *Drug metabolism reviews, 48*(3), 379-404. doi:10.1080/03602532.2016.1221960

U.S. Food and Drug Administration Center for Drug Evaluation (1997). Zyban NDA 20-711 Approval.

U.S. Food and Drug Administration, Center for Drug Evaluation and Research (2014). Contrave NDA 20006Orig1s000 Approval Letter.

Uchida, Y., Ohtsuki, S., Katsukura, Y., Ikeda, C., Suzuki, T., Kamiie, J., & Terasaki, T. (2011). Quantitative targeted absolute proteomics of human blood–brain barrier transporters and receptors. *Journal of neurochemistry, 117*(2), 333-345. doi:10.1111/j.1471-4159.2011.07208.x

van Gaalen, M. M., Schlumbohm, C., Folgering, J. H., Adhikari, S., Bhattacharya, C., Steinbach, D., & Stratford, R. E. (2019). Development of a Semimechanistic Pharmacokinetic-Pharmacodynamic Model Describing Dextroamphetamine Exposure and Striatal Dopamine Response in Rats and Nonhuman Primates following a Single Dose of Dextroamphetamine. *Journal of Pharmacology and Experimental Therapeutics, 369*(1), 107. doi:10.1124/jpet.118.254508

Volkow, N. D., Wang, G.-J., Fowler, J. S., Learned-Coughlin, S., Yang, J., Logan, J., . . . Xu, Y. (2005). The slow and long-lasting blockade of dopamine transporters in human brain induced by the new antidepressant drug radafaxine predict poor reinforcing effects. *Biological Psychiatry, 57*(6), 640-646. doi:https://doi.org/10.1016/j.biopsych.2004.12.007

Volkow, N. D., Wang, G. J., Fischman, M. W., Foltin, R. W., Fowler, J. S., Abumrad, N. N., . . . Shea, C. E. (1997). Relationship between subjective effects of cocaine and dopamine transporter occupancy. *Nature, 386*(6627), 827-830. doi:10.1038/386827a0

Volkow, N. D., Wang, G. J., Fowler, J. S., Gatley, S. J., Logan, J., Ding, Y.-S., . . . Pappas, N. (1998). Dopamine transporter occupancies in the human brain induced by therapeutic doses of oral methylphenidate. *The American Journal of Psychiatry, 155*(10), 1325-1331. doi:10.1176/ajp.155.10.1325

Wang, X., Abdelrahman, D. R., Fokina, V. M., Hankins, G. D. V., Ahmed, M. S., & Nanovskaya, T. N. (2011). Metabolism of bupropion by baboon hepatic and placental microsomes. *Biochemical Pharmacology, 82*(3), 295-303. doi:https://doi.org/10.1016/j.bcp.2011.04.014

Welch, R. M., Lai, A. A., & Schroeder, D. H. (1987). Pharmacological significance of the species differences in bupropion metabolism. *Xenobiotica, 17*(3), 287-298. doi:10.3109/00498258709043939

Wickham., H. ggplot2: Elegant Graphics for Data Analysis. . *Springer-Verlag New York, 2016.*

Wilens, T. E., Prince, J. B., Spencer, T., Van Patten, S. L., Doyle, R., Girard, K., . . . Biederman, J. An open trial of bupropion for the treatment of adults with attention-deficit/hyperactivity disorder and bipolar disorder. *Biological Psychiatry, 54*(1), 9-16. doi:10.1016/S0006-3223(02)01664-5

Woodcock , J., Khan , M., & Yu , L. X. (2012). Withdrawal of Generic Budeprion for Nonbioequivalence. *New England Journal of Medicine, 367*(26), 2463-2465. doi:10.1056/NEJMp1212969

Xue, C., Zhang, X., & Cai, W. (2018). Prediction of Drug-Drug Interactions with Bupropion and Its Metabolites as CYP2D6 Inhibitors Using a Physiologically-Based Pharmacokinetic Model. *Pharmaceutics, 10*(1), 1.

Yamamoto, Y., Välitalo, P. A., Huntjens, D. R., Proost, J. H., Vermeulen, A., Krauwinkel, W., . . . de Lange, E. C. M. (2017). Predicting Drug Concentration-Time Profiles in Multiple CNS Compartments Using a Comprehensive Physiologically-Based Pharmacokinetic Model. *CPT: pharmacometrics & systems pharmacology, 6*(11), 765-777. doi:10.1002/psp4.12250

Yeniceli, D., Şener, E., Korkmaz, O. T., Doğrukol-Ak, D., & Tuncel, N. (2011). A simple and sensitive LC–ESI-MS (ion trap) method for the determination of bupropion and its major metabolite, hydroxybupropion in rat plasma and brain microdialysates. *Talanta, 84*(1), 19-26. doi:https://doi.org/10.1016/j.talanta.2010.11.063

Zakaria, Z., & Badhan, R. (2018). Development of a Region-Specific Physiologically Based Pharmacokinetic Brain Model to Assess Hippocampus and Frontal Cortex Pharmacokinetics. *Pharmaceutics, 10*(1), 14.

Zamek-Gliszczynski, M. J., Ruterbories, K. J., Ajamie, R. T., Wickremsinhe, E. R., Pothuri, L., Rao, M. V. S., . . . Chaudhary, A. K. (2011). Validation of 96-well Equilibrium Dialysis with Non-radiolabeled Drug for Definitive Measurement of Protein Binding and Application to Clinical Development of Highly-Bound Drugs. *Journal of Pharmaceutical Sciences, 100*(6), 2498-2507. doi:10.1002/jps.22452

Zhu, A. Z. X., Cox, L. S., Nollen, N., Faseru, B., Okuyemi, K. S., Ahluwalia, J. S., . . . Tyndale, R. F. (2012). CYP2B6 and Bupropion's Smoking-Cessation Pharmacology: The Role of Hydroxybupropion. *Clinical Pharmacology & Therapeutics, 92*(6), 771-777. doi:10.1038/clpt.2012.186

Zhu, A. Z. X., Zhou, Q., Cox, L. S., Ahluwalia, J. S., Benowitz, N. L., & Tyndale, R. F. (2014). Gene Variants in CYP2C19 Are Associated with Altered In Vivo Bupropion Pharmacokinetics but Not Bupropion-Assisted Smoking Cessation Outcomes. *Drug Metabolism and Disposition, 42*(11), 1971-1977. doi:10.1124/dmd.114.060285